Structural-functional reciprocal affiliations between the phytochrome two-component signal transduction system and intra-domain cross talk in *Calothrix* PCC 7601

Shivani Sharda

HEINRICH HEINE
UNIVERSITÄT
DÜSSELDORF

Structural-functional reciprocal affiliations between the phytochrome two-component signal transduction system and intra-domain cross talk in *Calothrix* PCC 7601

Inaugural Dissertation

zur Erlangung des Doktorgrades
der Mathematisch-Naturwissenschaftlichen Fakultät
der Heinrich- Heine-Universität Düsseldorf

vorgelegt von

Shivani Sharda

Aus Jalandhar (Indien)

Düsseldorf, April 2010

Revisionsschein

Ich bescheinige hiermit, dass mir die Originalfassung der Dissertation

Von Frau ……Shivani Sharda……

mit dem Titel …` ‘**Structural-functional reciprocal affiliations between the phytochrome two-component signal transduction system and intra-domain cross talk in *Calothrix* PCC 7601’**.....…….....

vorgelegt worden ist und ich gegen den Druck dieser Dissertation nichts einzuwenden habe

_____

(Ort and Datum)

(Unterschrift Berichterstatter /in und Institütsstempel)

Der unterzeichnet revisionsschein ist zurückzusenden an :

Mathematisch-Naturwissenschaftliche Fakultät
der Heinrich-Heine-Universität Düsseldorf
DER DEKAN
Universitätsstr. 1, 40225 Düsseldorf

Acknowledgements

It is a pleasure to thank the many people who made this thesis possible.

This piece of work is an accomplishment of a long journey that has been blessed by God Almighty, and by people who were ever present behind me for inspiring and guiding me through thick and thin. The travel through the scientific corridors of phytochrome research was enlightened with words of encouragement and intellectual pauses that expanded my knowledge and ideas to greater heights.

The vitally pertinent gratitude is for my Ph.D. supervisor, Professor Wolfgang Gärtner whose perpetual energy and enthusiasm in research are exalted by all. For me, he was always accessible and willing to help during my stay in Germany and otherwise. It is difficult to overstate my sincere thanks to him for his continuous support during the study, his patience and motivation that guided me through the research and write up of this thesis. He set benchmarks for getting solutions to problems that has enthused me to look for brighter prospects in future. I could not have imagined a better mentor for my Ph.D. study.

I am earnestly grateful to Prof. Georg Büldt at Forschungszentrum, Jülich- my co-supervisor for giving me the opportunity to work with his group and his valuable insights on protein crystallography. The work was endearingly supported with his scrupulous appraisal that was amply constructive for my work.

Solemn gratitude goes to Prof. Georg Groth to agree to be my second referee for my thesis evaluation and helping me with his worthy inputs. I express my sincere gratitude to Professor Wolfgang Lubitz for the insightful discussions and permission to work in his lab.

Special thanks to Professor Silvia Braslavsky and Professor Aba Losi for their cheery and buoyant selves that put new energy into my work. I would also

like to gratefully acknowledge the support and valuable advice of Professor Jon Hughes to let me have extensive discussions around my work with him.

My regards to Professor Siebert and Pascale Schwinté at University of Freiburg, who gave me their critical analysis of the proteins I worked upon facilitating my knowledge into their molecular understanding.

I am indebted to trustworthy collaborations with Professor Martin Engelhard at MPI Dortmund, Professor Eckhard Hofmann at Ruhr University Bochum for their extended support during my protein explorations.

Frau Helene Steffen, Tanja Berndsen, Ingeborg Heise and Gül Kóc have been a constant source of espousal during my project work. I treasure all precious moments we shared and really like to thank them.

During this work I have collaborated with many colleagues for whom I have great regard, and I wish to extend my warmest thanks to all those who have helped me with my work with special mention to Norbert Dickmann, Michael Reus, Joung-Jun Kim at MPI Dortmund, and Christina Lang at University of Giessen.

I would like to thank the helpful and caring lab-mates at Max Planck, to make it a convivial place to work. This extends to all the colleagues who co-ordinate in good spirits at times of need, and make working more fun during the long hours in the lab.

My well wishers and friends in the institute gave me their steadfast help during my difficult times, their detailed review, constructive criticism and excellent advice has seen me sail through the project work. Amrit, thanks for tuning in with my frequency personally and working atmosphere in the lab.

Aruna, Julieta, Rashmi, Zhen, Gopal, were fun to work with and grow into a closely knit protein working group. I thank my fellow lab buddies for stimulating

questioning, for their undaunted help and their tireless hours that were spent in the green aura of the dark room. Christoph, Christian, Anke, Alessandra, Dr. Zakir Hussain, Dr. Hideaki Ogata, Petra were very supportive in their role as co-workers and friends.

Daniela and Barbara were two nice girls who worked with me and showed their skill in learning and adapting to the protein work. There are others who have assisted me in numerous ways in my work and stay there. Thanks.

I am especially grateful to my friend Dr. Bettina Berendonck for helping me get through tough times, be it in Germany or during her visit to India, and for all the emotional support, comraderie, entertainment and care she provided.

The provident staff at MPI had been always welcoming and helpful with special allusion for Herr Schlamann, Herr Klotzbücher, and Herr Stephan Kempkes for their timely help. The librarians for providing me documents at short notices and finding the needed literature for my study. I also thank the administration staff for their sympathetic help in all paper work.

And to the rest, whom I failed to mention, thank you very much for your prayers. It really helped a lot. To everybody that has been a part of my life but I failed to mention, thank you very much.

The words might fall short for my hearty gratitude for my mentors and very special individuals who showed me the path for a successful career in spite of all my backtracking experiences. The word document doesn't sum up my heartfelt emotions for the endurance showered upon me. They reflected back my ideas of work and life, so that they echoed in my mind to shape this thesis and future work. I can only say proper thanks by practically getting high on your expectations through my future work.

ADDENDUM

To wrap it up, thanks everyone, for making my MPI - Germany life fun, enjoyable and unforgettable. And thanks for making the "morning at nights" session untiring and enjoyable experience. Thank you doesn't seem sufficient but it is said with appreciation and respect. Thank you all for encouraging me to grow and expand my thinking and allowing the freedom to pursue my doctoral degree.

Last and stupendously, I am indebted to my parents Promila and Jatinder Kumar Sharda. They bore me, raised me, trained me, propped and loved me to reach my dreams. To them I devote this thesis.

I cannot end without my deepest gratitude for my family for their stanch and unswerving belief and eternal spiritual support system throughout my life. I wish to thank my entire extended family for providing a loving environment for me. Their unflinching courage and conviction will always instigate me, and I hope to continue, in my own ways to refurbish their confidence in me and to them I dedicate this work.

Sagacious approbation goes to my partner, Shailander, for his endorsement and time to finish this work. His aura would always be surmised in framing my work and life. The pristine elite element in my life, Sveysha, angelic daughter born on Christmas Eve, whose innocent smile puts me in a trance, and melts down my distress into nowhere.

The generous support from MPI/DFG Foundation is greatly appreciated for funding my ambition to study abroad in their prestigious institute.

Last but not least, thanks to God, his power bestowed in my life has seen me through all tests in the past five years. You have made my life more plenteous. May your name be exalted, honored, and glorified.

Shivani Sharda

MPI Muelheim, 2010

Curriculum Vitae

Personal Information

Name	Shivani Sharda
Birth date	13.07.1976
Birth place	Jalandhar, India

Education

1994	12th grade schooling (Physics,Chemistry,Biology)
1998	Bachelors of science (Physics, Chemistry, Biology) at G.N.D. University, Amritsar, India
2000	Masters of Science (Biotechnology) at G.N.D. University, Amritsar, India
2000	Two months summer training at Department of Microbiology in All India Institute of Medical Sciences, New Delhi, India
2000-2002	Research assistant at International Centre for Genetic Engineering and Biotechnology, New Delhi. Worked on synthetic unnatural peptides and wrote project for who grant on the biological impact of the unnatural synthetic peptides.
2003-2007	Worked on doctoral thesis Structural-functional reciprocal affiliations between the phytochrome two-component signal transduction system and intra-domain cross talk in *Calothrix* PCC 7601' under supervision of Prof. W.Gärtner, at MPI-BAC, Muelheim an der Ruhr, Germany
2007-08	Six months of Research fellowship at ICGEB, New Delhi.

Publications :

- Quest, B., Hübschmann, T., **Sharda, S.**, Tandeau de Marsac, N., and Gärtner, W. (2007)

Homologous expression of a bacterial phytochrome. The cyanobacterium Fremyella diplosiphon incorporates biliverdin as a genuine, functional chromophore. **FEBS J. 2007 Apr;274(8):2088-98.**

- **Sharda, S.**, Shah, R., and Gärtner, W. (2007)

Domain interaction in cyanobacterial phytochromes as a prerequisite for spectral integrity. **Eur Biophys J. 2007 Sept; 36(7) : 815-21.**

- Murgida, D.H., v. Stetten, D., Hildebrandt, P., Schwinté, P., Siebert, F., **Sharda, S.**, Gärtner, W., and Mroginski, M.A. (2007)

The chromophore structures of the Pr states in plant and bacterial phytochromes. **Biophys J. 2007 Oct 1; 93 : 2410-17.**

- Schwinté, P., **Sharda, S.**, Gärtner, W., and Siebert, F. (2009)

The photoreactions of recombinant phytochrome CphA from the cyanobacterium Calothrix: A low-temperature UV-Vis and FTIR study.

Photochemsitry and Photobiology 2009, 85 : 239-249.

- Schwinté, P., **Sharda, S.**, Gärtner, W., and Siebert, F. (2009)

The photoreactions of recombinant phytochrome CphB from the cyanobacterium Calothrix: A low-temperature UV-Vis and FTIR study.

Biochemistry (submitted).

- **Sharda, S.**, Koay,M.S., Young-Jun, K., Engelhard,M., and Gärtner, W. (2009)

Detection of an active complex formation in a light inducible signal transduction system.

Journal of Biological Chemistry 2009,Vol. 284 (49) : 33999-34004.

Poster presentations/ Conferences attended :

6th International Conference on Tetrapyrrole Photoreceptors in Photosynthetic Organisms, 2005 – Luzern, Switzerland.

Identification of the chromophore binding site in cyanobacterial phytochrome from *Calothrix* PCC 7601

Sharda, S[1]., Quest, B.[2], Tandeau de Marsac, N.[3] and Gärtner, W.[1]*

1, MPI Bioanorganische Chemie, Mülheim, Germany, 2, Institut de Biologie Structurale - J.-P. Ebel Laboratoire des Proteines Membranaires Grenoble Cedex 1, France; 3, Unite´ des Cyanobacte´ries, Departement de Microbiologie Fondamentale et Medicale, Institut Pasteur (URA-CNRS 2172), Paris, France

International Plant Photobiology Meeting 24 – 28, April 2006 – Paris, France

Chromophore binding site in cyanobacterial phytochrome CphB from *Calothrix* PCC 7601- still a query.

Sharda, S[1]., Quest, B.[2], Tandeau de Marsac, N.[3] and Gärtner, W.[1]*

1, MPI Bioanorganische Chemie, Mülheim, Germany, 2, Institut de Biologie Structurale - J.-P. Ebel Laboratoire des Proteines Membranaires Grenoble Cedex 1, France; 3, Unite´ des Cyanobacte´ries, Departement de Microbiologie Fondamentale et Medicale, Institut Pasteur (URA-CNRS 2172), Paris, France

INDEX

'Phytochromes' -- resplendent light sensors

Zusammenfassung

Phytochrome (rot-, dunkelrot-detektierende biologische Photorezeptoren) finden sich sowohl in der prokaryotischen als auch in der eukaroytischen Welt. Zwei derartige Chromoproteine, CphA und CphB aus dem Cyanobakterium *Tolypothrix* PCC7601, wurden in dieser Promotionsarbeit untersucht. Phytochrome schalten zwischen rot- (664/704 nm, Pr Formen) und dunkelrot-absorbierenden Formen (707/750 nm, Pfr-Formen) in Abhängigkeit von Belichtungen mit entsprechenden Wellenlängen. Die Photochemie des Chromophors induziert strukturelle Änderungen des Proteins , die dann in ein physiologisches Signal übersetzt werden. Phytochrom-Apoproteine assemblieren autokatalytisch mit Phycocyanobilin oder Biliverdin IX α zu Holoproteinen, wobei je nach Protein eine Chromophorselektivität und auch eine andersartige Bindeposition im Protein vorgefunden wird.

In einem systematischen Ansatz der Wachstums- und Induktionsbedingungen wurde die Expression in qualitativer und quantitativer Weise optimiert. Die Assemblierung und Aufreinigung zur Homogenität ergab voll reversible Holoproteine, die u.a. Kristallisationstests unterworfen wurden. Eine systematische Einteilung an Hand von Sequenzvergleichen und Domänen-Homologie identifizierte diese bakteriellen Phytochrome als photoaktive Unterfamilie des Zweikomponenten-Signalsystems. Entsprechend wurden verkürzte Proteine erzeugt, denen entweder die Histidinkinase oder zusätzlich auch die „PHY“ Domöne fehlte. Ein Vergleich der Bindeeigenschaften und der spektroskopischen Parameter mit den Vollängenproteine zeigte deutliche Unterschiede auf, obwohl Chromophorbindung und Photoreversibilität erhalten blieben. Die hieraus erhaltenen Ergebnisse ergaben wichtige Informationen über die für Funktion und Stabilität wichtigen Wechselwirkungen zwischen den Domänen.

Thermodynamische Studien (Isotherme Calorimetrie) ergänzten die biochemischen und spektroskopischen Charakterisierungen. Diese Experimente zeigten, dass die Interaktion der Histidinkinase und des zugehörigen „response regulators“ als auch die gegenseitige Aktivierung essentiell von der Funktionsfähigkeit und Anwesenheit der lichtdetektierenden Domäne abhängig sind.

In Ergänzung durchgeführte Fourier-Transform Infrarot Untersuchungen der Vollängenproteine und der Vergleich mit verwandten Proteinen ergab wichtige Informationen über strukturelle und elektronische Veränderungen, die bei der reversiblen Photokonversion auftreten.

Insgesamt tragen die hier erhaltenen Ergebnisse – unter Einbeziehung vorhandener Kristallstrukturinformationen – dazu bei, die noch immer unzulänglich verstandene Funktion Signal-gebender biologischer Photorezeptoren besser zu verstehen.

Summary

Phytochrome systems (red-, far red-sensing biological photoreceptors) are established throughout the prokaryotic and eukaryotic world. Such chromoproteins, CphA and CphB from the cyanobacterium *Tolypothrix* PCC 7601 were investigated through the thesis work presented here. Phytochromes swap between red light (664 / 704 nm, Pr-states) and far-red light (707 / 750 nm, Pfr states) absorbing forms where the photoconversion between two states (a double bond photoisomerization) is instigated by these bilin binding protein units due to irradiation with alternate light wavelengths. These two phytochromes autocatalytically form photoconvertible holo-phytochromes with phycocyanobilin and biliverdin IXα respectively, though being disparate in their chromophore specificity as well as the binding region of the bilin. The photochemistry of the chromophore in turn induces structural changes of the protein allowing it to transmit a physiologically relevant signal.

Systematic quantification in terms of growth and induction conditions, yield and quality was performed for heterologously expressed proteins. Homogenously purified and reconstituted photoreversible phytochromes were subjected to crystallization trials. Cataloging of the phytochromes into discrete domains based on sequence as well as motif homology illustrated them as a light sensing subgroup of the bacterial two component signal transduction. Truncated constructs were designed lacking the histidine kinase module alone or the kinase along with the PHY module, respectively. The comparative spectrophotometric evaluation of the conformational changes of the truncated proteins proportional to full length proteins showed significant variations during assembly, nonetheless depicting photoreversibility after chromophore incorporation. The results yield valuable insights into the sub-domain interactions essential for photo-isomerization and stability.

Thermodynamic profiling employing isothermal calorimetry comprehended the above biochemical characterizations of domain specific interactions. Studies ensued to divulge into the photo-receptor and cognate response regulator interactions proved that the signaling here, apparently mediated through the C-terminal histidine kinase domain of the photo-receptor, is functionally controlled by the presence of the photo-sensitive fragment.

Fourier transformation infra-red spectroscopic investigations of the full length proteins and their comparison with related proteins generated information about the significant electronic modulations occurring during the reversible photo-conversion. The data of the work undertaken in the light of the known crystal structures of related proteins significantly contribute to unraveling the enigma of signaling photoreceptors.

Chapter 1

Conceptual Study Target

1.1 Aim of work

Biological photoreceptors have always attracted the research activities of scientists, probably also triggered by the fact that for human beings vision is the major sense for communicating with natural and social environment. In addition, the conversion of light energy into either chemical energy (e.g., photosynthesis) or the generation of a physiological response to various light qualities might have gained strong interest in this protein class. Plants, due to their sessile life, are outstandingly dependent on the precise determination of all parameters of light, be it the spectral composition, the duration of the illumination period, the direction, and in some cases even its polarization. The intricate organization of plant light perception is rooted upon several photoreceptors: phytochromes (600–750 nm), cryptochromes and phototropins (320–500 nm) and a putative UV-B receptor (280–320 nm). As concerns phytochrome, it is the most imperative class of photoreceptor proteins well characterized biochemically and physiologically.

Phytochrome research had been under the structural elucidation demands from the last 50 years of work in the area (Butler et al., 1954). The interest for the molecular and atomic level screening of the phytochromes as per their characteristic function and photochemical reactivity has led to an application of numerous techniques that would circumscribe these details for the benefit of the scientific world. Phytochromes are photoreceptors that utilize light as a source of information for controlling numerous biological processes (Schäfer and Nagy, 2006; Rockwell and Lagarias, 2006). The bilin chromophore, a methine-bridged tetrapyrrole acts as a photoswitch between two photoconvertible, spectrally distinct forms, denoted as Pr (λ_{max} = 664 nm) and Pfr (λ_{max} = 730 nm) according to their red and far-red absorption maxima, respectively. The photochemical switches resulting in the biologically active Pfr form, initiate an array of morphological, physiological and biochemical responses by controlling the recognition by reaction

partners of the downstream signaling processes (Smith, 2000; Kevei and Nagy, 2003; Schäfer and Nagy, 2006; Rockwell et al., 2006; Rockwell and Lagarias, 2006).

At the outset to being limited to plants, their revelation in cyanobacteria (Hughes et al., 1997) and other bacteria points towards the prokaryotic origin of this family of photoreceptors. The plant and bacterial phytochromes have evident structural and mechanistic similarities regardless of the difference in regulatory functions (Vierstra and Davis, 2000; Lamparter, 2004). Bacterial and plant phytochromes bind different, but chemically related tetrapyrrole cofactors i.e. plants binding phytochromobilin (PΦB), while phycocyanobilin (PCB), or biliverdin IXa (BV) are the dominant chromophores in bacterial phytochromes (Figure 2.3) (Lamparter et al., 2004; Karniol et al., 2005; Sharda et al., 2007). The bilin ligates to the cysteine residues present either at the canonical bilin binding pocket in the GAF domain (in plants and cyanobacterial phytochromes) or to cysteines located in the N-terminally present PAS-like-domain, subsequently coined as PLD-Cys (in bacteriophytochromes) (Kendrick and Kronenberg, 1994; Hughes et al., 1997; Vierstra and Davis, 2000; Bhoo et al., 2001; Quail, 2002; Lamparter, 2004; Lamparter et al., 2002, 2004). Bacterial phytochromes as their plant counterparts are specified with homologously present individual domains, the N-terminal sensory part that folds into a Per-Arnt-Sim (PAS) domain, the chromophore-binding GAF- (found in cGMP-specific phosphodiesterases) and a PHY- (phytochrome) domain followed by a C-terminal transmitter histidine kinase module (Karniol et al, 2005; Rockwell and Lagarias, 2006) (See Figure 2.6). The bacterial phytochromes and plant phys share such structural domain arrangement with slight modifications concurrently encoding the signaling two component system.

Since their discovery, the acquiescent microbial phytochrome systems are subjected to various biochemical and structural illustrations that are difficult for the plants, thus showing light to the underlying molecular mechanisms of such

chromoproteins. Typical bacterial phytochromes are considered as light – regulated histidine kinases constitutive of the well known two – component signal relay system of bacteria with receptive sensor domain hinged to the output kinase domain. The biological functions of such TC-HK relays in phytochromes are still enigmatic though initial findings are supportive of the above mechanism of gene regulation controlled by light activation of such proteins. The finding of a two component system in many bacterial phytochromes has highlighted the importance of these proteins, triggered by the fact that TC-HK systems represent a most generic stimuli-response system in prokaryotes which was already formerly investigated in great detail and are well characterized in many microorganisms (West and Stock, 2001; Stock and West, 2003) as well as in cyanobacteria (Ashby and Houmard, 2006). The fact that such signaling system is found in conjunction with light-stimulated sensing domains, make it an excellent object for the study of protein function.

Calothrix PCC 7601 forms an intriguing system with two different types of photochromic proteins present, an evolutionary switch indication for the cyanobacteria (from the precursor BV chromophore to more reduced PCB chromophore) as an adaptation to allow greater sensitivity to the most photosynthetically active light. The study undertaken during this project, the biochemical studies into the full length phytochromes were done to divulge in depth information about the domains indispensable for the photoreversibility of the two proteins. The chromophore selectivity and binding studies have led to the description of the discrete patterns of evolution for the two types of phytochromes studied in *Calothrix*.

The present study abstracted on the crystallography trials for the full length phytochromes, CphA and CphBm from *Calothrix PCC* 7601. An increment in the expression of soluble proteins was desired which could be purified substantially for the crystallization screening requirements. The soaring level of protein purity of

the two proteins was achieved by polishing the proteins including assorted purification steps so as to upgrade upto 99% purity levels. Previous attempts to get pure protein at high concentration usually were not successful, so this also formed another aim to achieve.

The molecular level structural details of the full length phytochromes and its chromophores had been quite a challenging task since years, so alternatively, to have vivid details of the structural modulations of the phytochrome proteins as per their function and protein domain dissection, techniques such as FTIR and protein – protein interactions were implied in this project. The aim was to elucidate the chemical changes occurring during the photoreversion of the phytochromes with respect to their respective chromophores. Isothermal titration calorimetry focuses on the quantitative analysis of protein – protein interactions which would add to the available structural details of the proteins, putting light on the mechanism of photoconversion and the downstream signaling mechanism.

The intra-domain cross talk formed another aspect for studying these photoactive proteins, where the biochemical characterization of the individual domains was approached to decipher their contribution to the activity of these proteins in vitro. Genetic modifications to the full length phytochrome genes were done to provide for the intra-domain activity and stability studies. The knowledge of the domains mapped for different functions with the truncated clones would give the insight into the bilin chromophore interactions with the sub domains as well as the basic functioning of the most sought after light perception system. The crystal structures available have given the basic features of the protein folds adopted by the phytochromes and the biochemical investigations add upto the information on the functional unit of such bili-proteins.

Chapter 2

Introduction

2.1 Light perception -Photoreceptors

Nature has in its folds numerous mysteries of life on earth. The intricate distribution of genera of prokaryotic and eukaryotic organisms has evolved during the unknown years in the history and the process still continues. Whereas the motility of animals gives them an added benefit for survival, the highly developed molecular processes in the non-motile plants contribute towards their life sustenance. Light forms the most revered source of energy for plants and other cellular organisms, which drives the molecular changes leading to growth and development processes. The light source forms the sensory signal utilized by a suite of photoactive receptors, which assess specific irradiance combinations, its composition, photoperiod duration, intensity, angle of irradiance and quality in their environment (Kendrick and Kronenberg, 1994; Batschauer, 1999; Schäfer and Nagy, 2006; Rockwell et al., 2006; Rockwell and Lagarias, 2006). Photoreceptors are critical molecules that function at the interface between organism and environment thus forming the innovating field of research for adaptation and diversification of organisms.

Plants synchronize their sophisticated transcriptional networks through perception and transduction of signals to the environments in which they occur through the network of three classified groups of photoreceptors – the phytochromes, cryptochromes, and phototropins, and their downstream signaling elements (Batschauer, 1999; Briggs, 2001; Schäfer and Nagy, 2006) along with the photosynthetic apparatus utilizing the red and blue wavelengths of the visible spectrum. Recent genomic studies have revealed that light induces massive reprogramming of the plant transcriptome, and that the early light-responsive genes are enriched in transcription factors (Jiao et al., 2007). The genre of photoreceptors described above has different light perception wavelengths in the visible and near-infra-red regions of the light spectrum (400 - 850 nm). Phytochromes (phy) predominantly detect red/far-red light (600 - 850 nm); the

cryptochromes (cry) and the phototropins (phot) detect light in the UV-A / blue region (400 - 500 nm) of the spectrum (Fig. 2.1) (Quail, 2002). A majority of the photomorphogenesis events occurring in plants and prokaryotes are induced by blue or red/ far-red signals through the aforementioned three classes of photoreceptors. Evolution of the photoreceptor genes from the prokaryotic species to higher plants have led to the occurrence of multiple cry, phot, and phy receptors allowing efficient sampling of the light wavelengths over a varied range of environmental and developmental conditions.

Genome sequencing and annotation projects unveil the prokaryotic structural regimes that are primed to enfold a range of putative photosensor proteins, whose physiological substance is still under scrutiny. The analysis of the different light sensing/light responsive protein modules and the elucidation of their light-triggered reactions, incessantly exemplify an explicit setting of photosensing prototypes (*e.g.* phytochromes, flavin-based photoreceptors, BLUF proteins) providing a connecting link amid eukaryotes and prokaryotes (Losi and Gärtner, 2006, 2008). The prokaryotes are equipped with a variety of open reading frames (ORFs) encoding both blue light and red / far red light sensing photo switchable signaling photoreceptors i.e. the bilin-binding phytochromes and the flavin-binding cryptochromes, phototropins, photoactived adenylyl cyclases (PAC) as LOV and BLUF proteins, indicating that about 1/4 of bacteria do possess at least one of these photosensory proteins (Butler et al., 1954; Ahmad and Cashmore, 1993; Briggs et al., 1997; Watanabe et al., 2002; Gomelsky and Klug, 2002; Losi and Gärtner, 2008).

The sighting of photoactive proteins through microbes, algae and fungi commences fresh research to unlock the field of light sensing and significance, apt for the future of 'visualization' of the world from microorganism perspective. These light systems creating the light perception to signal transduction mechanism providing a modular protein architecture that could be utilized in understanding the modalities of interdomain communication in sensor proteins.

2.1.1 Blue light perception

Light in the blue region of the spectrum [blue light (BL), 400 – 480 nm] is a quintessential environmental signal mediated through intracellular photosensitizers e.g., porphyrin derivatives and flavins. Therefore, living organisms detect and respond to BL either by photoprotection mechanisms or by maximally exploiting this environmental input, e.g., to entrain circadian rhythms and optimize photosynthetic efficiency. Blue light modulates quite a number of responses in plants ranging from reversible physiological changes to changes in gene expression due to light activation. These functions in plant modulation and development are a result of the complex array of photoreceptor chromoproteins which work either singly or in co-ordination with other receptors to organize the complex web of the spectacular molecular machinery in the light adaptive sessile plants and even in prokaryotic genera (Lin, 2002; Briggs, 2006).

2.1.1 (A) Cryptochromes

The term "cryptochrome" is a generic label for photoreceptors in plants that were responsible for plant responsiveness to blue light. Cryptochromes are the members of a large blue-light absorbing chromoprotein superfamily (Kanai et al., 1997) that also embrace the DNA photolyases, an observation made by the discovery of a mutation conferring anomaly in blue light signaling in Arabidopsis, marked to a gene encoding protein similar to DNA photolyases (Ahmad and Cashmore, 1993). Cryptochromes (CRYs) are thought to have evolved from photolyases several times independently. Cryptochrome is portrayed as a photolyase-like photoreceptor with sequence similarity to photolyases, DNA repair flavoproteins that mediate the repair of pyrimidine dimers, generated as a result of exposure of DNA to UV-B light (Sancar, 2003). All members of the cry/photolyase family share a highly conserved amino-terminal photolyase-related (PHR) domain that is responsible for chromophore binding (both a primary/catalytic flavin and a

second light-harvesting deazaflavin or pterin) and light-absorbing capacity (Fig. 2.1).

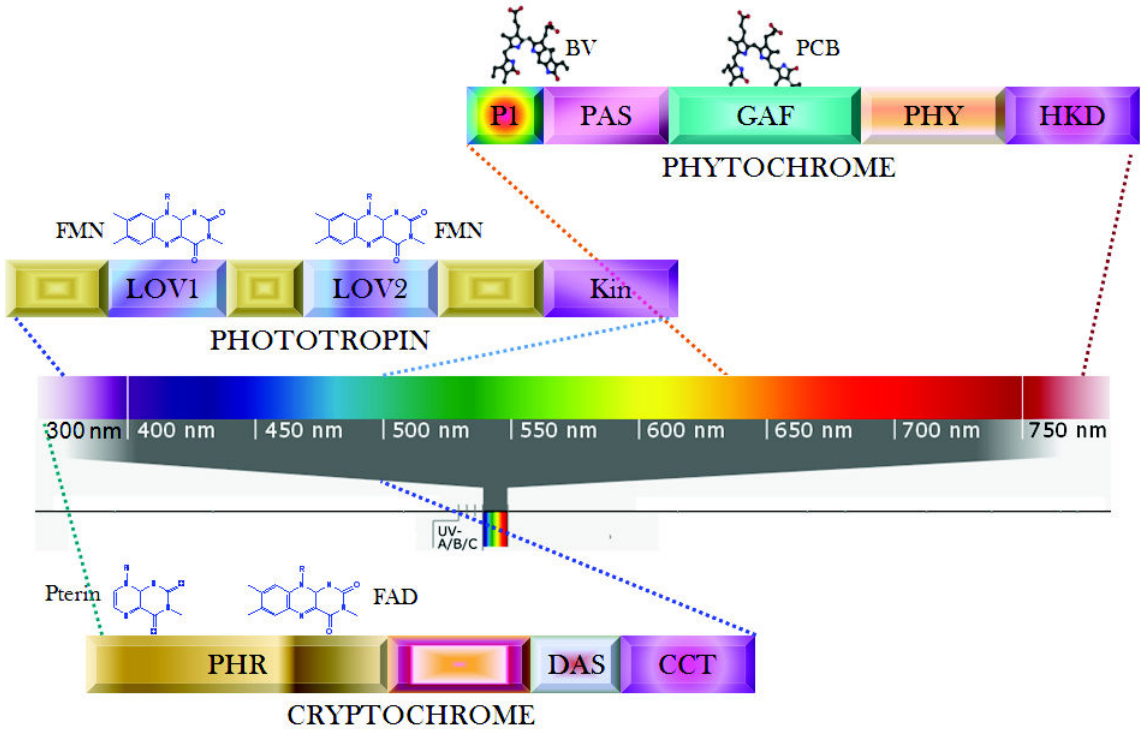

Figure 2.1 : Diagrammatic display of the electromagnetic light spectrum with identified photoreceptor groups active under the respective light wavelengths : Representation of the functional domains of phytochrome, phototropin and DNA photolyase / cryptochrome families. The phytochrome family ligates linear tetrapyrroles such as PΦB, PCB and BV as chromophores, phototropins and blue light receptors bind FMN while the cryptochromes ligates either Deazaflavin or Pterin and FAD. The homologous known domains are depicted in the scheme alongwith the light wavelength where these light receptors are functionally active. The domain specific homology regions of the proteins are also shown, details of which are described in the text. The figure is adapted from Lin (2002) and Lagarias et al. (2006).

These receptors for blue and ultraviolet (UV-A) light, have sequence similarity to photolyases but differ in their lack of DNA repair activity which is hallmark for DNA photolyases, except for CRY-DASH proteins with the presence of DQXVP – Acidic – STATES (DAS) motif (Lin and Shalitin, 2003), a carboxy-terminal extension beyond the signature of the PHR domain in the crys (Sancar 2003, 2004) (Fig 2.1). The cryptochromes bind pterin and flavin chromophores at their amino terminal domain that are activated by blue/UV-A light generating a

signaling cascade through their carboxy terminal domain. Cryptochromes are widely distributed in bacteria and eukaryotes and can be clustered into three subfamilies as plant cryptochromes, animal cryptochromes and cryptochrome-DASH proteins (CRY-DASH, as related proteins in Drosophila, Arabidopsis, Synechocystis and Homo cryps). The CRY-DASH proteins exceptionally have single stranded DNA splitting photolyase activity and are reported in the photosynthetic cyanobacteria, non-photosynthetic bacteria, fungi, plants and animals (Brudler et al., 2003; Selby and Sancar, 2006; Losi, 2006).The cry family of blue light receptors regulates various aspects of plant development, most notably seedling de-etiolation—the transition from a pale nonautotrophic seedling to a green photosynthetically competent one, entrainment of the circadian clock, and day length-sensitive timing of flowering (Cashmore 2003; Lin and Shalitin, 2003; Sancar, 2004). The cryptochrome proteins are mostly alluded with circadian rhythms (transcriptional / translational feedback loops) that synchronize the temporal relationships of cellular, physiological and behavioral processes omnipresent in genera ranging from cyanobacteria to vertebrates associated with environmental cues of light and temperature. In *Arabidopsis*, a role in circadian entrainment has been demonstrated for CRY1 and CRY2, as well as for the phytochromes (the red/far red photoreceptors) PHYA and PHYB (Somers et al., 1998).

2.1.1 (B) Phototropins

Phototropins were determined to be the photoreceptors for phototropism of the hypocotyl in *A. thaliana*, blue light induced stomatal opening, and blue light-activated leaf expansion and chloroplast movements in response to changes in light intensity (Briggs and Christie 2002). The phototropins extensively studied physiologically, photochemically and biochemically, have been annotated as blue-light receptors controlling a range of responses that serve in auxiliary optimization of the photosynthetic efficiency of plants. Phototropins are structurally designated

as blue light chromoproteins with light-activated serine/threonine protein kinase activity, resulting from two bound flavin mononucleotides (FMN) linked in a tandem repeat arrangement in the N-terminal region of the protein known as the LOV domains (Briggs et al., 1999, 2001, 2002).

Starting from their discovery in *Arabidopsis thaliana* using the mutant nph1 (non-phototrophic hypocotyls mutant 1) found deficient in blue light induced phototrophic curvature, hence named phototropin after the phenotype, many orthologous sequences have been identified in several plants structurally conserving two LOV domains (1 and 2). Photoexcitation of the LOV domain by absorption of blue light triggers the formation of covalent adducts between FMN and cysteine residues in the PAS/LOV domains, which induce a conformational change that is thought to initiate a signaling cascade through activation of the serine/threonine kinase activity at the carboxy-terminal domain.

Since their discovery in plants, LOV (light, oxygen, voltage) domain proteins have been identified in many prokaryotic species, where they are combined with histidine kinase motifs and many other output domains (Losi and Gärtner, 2008). Phototropins thus comprise the founding members of a larger superfamily known as LOV domain family that includes such proteins as WHITE COLLAR-1 of *Neurospora crassa* and YtvA of *Bacillus subtilis* (Losi et al., 2002; Crosson et al., 2003). The hallmark feature of the phot/LOV domain superfamily is the LOV (light, oxygen, and voltage) domain, an approximately 110-amino acid motif that is responsible for chromophore (flavin)-binding and the light-sensing capacity in photoactive LOV domain-containing proteins (Fig. 2.1). The other members of the superfamily couple diverse and unrelated output domains e.g. kinases, phosphodiesterases, constituting modular light switch protein entities to the LOV sensor domain (Crosson et al., 2003; Losi, 2006; Losi and Gärtner, 2008) when compared to plant phots containing two LOV domains (LOV1 and LOV2) coupled to C-terminal Ser/Thr protein kinase output domain. Photoexcitation of

the LOV domain results in receptor autophosphorylation and an initiation of phototropin signaling.

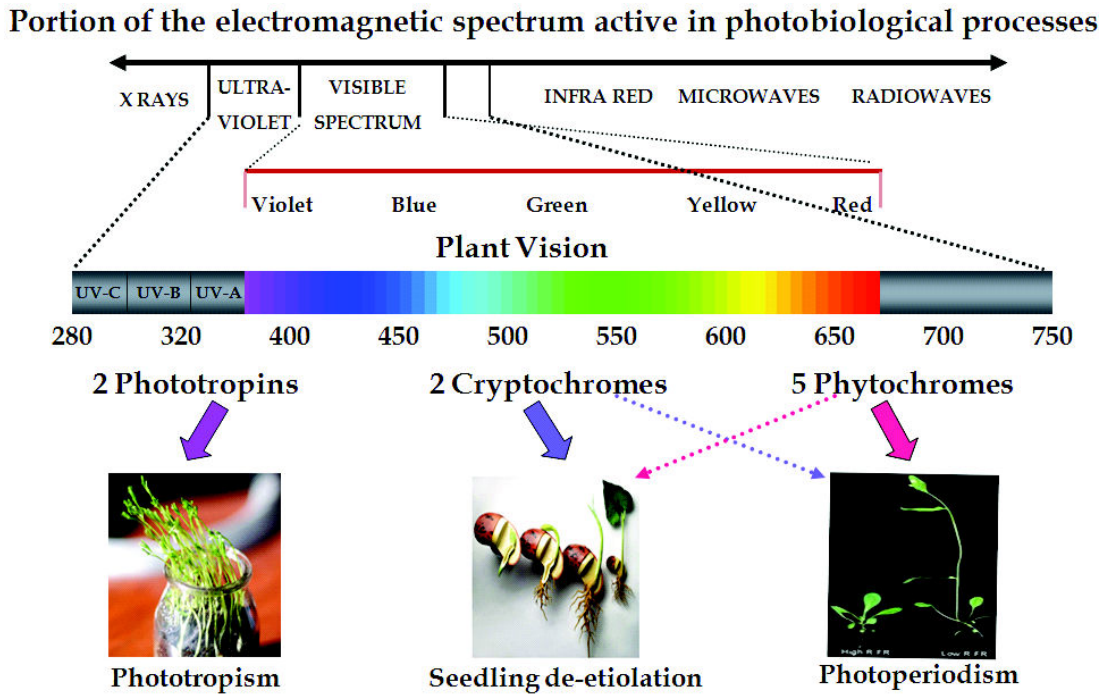

Figure 2.2: Functional facet of various light receptive proteins: Depiction of the three types of photoreceptors comprehensible for the plants with the assigned functions of each photoreceptor as described by various studies. The figure is adapted from Lin et al., 2002.

Phototropins regulate a number of blue light induced responses like chloroplast relocalization, stomatal opening and phototropism (Liscum et al., 2003; Christie, 2007) in response to light which serves to optimize the photosynthetic efficiency of plants (Fig. 2.2).

2.1.1 (C) BLUF proteins

BLUF domain proteins form the third type of blue light sensors using flavin adenine dinucleotide, FAD. The flavin photosensor identified in *Euglena gracilis* as the PAC (PAS associated C-terminal domain) responsible for phototaxis in this protist where protein employs BLUF domain for cellular functionality after blue light sensitization (Gomelsky and Klug, 2002; Watanabe et al., 2002). Similarly BLUF domain is the light sensing unit of AppA, a blue light and redox sensor involved in the regulation of photosynthesis genes in *Rhodobacter sphaeroides* (Masuda and Bauer, 2002; Laan et al., 2006).

BLUF domains are present in various proteins from Bacteria and lower Eukarya (euglenoids). They are fully modular and can relay signals to structurally and functionally diverse output units, most of which are implicated in nucleotide metabolism. The structural insights have suggested along with other lines of evidence, the mechanistic aspects for the photocycle that is characterized by a red-shifted absorbance of the flavin. The structure suggests a unique photochemical signaling switch in which the absorption of light induces a structural change in the rim surrounding the hook, thereby changing the protein interface between BLUF and the output domain.

2.1.2 Red/Far-red light perception

2.1.2.1 Phytochromes (Phys) - discovery, distribution and general features

Phytochromes command the most impending occurrence in various organisms from green algae to higher plants, forming the intensely characterized form of the light receptors, mediating diverse array of photomorphogenetic responses (Quail et al., 1995; Han et al., 2007). Plants have developed light-receptor systems to recognize and respond to light quality, fluence rate, direction and duration from their environment. The blue-protein entities, phytochromes, extracted from plant tissue half a century ago (Butler et al., 1959) have functions impacting seed germination, seedling growth, flowering, stem elongation, shade avoidance, and circadian rhythms along with the regulation of many molecular signaling pathways directing various physiological and biochemical aspects of plant development like organization of plastids, vertical movement of leaves (Fig. 2.2) (Kendrick and Kronenberg 1994; Neff et al. 2000; Casal et al. 2000). The diversity of phytochrome-mediated phenomena has been established using molecular genetic analysis of these bili-proteins (Clack et al., 1994; Pratt, 1995).

The phytochrome group here was addressed as the red and far-red reversible receptors with a bilin chromophore. The cyanobacterial chromatic adaptation sensor, RcaE, from *Fremyella diplosiphon* was the very first phytochrome related protein to be isolated (Kehoe and Grossman, 1996; Schäfer and Nagy, 2006), however no solid information on the type and binding of chromophore could be presented for this protein. The recent years have seen exponential growth in research on the physiological, biochemical and functional properties of phytochromes (Quail 1997; Fankhauser 2001; Nagy and Schäfer 2000). Phytochromes perceive red and far – red light between 600 and 800 nm wavelength of the electromagnetic spectrum. The phytochrome apoprotein contains an N-

terminal photosensory domain and a C-terminal kinase domain that have been shown to function as protein – protein interaction motif as also small ligand response module.

The thrusting research into these receptors has led to decode the evolution of phytochromes deep into representative organisms from prokaryotes, in oxygenic photosynthetic organisms, non-oxygenic photosynthetic bacteria, cyanobacteria (Cph1/CphA, Cph2, and CphB/BphP), and non-photosynthetic eubacteria (bacteriophytochromes or BphPs) as well as in fungi (fungal phytochromes, Fph family) (Hughes et al., 1997; Yeh et al., 1997; Davis et al., 1999; Lamparter et al., 2002; Suetsugu and Wada, 2003; Lamparter, 2004; Blumenstein et al., 2005; Froehlich et al., 2005; Karniol et al., 2005; Karniol and Vierstra, 2006) except archaea (Vierstra and Davis 2000; Giraud et al., 2005).

The in-depth research findings have put enough weight on the independent assortment of these receptors as entities responsible for various physiological responses in diverse living systems. The phytochrome genes may have specific or overlapping functions to regulate various responses as has been identified by unlocking many of the downstream components of phytochrome signal transduction (Nagy and Schäfer, 2000; Quail, 2002). It is thought that phytochromes directly modulate gene expression through interaction with transcription factors in the nucleus (Quail, 2002).

2.1.2.2 Phytochrome Chromophore and Photointerconversion

The phytochromes and phytochrome-related proteins use open chain tetrapyrroles as their chromophores. Biliverdin IXα is both the biosynthetic precursor of plant phy chromophore, phytochromobilin (PΦB) and of cyanobacterial Cphs chromophore, phyocyanobilin (PCB), and also a chromophore itself bound by Bph proteins. The basic chemical structure of these three bilins is

similar, only differing in the number of double bonds they contain (refer Figure 2.3). The differences in the bonds lead to differences in terms of absorption light wavelengths that are a function of conjugated electron system. The more reduced phytobilins i.e. PΦB and PCB, have shortened electron systems, preferentially absorbing light of shorter wavelength (i.e. closer to the blue end of the spectrum) resulting in slight differences in the spectral properties of assembled proteins.

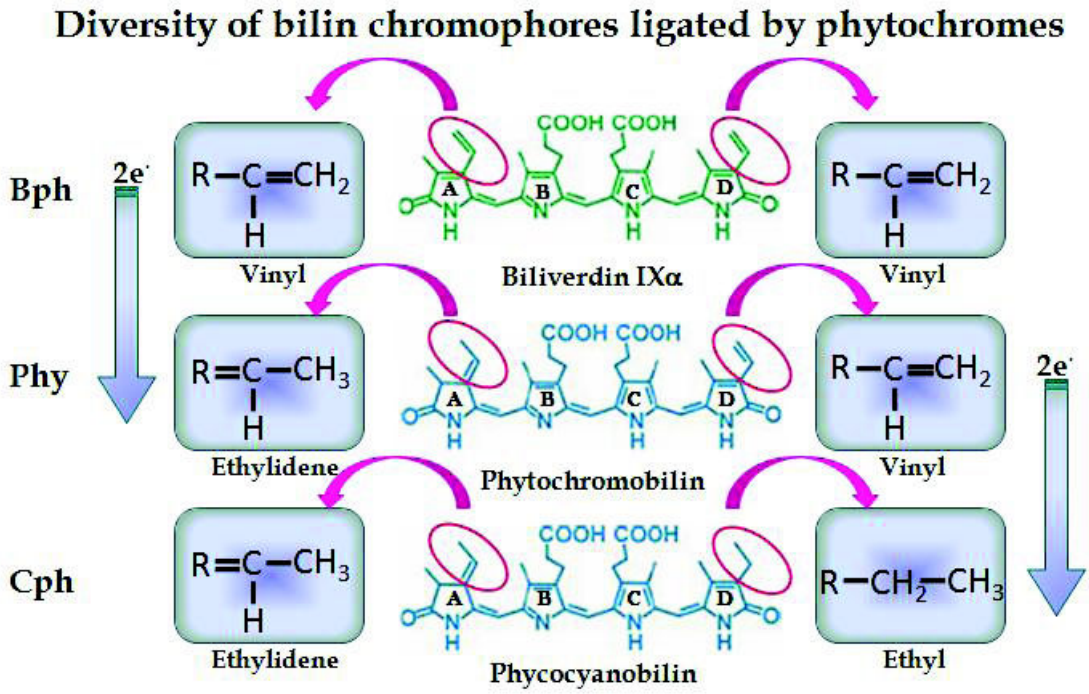

Figure 2.3. Diversity of bilin chromophores utilized by the phytochrome systems found in proteobacteria, plants and cyanobacterial : The structural differences and oxidation relationships of these natural chromophores are highlighted. The conversion from biliverdin to PΦB is also connected to a rearrangement of electrons in ring A.

The attachment of PΦB and PCB chromophores by Phy and Cph proceeds via a common mechanism of thioether formation with the ethylidene group present at the $C3^1$ carbon of the bilin A-ring (Fig. 2.3 and Fig. 2.5). In contrast to PΦB and PCB, BV does not contain the A-ring ethylidene group required for formation of a thioether linkage with the GAF domain cysteine of Phy and Cph (BV has a vinyl group at this position), and therefore, it does not covalently bind

to Phy or Cph. Structural work has revealed that BV binding to Bph proceeds via linkage at the $C3^2$ carbon and that this reaction may be favored by the geometry of the attachment site. The chromophores structure in the protein have been evaluated as per the crystal structures (Wagner et al., 2007; Essen et al., 2008; Yang et al., 2008) and also from QM/MM (Mroginsky et al., 2009) calculations as ZZZ_{ssa} (Pr) and ZZE_{ssa} with no other formal changes but plenty rearrangements occurring along single bonds and dihedral angle rearrangements. The details of the chromophores structure are dealt with while detailing about Cph1 crystal structure.

Phytochromes are chromophoric proteins absorbing visible light of the electromagnetic spectrum both in the blue and red regions with maxima at around 380 nm and at wavelengths longer than 650 nm. The energy of this absorbed light is converted into signals which exert photomorphogenic controls, primarily as a function of the spectral composition of the absorbed light (Nagy and Schäfer, 2002; Quail, 2002). These protein entities have the definite feature of photoreversibility upon irradiation with either red or far-red light wavelength (Butler et al., 1964). This reversible photoisomerization reaction is conferred by an open chain tetrapyrrole (phytobilin) prosthetic group that is covalently attached to the phytochrome apoprotein, a feature related to other photoactive proteins that are associated with light absorbing chromophores, linked within the binding pocket of these proteins (Briggs and Olney, 2001). The chromophores undergo upon light activation chemical modifications producing two reversible forms of the phytochromes, Pr and Pfr. Synthesized in the red light-absorbing Pr form (λ_{max} = 660 nm/ 700 nm, wavelength dependent on type of chromophore), all phytochromes are transposable while being synchronized by red light (R) absorption which initiates the photochemical interconversion to the far-red (FR) light-absorbing Pfr form (λ_{max} = 700 nm/ 750 nm) (Figure 2.4). FR promotes the reverse conversion of Pfr to Pr – a process which typically abolishes the R-dependent activation of the photoreceptor either by absorption of an FR photon or

by prolonged incubation in the dark via a thermal process known as 'dark reversion' (Braslavsky et al., 1997; Gärtner and Braslavsky, 2003). The two isomeric forms, Pr and Pfr (Fig. 2.5) of the phytochromes have slighlty different conformations linked with the attached chromophores which have been substantially supported by well documented experiments including circular dichroism, chromatography, and cysteine labeling (Eilfeld and Eilfeld, 1988; Noack and Lamparter, 2007). The photochromic Pr/Pfr equilibrium is consonant with the absorption spectra of the two phytochrome forms (Fig. 2.4). The photoconversion between the forms is though unequal as the absorption of light at wavelength 730 nm, Pfr is converted entirely to Pr while the reverse phototransformation with shorter wavelengths is not quantitatively favourable for Pfr, having overlapping absorptions of the two forms. This makes isolation of pure Pfr form inaccessible by any photochemical means and an enrichment of only 87% Pfr at best can be obtained by saturating irradiation with red light of 660 nm (Braslavsky, 1997; Gärtner and Braslavsky, 2003).

The field of light activated interconversions of phytochromes has been extensively studied for getting insight into the biochemical modulations occurring during the reversible phenomenon (Butler, 1972; Braslavsky et al., 1997; Gärtner and Braslavsky, 2003). Since Pr and Pfr have overlapping absorption spectra in most regions of the light spectrum, Pr-to-Pfr and Pfr-to-Pr photoconversion processes lead to the formation of a photoequilibium consisting of a mixture of Pr and Pfr forms under saturating illumination. Photoequilibrium statistics stand at red light producing a mixture of roughly 87% Pfr and 13% Pr whereas far-red light irradiation can convert >99% of phytochrome to the Pr form owing to the lack of Pr absorption in the far-red (FR) region of the light spectrum (Lagarias and Lagarias, 1989).

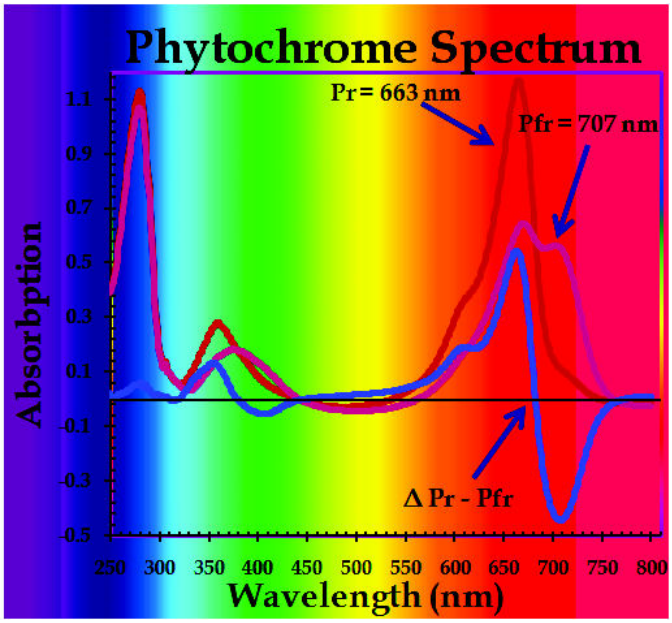

Figure 2.4 : Spectral properties of typical cyanobacterial phytochrome : Absorption spectra of purified phytochrome (88kDa) from *Calothrix PCC* 7601. The spectrum of Pr was measured after saturating irradiation with far-red light (λ_{irr} = 710 nm), while the Pfr spectrum corresponds to red light (λ_{irr} = 680 nm) adapted absorbance. The difference spectrum is between the corresponding spectra thus obtained after irradiation.

(i) Pr to Pfr The time resolved absorption and low-temperature trapping spectroscopic techniques applied to observe the inter-conversion between the two Phy isoforms have led to ascertaining the intermediates formed during this process (Remberg et al., 1997; Sineshchekov et al., 1998, 2002; Foerstendorf et al., 2000). The first stable photoproduct after irradiation of the Pr state form with red light yields 'Lumi-R' absorbing near 700 nm. This initial photoconversion accounts for the Z_{anti} (data shows that there is no single bond isomerisation) to E_{anti} isomerization of the C-15 double bond of the bilin, an interpretation based on resonance Raman analyses (Andel et al., 1996) and consistent with low temperature kinetic measurements. Lumi-R decay occurs in microseconds to Meta-Ra, followed by its conversion into Meta-Rc in milliseconds that ultimately yields Pfr. The chemical structure of these intermediates is subject of debate, with some investigators favoring a deprotonation-reprotonation mechanism while others assert that the

chromophore remains protonated throughout (Foerstendorf et al., 2001; Gärtner and Braslavsky, 2003). The recently available data of the crystal structure of phytochromes depicts the chromophore conformation in the Pr as well as the Pfr dark state (Yang et al., 2007, 2008) that opens up the arena to look into its conformational changes upon photoconversion (Karniol et al., 2005, 2007; Yang et al., 2007; Essen et al., 2008).

(ii) Pfr - Pr The reverse Pfr to Pr interconversion is less well characterized due to presence of multiple intermediates as a result of partial conversion or parallel interconversions of the two forms after irradiation. The Lumi-F intermediate formed after Pfr irradiation is assumed to include a concerted configurational and conformational isomerization about the C-15 double bond (Figure 2.5) with spectroscopic evidence indicating strong Pfr/Lumi-F coupling that favours the concerted C-15 E_{anti} to C-15 Z_{anti} isomerization mechanism (Andel et al., 2000). The low abundance of Pfr is suggestive of thermal reversion of Pfr to Pr intermediates back to Pfr-like Meta-Ra intermediates of the forward reaction or presence of second reversible photochemical reactions occurring in parallel with the photoisomerization that quenches the Pfr excited state.

The generally accepted theme in plant phytochromes indicates Pfr as its active form related to physiological responses such as in R-FR-reversible low-fluence responses (LFR) and for R-dependent very low fluence responses (VLFR) (Shinomura et al. 1996), however, exceptions have been outlined in FR high irradiance responses (HIR) that contradicts this simple view of phytochrome action (Casal et al. 1998; Shinomura et al. 2000). Studies indicate the collective role of Pr, Pfr, photocycled-Pr, as well as intermediates produced during Pfr to Pr photoconversion to transduce the light signal for different phytochromes.

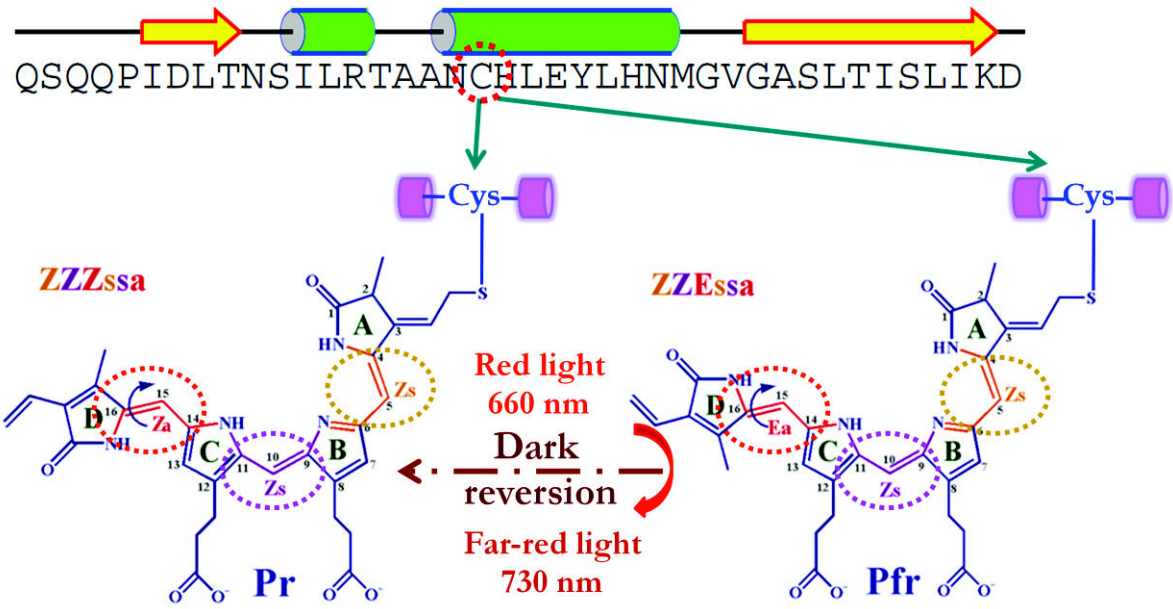

Structural changes of the PCB chromophore during the Pr-to-Pfr photocycle in CphA

Figure 2.5. Reversible photoreaction of chromophore upon light irradaiance : The chromophore phycocyanobilin appended to the cysteine in the protein undergoes structural modulation during the photoreversible Pr/Pfr transition. The ground state Pr chromophore assumes the ZZZ_{ssa} conformation at the AB, BC and CD rings as depicted. Red light (660 nm) absorbing Pr form isomerizes as a result of C-15/C-16 methine bridge between rings C and D generating the red-shifted ZZE_{ssa} spatial chemical module as Pfr photoproduct. The reversible isomerization, of the Pfr form absorbing far-red light (730 nm) or thermal dark reversion process regenerates the Pr state.

(iii) Dark Reversion In addition to photochemical interconversion processes, a non-photochemical Pfr-to-Pr dark reversion plays an important role to attenuate the signal output by altering the lifetime of the Pfr form. Atypical bacteriophyto-chromes, or BathyBphPs, described through various studies have the far-red absorbance maxima in the thermal ground state with photoconversion to Pr like species (Giraud et al., 2002; Karniol and Vierstra, 2003; Tasler et al., 2005). Whether this spectral inversion is either through the reversion mechanism of the normal dark reversion pathway or by some other mechanism is still under scrutiny. The Pr/Pfr ratio, holophytochrome synthesis, the two photochemical interconversion processes and the dark reversion are the processes that coordinate the biological

outputs from phytochromes inspite of the spectral variation amongst different types of these proteins.

The process of non-photochemical Pfr to Pr dark reversion process was manifested early in the phytochrome spectroscopic measurements (Fig. 2.5). The process has been of physiological significance as it has been evidently found both *in vitro* using Phy protein spectroscopy (Jorissen, 2002- doctoral thesis) as well as *in vivo* using dark adapted plant seedlings (Bulter et al., 1964). The development of methods to isolate and purify phytochromes has facilitated analysis of the molecular basis of dark reversion – a process that has been shown to be modulated by temperature, pH, various denaturants, proteases and reductants.

2.1.2.3 Phylogenetic Analysis - Phytochrome superfamily evolution and distribution

Recent advances in the genomic data analysis of phytochromes have provided a potential route for the evolution of the Phy superfamily. Their distribution amongst non-photosynthetic, photosynthetic eubacteria and cyanobacteria highlights the BphP family to be the progenitor for all the bilin binding photochromic proteins. The utilization of biliverdin (linear bilin synthesized by one enzymatic step from the cyclic heme precursor) as their preferred chromophore, and incorporation of the HKD for light directed signaling networks (Bhoo et al., 2001) strengthens this belief. Cyanobacterial and fungal phytochromes are also considered to have evolved from BphPs. While the fungal phytochromes (Fphs) use BV as their bilin as being unable to synthesize other chromophores, cyanobacterial phytochromes (Cphs) have advantageous acquisition of phycocyanobilin (PCB) as their tetrapyrrole ligand, which is an accessory pigment of photosynthetic machinery present in such bacteria. Adaptation for binding PCB might have resulted in the modification of the bilin linkage site, and various other modifications of Cphs are believed to be responsible

for evolution of Phy like family i.e. modified bilin binding pocket or replacement of HKD with other signaling motifs. Gene duplications and lateral gene transfers from the endosymbiont cyanobacteria is believed to be the evolutionary shift to the more complex plant phytochromes, that use phytochromobilin (PΦB) as their chromophore and the HKD domain being replaced with serine/threonine kinase. Atypical phytochromes, BathyBphps, exhibiting the thermally stable Pfr form are presumed to have evolved from BphPs as an adaptative trait to exploit FR as an environmental signal (Giraud et al., 2002; Karniol and Vierstra, 2003).

The true extent of the phytochrome family now apparent to have formed inroads from simple prokaryotic organisms to highly developed plants thus organize into the largest known population of photoreceptors across plant, microbial and fungal kingdom. The growing number of phytochrome sequences across organisms has led to their classification under representative sub-families (Montgomery, 2007; Karniol et al., 2005) described further ahead. The superfamily can be distinguished according to the generic presence as well as the chromophore assembled by these proteins. There has been extensive evolution of the phytochromes, albeit their similarity in biochemical and modular structure. This class of receptors is divided into majorly two types, eukaryotic and prokaryotic, based on the generic distribution and further sub-divided into representative forms in the microbial world.

The delineation of the prokaryotic phytochromes is based on their grouping as per specific differential utilization of phytobilins and their binding sites (Bhoo et al., 2001; Jorissen et al., 2002b; Lamparter et al., 2004). There are queer exceptions to the sub-division and grouping of phytochromes e.g. BathBphPs, an extraordinary subset of Phys using the Pfr and not Pr form as the ground state, indicative of backward functioning i.e. require FR and not R to photoconvert the photoreceptor following bilin assembly (Giraud et al., 2002; Karniol and Vierstra, 2003). Some cases might be mentioned where a variety of light signaling systems co-exist as in

Synechocystis (Cph1/Cph2 and Phy like sequences) and *Calothrix*, Cph/ BphP (CphA / CphB) type phytochromes (Wilde et al., 1997, 2002; Yeh et al., 1997; Park et al., 2000b; Jorissen et al., 2000b).

2.1.2.3(A) Phytochromes in Eukaryotes - Molecular properties, Spectra and Modular architecture

In early diverging flowering plants, episodes of periodic selection and gene duplication have led to the evolution of a family of phytochromes encoded by a small nuclear gene family under a eukaryote phytochrome progenitor (Mathews et al., 2003). The model plant *Arabidopsis thaliana*, is governed by a phytochrome family of five genes, denoted phyA–phyE based on differential sequence patterns (Clack et al., 1994), while monocot species (eg. rice or maize) appear to possess only representatives of the phyA–C families (Mathews, 2005, 2006). The non-photosynthetic plants possess the signature phytochromes and other photoreceptors though there are functional differences and downstream signaling mechanisms different than in the photosynthetic species. The overall modular structure of phytochromes is preserved throughout the eukaryotic photosynthetic organisms albeit the reports of atypical phytochromes in mosses and ferns (Thümmler et al. 1992).

Eukaryotic phytochromes are soluble homodimeric proteins consisting of two subunits of ca. 120 kDa. Each monomer is dissected into an N-terminal 'photosensory' core (60-70kDa) and a 55 kDa C-terminal 'regulatory' core joined by a protease-sensitive hinge region. The photoactive domain programmed to sense and respond to light is further composed of small sub-domains that is the serine rich N-terminal P1 domain, a PAS related P2 domain, the bilin binding P3 GAF domain and the P4 PHY domain (Fig. 2.6). Overall, the N-terminal photosensory module is combined with a C-terminal histidine kinase related domain (HKRD). The concatenation of PAS, GAF, and PHY domains attached to HKRD modules

typify all classes of phytochromes and phytochrome-related proteins. Plants have two additional regulatory PAS domains important for nuclear localization (Chen et al., 2005) and have sites of homodimerization (Edgerton and Jones, 1994).

The tetrapyrrole chromophore is covalently linked to a conserved cysteine residue found in the GAF domain, a fact proven by various mutational studies (Lagarias and Rapoport, 1980; Davis et al., 1999). The presence of this conserved cysteine residue is one of the key structural features that distinguishes the phytochrome photoreceptors from members of the phytochrome-related BphP family. The PAS and PHY domains though not directly binding the chromophore had been found to stabilize the three dimensional protein folding and are indispensable for the stability and photoreversibility of the phytochrome (Karniol et al., 2005; Sharda et al., 2007; Essen et al., 2008; Yoon et al., 2008).

The presence of transmitter kinase related 'output' domains at the C-terminus in all eukaryotic phytochromes implicates their role in ATP-dependent phosphorylation and downstream signaling. Thus, plant phytochromes are also labeled as serine-threonine kinases with an ATP dependent auto- and transphosphorylation mechanism of signal transduction pathway (Cashmore, 1998; Yeh and Lagarias, 1998). The mechanism of plant phytochrome signaling indulges light mediated nuclear translocation and regulation of transcription factors (Chen et al., 2004; Schäfer and Nagy, 2006). The C-terminal here is responsible for homodimerization and light activated nuclear targeting, both required for signal transmission (Matsushita et al., 2003; Chen et al., 2005). There have been reports stating the role of the protein-protein interactions in mediating the light modulated signaling (Ni et al., 1999) involving the N-terminal domain, though whether alone the Ser/Thr rich stretch is sufficient or the whole photosensory core (P2-P3-P4) takes part during signaling is still under question. In more primitive plants and algae, atypical phytochromes have been described in which the C-terminal region

has been replaced by fortuitous gene fusions with phototropins and other eukaryotic Ser/Thr kinases (Thümmler et al., 1992; Suetsugu et al., 2005).

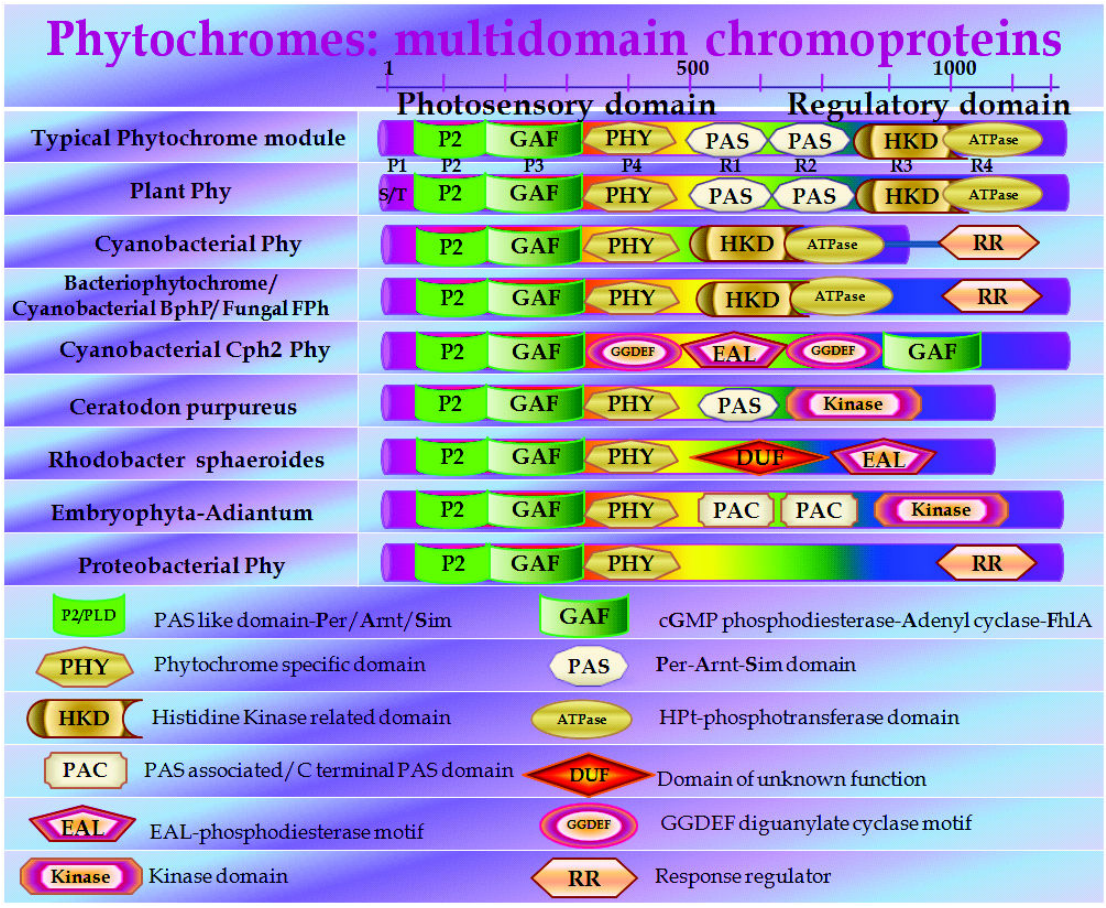

Figure 2.6. Schematic domain architecture of selected phytochromes and phytochrome like proteins : The figure enlists the sequential assortment of phytochromes and phy-related proteins based on the conserved motifs and sub-domains in the representative classes. Domain analysis was performed at the InterProScan system of the SMART service. Proportions are respected (for groups of proteins, the name and structure for the organism in bold is shown). The bottom half of the figure depicts individual details of the domains.

2.1.2.3(B) Phytochromes in Prokaryotes - Molecular properties, Spectra and Modular architecture

Bacteria, like the fellow living organisms are sensitized by environment and changes thereof. The most abundant world of microorganisms has evolved metabolic diversity to authorize maximum utilization of their available resources

for life processes. The extensively developed metabolic processes have sufficient flexibility as well as sophistication to regulate gene expression and physiological responses. Bacteria respond to the stimuli by adjusting to the environment by various processes that correspond to a cascade of reactions followed by the reception of stimulus, which has been termed as signal transduction. There are various players in this process that have been widely accepted through various activities they perform in the signaling. The very first being the receptors, then transducers and finally the regulators of such responses in the cell. Phytochromes here are epitomized as photosensitive receptors which employ classical two-component phosphotransfer relays, the signaling mechanism consisting of two proteins – sensor histidine kinase (HK) coupled with the response regulators (RR) to generate a very exquisite system to study the processing of receipted signals (Stock and West, 2003).

RcaE, essential for response to chromatic adaptation, was the very first phytochrome related protein isolated from the cyanobacterium *Fremyella diplosiphon* (Kehoe and Grossman, 1996). The protein was found to associate with the higher plant phys in terms of its modular structure, with the bilin binding photosensory core at its N-terminus followed by prototypical histidine kinase domain (HKD) found in two component systems (TC-HKs). The HKD consisted of all motifs and residues essential for phosphotransferase activity, including the H box that contains the histidine that becomes phosphorylated, and the N, F and G boxes that participate in ATP binding. This protein was hence put forth as the phytochrome that has the TC-HK phosphorelay pathway (Kehoe and Grossman, 1996). The completed genome of *Synechocystis* sp. PCC 6803 was eventually found to sustain the belief in bacterial phytochromes, as it contained atleast three proteins with varying degree of relatedness to RcaE and higher plant phys (Kehoe and Grossman, 1996; Hughes et al., 1997; Wilde et al., 1997; Yeh et al., 1997; Park et al., 2000b).

Phytochrome C-terminal domains mediate the transmission of photosensory signals perceived by the N-terminal region to signal transduction pathways within the cell. The C-terminal transmitting core is typically a histidine kinase related domain that catalyzes autophosphorylation and phosphotransferase activity, with ATP acting as the source of phosphoryl groups. Response regulators (RRs) here are phosphorylated by the phosphoryl group, under light activation, from the conserved histidine residue on HK to a conserved aspartate residue, with the degree of phosphorylation typically determining the extent to which the RR turns expression of appropriate genes on or off (Yeh et al., 1997; Yeh and Lagarias, 1998; Bhoo et al., 2001; Hübschmann et al., 2001; Lamparter et al., 2001; Karniol and Vierstra, 2003; Giraud et al., 2005; Tasler et al., 2005). Bacteriophytochromes that lack recognizable kinase output domains have also been reported (Giraud et al., 2002; Karniol et al., 2005). It thus appears that the primary mechanism of light perception, arguably shared by the conserved photosensory core of all phytochromes, has been evolutionarily co-opted to regulate output domains with different molecular architectures. The prokaryotic phytochromes are diversified under different sub-families as described below.

(i) Cyanobacterial Phytochromes – molecular properties

Synechosystis and Calothrix (Tolypothrix)

Cyanobacteria possess the most studied and highly developed system of photoreceptor phytochromes with the greatest similarity to their plant counterparts. Cph1 (cyanobacterial phytochrome 1) protein from *Synechocystis* sp. PCC 6803 was the pioneering protein in this family of photoreceptors that behaved as a true phytochrome. The recombinant apoprotein autocatalytically assembled with bilins like PΦB and 3-Z-phycocyanobilin (PCB) at the canonical cysteine to generate a dimeric R/FR photochromic chromoprotein *in vitro* (Hughes et al., 1997; Yeh et al., 1997; Park et al., 2000a, 2000b; Hübschmann et al., 2001a; Jorissen et al., 2002a). The slightly blue-shifted Pr and Pfr absorbption maxima for Cphs (654/660

nm – 707 nm) as compared to plant phys (666 nm – 730 nm) is consistent with the loss of a double bond in the π–electron system of PCB versus PΦB. The resulting holoprotein displayed HK activity with the Pfr form being more active than the Pr form. All the members of this family, including the bacteriophytochromes, possess the PAS, GAF, PHY domains (similar to P2-P3-P4 domains designated for plant phytochromes) as well as the two conserved sub-domains found in the transmitter modules of histidine kinases comprising two-component signaling (Stowe-Evans and Kehoe, 2004). A similar bilin attachment site and R/FR spectra were confirmed for two other members of the Cph family, *Synechocystis* Cph2 (Park et al., 2000b; Wu and Lagarias, 2000) and *Calothrix* CphA (Jorissen et al., 2002b), suggesting that the bilin-BBP (bilin binding pocket) interactions among this group have been conserved.

The discovery of the microbial phys led to investigations into related bacterial genomes to circumscribe the confines of the prokaryotic Phy kingdom. Of the numerous cyanobacterial species surveyed, including *Calothrix* PCC 7601, *Oscillatoria* PCC 7821, and several *Anabaena*, *Pseudoanabaena*, and *Nostoc* species, all were found to contain one or more Phy-like protein sequences, indicating that these photoreceptors may be common to this phylogenetic group (Lamparter et al., 1997; Lamparter et al., 2001; Herdman et al., 2000; Wu and Lagarias, 2000; Park et al., 2000b; Hübschmann et al., 2001a; Jorissen et al., 2002). These phytobilin-binding, R/FR photoreversible chromoproteins described have been implicated in cyanobacterial photobiology e.g. CikA, a Phy-like protein from *Synechococcus elongatus* PCC 7942 that was identified to reset the circadian clock (Schmitz et al., 2000).

The chromoproteins in cyanobacteria have the highly conserved histidine kinase domain at their C-terminus, where histidine autophosphorylation and aspartate phosphotransferase activities to downstream signaling partners are both light dependent (Yeh et al., 1997; Hübschmann et al., 2001b). These light activated

catalytic functions of the proteins require both HPT (histidine phosphotransferase) and H-ATPase domains forming the phosphohistidine donor/acceptor and ATP-binding sites respectively (Yeh et al., 1997; Jorissen et al., 2002b). Size–exclusion chromatographical experiments evidently show that light dependent binding of the apoproteins to the bilins promotes sub-domain association and a dynamic equilibrium of monomeric and dimeric forms of Cph1 as result of the kinase activity that promotes homodimerization and autophosphorylation (Park et al., 2000b; Lamparter et al., 2001).

The PAS (P1) and GAF (P2) domains in plants, cyanobacteria and bacteriophytochromes are required for the covalent attachment of the bilin chromophore whereas the PHY (P3) domain is dispensable (Vierstra, 1993; Wu and Lagarias, 2000; Oka et al., 2004; Karniol et al., 2005). The PHY domain is critical for the efficient photochemistry and for normal Pr spectrum, probably resulting from optimal bilin chromophore conformations in the protein folding. Thus, the PHY domain is essential for photoreversion, perhaps by conferring rigidity to bound bilins and minimizing deexcitation of chromophores (Wu and Lagarias, 2000; Fischer and Lagarias, 2004; Karniol et al., 2005; Sharda et al., 2007; Essen et al., 2008).

P2 domains of some phytochrome protein sequences have been identified by domain database searches to be PAS motifs (named for **P**eriod clock/ **A**RNT/ **S**ingle minded proteins), while P3 is identified as a GAF domain (named for vertebrate c**G**MP-phosphodiesterases, cyanobacterial **a**denyl cyclases, and the transcription activator **F**hlA) (Aravind and Ponting, 1997). The P4 domain of phytochromes, classified as a PHY domain by domain family database searches, also exhibits much weaker homology to GAF domains. This typical phytochrome sub-domain is proven to be indispensable for the spectral integrity and stability of the phytochrome protein. The tryptic digestion of proteins (Esteban et al., 2005; Yoon et al., 2008) or truncated engineered phytochrome proteins (Sharda et al.,

2007) has evidently shown that the phy sub-domain is essential for full phytochrome functionality although in its absence the chromophore is still adhered to the bilin binding pocket albeit weakly. The crystal structure of the PAS-GAF-PHY domain of the cyanobacterial phytochrome Cph1 has given support to the biochemical findings as the phy domain is required to provide strength to the bilin binding and photoreversibility (Essen et al., 2008). These studies prove that proper protein folding resulting from the presence of the essential sub-domains is vital for proper chromophore assembly and Pfr form stabilization, thus attaining spectral integrity of the holoprotein.

Many cyanobacterial species have two representatives of this family in their genome e.g. *Calothrix* sp. PCC 7601 has CphA resembling Cph1 and CphB, a bacteriophytochrome with the conserved cysteine residue missing from the GAF domain (Herdman et al. 2000). The second type of prokaryotic phytochromes, that is the Cph2s / CphBs, have also been found exclusively in cyanobacteria (Montgomery, 2007). *Synechocystis* Cph2 is unusual because it contains three predicted GAF domains, though the phytobilin binding activity and R/FR photoreversible signature spectroscopic properties of the full length recombinant Cph2 protein were retained within the two N-terminus GAF domains in spite of all three GAF domains binding the chromophore *in vitro* (Fig. 2.6)(Park et al., 2000a, 2000b; Wu and Lagarias, 2000). The N-terminal GAF domains of Cph2s are most similar to the P3 GAF domains of plant and Cph1 phytochromes in which the conserved cysteine residue is located (Montgomery, 2007). The experimental results prove the evident role of the P3 GAF and P4 PHY subdomains in the chromophore binding, with phytobilin lyase activity limited to the P3 GAF subdomain. Cph2 is also exceptional in terms of the C-terminal HKD domain being replaced by a pair of domain of unknown function (DUF-1 and DUF-2 motifs). Although missing the N-terminal P2/PAS domain it still retains normal R/FR photochromic absorption indicating that here PLD is not essential photochemically.

The CphB subset of the cyano-bacteriophytochromes are more related to the bacteriophytochromes (Bphps) representative in the non-photosynthetic eubacteria, with the chromophore binding activity imminent in the N-terminal PAS fold at a non-canonical cysteine residue (Lamparter et al., 2001; 2002, 2003). The GAF domain is quintessential in forming the bilin binding pocket for such phytochromes as also the indispensable PHY domain for maintaining the spectral intergrity of such proteins (Karniol et al., 2005; Sharda et al., 2007). Thus, the Cph2 / CphB type phytochromes preserve the GAF-PHY molecular architecture for its members pointing at the similarity of the molecular changes associated with light activation of the phytobilin prosthetic group albeit differing in the site for attachment of the bilins.

(ii) Bacteriophytochromes

The second most abundant class of phytochromes is that of bacteriophytochromes (BphPs) that distinguishes itself from Cphs by the utilization of BV as chromophore as also by the differential binding assessed by the bilin (Bhoo et al., 2001; Lamparter et al., 2002; Karniol and Vierstra, 2003). The bacteriophytochromes are spread widely through the bacterial kingdom, with most known members from non-photosynthetic eubacteria and photosynthetic purple bacteria (Davis et al., 1999b; Bhoo et al., 2001; Giraud et al., 2002). There are other potential BphP candidates evidently in some cyanobacteria e.g. *Calothrix*, *Nostoc* and *Oscilatoria* (Herdman et al., 2000; Bhoo et al., 2001) which are reported to contain both Cph anf BphP type phytochromes (Jorissen et al., 2002b). The expanding distribution of BphPs through the microbial genera is indicative of their important role in the evolution of phytochromes. BphPs bind the PΦB/PCB precursor BV as the chromophore, while Cphs and plant phys bind BV poorly or not at all. The absorption maxima of the Pr and Pfr froms of the chromoproteins is slightly red-shifted (λ_{max} 700 nm and 750 nm, respectively) compared to plant phys,

consistent with the addition of one double bond in the π- electron system of BV versus PΦB.

The BV binding is genetically well supported by the presence of a Heme oxygenase (HO) gene physically linked to the phytochrome genes in the same operon (e.g. in Bph operons of *Deinococcus radiodurans, Pseudomonas aeruginosa, Pseudomonas syringae,* and *Rhizobium leguminosarium* as *BphO*) or included within the operon (*Bradyrhizobium* and *Rhodopseudomonas palustris* genomes as *HmuO*) that convert heme to BV, though no further reduction of BV to PCB or PΦB is possible due to absence of reductase activity of HO (Bhoo et al., 2001; Giraud et al., 2002; Frankenberg-Dinkel et al., 2004). These bacteria are believed to coordinate synthesis of the chromophore with the apoprotein via such genetic linkages. The crystal structure available from *Deinococcus radiodurans*, *Rhodopseudomonas palustris* and *Pseudomonas aeruginosa* (Wagner et al., 2005, 2007; Yang et al., 2007, 2008) clarifies the binding accounted by these phytochromes to the bilin ligand. The preferred binding of BV to either PCB or PΦB as chromophore distinguishes it from Cphs and plant phytochromes.

Another marked characteristic of bacteriophytochromes is the presence of an N-terminal PAS like domain (PLD) that houses the invariant cysteine residue for bilin linkage instead of the GAF domain canonical cysteine found in plant phys and Cphs to attach bilins that is suggestive of different binding mechanism of the bilin (Lamparter et al., 2002, 2004; Karniol et al., 2005, 2007; Vuillet et al., 2007).

The alternative binding site was first suggested for *Agrobacterium tumefaciens* BphP1 (or Agp1) by using cysteine modification reagents to block BV binding to the apoprotein (Lamparter et al., 2002). Assembly reactions with site-directed mutants, various BV derivatives and peptide mapping corroborated the conserved cysteine (Cys 20) in the PLD as binding partner for the bilin (Lamparter et al., 2003, 2004). Spectroscopic studies were indicative that most BphPs function as typical Phys, with the Pr form generated first following autocatalytic attachment of the

bilin. Pfr is created only upon light absorption; Pfr can either photoconvert back to Pr by FR or revert nonphotochemically from Pfr back to Pr. Pfr conformation is reported to be less stable for some of these prokaryotic phytochromes as the dark reversion process is quite fast compared to plant phys (Lamparter et al., 2002; Karniol and Vierstra, 2003).

Bacteriophytochromes are organized to function as TC-HKs as often a canonical HKD is found C-terminal to the photosensory core. Some species also have a response regulator (RR) domain appended to the HKD (Fig. 2.6) or in some cases have a new type of HKD designated as HWE-HKD (conserved histidine, tryptophan and glutamic acid residues in HKD) (Dutta et al., 1999; West and Stock, 2001; Inouye and Dutta, 2003; Karniol and Vierstra, 2003, 2004). This new type of domain also having TC-HK relay differs from HKD by substantial sequence alterations within the H, N and G boxes and the absence of an obvious F box. There are some exceptions to this arrangement of domains, as the C-terminus of some phytochromes in this family bear other prolific domains that are implicated in light regulated protein – protein interactions and downstream signaling (e.g. PAC domain in *Bradyrhizobium* or PYP in *Rhodospirillum centenum* Ppr) (Giraud et al., 2002; Jiang et al., 1999). Bacteriophytochromes with some unusual behavior are called atypical bacteriophytochromes described as follows.

(iii) Bathybacteriophytochromes– atypical photoreceptors

The analysis of several BphPs distributed across prokaryotes using the advancements in sequencing and gene mapping has revealed a novel subfamily of BphPs that works in reverse (Giraud et al., 2002; Karniol and Vierstra, 2003). These backwards or bathy BphPs assemble BV to generate a Pr-like transient intermediate that rapidly converts non-photochemically to a stable Pfr ground state. The photoreceptors behaving in contrast to the BphPs and other Phys have absorption spectra after assembly that resembles the envisaged Pfr spectrum without Pr

contamination while Pr, generated after photoconversion with FR is unstable and dark reverts to Pfr. To date, members of the bathyBphP subfamily have been discovered in three species, *Agrobacterium tumefaciens*, *Bradyrhizobium*, and *Rhodopseudomonas palustris*, with more likely to be found (Giraud et al., 2002; Karniol and Vierstra, 2003).

(iv) Fungal Phytochromes

Identification of the bilin binding sequences in various filamentous fungi is suggestive of the incursion of light receptive phytochromes in fungal kingdom, thereby broadening the precincts of phytochrome distribution outside bacterial and plant kingdoms (Bhoo et al., 2001). This family of phytochromes is apparently closely related to bacteriophytochromes. The fungal phytochromes (Fphs) contain a GAF domain with the conserved histidine preceded by hydrophobic residue and an N-terminal PLD with the symbolic cysteine similar to that in BphPs (Fig. 2.6). The Fphs can covalently assemble with BV *in vitro* and yield photochromic proteins after irradiation with R/FR light wavelengths (Blumenstein et al., 2005; Tasler et al., 2005). The fungal Fphs have distinct N-terminal extensions in the photosensory core linked to typical HKD followed by response regulator domains (RR/REC), hence likely to function in TC-HK cascades (Catlett et al., 2003).

(v) Phy-like Sequences

Extensive phylogenetic and biochemical investigations have revealed an assortment of Phy-like sequences alienated from the main Phy families by one or more criteria. Homology alignments of these sequences reveal major differences in terms of GAF or PLD domains, the two domains that unify the collection of phytochromes under a family. These unorthodox polypeptides either do not bind bilins, ligate them in unconventional ways but are still photochromic, or bind bilins but are peculiar in being not photochromic. The GAF domains in such sequences have a small deletion upstream of the putative chromophore-binding residue that

maybe photochemically significant (Wu and Lagarias, 2000). Some examples of the Phy-like group are *Fremyella diplosiphon* RcaE, *Synechocystis* TaxD1 and *Synechococcus elongatus* CikA. Biochemical investigations designate their dilienation from other main phytochrome clades. *Fremyella* RcaE for example, has a recognizable GAF domain with cysteine near the expected site that is not essential for bilin attachment (*in vitro*) but still can bind bilins both *in vivo* and *in vitro* (Terauchi et al., 2004). The resulting holoprotein though non-photochromic is implicated in photoreception during complementary chromatic adaptation but still debatable as a true phytochrome. *Synechococcus elongatus* CikA, missing the positionally conserved cysteine and histidine residues in the GAF domain as also missing PLD, can still bind PCB and PΦB *in vitro*, resulting in a non-photochromic protein though seemingly participate in photoreception (Schmitz et al., 2000; Mutsuda et al., 2003).

Multiple Phy like sequences were also delineated from the genomes of several purple bacteria like *Bradyrhizobium*, *Rhodospirillum centenum*, *Rhodobacter sphaeroides*, and *Rhodopseudomonas palustris*, henceforth channeling the prokaryotic Phy subfamily to include these unorthodox proteins (Jiang et al., 1999; Wu and Lagarias, 2000; Bhoo et al., 2001; Giraud et al., 2002). The proteins contained canonical HKD appended to bilin binding core, strengthening the view of evolution of plant phys from a prokaryotic TC-HK progenitor.

2.1.2.4 Phytochrome chromophore structure

The phytochromes with their characteristic absorbance spectra and photoconversion reflect the association with a linear tetrapyrrole bilin chromophore. Photoconversion involves a *Z*– *E* isomerization about the C15–C16 double bond of the bilin for generating the signature absorption spectra (Gärtner and Braslavsky, 2003). The distinct bilin chromophores of the various phytochrome classes are all derived from the oxidative metabolism of heme. Heme oxygenases

are reported to convert heme to biliverdin IXa (BV), the precursor of the chromophores of bacteriophytochromes and also of fungal phytochromes (Bhoo et al., 2001; Giraud et al., 2002, 2005; Lamparter et al., 2003, 2004; Tasler et al., 2005; Blumenstein et al., 2005; Froehlich et al., 2005). Biliverdin is reported to be used as the tetrapyrrole ligand in phytochromes from non-photosynthetic bacteria, as well as in the CphB type phytochromes (Giraud et al., 2002; Lamparter et al., 2003, 2004; Quest and Gärtner, 2004; Karniol et al., 2005; Tasler et al., 2005). In cyanobacteria and algae, BV is converted to phycocyanobilin (PCB) via a four electron reduction mediated by ferrodoxin dependent bilin reductases of the PcyA subfamily (Frankenberg et al., 2001). In higher plants, BV is converted to phytochromobilin (PΦB) through the action of the homologous two–electron bilin reductase phytochromobilin synthase (HY2) (Kohchi et al., 2001). The bilin chromophore is covalently linked to the protein via a thioether bond between a Cys residue and the bilin A-ring (Fig. 2.3 -2.5). Plants and cyanobacterial (Cph1s/Cph2s) phytochromes utilize a conserved cysteine residue in the GAF (P3) domain (Lagarias and Rapoport, 1980; Park et al., 2000; Wu and Lagarias, 2000; Hübschmann et al., 2001; Lamparter et al., 2001), whereas bacteriophytochromes (CphB) and fungal phytochromes instead utilize Cys in the PAS (P2) region at the N-terminal of the protein (Lamparter et al., 2004; Wagner et al., 2005; Tasler et al., 2005) (Fig. 2.3 – 2.6). The report suggesting the weaker binding of the BV to the P2 domain as an outcome of intra-reversibility of binding either BV or PCB (Quest and Gärtner, 2004) is supported by the observation of a mutant BphP that lacks the nucleophilic Cys residue being a functional enzyme for producing C15–C16 *E* bilins (Lamparter et al., 2005). *Calothrix* CphB phytochrome protein mutated at the N-terminally located Cys (Cys-24-Ser) could ligate BV and showed photoreversibility (Quest et al., 2007), though covalent attachment likely provides a more stable holoprotein that is better suited to reversible photoswitching. The P2 domain is attributed the accessory role in maintaining the holophytochrome assembly in cyanobacteria supposedly by stabilizing the bilin binding pocket in the P3 domain (Zhao et al.,

2004), though the Cph2 subfamily lacking this domain altogether still supports bilin attachment (Wu and Lagarias, 2000). Introduction of Cys residue in bacteriophytochromes at the canonical position at P3 restores PCB attachment thus resulting in the structural conservation of the chromophore binding pocket (Davis et al., 1999; Lamparter et al., 2004; Quest and Gärtner, 2004).

The chromophores for phytochromes are open chain tetrapyrroles with spectroscopic properties under strong influence of their conformation, protonation state and chemical environment (Falk, 1989). The phytochrome crystal structure has given some evidence for the configuration adopted by the chromophore in the Pr state. The chemical structure of the phytochrome chromophore involves a covalent carbon-thioether linkage between chromophore ring A and the sulfur of Cys residue on the phytochrome proteins (Cys-259 in Cph1, and the N terminal Cys in bacteriophytochromes). The chromophore is evidently seen as ZZZ_{ssa} conformer linked to the protein (Essen et al., 2008), rather than a linear ZZZ_{asa} conformation as predicted by vibrational spectroscopy (Mgorinski et al., 2006). This assignment was due to an incomplete theoretical calculation (ab initio calculation for solely the chromophore in vacuo; including the protein environment via QMMM calculations reassigned the Raman bands, now in agreement with the crystal structure prediction; Mroginsky et al., 2009).

2.1.2.5 Physiological attributes of phytochromes

The varied structural and spectral properties of the phytochrome proteins accredit them to be involved in a diverse array of photosensory processes. The phy systems scrutinized at the physiological level are at very elementary stages in case of microbial phytochromes. The higher plant phytochromes have been screened for a number of functions they perform either singly or in conjunction with other photoreceptors. Some of the potential functions of these proteins include both

photosensory roles (i.e. phototaxis, light-intensity sensing, chromatic adaptation) as well as non-photosensory roles (i.e. regulators of tetrapyrrole and/or iron metabolism or oxygen sensors).

In most cases, the transcriptional control of gene expression is the ultimate output, thus implicating the associated TC-HK cascades in the regulation of DNA-binding proteins. Predictably, many of these same responses are also regulated by phys in higher plants (Smith, 2000; Quail, 2002).

Although microbial phytochromes have proven amenable systems for biochemical and spectroscopic analyses, much remains to be determined about the function of many of these molecules *in vivo*. The physiological functions of phytochromes in microbes are conceptually analogous to functions of plant Phys i.e. phytochromes regulate the metabolic response of the organism to its light environment. To date, one or more microbial Phys have been connected to the roles explained further here.

Phytochromes are used for physiological functions in various organisms in conditions where light is attenuated. Cyanobacterial phytochrome-like proteins embracing weak GAF domain homology have been assigned a number of light effects such as phototaxis (Yoshihara and Ikeuchi, 2004), control of circadian clock (Schmitz et al., 2000), chromatic adaptation (Kehoe and Grossman, 1996) and adaptation to blue light conditions (Wilde et al., 1997, 2002), while the biological function of prototypical phytochrome is known for only a few bacteria. Cph1 from *Synechocystis* sp. PCC 6803 is known for its role in adaptation to strong light conditions (Fiedler et al., 2004) and regulation of several genes, e.g. *gif*A, that encodes glutamine synthase regulator (Hübschmann et al., 2005), though having obscure links to the signal transduction mechanism due to the observed light effects.

The most obvious effects controlled by bacterial phytochromes have been found for *Bradyrhizobium* spp., a photosynthetic plant symbiont, and the purple bacterium *Rhodopseudomonas palustris*. The BphPs from these two species are involved in alleviation effects from high light fluencies as well as damaging UV irradiation by regulating the biosynthesis of the photoprotective pigments such as the photosynthetic apparatus, bacteriochlorophylls and carotenoid pigments (Giraud et al., 2002, 2005). It is not known why phytochrome proteins are retained in non-photosynthetic bacteria, as also intriguing is the fact that many observable light dependent processes in cyanobacteria are rather controlled by Phy-like proteins RcaE, PlpA, CikA or PixJ (Kehoe and Grossman, 1996; Wilde et al., 1997; Schmitz et al., 2000; Yoshihara et al., 2000) that have no direct plant homologs. The non-photosynthetic bacteria, *Deinococcus radiodurans* BphP control the regulation of carotenoid biosynthesis (Davis et al., 1999). The phytochrome from the filamentous fungus *Aspergillus nidulans* was recently implicated in sexual development (Blumenstein et al., 2005).

2.1.2.5(A) Phytochromes as kinases – Downstream signalling cascades

Histidine Kinases in Signal Transduction

Phytochromes as receptors involved in signal transduction is an area where enough recognition of functionality is still amiss. These proteins constitute the resplendent field of one of the most important receptor types, the histidine kinase. Histidine kinases (HKs) are the first component of the widely studied 'two-component' signal transduction systems used extensively by bacteria to modify their cellular behaviour in response to their environment. The second component of this systematic information flow pattern, the response regulator (RR), has been implicated in various downstream signal processing. Progressive approaches

during recent years have led to elucidate the molecular structures of these enzymes, thus taking our understanding of these signaling proteins into a new era.

The signaling systems about which we know most, those involving the HK enzymes are EnvZ and CheA, where partial structural details have been solved by NMR and X-ray crystallography. The HK core structure has been shown to belong to the GHL - ATPase superfamily, which informs us of the possible HK catalytic mechanism. Structure based sequence analysis leads to the speculation that HKs arose from an ancestral ATPase fold and coevolved with their signaling partners, the RRs. The RRs reportedly have interactions with HKs and with effector domains, and also with respect to structural changes induced by RR phosphorylation. The dual functionality of HK proteins is assessed as per their kinase as well as phosphatase activity. There is evidence of the kinase versus phosphatase activity, and contrasts a switch-type mechanism (i.e. kinase on – phosphatase off and vice versa) with a rheostat model encompassing many different intermediate states (Inouye and Dutta, 2003).

A much deeper understanding of the molecular operation of HKs and two-component systems is essentially one of the fundamental questions addressed through vigorous research so as to reach details about signaling specificity achieved in these pathways. Signal transduction pathways can be dissected in the prokaryotes and eukaryotes as His/Asp phosphorylation and Ser/Thr/Tyr phosphorylation regulatory systems, respectively. These biological signaling mechanisms though seemingly divergent have more fundamental similarities than differences across phylogenetic domains. The fundamental attributes of such systems are reception/detection of stimulus, internal processing of signal amplification and adaptation that leads to appropriate responses. Phytochromes accomplish as photoreceptor proteins in the biological signal transduction system, modular in their architecture and employing different permutations of similar elements to create unique circuits in different organisms.

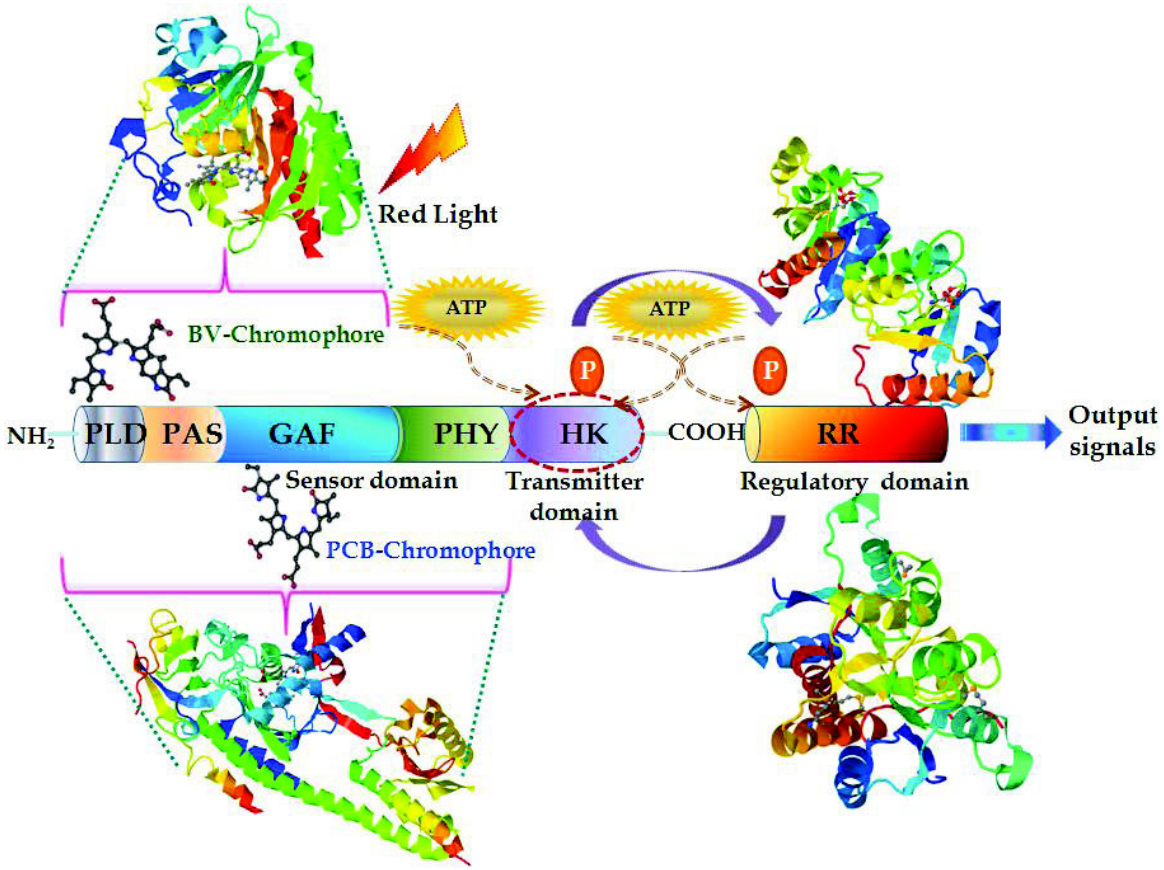

Figure 2.7 : Schematic organization of the phytochrome structural domains : Generalized function of the photoreceptor as bacterial light driven kinases described by conformational changes of bilin/protein that induces interaction/activation with intracellular signal transduction proteins. The figure credits a diagrammatic view of *Calothrix* phytochromes CphA / CphB structural domains interacting with response regulator protein constituting the two component signaling system. The specific region crystal structures of the related proteins are shown. The ATPase domain of the histidine kinase is depicted with the circled P : phosphate group, with the auto- / trans- phosphorylation capacity.

Two-component regulatory systems dominate bacterial signaling and have been under pervasive investigations in the recent assessment (Galperin et al., 2001). The structural organization of microbial Phys indicates that many, if not all, function either directly or indirectly in TC-HK phosphorelays. This connection is ancillary supported by the presence of a RR domain, either translationally coupled to the HKD thus creating a hybrid HK, or expressed as a separate polypeptide within the operon that encodes the Phy apoprotein (refer Figs. 2.6 – 2.7). The

phytochrome bili- proteins are therefore light regulated histidine kinases, which form the vastly famous two component signal transduction cascade with second protein known as response regulator (RR). The HK phosphorylated after irradiation with appropriate light then transphosphorylate the RR at a conserved aspartate residue, a phenomenon biochemically shown in various Cphs and BphPs (Yeh et al., 1997; Bhoo et al., 2001; Hübschmann et al., 2001b; Karniol and Vierstra, 2003). A recent study has formulated different classes of these phytochromes, putting them together according to their distribution among various genera, as also differentiating them according to chromophores they ligate (Lagarias et al. review 2006). There has been evidence of presence of the phytochrome proteins amongst the microbial world living under extreme conditions thus suggesting the evolutionary importance of these bili-proteins.

The downstream signaling links after RR phosphorylation by phy HK are still incomprehensible making the understanding of this protein interaction network quite alluring. In lieu of the available structural details of both the partners of the phytochrome system from microbes, much can be deduced to decipher the signaling of modular phys. The absence of appended output module on RR is suggestive of microbial phys participating in a four step his-asp-his-asp phosphorelay before signal output as depicted in Figure 2.7, similar to the model TC-HKs (West and Stock, 2001; Inouye and Dutta, 2003).

2.1.2.5(B) Biochemical mechanism of signal transmission

The underlying biochemical mechanism behind the signal transfer from photoactivated phys to their immediate signaling partners is still a challenging question. The homology of phytochromes to histidine kinases (Schneider-Pötsch et al., 1991; Schneider-Pötsch, 1992; Quail, 1997a,b; Hughes et al., 1997) had given a direction for phytochrome functional research. The cyanobacterial phy has light regulated histidine kinase activity (Yeh et al., 1997) while plants have been shown to contain Ser/Thr protein kinase activity (McMichael and Lagarias, 1990). The

autophosphorylation of oat phyA and resultant transphosphorylation of phy-interacting factor, PKS1, has been proven with valid experiments (Yeh and Lagarias, 1998). Studies have shown that the protein kinase activities of both Cph1 and eukaryotic phytochromes are bilin and light-regulated (Yeh et al., 1997; Yeh and Lagarias, 1998). The holoprotein dimeric formation is stimulated by phytobilin binding as a result of activation of the histidine kinase dimerization domain (Park et al., 2000b; Lamparter et al., 2001). However, the precise biologically significant activities related to this phosphorelay mechanism of signaling are still under lens, as some reports suggest that the C-terminal domain responsible for kinase activity is apparently completely dispensable for phy activity in vivo (Matsushita et al., 2003).

2.1.2.5(C) Phy Signaling components

(i) Second Messenger hypothesis

The phytochrome function linked to their widespread distribution across genera is related to the protein stretches with homology to known photosensitive domains as well as kinase output domains. The obvious approach of biochemical delineation of phy function included identifying second messengers that are hypothesized to function in transducing phy signals e.g. in plants the signaling from cytosol to the nucleus where gene expression is altered. Pharmacological and microinjection techniques implicated the involvement of G-protein, cGMP, and Ca^{2+}/ Calmodulin in phy signaling (Neuhaus et al., 1993; Bowler et al., 1994; Okamota et al., 2001). There have been reports of mutational analysis and genetically engineered co-ordinated studies which suggest different pathways for the biological functions of the phytochromes (Jones et al., 2003; Huq et al., 2003).

(ii) Phy interacting partners

Another approach related to physiological phy function involved yeast two hybrid assays that identified factors binding to phytochromes that have also been

proved by subsequent reverse genetic analyses (Quail, 2000; 2002a,b). The basic helix-loop-helix (bHLH) family of transcription factors e.g. PKS1, NDPK2, ARR4, PIF1-4, are studied to be meshed with phytochrome function as also their interaction also with other photoreceptor proteins like cryptochromes or hormones (Quail, 2002; 2002ab; Huq and Quail, 2002; Kim et al., 2002; Al-Sady et al., 2006).

2.1.2.6 Crystal Structure of phytochromes – structure and assembly of photosensory core

The quest for the mechanism of light reception by the biliproteins assembling various linear or tetrapyrrole chromophores has been nostalgic, though various biochemical, spectroscopic and biophysical techniques have been deployed for the elucidation of the same. The modular domains credited with specific roles in the phytochrome photoreaction have been put to test through a number of approaches where the inter-domain interactions have been given thorough study. The results have designated inimitable functional coherence between the domains though still highlighting substantial variability among the PAS, GAF and PHY domain interactions as per published protein structures resembling the said motifs in phytochromes (Ho et al., 2000; Martinez et al., 2002, 2005; Kurokawa et al., 2004). Thus, it has been elusive to predict how the domains in phytochrome might assemble after light absorption or how the signals are transmitted across from C-terminal portion of the protein to the downstream receptors. Similarly the mechanistics behind the chromophore assembly and its structure in the two forms of phytochromes have been deduced by various bio-physical and biochemical analysis. The chromophore structure itself has generated heightened interest as per the sundry chemical conformations adopted during various studies that has put forth Pr chromophore to adopt C5-Z,anti/C10-Z,syn/C15-Z,syn, C5-Z,anti/C10-Z,syn/C15-Z,anti, C5-Z,anti/C10-E,anti/C15-Z,syn, or C5-Z,syn/C10-Z,syn/C15-Z,anti conformations on the basis of vibrational spectroscopy and theoretical approaches (Fig. 2.5) (Andel et al., 1996, 2000; Kneip et al., 1999; Mroginski et al., 2004; Fischer et al., 2005; Mroginski et al., 2009).

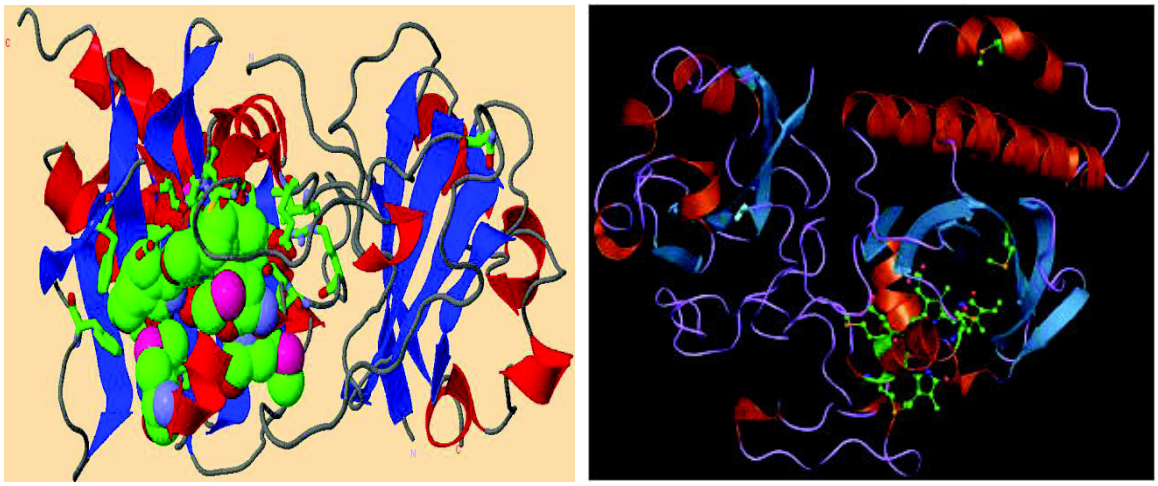

Figure 2.8 Ribbon and ball represented crystal structure of the PAS-GAF domain : Three dimensional phytochrome bi-domain structure of the N-terminus PAS-GAF of *Deinococcus radiodurans* – the BV chromophore bound to the Cys 20 residue in PLD is tethered tightly by the GAF domain trefoil knot. PDB accession number for the structure is 1Ztu.

The much awaited phytochrome structure delivered by the truncated PAS-GAF stretch of BphP from Deinococcus radiodurans (Wagner et al., 2005), with attached chromophore at the N-terminal PLD cysteine alleviated the basic obscurity about domain folds and chromophore linkage. The three dimensional crystal structure (Fig. 2.8), thus provided conformational evidence to the many suppositions, albeit being hampered by the fact that this stretch of phytochrome is not photochemically active as it assembled to generate only the Pr ground state while the Pfr state does not result due to the absence of the PHY domain from the holoprotein. This limitation has now been partially permeated by the abysmal efforts from the groups of Jon Hughes and Lars-Oliver Essen (Essen et al., 2008), who has now provided the structure of Cph1 phytochrome from *Synechocystis* PCC 6803 in the Pr form, and the continued exploration would generate the photoactive protein structure as the PAS-GAF-PHY module of the phytochrome crystal here resembles the full protein in terms of its photoreactivity (Fig. 2.9) (Sineshchekov et al., 2002).

Unearthing the three dimensional folds appropriated by the truncated domains of the phytochrome yielded important insights into their chromophore binding and photoconversion. The BV chromophore of Deinococcus radiodurans bacteriophytochrome (DrBphP) holoprotein is deeply buried within the GAF domain fold with the covalent linkage evidently at the cysteine in the PLD motif utilizing the A-ring vinyl side chain. The noticeable difference for the chromophore linkage was that the C-3^2 carbon of the A-ring vinyl group was used as opposed to the thioether linkage between the GAF cysteine and C-3^1 carbon of PΦB or PCB in plant and cyanobacterial phytochromes (Lagarias and Rapoport, 1980; Hübschmann et al., 2001).

The initial 2.5 Å crystal structure thus confirmed the P2/P3 domains as adopting the PAS and GAF folds respectively, with highly conserved cores throughout the phytochrome family as per the secondary structure folds (Figure 2.8). The BV chromophore covalently bound to cysteine 24 in the PLD motif via C-3^2 linkage is buried deeply within the GAF bilin pocket (Figure 2.8) as proven by biochemical illustrations (Lamparter et al., 2004). The PAS and GAF folds are interlinked through a stretch of amino acids lying between cysteine 24 and the start of the PAS fold that turn to form a deep trefoil knot. The trefoil knot passes through a 'lasso' formed by the GAF motif sequence between the fourth and fifth strands of the central GAF β-sheet. The knot centering on conserved isoleucine 35 (Zhao et al., 2004; Wagner et al., 2005) within the N-terminal sequence also contains the omnipresent phytochrome arginine 254 residue that interacts with the carboxyl group of the biliverdin chromophore, thus registering the knot that has been proposed as more or less preserved architecture in the phytochrome family. Phytochrome biosynthesis thus holds the promise of providing new insight into knot formation. The site mutations that have been previously studied quite vigorously in the phytochromes can be correlated now to the structural folds held by the P2/P3 domains that result in altered biochemical functions. This opens up a new arena to investigate in phytochrome signal transduction via direct or indirect

modulation of intra and inter- molecular interaction among the known domains of the full length phytochrome and other downstream signaling molecules. The crystal structure was further refined to have 1.45 Å data (Wagner et al., 2007) that proved the hazy assumptions with more certainity regarding the chromophore binding interactions. Thus, BV is unequivocally bound in the C5-Z,syn C10-Z,syn C15-Z,anti configuration in the Pr form (Figure 2.8, 2.5) deeply buried in the GAF domain with side chains excluded from the bulk solvent. The BV ring system is predicted to be protonated due to the residues surrounding the bilin in the BBP (bilin binding pocket).

The chromophore structured inside the binding pocket gave valuable insights into the similar patterns that would be evident in the cyanobacterial and higher plant phytochromes as the substitution of the hydrophobic residue present at the canonical cysteine position in the GAF domain assesses the vinyl group interaction at the A-ring of the tetrapyrrole utilizing either PCB or PΦB as chromophore. Wagner et al. (2005) put forth the inference of plant and cyanobacterial phytochromes originating from a bacteriophytochrome progenitor as per the structural details via the gain of the GAF cysteine instead of PLD cysteine along with the appearance of bilin reductases capable of the conversion of BV to the more reduced bilins, PCB and PΦB. Thus, the photosensory core of the extended family of phytochromes assumes similar three dimensional folds to that of DrBphP. The three lobed knot, covalent binding and close proximity of certain residues to the chromophore as seen in the crystal structure are indicative of a more rigid structural entity than have been assumed from other biophysical analysis of inter-domain interactions. This extra rigidity however gives support to the assumption that photoconversion process is facilitated as such due to reduction in the de-exciatation potential associated with protein domain vibrations (Wagner et al., 2005).

The breakthrough crystal structure of the chromophore binding domain (CBD) of the Bph from *Deinococcus radiodurans*, DrBphP, though providing for definitive structural insights into the photosensory crux of phytochromes lacked in giving the molecular and mechanistic details of Pr/Pfr photoconversion. Crystal structure from *Rhodopseudomonas palustris* (RhBphP3) and *Pseudomonas aeruginosa* (PA-PCD, photosensory core domain) followed suite after DrBphP structure rendering most of the three dimensional facts true for bacteriophytochromes (Yang et al., 2007, 2008). The RpBphP3 - CBD crystal structure determined in the Pr state enhanced the appreciation of the structural basis of reversible Pnr/Pr/Pfr photoconversion and the factors bestowing unusual photoconversion behavior of RpBphP3. The vital residues directly moderating the photoconversion were realized by integrating structural and site-directed mutagenesis data carried out on longer constructs of RpBphP3 and RpBphP2 comprising the PAS, GAF, and PHY domains, which display photoconversion efficiency comparable to that of their full-length proteins. The PHY and HK domain was modelled to give insights into the full phytochrome three- dimensional structure and functioning. This crystal structure yielding several amino acid residues involved in the chromophore protein interaction using mutational analysis of crystals, also discussed the scenario common for bacteriophytochromes.

An unrivaled embodiment of phytochrome structure came soon after these reported crystal structures and biophysical characterizations of the chromophore in the binding pocket (Wagner et al., 2005; Yang et al., 2007, 2008; Strauss et al., 2005; Rohmer et al., 2006; Hahn et al., 2007) as the crystal structure of the PAS-GAF-PHY module of Cph1 phytochrome of cyanobacteria *Synechocystis* sp. PCC 6803 (Essen et al., 2008). This protein although truncated to exclude the HK domain, behaves similar to the full length protein in biochemical measurements (Esteban et al., 2005). Thus, it would give the complete picture of photochemically active phytochrome and the protein – chromophore modifications during photoconversion between the two types, Pr and Pfr.

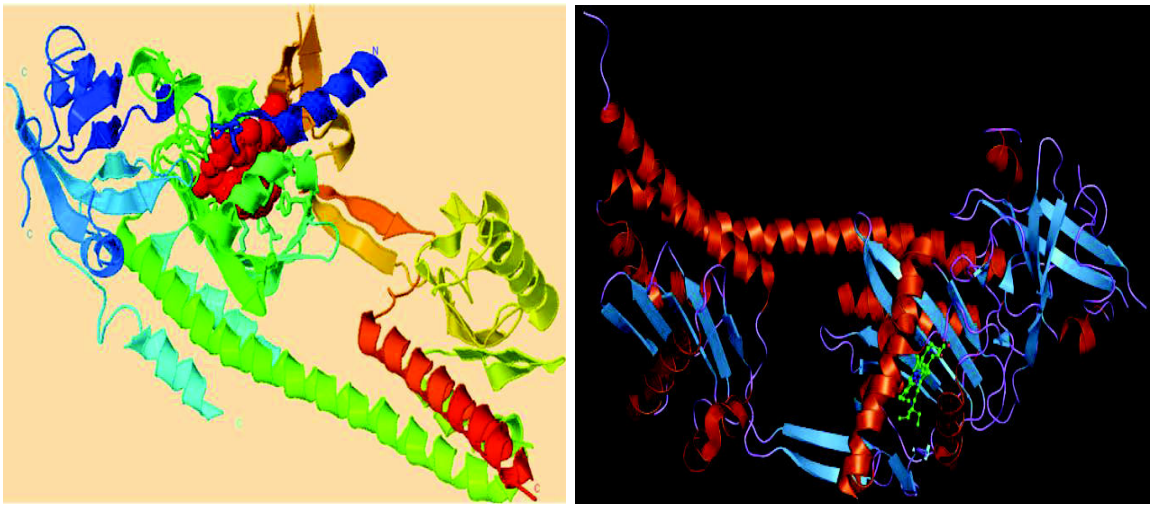

Figure 2.9. Three dimensional crystal form of Cph1 phytochrome : Crsytal structure of the PAS-GAF-PHY tri-domain of the *Synechocystis* PCC 6803 phytochrome, Cph1Δ2, in the Pr state. The protein depicts fully functional phytochrome photoreversibility present in the solution as well as in the crystal. The extended PHY domain forms a 'tongue' like flap that limits the PCB chromophore from solvent so that the bilin is deeply convened in the bilin binding pocket. The left panel in the figure diagrammatically represents the conserved domains with different colors while right panel is based on the secondary structure folds of the protein. The data base accession number from Protein data bank at NCBI is labeled as 2vea-Cph1.

The previous bacteriphytochrome structures obtained before this were marred by the fact that the bi-domain proteins were dysfunctional as they lacked the Pfr form attained after photon absorption by the ground Pr state due to the lack of PHY domain. The absolute requirement of this domain for full functionality of the protein has already been proven by mutational studies, where mutations at significant residues resulted in hypsochromic shifts or no photochromicity (Park et al., 2000; Wu and Lagarias, 2000; Oka et al., 2004; Hahn et al., 2006). This crystal structure provided details of phytochromes as evolved tandem 'GAF proteins' and chromophore conformations different from the biophysical Raman studies (Murgida et al., 2007) for Cph1. The protein contains the trefoil knot as reported earlier (Wagner et al., 2005) formed by the N-terminal extension of the PAS domain as well as a 'tongue' like protrusion formed by the PHY domain (see figure 2.9). The tongue representating highly conserved residues (PR x SF motif) extends back

as a long kinked hairpin from PHY lobe towards the GAF domain, maintaining intimate contact with the GAF domain and protruding through the knot. This chock a block trefoil knot and tongue-like folds effectively seals the chromophore from the solvent by closing the bilin binding pocket in the complete sensory module as was amiss from the PAS-GAF bidomain structural data. This symbolic docking site as such formed might be due to conformational restraints as a result of difference in chromophore attachment sites than from bacteriophytochromes (Lamparter et al., 2004; Wagner et al., 2005, 2007; Yang et al., 2007; Noack et al., 2007) or due to lack of the PHY domain tongue.

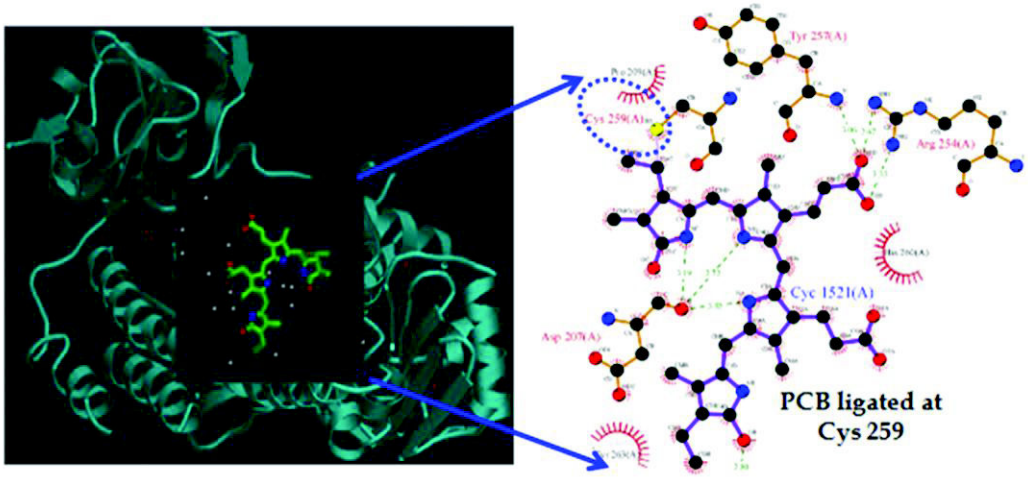

Figure 2.10. Chromophore structure in phytochrome : Chromophore bound to the protein in the biling binding pocket formed in the crystal structure of Cph1 with the right panel showing details of the amino acids closely involved in the protein-chromophore interactions.

The chromophore binding in Cph1 is substantiated to the single carbon-thioether link between chromophore ring A and the sulfur of canonical cysteine (C-259) in the GAF domain (Hahn et al., 2006) as compared to bacteriophytochrome where two carbon atoms link ring A of bilin to a cysteine near the N terminus in PLD (Lamparter et al., 2004). The N-terminal residues corresponding to the PLD cysteine in Cph1 (Leu-18, Leu-15 and Ile-20) form part of the hydrophobic walling

around rings A and B of the chromophore. The chromophore that is further shielded from solvent by residues from the PHY domain tongue, adopts a ZZZ_{ssa} conformation as evident in bacteriophytochromes (Fig. 2.5 and Fig. 2.10).

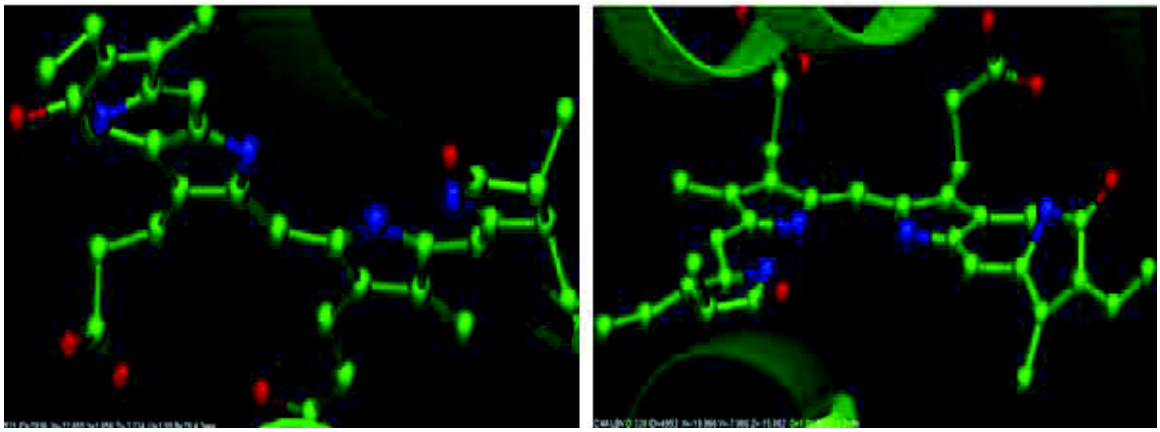

Figure 2.11. Chromophore ring rotation in the crystal structure : The chromophore tethered to the cysteine residue in the PLD domain of bacteriophytochromes or the GAF cysteine in the bilin binding pocket (left panel showing the lower view while right panel showing the upper view) of cyanobacterial phytochromes is seen through the crystal structure lens.

The meticulous details of the chromophore binding cleft of the complete Cph1 sensory module accentuate the similarities and differences from those of bacteriophytochrome PAS-GAF bidomains. These encompass the conserved amino acid residues around the chromophore form either salt bridges or hydrophobic subpockets around bilin rings as similarities, and segregation of the bilin from the solvent by the PHY tongue along with limited tilts in between the A, B, C and D rings of the chromophore distinctive from bacteriophytochrome structural reports. This detailed configuration of bilin binding in Cph1 gives more information on the biochemical effects of the photochromic proteins in terms of light absorption and photoreversible mechanism. The structure reported here consent to the expected ZZE_{ssa} Pfr conformation of the chromophore (Rüdiger, 1987, 1992; Inomata et al., 2006) while explaining the light-induced conformational changes transmitted to the protein. Contradictory to the weak NMR signals obtained for Cph1 (Strauss et al.,

2005; Rohmer et al., 2006; Rohmer et al., 2008) reflecting considerable chromophore mobility, the crystal structures for both bacteriophytochromes and Cph1 highlights close packing around chromophore rings A-C (Figure 2.11). Such tight packing rules out major conformational changes in that region of the bilin without associated dramatic changes in protein. These structural limitations along with the biochemical analysis of the amino acid residue mutants involved in the chromophore association with the protein explain the steps of photoconversion, importance of the PHY domain tongue association for photoreversibility as well as the signal transduction mechanism of the holoprotein (Heyne et al., 2002; Esteban et al., 2005; Hahn et al., 2006). The crystal structure thus augmented the era of research into these photoreceptors that would finally help in determining precisely their physiological functions.

2.1.2.7 Molecular interaction studies – analyzing structural function relationships in phytochromes

2.1.2.7(A) Isothermal titration calorimetry (ITC)

The biological necessity for molecule recognition and association to express and regulate signals are the two fundamental concepts that drive the thriving scientific research. The protein-protein interactions form an important aspect in studying the mechanism behind protein folding and downstream functions. The interactions of biological molecules e.g. protein – DNA, hormone – receptor, receptor – regulator exemplifies the complexity and diversity of molecular recognition. Such interactions form an integral part in signal transduction cascades as well as in gene expression. The nature of the interactions can be determined at various levels using highly advanced techniques in modern times. The understanding of molecular recognition processes of small ligands and biological macromolecules requires a complete characterization of the binding energetics and correlation of thermodynamic data with interacting structures involved. A quantitative description of the forces that govern molecular associations requires determination of changes of all thermodynamic parameters, including the stoichiometry of the interaction (n), the association constant (K_d), free energy of binding (ΔG), enthalpy (ΔH), and entropy (ΔS) of binding and the heat capacity change (ΔCp). Thus, the energetics of binding, in combination with the structural information can provide for the complete dissection of the molecular mechanisms and aid in identifying the most important regions of interface as well as energetic contributions in any such interaction.

The use of ITC has been upped by leaps with the increase in its sensitivity by the recent developments in instrument design permitting measurement of heat effects generated by nanomol (typically 10-100) amounts of reactants. The technical advances in microcalorimetry led us en route to measurements involving enthalpy

changes alongwith the thermodynamics for biomolecular processes in aqueous solution. It is the direct method to measure the binding equilibrium by determining the heat change during complex formation at constant temperature, where one binding partner is titrated into a solution containing the interaction partner, thereby generating or absorbing heat. The heat changes probed and quantified by the isothermal titration calorimeter are characteristic of most chemical and biochemical processes. ITC can be used for numerous applications, e.g., binding studies of antibody-antigen, protein-peptide, protein-protein, enzyme-inhibitor or enzyme-substrate, carbohydrate-protein, DNA-protein (and many more) interactions as well as enzyme kinetics (Velazquez and Freire, 2005).

A typical protein interaction system comprises complex mechanistic attributes through which polypeptides assume a functional conformation, and are involved in a multitude of weakly interacting groups, involving interactions variously described in terms of hydrogen bonding, van der Waals / dispersion forces, hydrophobic, and other polar and non-polar thermodynamic interactions in which the dynamics of solvent molecules are intimately involved. All these processes involve changes in solvation-hydration, and it is natural to assume that the uptake or relaease of heat associated with these processes should reflect, in some way, such changes in solvation. The processes accompanied by change in the heat capacity of binding (ΔCp) which is typically negative in annotation possibly due to decrease in the exposure of hydrophobic/ non-polar surfaces of proteins involved. Different contributions may be endothermic or exothermic, depending on circumstances and calorimetry provides a direct way of dissecting out the individual contributions e.g. enthalpic (ΔH) and entropic (ΔS) contributions, smaller variations in the free energy (ΔG) that ultimately determines the thermodynamic stability of any process. Such entropy-enthalpy assortment is encoded through microcalorimetry illustrating considerable information to understand the thermodynamics of macromolecular interactions that suffice the quest to define the parameters required for a successful reaction.

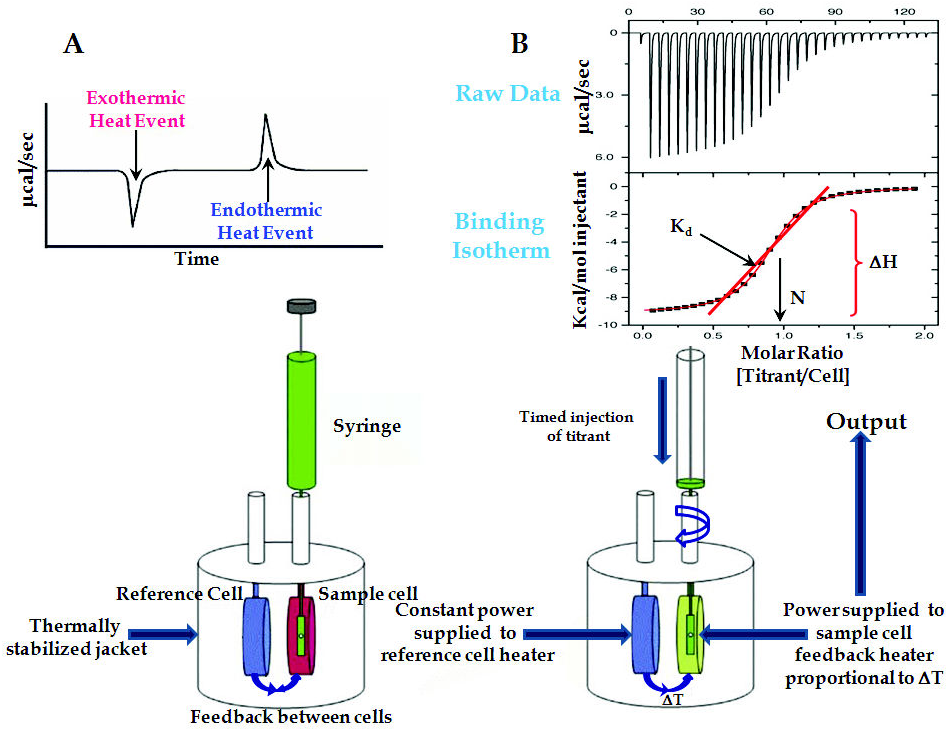

Figure 2.12: Schematic representations of isothermal titration calorimetry (ITC) instruments. (A) An ITC instrument prior to performing a titration. The sample cell and the reference cell as kept at the same temperature, which is typically 5°–10°C above the temperature maintained outside the jacket in which the cells are housed. The reference cell is always kept at the experimental temperature. The titrant component of the interaction is placed in the syringe and the reactant in the cell. The interaction can result in either exothermic or endothermic heat events as depicted in the panel above. (B) An ITC instrument performing a titration. When an injection is made, the change in heat associated with binding (endothermic or exothermic) results in a change in temperature in the sample cell. A change in power (heat/s) is required to return the cells to identical temperatures (T) (i.e., ΔT = 0). This change in power is recorded as a series of injections is made. In the raw data presented in the inset, each injection is accompanied by an interaction where heat is given out (exothermic). As the course of injections is completed, the binding sites on the sample in the cell are gradually saturated, and the exothermic effect becomes reduced.

The informational content of thermodynamic data is substantial playing an important role in the elucidation of binding mechanisms and, through the link to structural data, also in rational physiologically significant signaling mechanistics as well as resolving some of the ambiguities of protein-protein interactions. In this study we approached the comprehensive overview of phytochrome interactions, its sub-unit interactions involving domain specific functions to outline some critical experimental analysis utilizing the thermodynamic data collected using ITC technology.

(i) Isothermal Titration calorimetry (ITC) : General aspects

Calorimetric methods provide an invaluable tool for understanding the changes involved in the molecular processes. The advent of highly sensitive titration calorimeters has generated heightened interest in this technique. An ITC instrument consists of two identical cells composed of efficient thermal conducting material surrounded by an adiabatic jacket (Figure 2.10). The temperature of the cells is maintained by use of appropriate heating or cooling circuits around the cells, so that all the components of the reaction have identical temperature conditions. In an ITC experiment, the macromolecule solution is placed in the sample cell, whereas the reference cell (syringe) contains buffer or water for the blank or baseline measurement prior to the injection of the titrant. There is a constant feedback input of power required to maintain equivalent thermodynamic setup in the reservoir (sample) cell and the reference cell. During the injection of the titrant into the sample/ reservoir cell, heat is taken up or evolved depending upon whether the macromolecule association reaction is endothermic or exothermic. The exothermic reaction leads to increase in the temperature of sample cell, so that the feedback power is cut-off to maintain equal temperatures between the two cells while reverse of this occurs during endothermic reaction, when the feedback circuit increases power to sample cell to maintain constant temperature.

ITC directly measures the heats changes upon addition of small volumes (5-10 µl) of one solution to another in the calorimetric cell (1-2 ml), and is typically used to study protein-ligand binding or protein-protein interactions (Velazquez, 2004). In dilution mode it may also be used to determine monomer-dimer or oligomer-dissociation equilibrium parameters.

The fundamental thermodynamic parameters obtained through analytical calorimetric measurements i.e. binding stoichiometry (*n)* ,affinity (K_d), enthalpy (ΔH) which, together with free energy ($\Delta G^0 = -RT\ln K$), allows calculation of entropy (ΔS) and the heat capacity change (ΔCp) for the process as well. Typical

thermodynamic data for a protein-protein interaction as illustrated in Fig. 2.10 is evident of the strong temperature dependence of both ΔH and ΔS, a consequence of the large ΔCp effects that are a common feature of many biomolecular and other interactions in solution. The heat absorbed or evolved during a calorimetric titration is proportional to the fraction of bound ligand. Accurate determination of the initial concentrations of both macromolecule and the ligand is essential to determine the amount of heat evolved on gradual addition of the ligand. Initial interactions between the two proteins result in large endothermic or exothermic signals depending upon the nature of association as all or most of added ligand is bound to the macromolecule. As the ligand concentration increases, the macromolecule becomes saturated and subsequently less heat is evolved or absorbed on further addition of titrant.

(ii) Application of ITC in protein science

Isothermal calorimetry (ITC) has developed as a robust widely accepted specialist method for understanding molecular interactions and other biological processes of the likes of protein-protein interactions, protein-DNA/RNA interactions, protein-small molecule interactions, protein folding/misfolding mechanism and enzyme kinetics (Cliff et al., 2004; Ababou and Ladbury; 2006, 2007; Okhrimenkoa and Jelesarov, 2008). The recent development of commercially available high-sensitivity calorimeters (VP-ITC) from MicroCal (North Hampton, USA) has revived the microcalorimetry experiments as a preferred tool to understand mechanisms for protein interactions in signal transduction, hence becoming a necessary tool for protein complex structural studies. The increasing popularity of ITC in the field of protein science is due to several reasons, mainly its simple experimental setup that yields loads of thermodynamic data with only a small amount of protein. The dissociation constant values resulting in the determination of entropy and enthalpy changes allows further discrimination of thermodynamic – structural correlation of proteins by comparing subtle

conformational changes of proteins. ITC experiments performed at different temperatures provide an accurate, direct determination of the ΔC_p term representing the change in surface area on forming a protein interface that can be a useful tool in understanding protein interactions with respect to both structure and thermodynamics (Conelly et al., 1990). The protein association results in the formation of an encounter complex followed by desolvation and establishment of tight complex. The dissociation rate constant delivered by such changes observed in calorimetry can point out towards the design of the molecular switch by proteins for signal relays (Kiel et al., 2004).

(iii) Conclusions

The ITC method is gaining wider usage with respect to investigating protein interactions in signal transduction. The ITC critical data analysis combined with X-ray crystallography and nuclear magnetic resonance spectroscopy may be one method that will help provide greater understanding of the complexities of protein folding and protein interactions.

The phytochromes, both Cphs and eukaryotic are bilin- and light- regulated protein kinases proven by various biochemical interaction studies (Yeh et al., 1997; Yeh and Lagarias, 1998). The chromophore binding to the apoprotein stimulates its histidine kinase activity resulting in the dimerization of the monomeric apo-form to holoprotein (Park et al., 2000b; Lamparter et al., 2001). The auto- and trans-phosphorylation mechanism well documented for bacterial two-component histidine kinases (Stock and West, 2003) is concerned with the bilin stimulated and light inhibited phosphotransferase activities in Cph1 which include the regulation of ATP/ADP binding affinities, subunit association/dissociation constants, and ATP to histidine and phospho-histidine to aspartate equilibrium constants. There is limited information regarding the influence of bound ATP (and/ or ADP) and of the histidine phosphorylation state on the thermodynamics and kinetics of the various protein – protein interactions. Chromophore binding, light and ATP

working hand to hand modulate the phytochrome- protein interactions is surmised to be the guiding mechanism of phytochrome signaling.

The isothermal calorimetry technique applied here to the phytochromes would provide for the thermodynamic backdrop for the phytochrome protein interactions with response regulator proteins, or intra-domain interaction, kinetics behind such interactions. This data would therefore add to the biochemical and structural evidence available for phytochrome and pave way for further functional and applicative analysis of these bili-proteins.

2.1.2.7(B) FTIR

There are diverse biophysical and biochemical methods based on different approaches to study the structure function relationships in phytochromes. Spectroscopic techniques were among the first approaches to be used to study the biochemical properties of Phys (Butler et al., 1972). The relevance of the spectroscopic methods has made significant progress by improvement in spectral sensitivity, development of newer techniques for data acquisition and analysis, combination of different methods to unravel the structure-function relationships in the phytochrome family of photoreceptors.

The crystal structure of the three dimensional fold assumed by a protein is one of the strongest milestone in proteomics. The phytochrome structure thus would form the basis of the vastly applicative field of research in these photoreceptors. The phytochrome research has been carried out from last 50 years with various biochemical methods that had provided valuable insights into their chemical structural modifications and other interactions. The photoresponsive protein systems are mostly compliant to optical spectroscopy techniques. The biophysical spectroscopy techniques that are being used to investigate structural alterations in photoactive proteins include time resolved polarized absorption, fluorescence, multinuclear NMR, UV-Visible, Fourier transform infra-red, time resolved femtosecond spectroscopy, resonance raman, small angle X-ray scattering and X-ray diffraction spectroscopy. The Fourier transform (FT) spectroscopy technique used in the study is described here for the chromoproteins.

The *Calothrix* phytochromes here arrange into the light-activated signal transduction system, with C-terminal located histidine kinase domains. The apoprotein expressed in *Escherichia coli* incorporates the tetrapyrrole chromophores phycocyanobilin (PCB; Fig. 2.3) or biliverdin (BV; Fig. 2.3) autocatalytically, producing a holoprotein with fully reversible photochemistry in the red/far-red region (Hübschmann et al., 2001; Quest et al., 2007).

In the proteomics domain of scientific research X-ray structural analysis and NMR spectroscopy are established methods to determine the geometry of protein folding. The determination of the molecular reaction mechanism of the proteins remains to be determined by the valuable tool of time-resolved FTIR difference spectroscopy. Here, the FTIR spectroscopy is described for its application on the light driven photoreaction of the phytochromes that form the crucial step for downstream signal transduction and molecular interaction.

(i) Basis of Fourier transform infrared spectroscopy (FTIR)

FTIR spectroscopy is based on the fact that almost all molecules except for monoatomic (e.g. He, Ar - equal electronic fields of atoms or single atom) and homopolar diatomic (H_2, N_2, O_2) molecules absorb infrared light at frequencies that affect the dipolar moment of the molecules. The difference of charges in the electronic field of atoms produce a dipolar moment of the molecule that allow infrared photons to interact with the molecule causing excitation to higher vibrational states. Infrared spectroscopy measures these transitions between vibrational states of molecules that are induced by irradiating the sample with an infrared light beam. The plot of the intensity of light absorption versus the frequency of light is called the infrared spectrum. The infrared spectra consists of sharp peaks at certain frequencies that correspond to the vibrational frequencies of specific functional groups or bonding arrangements, that are used as fingerprints for identifying compound transitions. In infrared spectroscopy the peak position (vibration frequency) is commonly given as wavenumber (cm^{-1}), which corresponds to the frequency divided by the speed of light.

A Michelson interferometer is used to spread a sample with the infrared light spectrum and measure the intensity of the light not absorbed by the sample. FTIR spectroscopy is thus a multifarious technique, where all optical frequencies from the source are observed simultaneously over a period of time at constantly maintained conditions known as scan time. The spectrometer measures the

intensity of a specially encoded infrared beam after it passes through the sample, the resultant signal that is time domain digital signature, is called an 'interferogram'. This signal takes account of the intensity information about all frequencies present in the infrared beam, which can be extracted by switching this signal from a time domain digital signal to a frequency domain digital signal. This is achieved by applying a Fourier transform over the interferogram and producing a single beam spectrum. The higher number of scans of which the signal is composed can lead to a better estimate of the data of these statistically stationary signals. The output signals can be discerned on the basis of selective absorption of the molecule under investigation absorbing infrared light at certain frequencies. This paves the way for the molecular fingerprint identification (qualitative) and the amount of molecules (quantitative) in the sample.

(ii) Infra – red spectra of phytochromes

The advancements in the field of optical spectroscopy that monitors the photo-induced reactions providing the spectroscopically defined intermediates that could be accurately linked with X-ray crystal structures to synergistically reveal the underlying molecular mechanism or protein function. Time-resolved Fourier-transform infrared (trFTIR) difference spectroscopy can reveal great molecular details of the reaction mechanisms of proteins. These studies have led to a deeper understanding of the protein structural changes that determine the significant functions of the proteins. The integrated approach of difference spectroscopy related to the phytochrome photo-interconversion and the X-ray crystallography data would thus define the central dogma of the molecular action of these proteins.

Phytochromes are bili-proteins, using BV, PCB or PΦB as their prosthetic group in varied genera. Light induced Fourier transform infra-red spectroscopy has been proven to be an informative tool for investigations of such biological photoreceptors (Siebert, 1990, 1997). The infrared spectra of these proteins consist

of absorption bands from all the components i.e. the protein part, the chromophore, interactions between the chromophore and protein as well as water. The contributions from solvent components that are not specifically bound to the protein or to the chromophore are ascertained through the use of appropriate blank reference spectra and mathematical compensation procedure. Comprehensive insight into the photoconversions at the molecular level could be gained by the performance of difference spectra, the absorption bands of the protein groups involved in the reaction out of the background absorbance of the whole sample. The spectra can be demarcated according to molecular changes while measuring with time resolutions down to nanoseconds and followed for time periods ranging over six orders of magnitude. The technique can provide information that would complement the X-ray structure analysis, such as details of H-bonding, the protonation state of chromophores, charge distribution and the time dependence of the phytochrome photo-reaction.

(iii) Difference spectroscopy

Proteins have vibrational modes that describe the global information obtained through the absorption spectrum. The spectrum is dominated by the amide I (C=O stretch) and amide II (NH coupled with C-N stretch) bands, contributed by the amino acids. These backbone absorptions give information about the secondary structure of the protein. An FTIR difference spectrum is applied to a reaction between atleast two forms, e.g. in phytochromes the Pr and Pfr form, where substraction of the absorbance spectrum of Pfr from that of Pr gives the vibrational bands from groups that change during this reaction while the background similar vibrations are annihilated. Accurate similarity in the experimental set up is maintained to avoid any discrepancies and individual absorptions are resolved reliably. The photobiological system of the phytochromes is ideally suited to be studied by this technique as the intrinsic chromophores are differentially activated through light flashes enabling isomerization of the bilin and

subsequent reaction. The proteins can be assessed by FTIR spectroscopy by either the rapid scan method or step scan method. In the rapid scan method, ground state spectra of the protein are taken followed by activation of the protein by laser flash and the individual conversions of the protein are recorded at regular intervals. The step scan method constitutes the time resolved measurements of the protein activity, where time dependence of the intensity changes at different interferogram positions are recorded by the interferometer moving mirror. The interferograms are here a collection of data sets of step-wise mirror positions with time resolution upto a few nanoseconds.

The band assignments of the difference spectra recorded by FTIR are done by the tentative assignment of the vibrations of individual groups present in the protein after blank substraction. The band assignments point towards the information on the interaction of proteins, protonation states, charge distribution, and bond orders as well as involvements in the reaction mechanism. In this work the photoreactions of CphA and CphB, i.e. Pr $\longrightarrow$ Pfr and Pfr $\longrightarrow$ Pr, reconstituted with phyocycanobilin (PCB) and biliverdin (BV) respectively were investigated using optical and FTIR difference spectroscopy at low temperatures.

Chapter 3

Materials and Methods

3.1 Materials: chemicals and enzymes

All chemicals and reagents used throughout this work were of analytical grade or maximal purity available and were obtained from Merck (Darmstadt), Sigma (Deisenhofen), Serva (Heidelberg), DIFCO (Detroit, USA), Gibco/BRL (Eggenstein), Biomol (Hamburg), Pharmacia (Freiburg), ICN Biomedicals (Aurora, USA) and BioRad (München), unless otherwise indicated. Restriction enzymes and DNA-modifying enzymes were from Fermentas (St. Leon-Rot), General Electric (formerly Amersham-Pharmacia, Freiburg), Stratagene (Heidelberg), and NEB (New England Biolabs) (Schwalbach/Taunus). All solutions and labware for bacterial cell cultures and molecular biological techniques were autoclaved or sterile-filtered. All chemicals used for protein crystallization trials were of the highest purity available, and all solutions were sterile-filtered before use. Information on specific chemicals, reagents or labware is given below in the respective instruction and in the list appended to this paragraph, if reasonable. All numbers given in *per cent* (%) refer to either weight per volume or, in cases of liquids, to volume per volume. All experiments involving standard techniques were performed following the manufacturer's protocols and recommendations, when available, if not otherwise indicated.

3.1.1 Equipment

Instruments

Chromatography media	Ni-NTA, Qiagen, Hilden; Superdex 26/60 (Amersham), all other media were purchased from Amersham Pharmacia Biotech, Freiburg and Ni-IDA, Serva.
FPLC System and Accessories	Äkta-system, General Electric formerly Amersham Pharmacia Biotech, Freiburg
French Press	Aminco 20K French Pressure Cell, Polytec GmbH, Waldbronn
UltraTurrax	Ultra Turrax T25, Jahnke & Kunkel GmBH, Staufen, Germany
Incubator	Heraeus , Hanau

PCR machine	Thermocycler gradient PCR System, Eppendorf , Hamburg
Phosphoimager	FujiFilm FLA-2000, Fuji Photo Film Co., Ltd., Tokyo, Japan
Sonifier Sonifier	Cell Disruptor B-30, Branson Sonic Power Co. Danbury, CT, USA
Microcal	Northampton, USA
MALDI-TOF	Voyager-DE™ PRO Biospectrometry Workstation, Applied Biosystems (USA)

3.1.2 Chemicals and Consumables

Consumables

Centriprep	Centriprep K, Millipore, Eschbronn
Crystallization consumables	Hampton Research, Laguna Niguel, CA, USA
Dialysis Tubing	10 kDa or 30 kDa exclusion limit, Sigma-Aldrich , Deisenhofen
Electroporation cuvettes	0.2 mm gap, BioRad, Richmond, CA, USA
Filter paper	Whatman 3MM, Whatman, Fairfield, NJ, USA
Microfuge Tubes	0.5 and 1.5 ml, Eppendorf AG, Hamburg
PVDF Membrane	Bio-Rad and Sigma-Aldrich, (Deisenhofen)

Kits

DNA purification kit	QIAquick, Qiagen, Hilden, Amersham Biosciences (GE Healthcare)
Plasmid isolation kit	QIAprep, Qiagen, Hilden, Amersham Biosciences (GE Healthcare)
Site directed mutagenesis kit	Quick Change mutagenesis kit, Stratagene, La Jolla, CA, USA

Enzymes

DNA Ligase	T4 DNA Ligase, Gibco BRL, Invitrogen GmbH, Karlsruhe
DNaseI	Roche Diagnostics GmbH, Mannheim
DNA polymerase	mi- Taq, Metabion GmbH, Munchen
	Pfx polymerase, Invitrogen, Karlsruhe
	Pfu polymerase, Stratagene, La Jolla, CA, USA
	Pfu DNA LigaseStratagene, La Jolla, CA, USA
Polynucleotide kinase	Amersham Biosciences (GE Healthcare)
Restriction endonucleases	New England Biolabs GmbH, Schwalbach/ Taunus
Shrimp alkaline phosphatase	USB, Cleveland, OH, USA

Fine Chemicals

Agarose	Serva, Heidelberg and Roth, Karlsruhe
Coomasie Brilliant Blue	Serva, Heidelberg
DNA size standard	One kb DNA size marker, New England Biolabs GmbH, Schwalbach/ Taunus, Fermentas GmbH, St. Leon-Rot
dNTPs	PCR nucleotide mix, Amersham Pharmacia Biotech, Freiburg
Gel filtration size standard	Gel filtration LMW and HMW Calibration kits, Amersham Pharmacia Biotech, Freiburg
IPTG	Serva, Heidelberg
Pefabloc	Biomol, Deisenhofen
Protease inhibitor cocktail	Complete Protease Inhibitor Cocktail, EDTA free, Hoffmann-La Roche Ltd., Basel, Switzerland
Protein MW marker	See-Blue Plus2; Benchmark 12, Invitrogen GmbH, Karlsruhe
SDS, 99%	Roth, Karlsruhe
Western Blocking Reagent	Hoffmann-La Roche Ltd., Basel, Switzerland

Antibodies

Primary antibody	Mouse anti His_6 IgG, Invitrogen, Karlsruhe
Secondary antibodies	Alkaline phosphatase conjugated goat anti mouse IgG, DAKO, Hamburg

Oligonucleotides

Primers/ Oligos	Metabion GmBH (Munchen)

Vectors

pET 28a	Novagen, concern of Merck GmBH.
pET 52b	Novagen, concern of Merck GmBH.
pQE His Strep Trisystem	Qiagen GmbH (Hilden).

Antibiotics

Ampicillin	Serva, Heidelberg
Kanamycin	Serva, Heidelberg
Chloramphenicol	Serva, Heidelberg
Spectinomycin	Serva, Heidelberg

3.2 Bacterial Strains

Transformations of ligation products (cDNA of interest into expression vectors) were done in bacterial cells *Escherichia coli L.* XL1-Blue (Stratagene, Heidelberg, Deutschland), and *Escherichia coli* DH5α (Invitrogen). XL1-Blue cells have one episome of laqI mutation- laq I^q , which produces the lac repressor (allowing for blue/white selection of ligations) while another episome has tetracycline resistance gene, resulting henceforth for the double antibiotic selection procedure.

BL21-CodonPlus® (DE3) strains derived from Stratagene's high performance BL21-Gold competent cells are engineered to enable efficient high-level expression of heterologous proteins in *Escherichia coli*. The rarity of certain tRNAs abundant in *Escherichia coli* required for efficient production of heterologous proteins limits the forced high-level expression which results in depletion of the pool of rare tRNAs and stall translation. This shortcoming is overcome with BL21-CodonPlus strains containing extra copies of genes that encode the tRNAs in *E. coli* thereby enabling the high-level expression of many heterologous recombinant genes. These strains (Table 3.1) are ideal for performing protein expression studies that utilize the T7 RNA polymerase promoter to direct high-level expression.

BL21-CodonPlus-RIL and BL21-CodonPlus (DE3)-RIL cells contain extra copies of the *argU*, *ileY*, and *leuW* tRNA genes. These genes encode tRNAs that recognize the arginine codons AGA and AGG, the isoleucine codon AUA, and the leucine codon CUA, respectively (Table 3.1). The BL21-CodonPlus (DE3)-RIPL cells contain extra copies of the *argU*, *ileY*, and *leuW* as well as the *proL* tRNA genes. Both these strains rescue expression of heterologous proteins from organisms that have either AT- or GC-rich genomes.

The BL21 Star (DE3) and BL21 Star (DE3) pLysS *E. coli* strains have the λ DE3 lysogen which allows high-level expression of T7-regulated genes under control of the lacUV5 promoter as well as the rne131 mutation which encodes a truncated RNase E enzyme lacking the ability to degrade mRNA, resulting in an increase in mRNA stability leading to enhancement of the expression capabilities of each strain. Expression in these cells is performed by addition of IPTG, which induces expression of the T7 RNA polymerase. The table below lists the various strains of bacteria used during this study, and their genotype.

Table 3.1– Bacterial strains used with detailed genotypes

Host Strain	Genotype
***E. coli* Top10F′**	F′ {*lac*I^{q} *Tn10* (Tet^{R})} *mcr*A Δ(*mrr-hsd*RMS-*mcr*BC) Φ80*lacZ*ΔM15 Δ*lac*X74 *deo*R *rec*A1 *ara*D139 Δ(ara-leu)7697 *gal*U *gal*K *rps*L(Str^{R}) *end*A1 *nup*G (Invitrogen)
***E. coli* XL 1 Blue MR**	Δ *(mcrA) 183 Δ(mcrCB-hsd MR-mrr) 173 endA1 supE44 thi-1 recA1 gyrA96 relA1 lac*
***E. coli* DH 5α**	*supE44 dlac*U169 (p80 *lacZd*M15) *hsdR17 recA1 endA1 gyrA96 thi-1 relA1*
***E. coli* BL21-AI**	F- ompT hsdSB (rB-mB-) gal dcm araB T7RNAP-tetA
***E. coli* BL21 Star(DE3)pLysS**	F- ompT hsdSB (rB-mB-) gal dcm rne131 (DE3) pLysS (Cam^{R})
***E. coli* BL21 Star(DE3)**	F- ompT hsdSB (rB-mB-) gal dcm rne131 (DE3)
***E. coli* BL21-CodonPlus(DE3)-RIL**	*E. coli* B F– *ompT hsdS*(rB– mB –) *dcm*+ Tetr *gal* λ(DE3) *endA* Hte [*argU ileY leuW* Camr]
***E. coli* BL21-CodonPlus(DE3)-RIPL**	*E. coli* B F– *ompT hsdS*(rB– mB–) *dcm*+ Tetr *gal* λ(DE3) *endA* Hte [*argU proL* Camr] [*argU ileY leuW* Strep/Specr]
***E. coli* BL21 - C41**	F-*ompT gal hsdSB* (rB –mB -) *dcm lon* _DE3 pLysS
***E. coli* BL21 – C43**	F-*ompT gal hsdSB* (rB –mB -) *dcm lon* _DE3 pLysS

3.3 Media and solutions

Media used are tabulated as per their composition per litre of volume. In general, the media were sterilized by autoclaving at 120°C and 1 bar pressure for 20 min. The heat-labile components of various media and other required solutions were otherwise sterilized by filtration of the stock solutions through a sterile filter. Tris-distilled water was used for all the preparations of the media as well as solutions. The water was monitored regularly for trace elements which were removed with an Organex column.

3.3.1 Media:

LB: 10 g/l NaCl, 5 g/l yeast extract, 10 g/l tryptone

LB-agar: 10 g/l NaCl, 5 g/l yeast extract, 10 g/l tryptone, 15 g/l agar

SOC: 20 g/l tryptone, 5 g/l yeast extract, 1% (v/v) 1 M NaCl, 0.25% (v/v) 1 M KCl, 1% (v/v) filter-sterilized 2 M Mg^{2+} stock (1 M $MgCl_2$; 1 M $MgSO_4$), 1% (v/v) filter-sterilized 2 M glucose stock

TBY: 16 g/l tryptone, 10 g/l yeast extract, 5 g/l NaCl

3.3.2 Solutions

3.3.2.1 Solution for Agarose-Gelelectrophoresis

10x TE-Buffer (mM)	10x DNA Loading Dye
100 Tris/HCl, pH 8.0	50 % Glycerol (v/v)
10 EDTA, pH 8.0	2.5 µg/ml Xylene cyanol
2.5 µg/ml Bromophenol blue	
5x TBE Agarose Running Buffer	**50x TAE Agarose Running Buffer**
54 g/l Tris.Cl	242 g/l Tris.Cl
27.5 g/l Boric Acid	57.1 ml/l Acetic Acid
20 ml 0.5 M pH 8 EDTA	100 ml/l 0.5 M pH 8 EDTA

3.3.2.2 Solutions for DNA Preparation and Modification:

Buffer P1: 50 mM Tris-HCl, pH 8.0, 10 mM EDTA, 100 µg/ml RNase A

Buffer P2: 0.2 M NaOH, 1% SDS

Buffer P3: 60% (v/v) 5 M potassium acetate, 11.5% (v/v) acetic acid

Buffer QBT: 750 mM NaCl, 50 mM MOPS, pH 7.0, 15% (v/v) isopropanol, 0.15% (v/v) Triton X-100

Buffer QC: 1 M NaCl, 50 mM MOPS, pH 7.0, 15% isopropanol

Buffer QF: 1.25 M NaCl, 50 mM Tris-HCl, pH 8.5, 15% isopropanol

Buffer PE: 1.25 M NaCl, 50 mM Tris-HCl, pH 8.5, 15% isopropanol, 75% ethanol

EP: 0.5 mM HEPES, pH 7.6, 10% glycerol

Kinase buffer: 50 mM Tris, pH 7.6, 5 mM $MgCl_2$, 2 mM EDTA

3.3.2.3 (a) Solutions for Phytochrome extraction from Bacteria

Wash Buffer (mM)	Extraction Buffer (mM)	Ammoniumsulfate Buffer (mM)
50 Tris	50 Tris	50 Tris
5 β–ME	5 β–ME	5 β–ME
250 NaCl	250 NaCl	250 NaCl
1 TCEP		3300 $(NH_4)_2SO_4$

The pH of the various solutions was buffered with HCl to pH 7.8. The phytochrome extraction was perfomed in the presence of Protease inhibitors such as Pefabloc (Biomol) as the concentration of 1 mM.

3.3.2.3 (b) Solutions for Affinity Chromatography

Equilibriation Buffer (mM)	Wash Buffer (mM)	Elution Buffer (mM)
50 Tris	50 Tris	50 Tris
5 Imidazole	10-50 Imidazole	250 Imidazole
250 NaCl	250 NaCl	250 NaCl

3.3.2.3 (c) Solutions for Analytical / Preparative Gel-Filtration

Gel filtration was perfomed with 20 mM Tris-Cl, 50 mM NaCl buffer of pH 7.8. The stock solution were made at 20X concentration, filter sterilized and de-gassed before the FPLC based Gel Filtration process.

3.3.2.3 (d) Solutions for Protein Analysis-SDS-PAGE & Western blot:

SDS-PAGE

Laemmli-buffer (2x)	SDS-stop buffer (1x)	Coomassie Stock and Staining solution
100 mM Tris	250 mM Tris-HCl	1 tablet Phastgel Blue R in 200 ml 60% (v/v) methanol (gives a 0.2% Coomassie Blue R solution)
4% (w/v) SDS	11% (w/v) SDS	
200 mM DTT	10% β-ME, 15 mM EDTA	1 volume Coomassie stock, 1 volume 20% acetic acid
0.2% Bromophenol blue	0.2% Bromophenol blue	
20% (v/v) glycerol pH 6.8 with HCl	30% glycerol pH 6.8 with HCl	

Solutions for Western Blotting:

SDS-PAGE-running-Buffer (mM)	Transfer-Buffer (ml)
50 Tris	800 SDS-PAGE-running-Buffer
39 glycine	200 methanol
1 EDTA	
0.037 % SDS	

Wash buffer: 10 mM Tris, pH 8.0, 150 mM NaCl, 0.05% (v/v) Tween 20

Block buffer: 3% (w/v) BSA in wash buffer

Incubation buffer: 0.75% (w/v) BSA in wash buffer

Substrate buffer: 100 mM Tris, pH 9.5, 100 mM NaCl, 5 mM $MgCl_2$

Western Blotting Substrate: 10 ml substrate buffer, 33 µl 50 mg/ml BCIP in DMF, 66 µl 50 mg/ml NBT in 70% DMF

3.3.3 Solutions for Protein Quantification

The protein concentration was determined using the Bradford assay kit from Biorad. The protein solution was assorted into different dilutions ranging from 0 - 2 mg / ml, with assay buffers. These dilutions were then read on a spectrophotometer as 540 nm and 700 nm. BSA was used as standard protein for the spectrophotometer analysis, and this range of protein concentration was used to calculate the experimental proteins.

3.4 Bilin chromophores

The phytochrome proteins have specific chromophore selection, and for their activity and assembly, bilin chromophores such as the tetrapyrroles phycocyanobilin (PCB), PEB (phycoerythrobilin) and BV (biliverdin) are used. The bilins PCB and PEB are extracted from Spirulina cells by methanol treatment, and purified to be used for phytochrome assays. BV was obtained from BR by an oxidation reaction.

3.4.1 Extraction of Phycocyanobilin

The crude PCB is extracted from the cyanobacterium *Spirulina geitlerii* using methanolysis (Kufer und Scheer, 1979; Arciero et al., 1988; Terry et al., 1993; Kunkel et al., 1993). The starting material is 50 g freeze-dried cell powder, washed in a sonifier at 4°C with 300 ml methanol, so as to remove the cholorophylls. The continuous washings remove the cholorophylls and the solution turns from green to blue. Crude extracts of phycocyanobilin are then prepared by methanolysis with 300-500 ml methanol for 3 h at 70 °C in a water bath that yields phycobilisomes and the released PCB molecules. The extract was filtered and evaporated to 30 ml. After the addition of 70 ml diethylether, the organic phase was first extracted with 100 ml 1 % (mass/vol.) citric acid, followed by 50 ml 0.5% (mass/vol.) $NaHCO_3$. The water phase was extracted with 50 ml chloroform and the organic phase was brought to 10 ml by evaporation. The remaining phycocyanobilin-containing

solution was slowly added to 150 ml hexane, stirred for 10 min and centrifuged at 5000 x *g* for 10 min at 4 °C. After the removal of the hexane by aspiration, the dry residue of PCB was dissolved in 5 ml diethylether, dispensed into small aliquots, dried *in vacuo* with a Bachofer Speed-Vac concentrator and stored in darkness at -80 °C. For reconstitution experiments of phytochrome apoproteins with phycocyanobilin, PCB was dissolved in dimethyl sulfoxide to give a final concentration of ca. 1.3 - 1.5 mM. The phycocyanobilin concentration was estimated using a molar absorption coefficient of 37,900 M^{-1} cm^{-1} at 680 nm (Cole et al., 1967) in HCl: MeOH (1: 19, by vol.).

3.4.2 Preparation of Biliverdin

The biliverdin chromophore was obtained by the method described by McDonagh et al., 1971. Bilirubin and solution of 2,3-dichloro-5,6-dicyanobenoquinone in dimethyl sulphoxide are mixed and stirred/purged continuously under argon. Addition of water resulted in the precipitation which was collected by filtration onto Whatman filter. The solid was washed extensively with water and re-dissolved by addition of 0.1 M NaOH. The filtrate was collected followed by centrifugation and crude biliverdin was re-precipitated by adding acetic acid. A slurry of silica gel in methanol/acetone (1:1) was poured into a Buchner funnel with a fritted sinter-glass disc, allowing gravity settling or under low vacuum with further solvent addition to get uniform gel layer. Crude biliverdin in methanol/acetone was added carefully and evenly to top of the column. The adsorbed was eluted with chloroform/methanol/acetic acid (700:300:3) and the deep blue-green eluates were collected here and evaporated to dryness under reduced pressure. The residue in 0.1 M-NaOH was filtered through a thin layer of Celite in a Buchner funnel containing a fritted sinter-glass disc, where further rinsing with 0.1 M-NaOH (3 x 1 ml) was done. Acetic acid (3 drops) was added to the combined filtrate and rinsings, and the precipitated product was collected by centrifugation, washed three times with an equal volume of water, and

mixed with acetone/water (4:1). An equal volume of water was added, the mixture was shaken, and acetic acid (5 µl) was added. The mixture was shaken, and left to stand for 10min. The precipitate was collected by centrifugation, washed twice with water, and freeze-dried, giving purified biliverdin as an amorphous green powder.

3.4.3 Spectral Measurements of PCB and BV

Analysis of PCB- and BV-Extinction

The bilin chromophores were tested for the spectroscopic properties prior to use by a UV-Vis spectrophotometer (Cole et al., 1967; Chapman et al., 1967). The extinction coefficients are measured as per tabulated below to analyse the concentration of the chromophores.

The absorption *A* of the dissolved chromophores here is a linear function of its concentration, as in the Lambert-Beer Law. The length of the light path (thickness of the cuvette) and the Extinction coefficient (substance specific constant) determine the slope of the linear plot.

$$A = \varepsilon\, cd$$

Where: c = Concentration; d = Thickness of the cell; ε = Extinction coefficient

ε ($mM^{-1}cm^{-1}$)		O.D. (nm)
PCB (A)	37,9	(680)
BV (A)	30,8	(696)
PCB (B)	16	(610)
BV (B)	13	(674)

Table 3.2 : Extinction coefficient (ε) of Bilins PCB (Cole et al., 1967), and BV (McDonagh, 1979). Spectrophotometric Measurement in HCl-(5%)Methanol (A) or in 50 mM Tris/HCl pH7.8, 5 mM EDTA Buffer (B).

In this experiment, we follow the behavior of the linear absorption increase of the chromophore solution with increasing concentration in order to determine its extinction coefficient at a given wavelength within its absorption area.

3.5 Oligonucleotides/ Primers

OLIGO-NUCLEOTIDE	SEQUENCE	CONSTRUCT
CphA Pas For_ss	*5'- TCC GGT CCA TGG TGA ATA GCT TAA AAG AAG CA -3'*	**CphA_PasGafPhy**
CphA GP_Rev pET	*5'- AAA **CTC GAG** CGC ATT CGA GCG TTC TAA GTC -3'*	**CphA_PasGafPhy**
CphA Pas For_ss	*5'- TCC GGT **CCA TGG** TGA ATA GCT TAA AAG AAG CA-3'*	**CphA_PasGaf**
CphA Gaf_Rev pET	*5'- AA**C TCG AG**A GCC GCA CCT TGA GCG CTA GT -3'*	**CphA_PasGaf**
CphA HisKa1F_ss	*5'- TAC TTT G**CC ATG** GTC AGC CAA ACA GAA GGA -3'*	**CphA_HisKin**
CphA HisConR_ss	*5'- ATT TAG **CTC GAG** TCC TCG ACC AAA AAG TGT -3'*	**CphA_HisKin**
CphBm Pas For_ss	*5'- TATA**CCATGG**GCTTAAGTCCTGAAAATTCTCCAG -3'*	**CphBm_PasGafPhy**
CphBm GP_Rev pET	*5'- AAA **CTC GAG** ATC GTT GCT GCG CTG CAG TTC -3'*	**CphBm_PasGafPhy**
CphBm Pas For_ss	*5'- TATA**CCATGG**GCTTAAGTCCTGAAAATTCTCCAG -3'*	**CphBm_PasGaf**
CphBm Gaf_Rev pET	*5'- AAA **CTC GAG** AAC AGC CGC GAA TGT AGC ATT -3'*	**CphBm_PasGaf**
CphBm HisKa1F_ss	*5'- TAC TTT **CCA TGG** CAG GAA ATC CTC ATA AGC CT -3'*	**CphBm_HisKin**
CphBm HisConR_ss	*5'- ATT TAG **CTC GAG** TTT GAC CTC CTG CAA AGT -3'*	**CphBm_HisKin**
CphBmC24S_sen	*5'- GAG GTG GAC TTG ACG AAT TCA GAT CGC GAA CCA ATT CAC*	**CphBm_C24S**
CphBmC24S_antisen	*5'- GTG AAT TGG TTC GCG ATC TGA ATT CGT CAA GTC CAC CTC*	**CphBm_C24S**

The table above depicts the name of the oligos used with information about restriction sites coding for specific enzymes as per the multiple cloning sites in vectors being underlined. Gene-specific sequences are given in italics. The positions of the gene-specific parts of the primers are indicated in the sequences in the Appendix. CphBm indicates a gene construct cloned by Benjamin Quest and the C24S notation comes from the mutant of CphBm wherein cysteine was replaced by serine.

3.6 DNA Methods - General Molecular Biological / Microbiology Techniques

3.6.1 DNA-Isolation from cyanobacterial cells:

The isolation of DNA from the Cyanobacteria *Calothrix* and *Nostoc* was performed according to the method from Sambrook and Russel, 2001. As an alternative method for genomic DNA preparation, the NucleoSpin Tissue Kit (Qiagen, Hilden) was used.

3.6.2 Plasmid DNA Preparation

3.6.2.1 Culture of *E. coli* XL-1 cells for plasmid growth

A single colony of *E. coli* XL-1 blue harboring the plasmid of interest was grown in a conical flask in 50 ml of LB broth (10 g Tryptone, 5 g NaCl, 5 g Yeast extract per liter; (Sambrook, et al., 1989). The media was supplemented with appropriate antibiotic and the culture was incubated overnight on a platform shaker at 37°C and 250 rpm. From this culture the cells were harvested by centrifugation (3000 x g_{max}, 5 min) and the plasmid DNA was purified as described.

3.6.2.2 Analytical plasmid DNA isolation (mini prep)

This method is a modification of the alkaline lysis method of Birnboim and Doly (1979). 2 ml of LB-medium supplemented with the appropriate antibiotic were inoculated with a single *E. coli* colony and incubated overnight in a rotary shaker at 37 °C. 1 ml of each culture was centrifuged in an Eppendorf tube for 2 min at maximal speed. The pellet was used to isolate DNA at small scale as per the manufacturer's defined protocol.

3.6.2.3 Preparative plasmid DNA isolation (midi prep)

For large-scale plasmid DNA isolations, the Plasmid Midi Kit from Qiagen was used, which is also based on the alkaline lysis method of Birnboim and Doly

(1979). After lysis, the DNA is purified on a Qiagen anion exchange column. The binding of DNA to this anion exchange resin depends on the salt concentration and pH conditions. RNA, proteins and other impurities are already eluted at low salt concentrations, whereas the DNA elutes only at higher salt concentrations. 20 – 50 ml of a bacterial culture was used for DNA isolation yielding upto 200 µg, using the Qiagen Midi prep kit. Qiagen-tips100 were used to obtain high quality DNA dissolved in 100 µl 10 mM Tris, pH 8.0.

3.6.3 Construction of expression plasmids from *Calothrix* phytochrome genes

The domains of the phytochromes were constructed by using PCR methods, from available templates of full length phytochrome genes or directly from genomic DNA extracted from cyanobacterial cells. A metal affinity tag was introduce through primers or integrated through the multiple cloning sites of the available vectors. The primers were designed to introduce specific restriction sites, sequences recognized by restriction endonucleases for the generation of overlapping ends. Subsequently, the resulting PCR fragment was cloned into an expression vector as described.

3.6.3.1 Polymerase chain reaction (PCR) for DNA amplification

The polymerase chain reaction is a method for selective *in vitro* amplification of DNA fragments, using two oligonucleotides flanking the DNA fragment to be amplified (Saiki et al., 1988).

The polymerase used here was the thermostable Pfx (Invitrogen), Pfu (Stratagene) and mi-Hot Taq Polymerase (Metabion). This polymerase also contains 3'-5' proofreading activity, reducing the error rate. The different polymerase enzymes were used under different experimental set-ups.

Components (50 µl) Reaction	Taq Polymerase	Pfx / Pfu Polymerase	End Concentration
Polymerase Buffer	5µl	5µl	1x
$MgCl_2$	3µl	1.5µl	1x / 0.5 x
Primer Forward (100µM)	2 µl	1.5 µl	0.5µM
Primer Reverse (100µM)	2 µl	1.5 µl	0.5µM
dNTPs (2.5 mM)	5µl	5µl	250 µM
Polymerase (5u/µl)	0.5 µl	0.5 µl	1.5u/µl
Template (10-20 ng)	2 µl	2 µl	Varied

The annealing temperature used was calculated depending on the melting temperature of the primers. The melting temperature was calculated using the equation (G + C) x 4°C + (A + T) x 2°C (Newton and Graham, 1994). For annealing, generally a temperature of about 10 °C below the melting temperature of the primers was used. In this work, in most cases, 58 °C was used as annealing temperature. The polymerization time depended on the length of the DNA fragment to be amplified (at least 1.5 min per 1000 bp).

The amplification was performed in a DNA Thermal Cycler 2.2 (Eppendorf) under the following conditions:

PCR STEP	Temperature (Celsius)	Duration (Min)	Cycles (Num)
Denaturation	94	3	1
Denaturation	95	1	30
Annealing	58	1	30
Amplification	68 / 72	1-3	30
Polymerization	68 / 72	10	1
Extension	72	20	1

3.6.3.2 Analysis of DNA by agarose gel electrophoresis

Horizontal agarose gel electrophoresis was performed for analysing the products from DNA extraction, PCR reaction and restriction digestion in commercially available submarine gel tanks of appropriate size following the method of McDonell et al., 1977 and Southern, 1979. The agarose gels were prepared and run in Tris-Acetate-EDTA-Buffer (TAE- as under section 3.3.2.1) at a concentration of usually 0.8- 1% gels. Samples containing an appropriate amount of DNA were mixed with 6x loading buffer (0.25% (w/v) bromophenol blue, 0.25% (w/v) xylene cyanol FF, 30% (v/v) glycerol) prior to sample application. The gels were run at 5 V/cm until optimal separation was achieved. The gels were stained with 0.1 µg ethidiumbromide/ml buffer for 10 min and visualized under UV light (fluorescence excitation at 302 nm) from a transilluminator. A 1 kb ladder (Fermentas) was applied as a size standard.

3.6.3.3 Isolation of DNA from agarose

Highly purified DNA is the basic requirement for the downstream utilization in cloning and other related molecular biology ministrations. Purified DNA can be obtained from agarose gels after determining the required size molecules. DNA molecules are extracted from excised gel patches and are bound to silica gel membrane in a solution with chaotropic salts and a pH below 7.5. The DNA can be eluted again in a solution with a low salt concentration and a higher pH (Vogelstein and Gillespie, 1979). The Amersham gel band extraction and purification kit was used throughout this work for this purpose. The DNA fragment was excised from the agarose gel and incubated in 2 volumes of DNA binding buffer at 65 °C until the agarose was solubilized. The solution was then bound to the silica based gel columns and centrifuged for 1 min at 16,000 x *g*. The flow-through was discarded and the column was washed once with 0.7 ml wash buffer. A dry run was performed for another min after the washing step to completely remove residual ethanol present in wash buffer from column. The

DNA was eluted with 30 µl 10 mM Tris-1 mM EDTA, pH 8.0. After 1 min of incubation, the column was centrifuged for 1 min at 16,000 x *g* to recover the DNA.

3.6.3.4 Desalting of DNA solutions

Desalting of DNA reaction mixtures for subsequent enzymatic reactions and for the removal of primers from PCR reactions was accomplished by the QIAquick PCR purification kit (Qiagen) and the Amersham Gel band and solution purification kit. It is based on the same principle of DNA-binding to silica gel as used for the isolation of DNA from agarose (Section 3.6.3.3). The DNA is bound to the appropriate buffers per the manufacturer's instructions and then applied to silica columns. DNA is bound to the column by centrifugation for 1 min at 16,000 x *g*. The column were washed with 0.75 ml of wash buffer (PE) and centrifuged twice for 1 min at 16,000 x *g* to completely remove buffer PE. The DNA was eluted with 50 µl 1 mM Tris, pH 8.0.

3.6.3.5 Preparation of PCR-derived DNA fragments for ligation reactions

The DNA fragments obtained after PCR were analysed by agarose gel electrophoresis as described under section 3.6.3.2. The appropriate size DNA fragments to be ligated into expression vectors were digested with the suitable restriction endonucleases to produce cohesive ends as follows: 70 µl DNA preparation (3.6.3.1), 10 µl of the restriction endonuclease reaction buffer and 100 units of each restriction endonuclease were mixed in a total volume of 100 µl. After incubation at 37°C for 1h, the DNA was purified from the reaction mixture as described under 3.6.3.3.

3.6.3.6 Preparation of vector DNA for ligation reactions

The vector DNA was prepared as described under 3.6.2.1. For restriction of vector DNA, 70 µl Miniprep™ plasmid DNA solution was digested with 100 units each of the appropriate restriction endonucleases in a total volume of 100 µl supplemented with reaction buffer as recommended by the manufacturer. After 1h

at 37°C, the DNA was purified from the reaction mixture as described under 3.3.3.3. The 5´-phosphate group was removed from the linearized DNA molecule to prevent re-ligation of vector DNA. Two different phosphatases were used: shrimp alkaline phosphatase (SAP) and calf intestinal phosphatase (CIP). The DNA was dephosphorylated with 1 unit SAP per pmol 5' ends in 1x SAP buffer or with 1 unit CIP per pmol 5' ends in 1x NEB3 buffer by incubation for 1 hour at 37 °C. The SAP was inactivated by incubation for 15 min at 75 °C, the CIP was inactivated by incubation for 10 min at 75 °C in the presence of 5 mM EDTA. The digested and dephosphorylated vector was purified via agarose gel extraction.

3.6.3.7 Restriction analysis of DNA for ligation reactions

Plasmid DNA isolated from transformed bacterial cells (3.6.1 and 3.6.2), and PCR products were generally analyzed via agarose gel electrophoresis. The plasmid DNA digested with restriction endonuclease(s) and the PCR DNA fragments for construction of desired recombinant plasmid was analyzed on an agarose gel as described under section 3.6.3.2.

3.6.3.8 Ligation of DNA molecules

The linearized and dephosphorylated vector DNA and the restriction digested PCR product were desalted using the Amersham PCR purification kit before ligation. The ratio between linearized vector and insert DNA in a ligation reaction was ideally 3:1, roughly estimated through agarose gel analysis. All ligation reactions were prepared by mixing 2 µl 5x ligase buffer (NEB), 2-4 µl insert DNA, 1 µl vector DNA, 1 µl 10 mM ATP and 2 µl T4 DNA ligase (NEB) to total 20 µl reaction volume (made up by adding water) in a standard PCR tube. The reaction mixtures were inserted in a PCR thermocycler and, after an initial step of 24°C for 15 min, cycled for 99 cycles of 22°C for 5 min, 18°C for 2 min and 16°C for 2 min followed by 1 h at 12°C. This reaction mixture was used for transforming bacterial cells (3.6.6) without further modification.

3.6.3.9 Sequencing of plasmid DNA

The sequencing of the plasmid DNA and the new domains were done as per Sanger dideoxy chain termination method for DNA sequencing (Sanger et al., 1977, 1980). Usually the DNA samples were prepared at the laboratory using the standard protocols described under section 3.6.3.1 – 3.6.3.8 and sent to commercial and academic companies for analysis of the whole sequence. The sequence data was analysed according to the available data at the NCBI website.

3.6.4 Site Directed Mutagenesis – introduction of point mutations

Point mutations were introduced into genes cloned in expression vectors, using the QuickChange™ site-directed mutagenesis kit (Stratagene). The recommended protocol and precautions were sternly followed to allow specific mutations to be introduced in the sequences. Primers were designed such that the respective mutations were flanked by approx. 30 complementary bases on either side to guarantee specific annealing. Successful mutagenesis was approved by DNA sequence analysis (3.6.3.9).

3.6.5 Cloning for Expression constructs in *E. coli*

The plasmids pET28a, pET52b (Novagen, Madison, WI, USA) and pQE-Trisystem (Qiagen, Hilden, Germany) were used for the cloning of expression constructs from the phytochrome genes in *E. coli*. The plasmid pET28a includes a T7 Promoter with a lac-operator gene and a Kanamycin resistance gene, while the plasmid pET52b has an Ampicillin resistance gene. The vector pQE-Trisystem has an UV-5 promoter region, with the multiple cloning site flanked by selectively available His and Strep tags. This vector is also acknowledged with an Ampicillin resistence selection of bla (beta lactamase) gene. The cloning is usually performed by the directional cloning method so that the start of the gene is oriented toward the inducible promoter in the plasmid. The various steps performed for such clonings are described under sections 3.6.3.1-3.6.3.9.

3.6.6 Transformation of DNA into competent *E. coli* cells

3.6.6.1 Preparation of chemically competent *E. coli* cells

Competent *E. coli* cells are prepared via the $CaCl_2$ method according to Mandel and Higa (1970). 100 ml LB-medium were inoculated with an overnight grown culture of *E. coli* XL-1 Blue or BL21 (DE3) RIL / RIPL cells, and following were grown in a rotary shaker at 37 °C and 180 rpm to an OD_{600} of 0.5. The cells were harvested at 4 °C by centrifugation for 10 min at 3000 x *g*. The cells were kept on ice during the whole procedure. The pellet was resuspended in 30 ml ice-cold 100 mM $MgCl_2$, and the cells were centrifuged again for 10 min at 3000 x *g* and 4 °C. The cells were then resuspended in 100 ml ice-cold 100 mM $CaCl_2$ and incubated on ice for 45 min, followed by centrifugation (10 min, 3000 x *g*, 4 °C). Another wash of the cells was performed using 20 ml of ice-cold 100 mM $CaCl_2$. After incubation on ice for 90 min, glycerol was added to the cells to a final concentration of 20%. The cells were either used directly or were frozen in liquid nitrogen in aliquots of 200 µl and stored at –70 °C.

3.6.6.2 Transformation of $CaCl_2$-competent *E. coli* cells

$CaCl_2$-competent cells were transformed according to the method of Cohen et al. (1972). An aliquot of competent cells was removed from the –70 °C freezer and thawed on ice. The DNA was added to competent cells, followed by gentle mixing and the solution was incubated on ice for 30 min. A heat shock was given to the cells incubated with DNA for a short time as 45 sec-1 min. The cells were then grown on a rotary shaker for 60 min at 37 °Cand 180 rpm, after adding 200 µl of SOC medium. The cells were later plated on appropriate antibiotic plates which were incubated overnight at 37 °C.

3.6.6.3 Preparation of electrocompetent *E. coli* cells

Electrocompetent *E. coli* cells were prepared according to Dower et al. (1988) by repeatedly washing and resuspending the cells in a high density in a buffer with low conductance. LB medium was inoculated with 1 ml of overnight culture of *E. coli* XL-1 Blue or expression cells (Bl21 DE3 RIL), and grown in a rotary shaker at 37 °C and 180 rpm to an OD_{600} of 1.0. The flask was removed from the shaker and cooled down to 4 °C in an iced water bath. After 20 min, the bacteria were harvested by centrifugation in 450 ml centrifuge tubes at 4 °C for 10 min at 3600 x *g*. The cell pellet was resuspended in a 6X volume of the original culture volume of ice-cold EP-medium. The cells are then repeatedly washed with ice cold EP buffer, and were centrifuged three more times under the same conditions as described. There is step wise reduction in the volume of the buffer used for three washings done. The final resuspension is in 2 ml EP-medium, supplemented with 15% glycerol. The cells were either used directly or frozen in liquid nitrogen in aliquots of 200 µl and stored at –70 °C.

3.6.6.4 Transformation of electrocompetent *E. coli* cells

For the transfer of DNA into electrocompetent *E. coli* cells as prepared in 3.10. 3, the cells were thawed on ice. The plasmid DNA preparations (50 -100 ng) were mixed with 70 µl of electrocompetent *E. coli* cells. A 5 µl aliquot of DNA from ligation reactions was used for transformation usually combined with 75 µl electrocompetent *E. coli* cells. The cells were transferred to ice cold electroporation cuvettes (0.2 mm gap width, Eppendorf) and incubated on ice for 5 minutes. Electroporation was performed using a Biorad Gene Pulser System (Bio-Rad) with the settings for *E. coli*: charging voltage 2.4 kV, resistance 200 Ω, capacitance 25 µF. The transformed cells were immediately resuspended in 0.5 ml SOC medium, transferred to 10 ml plastic cell culture tubes, and incubated for phenotypal gene expression in a shaker for 45 minutes at 37 °C. Bacteria were plated out (50 µl in all cases where plasmid DNA preparations were to be transformed and 300 µl in all other cases) on LB agar plates containing the appropriate antibiotic and were incubated overnight at 37 °C.

3.7 Protein Chemical Methods

3.7.1 Heterologous protein expression in *E. coli* BL21 DE3 RIL/RIPL

The coding regions of the full length phytochrome proteins and its respective domains were amplified as specified in section 3.7. The genes were subcloned into the pET28a (+) vector (Novagen, Merck), placing a His_6-tag at the carboxy terminus of the protein. The plasmids were transformed into the *E. coli* strain BL21 (DE3) Gold (Novagen) by electroporation of competent cells and subsequent selection on LB agar plates containing 50 µg ml^{-1} kanamycin. Expression was performed in TBY medium (Sambrook et al., 1989) at 30°C with vigorous shaking.

Single colonies were screened for the over-expression of the proteins with appropriate antibiotic selection medium. For the overexpression, an overnight *E. coli* cell culture in 50 ml LB broth was diluted 100-fold in a 5 l side baffled conical flask with TBY broth (Sambrook et al., 1989). This culture was then incubated on a platform shaker at 37 °C and 180 rpm until the cells reached an OD_{600} of 0.8. Expression of protein was induced by the addition of IPTG to a final concentration of 0.4 or 1.0 mM. Small aliquots were taken at every 2 hours of the upscaled culture, the bacteria collected by centrifugation in a microcentrifuge tube, and lyzed by the addition of 100 µl 2x SDS sample buffer. Total cell proteins were analyzed by 2x SDS-PAGE as described under 3.3.2.3(d). A Coomassie-stained prominent protein band of the appropriate molecular weight indicated the expression of the desired protein. As a reference, a sample of the bacterial culture taken prior to induction with IPTG was used.

The cells after induction were let grown further for 6-10 hours, and were harvested by centrifugation for 15 min at 2200 x *g* and 4 °C. After determining the weight of the pellet, it was stored at -20 °C or directly used for isolation of the expressed protein.

3.7.2 Extraction of proteins

The extraction of the proteins was carried out by resuspension of the wet cells either directly or after thawing on ice in protein lysis buffer. All steps were carried out on ice or in a cold room at 4 °C. The buffers used here were all degassed prior to use for purification of proteins either manually or using FPLC. Bacterial cells as obtained from 3.11.1 were resuspended in 0.5 volumes of lysis/extraction buffer (3.3.2.3(a)) supplemented with 0.2 mM EDTA, Complete™ protease inhibitor cocktail (Roche) and Pefabloc (final concentration 200 mM) and disrupted either by sonification or in liquid nitrogen with an Ultra Turrax T25 (Jahnke & Kunkel, Staufen Germany). After evaporation of the liquid nitrogen, the homogenate was thawed on ice. After the addition of appropriate amounts of DNase I the cytosolic proteins were separated from insoluble debris by centrifugation at 50,000 rpm at 4 °C for 45 min.

3.7.3 Purification of overexpressed proteins from *E. coli*

The protein purification was carried out either manually or utilizing an Äkta Basic 10 / 100 Amersham Pharmacia Biotech (General Electric- Life Sciences) was used. ÄktaTM basic is an automated liquid chromatography system designed for method development and research applications.

3.7.3.1 Ammonium sulfate precipitation

The protein lysate was purified and concentrated at the initial step by ammonium sulfate precipitation. For this, one volume of protein lysate was precipitated with 1 -1.5 volumes of 3.3 M $(NH_4)_2SO_4$ prepared in extraction buffer (Section 3.3.2.3(a)). The salt solution was added gradually during 1 hour to the protein solution on ice. The precipitate was pelleted by centrifugation for 30 min at 39,000 x *g* and 4 °C. The pellet was dissolved in an appropriate volume of 50 mM Tris, pH 7.8, 250 mM NaCl. Subsequently, the solution was cleared by centrifugation for 10 min in an Eppendorf centrifuge at 16,000 x *g* and 4° C.

3.7.3.2 His-tag affinity purification

The heterologously expressed proteins in *E. coli* have been designed to have a six- histidine tag at the N- or C-terminus, during gene modifications. This makes the purification of the recombinant proteins very handy by using affinity purification methods like Immobilized Metal Affinity Chromatography (IMAC). This method is based on the interaction between divalent metal ions (like Co^{2+}, Ni^{2+}, Cu^{2+} and Zn^{2+}) and the (unprotonated) imidazole ring of histidine. These metal ions have six coordination sites available for interaction with electron-rich ligands. In the Nickel-NTA, Nickel-IDA resin used here, tetradentate chelators bind the metal ions to the chromatographic substrate, leaving two sites available for interaction with histidine residues. Extensive washing of the resin with increasing concentration of Imidazole in the wash buffer leads to removal of the non-His_6 proteins. The desired His_6 proteins can hence be eluted by competitive elution with imidazole or by lowering the pH (resulting in protonation of the imidazole ring of the histidines, which is then repelled by the metal ions). Phytochrome spectral activity was found to be favored by purification method using increment of imidazole concentration rather than pH drop, where apoprotein lost most of the spectral activity (Mozley et al., 1997). Therefore, in this work, only elution with imidazole was used.

Manual purification: The NiNTA™ metal affinity resin (Qiagen) was washed 2 - 3 times with wash buffer (at least 1 ml resin per 5 mg His_6-protein). Then the reconstituted crude phytochrome solution obtained above was bound to the resin by incubation for 1-2 hours at 4 ^{0}C and 30 min at room temperature (in the dark) with gentle agitation to keep the resin in suspension (for most efficient binding, the resin should comprise 0.05 - 0.1 x the total volume). The resin was allowed to settle by gravity and the supernatant was removed. The resin was, resuspended in a small volume of buffer, transferred to a gravity column, and allowed to settle by gravity. The column was first washed with 20 ml of wash buffer. The His-tagged protein was eluted with 4 ml of elution buffer (containing 200 - 300 mM imidazole).

FPLC automated purification: The resuspended protein lysate was applied to a Ni-NTA column (1.6 x 10 cm) equilibrated in protein lysis buffer. The column was washed with 30 column volumes of the buffer containing 10 mM imidazole, at a flow rate of 1.5 ml min^{-1} and developed with an imidazole gradient (1 ml min^{-1}) from 25 mM to 250 mM imidazole in lysis (binding) buffer. Eluent fractions were analyzed by SDS-PAGE and those containing the protein of interest were pooled and concentrated using an Amicon centriprep device with appropriate cut off.

3.7.3.3 Preparative Gel-Filtration chromatography

The affinity purified proteins after concentration were applied (flow rate: 0.53 ml min^{-1}) to a HiLoad 26/60 Superdex™ 75 prep grade column (GE Life Sciences) pre-equilibrated with buffer (20 mM Tris HCl, 50 mM NaCl, 5% glycerol, pH 7.8). In general, the eluted proteins were essentially pure (>95%) as judged from SDS-PAGE analysis. Proteins were concentrated to 5-10 mg ml^{-1} by centrifugation with an Amicon centriprep 10, 30 or 50 ultrafiltration device. Quality and purity of the final samples were monitored by SDS-PAGE and ESI mass spectrometry.

3.7.3.4 Dialysis

The purified proteins containing high amounts of imidazole or any other salt were subjected to dialysis. Proper molecular size exclusion cut-off dialysis membranes were used for this purpose. The concentrated protein solutions were dialyzed against 400- 600 volumes of buffer with minimum salt concentration at 4 °C. Usually apo-proteins were dialyzed at this step, although sometimes holoproteins were also put through dialysis to remove unwanted salts.

3.7.3.5 Protein Concentration

The purified protein samples were concentrated before their biochemical characterization. The concentration was done using Ultrafiltration method with

Ultrafree 15 Biomax 10K, 30K or 50K (Milipore, Bedford, MA, USA), filter devices. The concentration of samples was perfomed by centrifuging at 4 °C and 2000 xg as per manufacturer's instructions.

3.8 Protein Content Estimation

3.8.1 Standard SDS-polyacrylamide gel electrophoresis (SDS-PAGE)

Complex protein mixtures or purified protein preparations were separated and analyzed by standard SDS-PAGE (Laemmli, 1970). NuPAGE minigels (Invitrogen) generally used were 4-12% acrylamide/bis-acrylamide gradient gels. Minigels were also prepared for the Bio-Rad apparatus with acrylamide/bis-acrylamide solutions (Serva™) with 13% in the separating gel and 7% in the stacking gel and were cast in a multiple gel caster (BioRad, Amersham Biotech). Protein samples to be analyzed were denatured by adding 2x SDS sample buffer (10 % SDS, 50 mM Tris HCl, 1 mM EDTA, 0.04 % bromophenolblue, 20 % 2-mercaptoethanol, pH 8.0) and incubation at 80 °C for 5 min. The gels were run in a Minigel Electrophoresis Unit (BioRad or Amersham Pharmacia) at 130 to 180 V until the tracking dye reached the bottom of the gel. Prestained Protein Marker (Invitrogen See Blue 2) was used as the molecular weight marker. After electrophoresis, the gel was fixed by 2 x 5 min incubation in 40% ethanol, 10% acetic acid. Proteins were visualized by staining with Coomassie brilliant blue solution (0.025% Brilliant Blue R250 (Sigma), 25% $ethanol_{tech}$, 8% acetic acid), and subsequent destaining (40% ethanol, 10% acetic acid) to remove background staining. To prevent cracking of the gel during drying, the gel was washed for 5 min in 10% glycerol and rinsed in water, before allowing it to air-dry.

3.8.2 Immuno-detection of immobilized proteins (Western Blotting)

Protein samples were separated by standard SDS-PAGE (3.3.2.3 (d)) and subsequently transferred to a nitrocellulose membrane in a tank transfer system (Invitrogen). The proteins on the gel were blotted, according to the method of

Towbin (Towbin et al., 1979), onto a PVDF membrane via wet or semi-dry electrophoretic transfer in the NuPAGE Transfer System. After removing the stacking gel, the running gel was equilibrated in transfer buffer (25 mM Tris, 192 mM glycine, 20% ethanol, 0.1% SDS) for 5-15 minutes. The transfer sandwich was assembled under transfer buffer in the following way: the gel and the wet (H_2O) nitrocellulose membrane were placed between two pieces of transfer buffer drenched blott paper (3 mm, Whatman). This sandwich was covered with a sponge on both sides and placed into a transfer cassette, taking care to remove all air bubbles from the layers. The transfer cassette was inserted into the tank filled with transfer buffer, such that the membrane was oriented towards the anode. The proteins were transferred at constant current (400 mA, approx. 100 V) within 1 hr. Prestained protein standard was run alongwith the protein preparations to verify transfer.

After disassembling the sandwich, the gel was generally stained with Coomassie blue and the blotted membrane was washed thrice in wash buffer for 10 minutes followed by incubation for 30 - 60 min (at room temperature) in block buffer to saturate nonspecific protein binding sites. The blocking buffer was washed out with 3 x 10 min washes with wash buffer containing Tween-20. The membrane was then incubated for 1 hour at room temperature with the primary antibody (anti penta-His, Qiagen), diluted 1:1000 in incubation buffer. The blot was washed again for 3 x 10 min in wash buffer and then incubated for 1 hour (at room temperature) with the secondary antibody (rabbit-anti-mouse-AP conjugate (with conjugated alkaline phosphatase), Dako), diluted 1:5000 in wash buffer. After washing 2 x 10 min in wash buffer and 2 x 5 min in substrate buffer, the blot was incubated in AP- (alkaline phosphatase) color development solution in dark. The chromogenic reaction was stopped by washing in distilled water.

3.8.3 Estimation of protein apparent molecular weights by gel filtration

To determine the apparent molecular weight of protein samples in solution, the gel filtration columns HiLoad 26/60 Superdex 75 prep grade and Superdex 200 prep grade (Amersham) were calibrated with protein standards of defined molecular weight and conditions used throughout all purifications (3.12). The reference proteins were dissolved in the same buffer used for purification of expressed proteins and separated at a constant flow of 0.53 ml min^{-1}. Standards used were ferritin (450 kD), aldolase (158 kD), bovine serum albumin (68 kD), albumin (45 kD), chymotrypsin (25 kD), cytochrome C (12.5 kD) (Boehringer-Mannheim). The molecular weights of the purified proteins were correlated accordingly with the respective fitted exponential equations for the calculation of apparent molecular weights (y, kD) for a given elution volume (x, ml).

3.8.4 Estimation of protein molecular weights by MALDI-TOF MS (matrix assisted laser desorption ionisation-time of flight mass spectrometry)

The purified proteins were also analyzed by MALDI-TOF MS that was considered a measure of purity as well as accurate determination of the molecular mass of a purified protein. The procedure involved embedding of the protein sample (prepared after gel filtration in 20 mM Tris.HCl buffer) in a solid matrix, which absorbs the energy generated by a LASER beam. The laser energy absorbed characteristicaaly ranging up to the order of 10^6 watts/cm^2, leads to intense heating and generation of a plume of ejected material that rapidly expands and undergoes cooling. High vacuum within the mass spectrometer assists in the process of gradual shredding of the protein from matrix and solvent molecules and hence its separation according to its apparent mass to charge ratio.

The experiments were conducted on either a Voyager-DE PRO Workstation or a Voyager-DE™ PRO Biospectrometry Workstation from Applied Biosystems (USA). The matrices used here were either α-cyano-4-hydroxycinnamic acid (CHCA) (M1),

or 2,5 - dihydroxybenzoic acid (2,5 - DHB)(M2), Sinapinic acid and a mixture of 2,5 - dihydroxybenzoic acid and 5-methoxysalicyclic acid (DHBs).

3.9 Protein Assays

3.9.1 *In vitro* reconstitution of heterologously expressed phytochromes with chromophore

Before reconstitution, the pH of the protein solution was readjusted to 8.0 with 1 M Tris. All steps involving phycocyanobilin (PCB) or biliverdin (BV) chromophores were carried out under inert green light conditions (Δ_{max} = 485 ± 20 nm). PCB was isolated from the alga *Spirulina platensis* following the method from Kufer & Scheer (Kufer and Scheer, 1979a,b). Approximately 2 mg (the tip of a micro spatula) of PCB were dissolved in 200 µl cold DMSO (dimethylsulfoxide) and diluted with 800 µl water. This stock solution was used to reconstitute the apo-protein by adding aliquots to a clarified cell lysate or purified samples from 3.12. The formation of holo-phytochrome was monitored by following the increasing characteristic absorption at 664 nm / 704 nm for PCB and BV, respectively, with a UV/VIS spectrophotometer (3.15.1). To guarantee complete assembly, the chromophore was added in small portions up to a 5- to 10-fold molar excess. After equilibration, excessive PCB was removed by gel filtration chromatography (3.12.3).

3.10 Spectroscopic Methods

3.10.1 UV/VIS Spectroscopy of recombinant phytochromes

For the spectroscopic characterization and the recording of P_r/P_{fr} difference spectra, a Shimadzu UV-2401 PC Spectrophotometer and quartz cuvettes (path length 10 mm) were used. Samples were generally illuminated for 30-120 sec (concentration dependent) with red light (658 ± 7 nm interference filter) and far-red light (> 715 nm RG9 cut-off filter), respectively, in order to generate the two

photoisomeric states P_r and P_{fr} respectively. The spectra were recorded in the range of 200 to 850 nm and difference spectra were calculated by subtracting the P_{fr} -spectrum from the P_r -spectrum.

3.10.2 Assembly kinetics

To determine the chromophore assembly kinetics, the rise in absorption at the λ_{max} of the P_r form directly after addition of the chromophore was measured at 10 °C. To be able to correct for possible changes in scattering or a shift of the absorption maximum, spectra were recorded from 600 - 750 nm at regular time intervals. A detection-interval of 2 nm was used instead of the normally used interval of 0.5 nm, enabling recording of a spectrum with high scanning speed every 20 s. The chromophore (about ten-fold molar excess to the apophytochrome) was dissolved in DMSO at high concentration and diluted to 30 µl in buffer. The cuvette with apoprotein (470 µl) was placed in the spectrophotometer and cooled to 10 °C. The chromophore was added to the apoprotein with a Hamilton syringe and mixed by "pipetting" up and down a few times. By this way it was possible to start recording the first spectrum within 15 s after the addition of the chromophore.

3.10.3 Pfr dark reversion

To determine the thermal stability of the Pfr form, the samples were first converted to Pfr by 5 min of irradiation with red light (658 nm interference filter). Directly after irradiation, spectral changes were recorded by measuring spectra from 450 – 850 nm at room temperature (20 °C) at regular time intervals. The increase of absorption in the Pr-maximum was used to determine the Pfr dark reversion. At start and end of the experiment, difference spectra were recorded to determine an eventual decrease of the absorption due to degradation of the protein.

3.11 Crystallization trials

Protein Crystallographic Techniques

The word 'crystal' is derived from the Greek root 'krustallos' meaning clear ice. Crystals are chemically well defined, with their flat faces and their physical anisotropy. They reflect the regular packing of molecules, atoms or ions in the crystal. Even though obtaining crystals of high quality that are suitable for X-ray structure determination is the compulsive basis, it is also the least understood step in the process of crystal structure analysis. Biocrystallization, the crystallization of biological macromolecules like proteins, DNA, RNA or their complexes, like any crystallization, is a multiparametric process involving the three classical steps of nucleation, growth, and cessation of growth. Usually, a solution containing the molecule to be crystallized must initially be brought to a state of supersaturation, which will ideally force the macromolecules to arrange in a regular 3-dimensional manner. Because of the complexity of the particles (proteins, nucleic acids etc.) involved in biocrystallization, the crystallization itself is often the primary obstacle that sometimes proves to be insurmountable.

All preliminary crystallization experiments were performed using the hanging or sitting drop vapor diffusion method (Davies & Segal, 1971) and a *sparse matrix* strategy (Jancarik and Kim, 1991). The latter was chosen because of the commercial availability of standardized kits covering a broad factorial space of crystallization conditions and providing the benefits of industry standards, meeting the high demands regarding purity and consistency over different charges. The *sparse matrix* strategy is an empirical approach, based on crystallization conditions that have successfully been utilized to crystallize biological macromolecules as introduced by Jancarik and Kim, 1991.

The initial screening of crystallization conditions was done randomly so as to address a variety of screening conditions with varied parameters such as pH

value, buffer type, type and concentration of precipitant etc. These set of experiments was selected based on factors making them compatible with a given protein. The experiments were studied under the microscope to gain knowledge about the conditions most compatible with the protein to be in solution, whereas conditions that immediately or within the first days produced brownish cloudy precipitate were excluded from further testing. Conditions that yielded any kind of crystalline arrangement in the droplets served as starting points for the optimization of the respective condition. This was accomplished by designing experiments where the conditions were varied as per the protein concentration as also the precipitant concentration, also allowing to put use of a two dimensional approach with two varying conditions, i.e. pH-value and precipitant and thereby narrowing the variation space of the crystallization parameters involved.

In the experiments involving phytochrome proteins, crystallization screens were set up under well defined light conditions, either inert green light (λ_{max} = 485 nm) or far red light (cut-off λ > 715 nm). Prior to incubation in the dark at 18 °C, the droplets were additionally exposed to far red or red (λ_{max} = 635 ± 7 nm) light in order to shift the photo equilibrium to either the Pr or the Pfr form. The crystallization screens utilized are listed in the Appendix in more detail.

3.12 Isothermal Titration Calorimetry- ITC

Isothermal Titration Microcalorimetry – Microcalorimetric experiments were performed on an MCS isothermal titration calorimeter (Microcal Inc., Northampton, MA) at the Max-Planck-Institute for Molecular Physiology in Dortmund (Dept. Prof. R. Goody). The purified proteins were used, where the concentration was determined by UV measurements for photochemically active proteins using the extinction coefficient of the relative chromophores, or by UV 260 / 280 ratio. The proteins were concentrated and their ratio in the cell versus syringe was adjusted to 1: 5 or 1: 10 as per their molarity. The ligand or the binding proteins was loaded into the syringe of the microcalorimeter. Both solutions were thoroughly degassed prior to loading. After temperature equilibration, the ligand was injected into the cell in aliquots under controlled volume conditions, and the evolved heat was measured with the first injection not considered for data analysis. A total of 24 injections were performed with 2-min equilibration times between injections. Data were corrected for heat of dilution by measuring the same number of buffer injections and subtraction from the sample data set. Dissociation constants were determined using the MicroCal Origin version 7 analysis software and the model of binding sites.

3. 13 FTIR spectroscopy

FTIR measurements were carried out in collaboration with the Biophysics Research Group of University of Freiburg (Prof. F. Siebert). Experiments were performed on a Bruker IFS-28 Fourier transform infra red spectrophotometer equipped with a MCT detector and a dry air purged sample chamber.

Sample preparation: The phytochromes, CphA and CphBm, were initially dissolved in a 10 mM Na-phosphate buffer, pH 8, containing 2 mM DTT and 200 µM Pefabloc. The stock protein concentrations were determined by measuring the UV absorbance of a diluted solution at 280 nm, where the extinction coefficient

used was the one for Cph1 from *Synechocystis* (83000 $M^{-1}.cm^{-1}$ (Murgida et al., 2007)). The concentration of CphA was 1.378 $g.l^{-1}$ ($2.12x10^{-5}$ M) while that of CphBm was 16.4 $g.l^{-1}$ ($2.5x10^{-4}$M). For both UV-vis and infrared measurements, sandwich samples were prepared: about 1 nmol concentration of CphA i.e. (60 µl of CphA protein and 4 nmol concentration of CphBm i.e. (16 µl of CphBm protein), were dried, using a gentle stream of nitrogen, on the central spot (7 mm diameter) of a BaF_2 infrared window, used for the so-called sandwich sample form described elsewhere (Vogel and Siebert, 2003). The obtained homogeneous film was rehydrated by adding 6-8 µl buffer and sealed by placing a second plane BaF_2 window on top of the first one, the higher rim serving as a spacer. This sample form guarantees full hydration at defined pH and buffer composition. The quality of the film was increased when the protein solution was first dialysed against a 5 mM Tris, 10 mM NaCl buffer, containing 2 mM 2-mercaptoethanol and 0.2% vol) glycerol.

For measurements in D_2O, exchange of water to D_2O was accomplished by 5 successive additions and evaporation of D_2O on the protein film, which was finally re-solvated using 6-8 µl of D_2O. The Pr:Pfr photoconversion was initiated by irradiating the sample with fiber optics connected to a 150 W slide projector fitted with a band-pass filter with peak transmission at 633 nm and half-width of 9 nm (BP633). A long pass filter (Schott, RG695) was used for the Pfr to Pr conversion. Observing the changes in the UV-vis spectrum between 400 and 800 nm as a function of illumination time, saturating Pr to Pfr photoconversion was obtained after 6 minutes. This duration of illumination was used for all intermediates.

Cryogenic experiments. Both for UV-vis and FTIR spectroscopy, the spectrometer was equipped with a home-built cryostat which allows measurements in the temperature range between -190 and 0 °C (±0.5 °C). Before insertion into the cryostat, the samples were converted, at room temperature, either into the Pr state for measurements of the intermediates of the Pr:Pfr pathway or into the maximum

Pfr state for measurements of the reverse reaction, using the above described filters.

UV-Vis measurements. The absorption spectra were measured on a Perkin-Elmer Lambda 17 spectrophotometer in the range between 250 to 800 nm at a scan speed of 120 nm/min and a slit width of 2 nm. Due to the low extent of photoconversion at low temperature, only difference spectra are shown, which are obtained from the absorption spectra measured before and after illumination of the sample.

FTIR measurements. The spectra were measured using a BRUKER IFS 28 Fourier-transform infrared spectrophotometer equipped with an MCT detector and a dry-air purged sample chamber. The degree of rehydration of the protein film was checked using the broad absorption band of water around 3300 cm^{-1}. Sealing the sandwich windows with silicone on the edges prevented dehydration of the film in the cryostat. The intermediates were accumulated by irradiation of Pr or Pfr at the temperatures given in the figure captions. The phototransformation back to the initial state had to be performed at ambient temperature. For each single-beam spectrum, 512 scans were accumulated with a resolution of 4 cm^{-1}.

3. 14 Bio-informatic methods- Software and databases

3.14.1 Data Banks

The proteins as well as the nucleotide sequences were collected and analysed using the data bank databases from Swiss-Prot and TrEMBL (http://us.expasy.org/sprot/). The protein molecular weight and trypsin digested proteins estimation was done using the TrEMBL software available online. The 3D structures were referred from Brookhaven protein data base (PDB) (http://www.rcsb.org/pdb/cgi/).

3.14.2 Structural visualization of Proteins

The program RasMol available for academic use at the website http://www.umass.edu/microbio/rasmol/ was put to use for the three dimensional molecular analysis of the proteins. The PSIPRED secondary structure prediction method (Jones DT, 1999) was used for the threading and secondary structure of various proteins.

3.14.3 Sequence analysis

BLAST and PSI-BLAST (http://www.ncbi.nlm.nih.gov/blast/) programs from the website were utilized for the sequence analysis of both nucleotides as well as proteins from the database available. The gene sequences were translated using ORF Finder at NCBI website.

3.14.4 Alignments

Multiple sequence alignments were performed with the shareware program CLUSTAL W (http://www.ebi.ac.uk/clustalw/) and processed using GeneDoc Multiple Sequence Alignment Editor & Shading Utility version 2.6.002 (Nicholas KB and Nicholas HB Jr, 1997).

The restriction pattern analysis for vectors and plasmids were carried out using the program Vector NTI version10 (InforMax, Inc., Gaithersburg, USA).

3.14.5 Other bioinformatics methods

The tools such as pI/Mw calculator programs at the Expasy server were used for calculating the molecular weight of the translated proteins in daltons. Website addresses are as follows (http://www.expasy.org/tools/pi_tool.html, http://www.expasy.ch/tools/peptide-mass.html).

The program WinPep 1.0 (L. Hennig, 1998) was used to calculate the molecular weight and the extinction coefficient at 280 nm of proteins using their amino acid sequence. Absorption spectra were processed with the program Microcal™ Origin™ version 10 (Microcal Software, Inc., Northampton, USA).

Chapter 4

Results

4.1 Optimization of expression of full length *Calothrix* phytochromes - Structural and functional analysis

4.1.1 Expression optimization of full length CphA and CphBm

Calothrix phytochromes, CphA and CphBm, from the cyanobacterium *Calothrix* PCC7601, with similar size (767 and 765 amino acids) and domain structure, were investigated for their spectral properties and subjected to various crystallization trials so as to get to the structural details of these light switch proteins. The full length protein expression was standardized to get optimal proteins with full functional characteristics through recombinant expression. *Calothrix* phytochromes, CphA and CphBm, respectively, are 88 kDa and 87 kDa proteins, which had been cloned previously in the group (Jorrissen et al.; 2002 and Quest, B. - 2004 doctoral thesis) to study the biochemical characteristics of these photoreceptors.

In brief, the plasmid pMEX8/pET 28a (+) carrying the coding sequence for the respective proteins, designed through genetic modulation so that these carry a C-terminal thrombin recognition site/His_6 peptide, was transformed into bacterial cells by chemical transformation or electroporation (3.6). The phytochrome ORFs CphA and CphBm (full length) were cloned in the pMEX8 / pET 28a (+) expression vector behind the tac /T7 promoter respectively, containing the lac operon and thus allowing for induction with IPTG. Positive transformants were selected on appropriate antibiotic agar plates and grown in TBY medium to an OD_{600} of 0.6-0.9. The expression was induced at various temperatures ranging between 18-30°C by adding IPTG to a final concentration of 400 µM to the culture and growth was continued for 10-16 hrs.

The concentration of phytochromes was analyzed by measuring the absorbance at 663 nm / 707 nm for CphA and 700 nm / 750 nm (Fig. 4.1) in difference spectra after assembly with their respective chromophores PCB or BV.

Both the full length proteins were relatively soluble, although the amounts of expression varied greatly during each expression. The highest expression achieved for CphA varied between 6-12 mg per litre, highest being 24 mg, while that for CphBm was 12-26 mg per litre of culture for the various experiments. The yields obtained were nearly double than previously reported for the same proteins. The expression in *E. coli* was improved using various strategies involving lowering of induction temperature, changes in media composition, and duration of induction thus resulting in higher amounts of reconstitutable phytochrome. The amount of the reconstituted phytochrome was determined by using the extinction coefficient of ε_{max} of 83,000 $M^{-1}cm^{-1}$ (Hughes and Lamparter et al, 1997). Cell lysis and the purification of proteins were done as described under 3.7.2 and 3.7.3. The quality of the final protein was verified by SDS-PAGE (Fig. 4.3) analysis. The specific absorbance ratio measured here is conclusive of the ratio of the total Pr to total protein absorbance i.e. A 660/700 : A 280.

Table 4 (a)- Detailed depiction of the heterologously expressed phytochromes

Sample	Weight of wet cells (g)	Concentration in 6 ml crude lysate	Expression level	SAR (Specific Absorbance Ratio)
88 kDa CphA	24	2 mg/ ml^{-1}	0.5 mg per g cells	1.1
87 kDa CphB	24	6 mg /ml^{-1}	1.5 mg per g cells	1

The total phytochrome concentration in the crude lysate or purified protein preparations were determined by measuring the amount of photoactive Phy samples, calculated from the maximal deflections in the Pr / Pfr difference spectra at 664/700 nm and 707/754 nm. The difference Δ(ΔA) between these peaks was

used for protein concentration calculation using the Lambert-Beer correlation between absorption and concentration of a given solution:

$$A = \varepsilon c d; \qquad A = \log_{10}(I_0 / I)$$

Molar extinction coefficient ε for the main absorption band at λ_{max} = 664 nm of the P_r-form of CphA is 80,000 [l mol^{-1} cm^{-1}] while for CphBm with λ_{max} = 700 nm is 88,000[l mol^{-1} cm^{-1}].

Here, ***A*** = absorbance of the sample in a quartz cuvette ; ***d*** = path length.

The table 4 (a) shown here summarizes the parameters of expression and purification of these two protein samples under standard conditions.

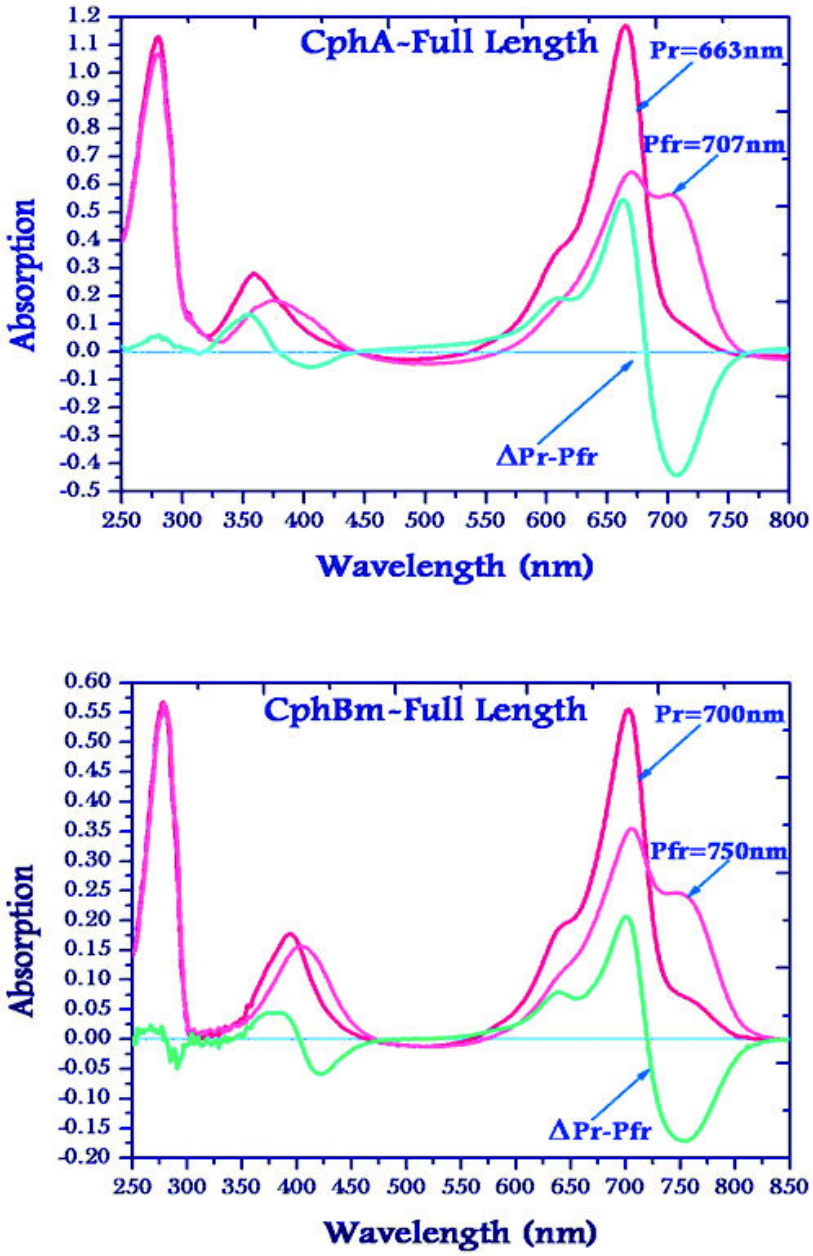

Figure 4.1 UV/VIS Absorption spectra of CphA and CphBm : Depicted are typical UV/VIS spectra of (a) CphA and (b) CphBm after standard purification processes. Both proteins exhibit the characteristic absorption band at 664/704 nm (P_r-form, marked red) and the photoinducible bathochromic shift (λ_{max} = 707/750 nm) after illumination with red light (635 nm ± 8; 680 nm), indicating the formation of the P_{fr} form (marked pink). The difference spectra (cyan line) were used to determine the protein concentration by calculating Δ(ΔA) between the Pr and Pfr absorption maxima. The spectra were recorded in quartz cuvettes after irradiation for 1 min for CphA and at least 2 min for CphBm for full photoconversion with the respective light quality (red for Pfr, far-red for Pr).

4.1.2 Increment in expression- methods used

The heterologous expression of phytochromes in *E. coli* had been standardized during this study so as to yield relatively high amounts of soluble proteins as compared to previous work done.

a.) Different expression cells: Expression of the His-tagged *Calothrix* phytochromes, both CphA and CphBm, was performed using various strains of expression cells *(E. coli)* which were modified to get at higher amounts of proteins (Table 4b). The amount of expressed protein varied in these different *E.coli* strains, with BL21 RIL and RIPL cells being best, individually as well as when grown together (mixed inocula of RIL and RIPL). CphA crude protein obtained thus was between 6 and 12 mg/litre while CphBm expression was increased from 6 mg (Quest doctoral thesis, 2004) to 12-26 mg/litre of culture.

Different strains of competent cells were used for transformation of plasmids housing the full length phytochromes, CphA-pMEX8 and CphBm-pET28a for over expression of protein. The different strains of *E. coli* used were BL21 (DE3) CodonPlus-RIPL, BL21 (DE3) CodonPlus-RIL, BL21, BL21 Star (Invitrogen), modifications of BL21 expression cells called C41 and C43 (Overexpress Tm, Paris). These strains have been engineered so as to yield highest expression of recombinant proteins (Section 3.2 and 3.7).

The transformed cells were grown on antibiotic medium, and single colonies were picked for the overnight inoculate. The up-scaling of the culture was done using 1-4% of this inoculum in baffled Erlenmeyer flasks and different parameters for expression were performed to get optimum protein in terms of quality and quantity. The test expressions were also conducted in 1 L culture medium using similar parameters. Soluble expression was compared to get best possible conditions of growth for all the proteins. An example of such experiment is represented graphically in the figure below (Fig. 4.2). The total amount of protein was measured spectroscopically, each such cuvette originally standardized to yield

photo-reactive proteins. Figure 4.2 depicts graphically the increase in the overall soluble yield of CphBm protein using different cell strains for expression conducted under same conditions of growth. Best expression results were obtained in the mix inoculum of BL21 (DE3) RIPL and BL21 (DE3) RIL.

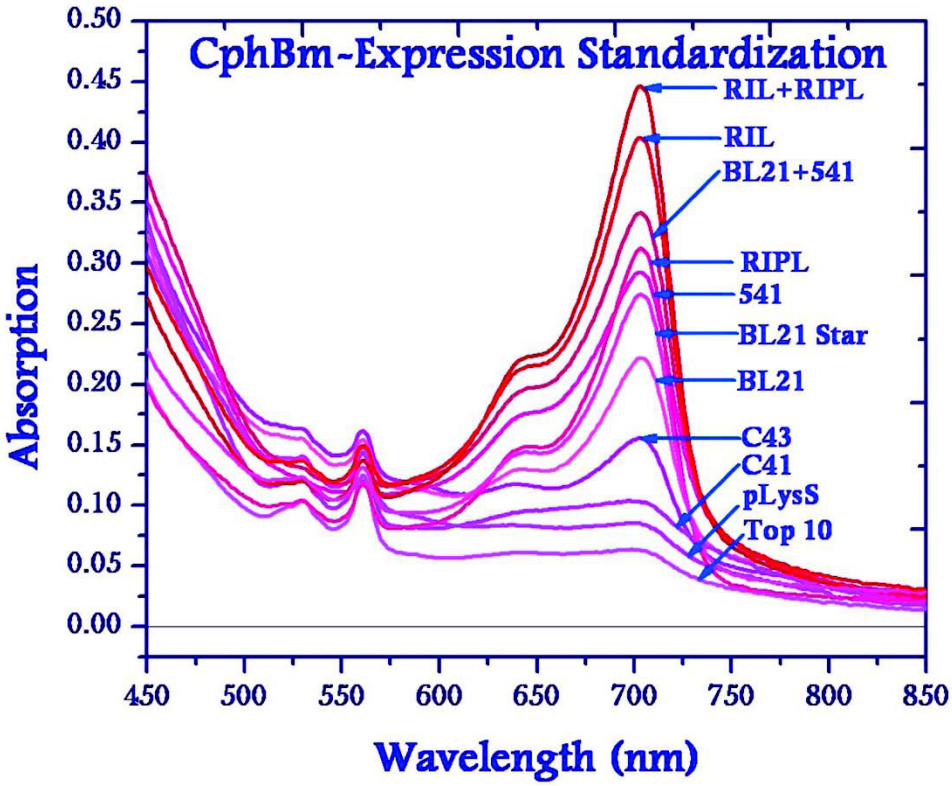

Figure 4.2 Spectrum of CphBm expressed in different competent cells : The mixed inoculum of BL21 (DE3) RIPL and BL21 (DE3) RIL expressed highly soluble protein.

b.) Chaperone co-expression: The plasmid p541, kindly provided by Prof. Bernd Bakau (LM-University of Munich), was also used for co-expression. This plasmid acts as GroEL/GroES chaperone system for improving the amounts of soluble proteins. There have been reports suggesting the role of the chaperone system in suppressing aggregation of the refolding native phytochromes after isolation (Grimm et al., 1993). The recombinant phytochrome was also co-expressed with this chaperone system in this study to attain properly folded homogenous protein.

Absorbance after 5 minutes irradiation in far-red light (Pr form) and amount of soluble protein obtained per milliliter of crude lysate is presented in table 4. This result showed that the amount of soluble protein depends on the used expression cells. After this result, a mixture of BL21 (DE3) RIL and RIPL was routinely used to grow the CphBm cells in further expression experiments.

c.) Lowering induction temperature: Another strategy applied for getting increased amounts of soluble proteins was lowering the temperature of induction. The induction temperature used here varied from 20-28 ˚C for different protein domains studied here.

All the above experiments evaluated for standardizing the highest expression of soluble phytochrome proteins here were performed under specifically similar conditions as per media composition, growth conditions, duration of expression, and protein extraction thus allowing a direct comparison of the spectral values (Figure 4.2).

Table 4 (b) – Soluble phytochrome yields using different competent cells

Competent cell strains	Pr Absorbance – Crude extract (20 ml) / liter expression (mAU)	Amount of soluble protein / ml crude lysate (in mg)
BL21 (DE3) RIL	0.445	0.490
BL21 (DE3) RIPL	0.403	0.443
BL21 (DE3) RIL and RIPL	0.538	0.600
BL21 (DE3)	0.010	0.118

4.1.3 Purification profile of the full length Phytochromes:

The purification of the full length proteins was done as described under the materials and methods section (3.7). Affinity purification was followed with

various steps of purification to get at least 85-95% purity of proteins to be used for crystallography trials. The extent of purification was checked using NuPAGE SDS gels as per manufacturer's instructions. 4 -12% Bis-Tris gels were used for the recognition of specific proteins and to analyze the purity of the protein with known molecular weight markers. Western blotting was also done for the recognition of specific proteins in a mixture of expressed proteins in the host cells. The proteins were run on the gel and blotted on the PVDF membrane. In the case of phytochromes from *Calothrix*, the western blot was done with the antibodies against the C-terminally located His tag. *Calothrix* CphA and CphBm showed the molecular weight of 88 and 87 KDa (Fig. 4.3). The molecular weights of the two proteins were according to those predicted using pI/MW calculator as well as previous biochemical estimations.

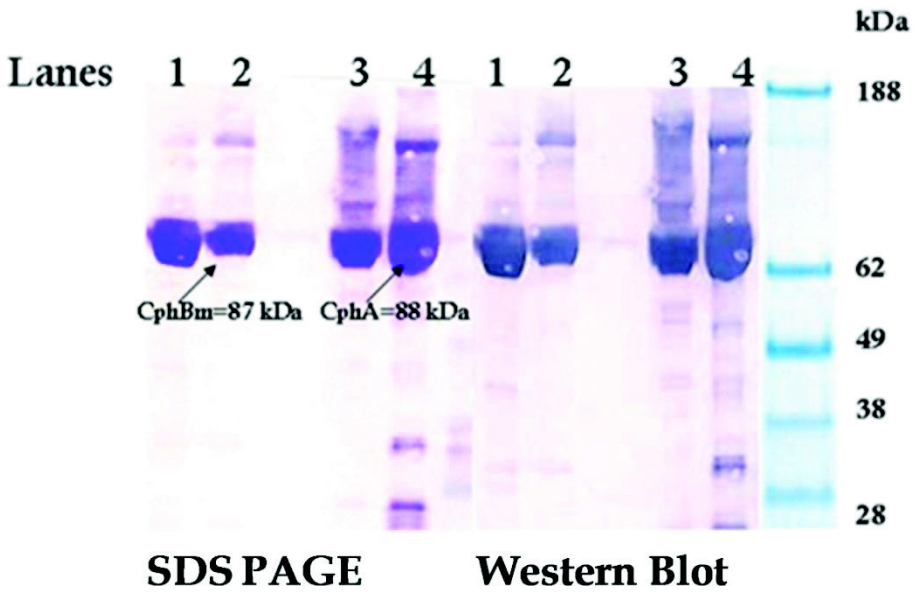

Figure 4.3 SDS-PAGE and Western blot analysis of Calothrix CphA and CphBm expression in *E. coli* : Lane 1 – 200 mM Imidazole eluate, lane 2 – 300 mM Imidazole eluate of *Calothrix* CphBm, Lane 3 - 200 mM eluate and lane 4 – 300 mM eluate of *Calothrix* CphA. M: molecular weight marker, the sizes (in kDa) are indicated on the right side.

4.1.4 Phytochrome crystallization

The protein obtained was passed through various purification steps so as to achieve maximum purity required for crystallography experiments. Set up for the crystallography experiments were done at FZ Juelich and at Ruhr University, Bochum. There has been partial success in terms of crystallography as these proteins were prone to aggregation and precipitation at high concentration required for crystallography trials.

Crystallization screening

The detection of atomic level structural organization of the proteins is achieved by X-ray crystallography, which is a challenging arena to work with such photoreactive proteins. The phytochromes present a very unique system to study for such purposes, so CphA and CphBm, both were extensively put through various crystallography trials in order to obtain single crystals. The extensively purified, polished and spectroscopically characterized proteins were incubated with standard crystallization conditions as generally described in section 3.16. The proteins were tested for both sitting drop and hanging drop methods per se used for such trials with conditions approaching sparse matrix methodology (Jancarik and Kim, 1991), covering a large space of well distributed conditions that could possibly lead to the progression and sustainability for crystal growth. The two proteins were tested with Crystal Screen I, II and Cryo Screen I-V (Hampton Research), altogether comprising 300 conditions. The proteins were tested as apo-proteins as well as assembled holoproteins. In conjecture with these conditions, the proteins were also tested after being pre-incubated with their cognate response regulators supposedly helping in the stability of such high molecular weight and photoactive proteins. The crystallization experiments were set up under safe green light, at 16-20^0 C in a dark room. There were also approaches to get the two photoactive reversible forms of these proteins by prior irradiation with either red (635 nm ±8; 680 nm in case of CphBm) or far-red light (>715 nm or 730 nm) before

pipetting. The crystallization droplets were divided as per variation of protein concentration alongwith different protein-to-precipitant ratios of 1:1 to 3:1 (three µl protein solution combined with one µl precipitant solution). The highest concentration of usual crystallography trials for any soluble proteins ranges from 10-25 mg/ml, but the tendency of precipitation of these two proteins as high concentration led to trials with maximal 4-8 mg/ml protein concentration. The droplets were inspected under a microscope, equipped with a green-light filter for inert illumination. This was done immediately after the crystallization set-up was completed, and subsequently each day for one week. Crystallization set-ups were inspected two to three weeks after pipetting, in order to keep the droplets unperturbed, for as long as possible. In some cases, the droplets were observed for as long as six months.

The full length holoproteins were tested with at least 8 different crystal screens, with varying precipitants, their concentration, and differential pH. The experiments were set up at two different protein concentrations with the same precipitant used. The crystal screens used for crystallization trials were namely: Crystal Screen I and II, Cryo Screen I and II, Peg Ion Screens I and II, Hampton Wizard I, II and III. Extensive screening using these combinations of initial conditions with a diversity of additives listed below was tested.

Precipitation agents tested:

PEG (up to 8000)

Glycerol (upto 50%)

Triton X-100 (up to 0.2 mM); CMC = 0.20 mM

Detergent Screen, Hampton Research

Cryo Screen I & II, Hampton Research

Variability in terms of hydrophobicity, as well as concentration of the precipitants present in the crystallization screens were also done to probe further

into the conditions favourable for the proteins in solution. The details of the crsytal screens tried for the full length phytochrome crystallization are presented in the Appendix II. The addition of PEG and detergents was derogatory for the proteins as there was mostly immediate precipitation.

The elevation of the phytochrome concentration above 4 mg ml^{-1} usually led to protein precipitation in most of the conditions tested. The experimental droplets, where the protein concentration was below that, remained clear in some cases even after several months, indicating that supersaturation was not achieved in the respective condition. A total of more than 1000 different conditions were tested with both phytochrome fragments, but crystal growth was not attained.

4.2 Domain Representation of Phytochrome proteins

The limited successes with the crystallography trials of the full length proteins lead us to explore with various aspects at the molecular level of the photoreceptor proteins. On the molecular level these proteins are composed of different domains which collectively form the fully functional phytochrome. These domains are based on the high similarity alignment of the amino acid composition of the phytochromes and have been well tabulated as per literature. The modular structure delineation of the phytochromes has been described in the introductory chapter. The purpose of the study was modulated so as to have deeper understanding into the inter-domain interaction of the constitutive domains of the phytochromes as well as to discern the essential length of their protein moiety required to maintain the spectral integrity. The study would henceforth lead to achieve the goal of modular structure identification with functional characteristics assigned to the respective domains.

The *Calothrix* phytochromes here arrange into the light-activated signal transduction system, with C-terminal located histidine kinase domains. The two phytochromes, CphA and CphB proteins fold into PAS-, GAF-, PHY-, and Histidine-kinase (HK) domains. CphA autocatalytically binds a phycocyanobilin

chromphore at a "canonical" cysteine within the GAF domain, identically as in plant phytochromes. CphB binds biliverdin IXα at cysteine24, positioned in the N-terminal PAS domain. The following results are described for the intra-domain cloning, biochemical characterization and their crosstalk studies.

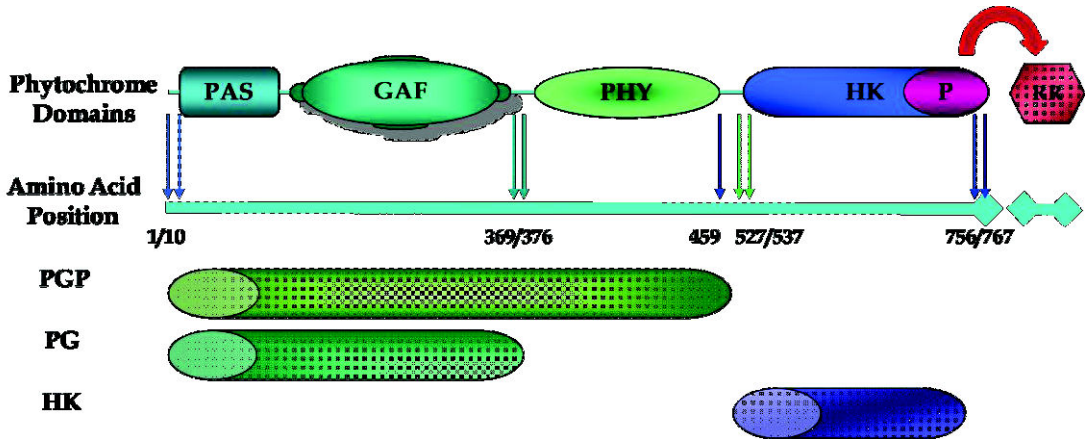

Figure 4.4 Schematic assay - molecular organization of the functional entities in *Calothrix PCC* 7601 Phytochromes : The N-terminal halves of the proteins contain a PAS (Per-Arndt-Sim) domain and the photosensor GAF domain (Guanylate Adenosine FhlA) forming photosensory core where BV is bound at N-terminal PLD domain cysteine while PCB binds to GAF domain cysteine, followed by the phytochrome specific PHY domain. The C-terminal half harbors a histidine kinase domain (HK) with an ATPase activity. The expression constructs are indicated by the abbreviated notations as PAS/GAF/PHY (PGP) domain, PAS/GAF (PG) domain, and Histidine kinase constructs (HK) domain. The amino-acids representing the beginning of the protein expressed with such constructs are indicated at the arrow, initial numbers indicative for CphA and later ones for CphBm domain specific proteins. The green panel represents photoconvertible receptor domains and the blue panel is the phosphotransfer histidine kinase domain, which were selected as targets for physicochemical characterization and crystallization.

Cloning

The gene product from phytochrome CphA, as from the plasmid construct (Jorrisen et al., 2002) has 767aa, while CphBm (Quest et al., 2004), where the construct starts 10 aa less than the assumed translation start of CphB, has 756 aa, both terminating by a C-terminal His_6 tag. The full length proteins were truncated so as to get some more detailed information about the activity of the respective domains by using different biochemical studies. The details of the constructs made

for this purpose are given in Table 4 (c). Graphical representation of the constructs is given under figure 4.4.

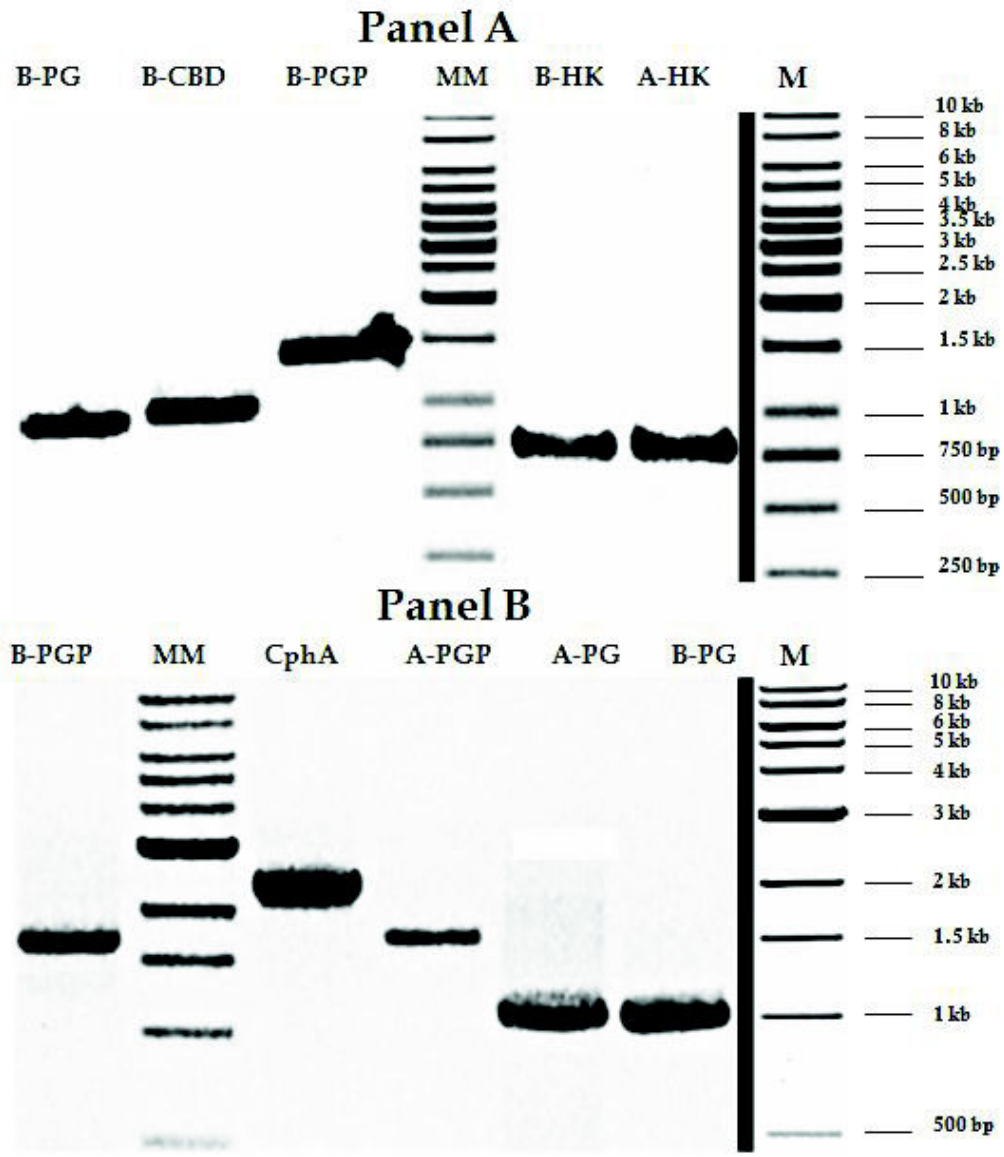

Figure 4.5 : PCR amplification of CphA and CphB genes from *Calothrix* PCC7601 : The agarose gel electrophoretic analysis shows the ethidium bromide stained DNA fragments. Panel A shows the PCR amplified fragments (i) CphB- Pas-Gaf Domain (Abbr. B-PG), (ii) CphB- Chromophore binding Domain (B-CBD), (iii) CphB-Pas-Gaf-Phy domain (B-PGP), (iv) DNA Marker (Fermentas-1 kb ladder), (v) CphB-Histidine Kinase domain (B-HK) and (vi) CphA- Histidine Kinase domain (A-HK). Panel B depicts (i) CphB- Pas-Gaf-Phy domain (B-PGP), (ii) DNA Ladder (1kb-New England Biolabs), (iii) CphA- Full length phytochrome, (iv) CphA-Pas-Gaf-Phy domain (A-PGP), (v) CphA-Pas-Gaf domain (A-PG) and (vi) CphB-Pas-Gaf domain (B-PG). Lanes M contain DNA molecular weight standards; numbers refer to kilo bases.

The respective domains from the coding sequence of the full length phytochrome proteins, CphA and CphBm, from *Calothrix* PCC7601 were cloned into the pET 28a vector for expression in *E. coli*. PSIPRED and SWISS Pro protein secondary structure prediction and threading programs were made use before attempts of cloning. The predicted structures were examined for secondary elements and the primer design was done so as not to intersect the continuity of the secondary structure predicted for such domains. This step was done as a precaution so that the soluble expression of the truncated domains is not affected. The primers for the respective domains are described in Table 4 (c). The genes were amplified using PCR as described in section 3.6.3.1- 3.6.3.5, using either cDNA or already present full length phytochrome constructs as templates. The PCR primers were designed to include the C-terminal His_6 tag provided with the vector (see Fig. 4.4, 4,5 and table 4 (c) for details), to ensure complete translation of the proteins.

Restriction digestion and ligation were performed as explained in section 3.6, and recombined plasmids were selected and propagated in the *E. coli* strain XL1-Blue. The correctness of the cloned genes was controlled by sequence analysis.

Table 4 (c) – Description of the cloned domains with amino acid position of full length phytochromes

Gene	Domain	5′-Restriction site	3′-Restriction site	Amino Acid	Final plasmid
CphA	Pas-Gaf-Phy	NcoI	XhoI	10-527	CphA-PGP
CphA	Pas-Gaf	NcoI	XhoI	10-369	CphA-PG
CphA	His- Kin	NcoI	XhoI	459-767	CphA-HK
CphBm	Pas-Gaf-Phy	NcoI	XhoI	1-537	CphBm-PGP
CphBm	Pas-Gaf	NcoI	XhoI	1-376	CphBm-PG
CphBm	His- Kin	NcoI	XhoI	459-756	CphBm-HK
All the domains were cloned in pET 28a (+) vector from Novagen, having Kanamycin selectivity.					

4.2.1 Pas-Gaf-Phy Domains from CphA and CphBm: cloning, expression, *in vitro* reconstitution, purification and biochemical characterization

Cloning

Phytochromes CphA and CphBm are built up internally of the representative domains as shown in Fig. 4.4. In the case of the bacterial phytochromes, the N-terminal domains were separated from the C-terminal Histidine Kinase domain by cloning the first three consensus domains, named as PAS, GAF and PHY separately (introducing a stop codon after the Phy domain and a C-terminal His tag introduced from the vector for affinity purification). The PGP (short term including Pas, Gaf and Phy) domains were predicted to be A-PGP as 61.2 kDa /B-PGP as 61.7 kDa proteins consisting of 518/535 amino acids, respectively, for CphA and CphBm. The DNA encoding for PGP domains was amplified by PCR from either cDNA or the plasmids containing full length phytochromes and cloned into the vector pET-28a (+) between the NcoI and XhoI restrictions sites (described in section 3.6.3). Both these constructs were assumed to still assemble their respective chromophores as explained in the introductory chapter. Such domain would predictably have functional photo reversibility as all the domains required for such activity would be intact in such as construct (Esteban et al., 2005). The figure 4.4 shows the graphical representation of the PGP domains from both CphA and CphBm. The details of the various constructs designed for CphA and CphBm are summarized in the table 4 (c).

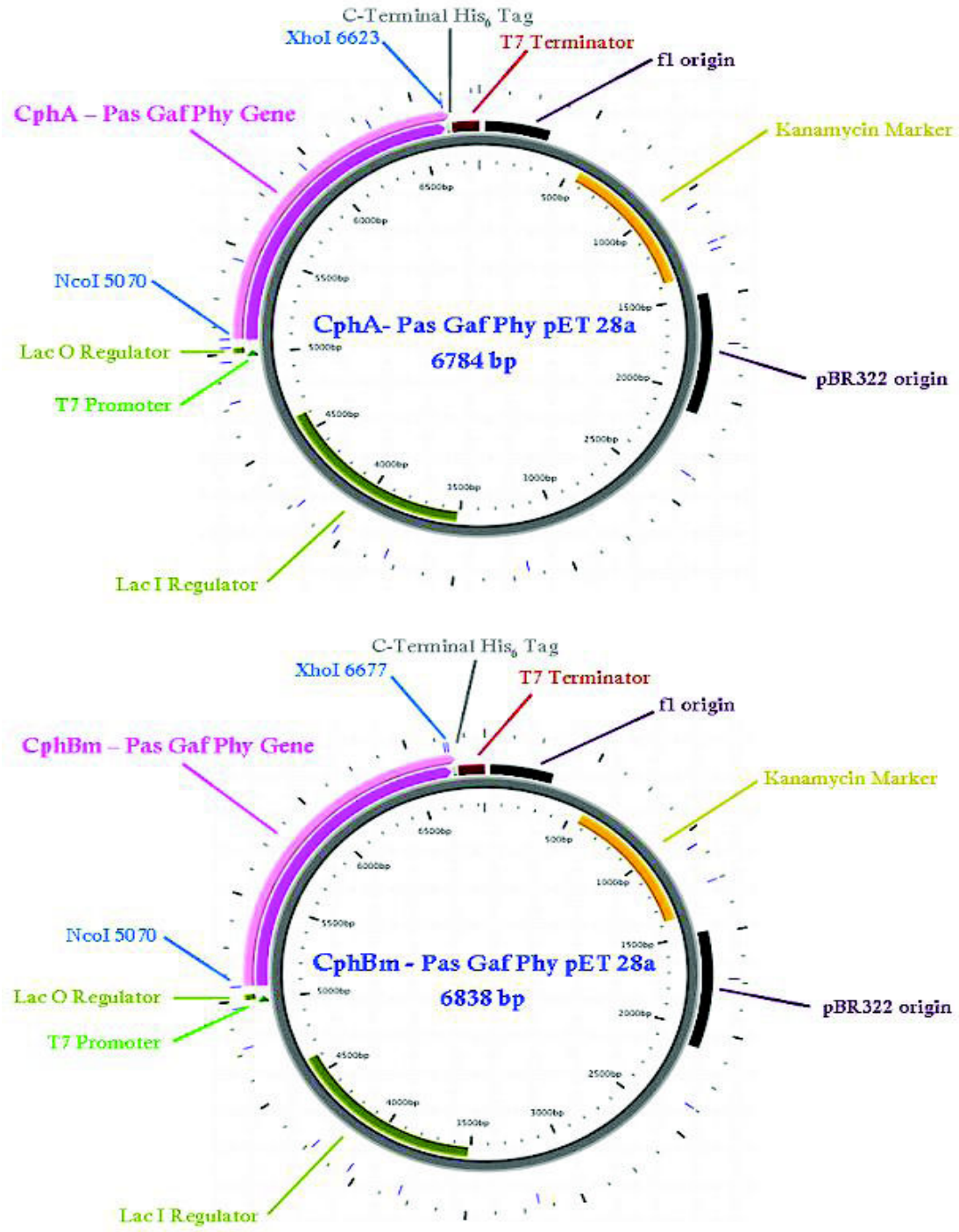

Figure 4.6 Graphical representation of the expression constructs in vector pET28a (+) : CphA-Pas-Gaf-Phy (A-PGP) and CphBm-Pas-Gaf-Phy (B-PGP) showing detailed vector construction with various components used for directional cloning, selection, expression and purification. E.g. CphA Pas/Gaf/Phy ORF with His6 tag, Kan: Kanamycin resistance gene, Ori: origin of replication, T7P: T7 promoter, T7T: T7 terminator.

Expression, *in vitro* reconstitution and purification

The heterologous expression of the N-terminal photoreceptor domain of the phytochromes CphA and CphBm from *Calothrix PCC 7601* was accomplished in *E. coli*, where the genes for the two proteins were designed so as to include C-terminal poly-histidine tags for facile affinity purification. The PGP domains of the phytochromes were subjected to UV-Vis spectroscopic characterization as well as crystallization trials. The proteins were purified as per standardized protocol used in this study (3.7).

Recombinant heterologous expression of the cyanobacterial phytochromes was aimed at high cell mass production and to obtain soluble proteins for biochemical studies. For this purpose the transgene *E. coli* strains BL21 (DE3) RIL/RIPL Gold cell strain were selected for positive transformants under kanamycin addition. The recombinant plasmid hosting the genes of interest were cultivated using Erlenmeyer flasks (5 liter) with constant shaking at 37 ˚C as described in detail under 3.11. From a standard per litre bacterial culture, a total of approx. 20-35 g wet cell mass was obtained. The cells were usually divided into aliquots of 10 g, flash frozen in liquid nitrogen and stored at -80 ˚C until further processing. The cells were thawed on ice and disrupted as explained in 3.7.2 to obtain raw lysate of the recombinant proteins.

Preliminary test expressions were done according to the standard protocol for full length proteins that yielded proteins of expected sizes. CphA-PGP protein was exclusively found in inclusion bodies while most of CphBm-PGP was soluble. Modifications to the expression conditions as were done with the full length phytochromes (Section 4.1) led to better yields of soluble protein for both the A- and B-type domains, although CphA-PGP still expressed poorly. The yields for CphA-PGP and CphBm-PGP per litre were 1 mg and 4-9 mg, respectively. Lowering of induction temperatures (18 ˚C for 16 hrs or 24 ˚C for 6 hrs) was used

for PGP domain expression with induction with 400 µM IPTG resulted in obtaining the best amounts of soluble proteins.

Purification and *in vitro* reconstitution

Purified receptor domain proteins were tested by UV/VIS spectroscopic analysis in order to assess the absorption profiles and photoreversibility of the photochromous proteins. The reconstitution of the apo-proteins with the desired chromophore (PCB or BV) was either done in the clarified cell lysate or after purification, as explained in 3.7 and 3.7.3. The purification of all the truncated domains was attained *via* a predescribed protocol that involved the basic step of preliminary separation from residual cellular proteins by metal affinity chromatography.

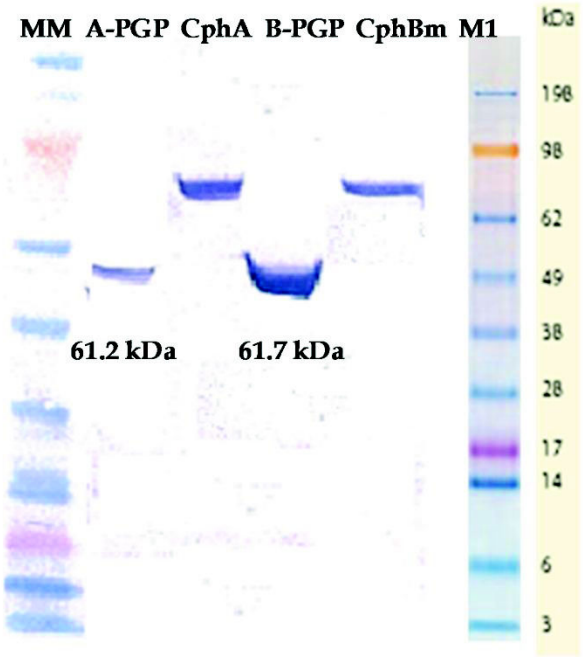

Figure 4.7 SDS-PAGE analysis of *Calothrix* CphA-PGP expression in *E. coli* : Lane 1: *Calothrix* A-PGP , Lane 2: *Calothrix* CphBm and lane 3: *Calothrix* B- PGP. The sizes (in kDa) indicated at the right for the pre-stained molecular weight marker used.

After the His-tag purification of the apoproteins, the molecular weight of the A-PGP and B-PGP was checked via SDS-PAGE (Fig. 4.7). Single bands migrating

at approx. 61 kDa and 62 kDa were obtained on SDS-PAGE, which correlate with the predicted molecular mass calculated from amino-acid composition. Additional information on the purity of the proteins and concentration was deduced from the UV-Vis spectrum analysis. Specific absorbance ratio (SAR) between the Pr absorption band maxima (λ_{max} = 663, 700 nm) and the absolute protein absorption at λ_{max} = 280 nm is used, where the range of 1 to 1.6 is considered as optimal purity with 95% of protein assembled with the chromophore *in vitro*.

UV/VIS Spectroscopic characterization

The respective domains of the phytochromes CphA and CphBm, (PGP and PG) were subjected to UV/VIS spectroscopical analysis in order to have evidence which role the various domains played in the absorption properties and photoreversibility of the photochromous proteins. The spectral analysis of the PGP domains was done by irradiating with the red and far-red wavelength of light as done with the full length phytochromes. The ground state of the proteins consisted of the red absorbing Pr, which was then irradiated appropriately to get the photoreversible forms of the two proteins, Pr and Pfr.

After the His-tag purification and reconstitution with PCB, A-PGP showed photoreversibility with a Pr maximum of 663 nm and a Pfr maximum of 707 nm (Fig. 4.8). The difference spectrum was used to calculate the amount of protein which was found to be ca. 1-2 mg per liter culture.

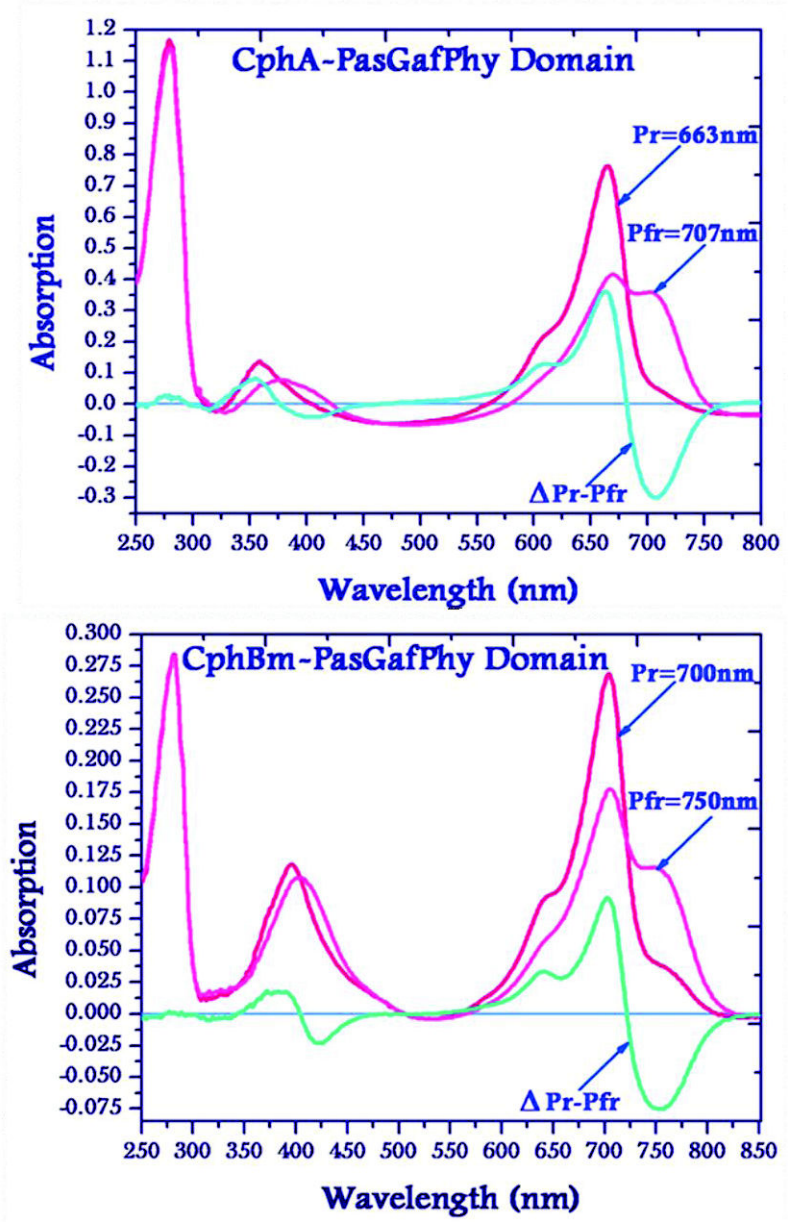

Figure 4.8 UV/VIS spectra from highly purified receptor domains : The specific absorption ratio (SAR) between the P_r absorption band ($\delta\blacktriangle_{max}$ = 664,704 nm) and the absorption at $\delta\blacktriangle_{max}$ = 280 nm is used. The SAR values for protein samples with the highest purity obtainable through the applied methods were generally in the range of 0.4 to 1.2. SDS PAGE analysis was utilized to determine further purity of samples which was found to be at least 95 % pure indicating some residual apoprotein that does not assemble with chromophores. Pr and Pfr absorption spectra and difference spectrum of *Calothrix* CphA-PGP and CphBm-PGP expressed in *E.coli* and reconstituted with PCB and BV, after His tag affinity purification and concentration.

Similarly, reconstitution of B-PGP with BV having Pr maximum of 700 nm and Pfr of 750 nm was used to measure the difference spectrum, hence calculating the amount of protein which was found to be 6-10 mg per liter culture.

The binding of chromophore biliverdin (BV) was found to be slow in B-PGP in comparison to binding of phycocyanobilin (PCB) to A-PGP. The difference in absorbance, P_r - P_{fr} (Δ absorbance) maximum of apoproteins was found to be 0.250 with BV after 5 min irradiation in far red light and red light. Whereas, after an overnight (approx 16 h) incubation of apoproteins with BV, the full conversion of Pr form to Pfr form yielded Δ absorbance of 0.310.

P_{fr} dark reversion of A-PGP and B-PGP

After extensive irradiation with red light to obtain a maximal formation of Pfr, dark reversion was checked at room temperature (20°C) by measuring spectra at regular time intervals. Even after 14 days at room temperature, no clear Pfr to Pr dark reversion could be detected but the degradation of protein was found to be as the 4.34% and 2% for A-PGP and B-PGP respectively (table 4 (d)).

Table 4 (d) - Percentage of degradation of Apgp and Bpgp

Domain	ΔA (t = 0)	ΔA (t = 14 days)	Degradation
A-PGP	0.092	0.088	4.34%
B-PGP	0.311	0.305	2%

B-PGP had shown 0.155 ΔA, after 30 days of incubation which is the degradation of 50%. The degradation was assumed due to the precipitation of the purified protein.

Mass spectrometric analysis

The detection of homogeneity of samples was also ascertained using MALDI-TOF mass spectrometry. According to the resulting mass spectra, all samples were analyzed for the theoretical and actual obtained molecular masses.

The mass spectra for B-PGP here shows the expected molecular mass in the range around 60 and 65 kD (Fig. 4. 9), a broad distribution of some minute unrelated bands are seen indicating either unspecific proteolytic activity which might happen during expression, purification, or unspecific chemical modification of the protein molecules in the cell's cytosol such as phosphorylation, deamidation or oxidation.

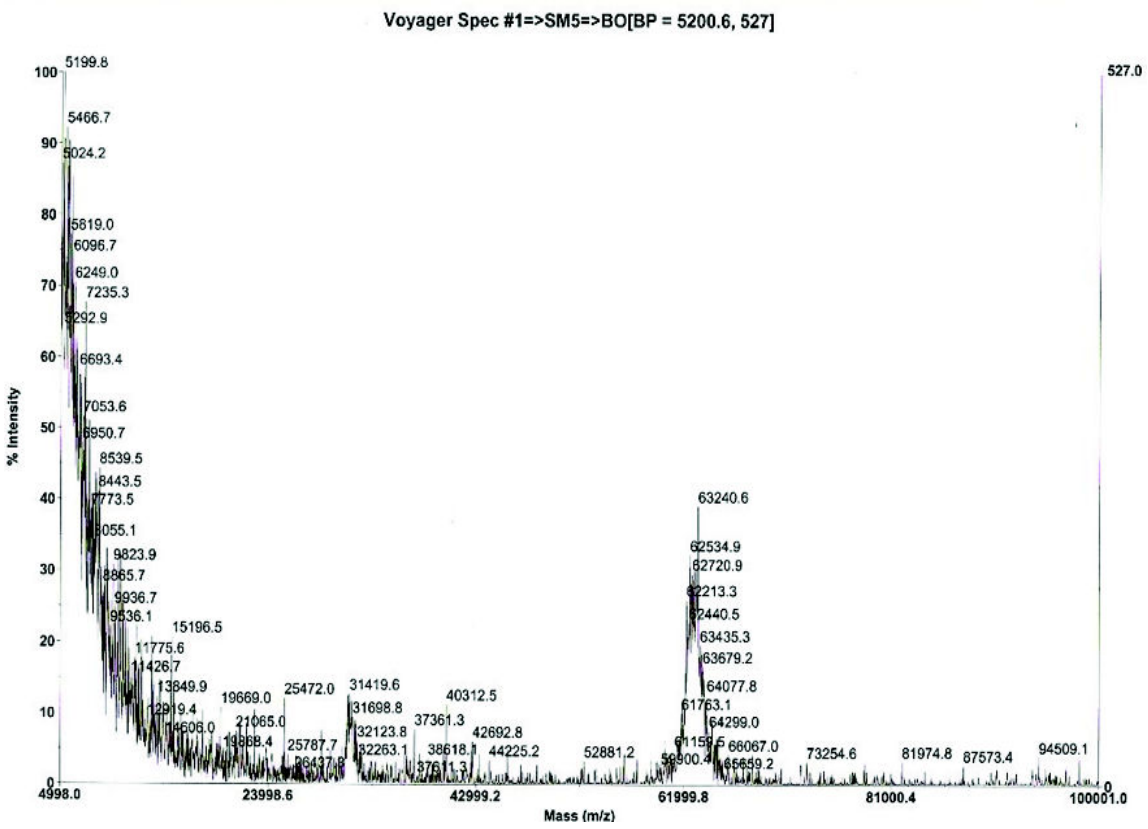

Figure 4.9 : The MALDI-TOF MS molecular weight analysis and purity profiling of CphBm-PGP domain protein. The molecular mass hitherto determined through online mass analysis as well as using SDS-PAGE and Western blotting techniques was ascertained to be 62 kDa (error of ± 1 kDa).

4.2.2 Pas-Gaf from CphA and CphBm: cloning, expression, *in vitro* reconstitution, purification and biochemical characterization

Cloning

The most N-terminal part of the phytochromes comprise of the PAS and the chromophore-binding GAF domain. The spectroscopic property of the truncated domains would be interesting as this would give the specific roles for the individual domains. Here the phytochrome was truncated at the end of the GAF domain introducing a stop codon at appropriate site. A-PG (Pas/Gaf) comprises of amino acids 10 to 370 while B-PG (Pas/Gaf) is from amino acid 1 to 377. The interesting aspect was to see if the Phy domain plays any role in the integral property of photo reversibility and stability of these proteins or these two domains themselves are capable of doing so.

Expression

The plasmids pET28a-CphA-PG (A-PG) and pET28a-CphBm-PG (B-PG) were transformed into *E. coli* BL21 (DE3) RIL and RIPL expression cells. Subsequently, the A-PG and B-PG apoprotein with His_6-tag was heterologously expressed in *E. coli* BL21 (DE3) RIL+ RIPL cells. 500 µl of crude lysate of A-PG and B-PG was reconstituted with PCB and BV, respectively, for the observation of expression of soluble protein.

The A-PG protein was expressed in very low soluble amounts as compared to the B-PG protein. Low temperature induction led to some increase in the expression of both these proteins although A-PG still expressed relatively poorly. One more factor applied here during expression yielded more amount and stability of the expressed proteins was growth after induction was limited to 4-8 hours, with decreasing temperatures of growth. A decrease of 4 °C every hour was made during the expression. There had been no scientific backdrop for this but it was tried to have minimal inclusion bodies during the growth after IPTG induction.

The Pas-Gaf domain protein from CphBm, although expressed at higher amount than the CphA-PG domain under the same growth and induction conditions, which were- 37 ˚C optimal growth, with induction at lowered temperature of 28 ˚C and gradual reduction of temperature till 16 ˚C final growth temperature. The cultures were induced with 0.5 mM IPTG.

The PAS-GAF truncated domain proteins were found to be quite deviant from the full length phytochromes in terms of their expression, purification and their stability. The proteins expressed at very low amount during the culture that involved also experiments at small scale about expression standardization with almost negligible changes from the already set protocol. The low yielded proteins were also labile to precipitation and degradation during purification which futher reduced the amount of purified proteins.

The proteins assembled with chromophore extremely slowly as compared to the PAS-GAF-PHY partners or full length proteins. This slow assembly maybe a resultant of the truncation of the PHY domain which is now known to stabilize the chromophore in it binding cleft (Essen et al., 2008) as the truncated protein residues become more exposed to the solvent and therefore might be responsible for the weak protein-bilin binding.

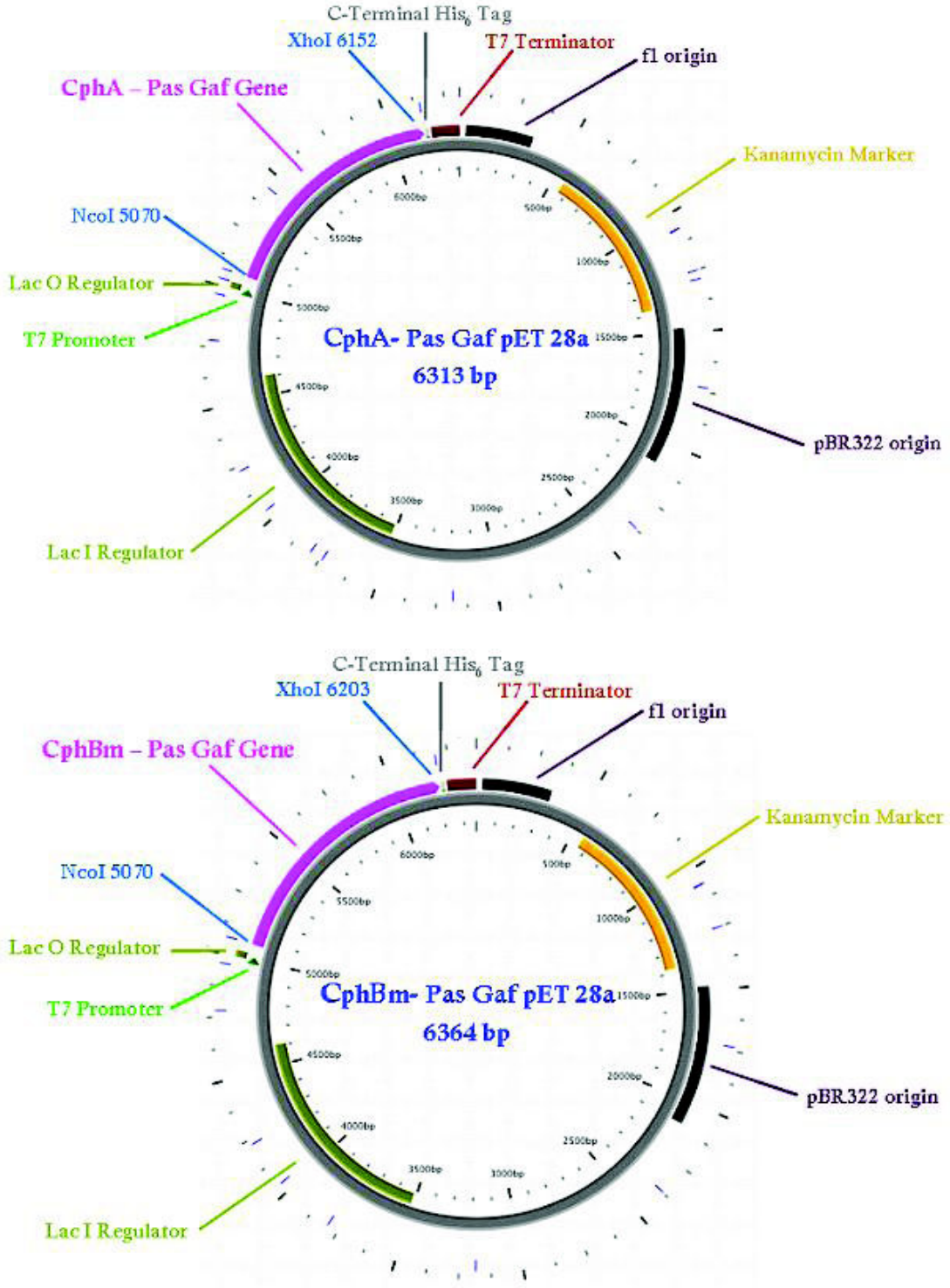

Figure 4.10 Graphical representation of the expression constructs in vector pET28a(+) : CphA-Pas-Gaf- (A-PG) and CphBm-Pas-Gaf (B-PG) showing detailed vector construction with various components used for directional cloning, selection, expression and purification. E.g. CphA Pas/Gaf ORF with His6 tag, Kan: Kanamycin resistance gene, Ori: origin of replication, T7P: T7 promoter, T7T: T7 terminator.

Purification and *in vitro* reconstitution

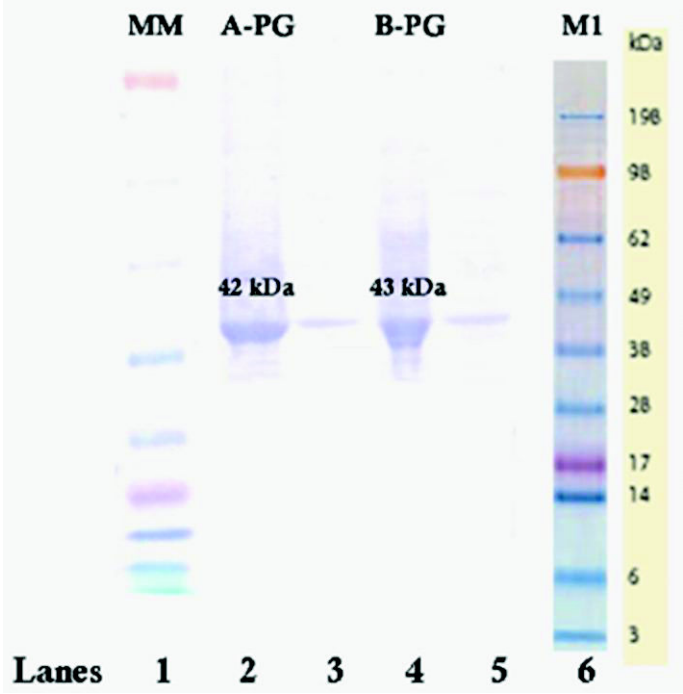

Figure 4.11 Western blot analysis of *Calothrix* CphA-PG and CphBm-PG expression in *E. coli* : Lane 1: MM: molecular weight marker, Lane 2: CphA-PG-elution 125 mM Imidazole, Lane 3: CphA-PG-elution 150 mM Imidazole, Lane 4: CphBm-PG- elution 125 mM Imidazole, Lane 5: CphBm-PG- elution 150 mM Imidazole and Lane 6: the sizes (in kDa) of the protein molecular marker (M1) are indicated on right side.

The His-tag purification of the domain apoproteins was followed according to the standardized protocol. The yield of the two proteins, CphA-PG and CphBm-PG was however very different, where A-PG domain was mostly (70%) found in inclusion bodies while B-PG was soluble protein with higher expression. The molecular weight of the A-PG protein was 42 kDa while that of B-PG was 43.5 kDa as predicted by EXPASY Server and confirmed via SDS-PAGE and western blot (figure 4.11).

UV/VIS Spectroscopic characterization

The reconstitution of the domain proteins was done with PCB for A-PG and BV for B-PG. The spectral analysis of the PG domains was performed in similar manner as with PGP domains. The ground state of the proteins consisted of the red absorbing Pr, which was then irradiated appropriately to get the photoreversible forms of the two proteins. The graphs below depict the UV-Vis spectra of the Pas-Gaf Domains from both the proteins. It was quite interesting to find out that behaviour of the A and B type of phytochromes differ as per the spectral aspects of the domains are concerned. This is the first indication that there would be differences in terms of the ligand assembly and the photochemistry of the two types of phytochromes present in *Calothrix*.

The deletion of the "PHY" domains caused a slight blue-shift of the Pr and Pfr absorption of CphA (λ_{max}: 658/698 nm), however, in CphBm it practially impaired the formation of Pfr, whereas the Pr form remains unchanged (702 nm). This finding clearly indicates a different interaction between domains in the "typical", phycocyanobilin binding- and in the biliverdin-binding phytochromes, and demonstrates a loss of oscillator strength for the latter, most probably due to a strong conformational distortion of the chromophore in the CphBm Pfr form.

The reconstitution of PCB with the both crude and purified protein of A-PG and B-PG was very slow in comparison with full length proteins or PGP domain proteins. The crude lysate obtained for these domains was incubated with their respective chromophores overnight for the proper assembly. There was an increase in the amount of reconstitutable proteins with increasing time of incubation. The spectrum was measured at different time intervals to assess the binding, which is shown in Fig 4.12. Purification of the reconstituted A-PG via His-tag affinity chromatography resulted less than the original amount of photoreversible phytochrome. However, addition of PCB restored the photoreversibility as found for the unpurified protein-PCB complex (Fig. 4.13).

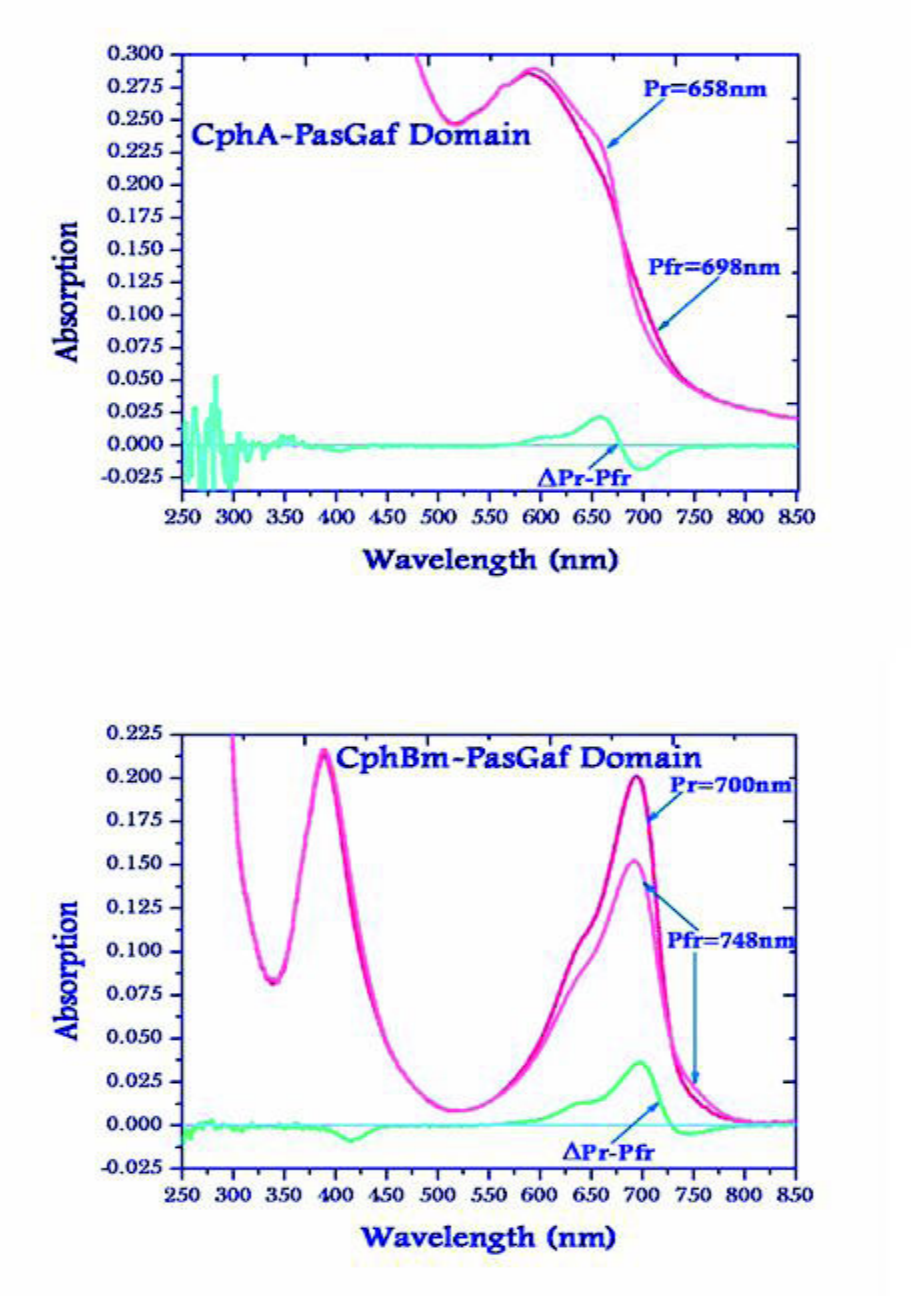

Figure 4.12 The Pr and Pfr absorption spectra and difference spectrum of *Calothrix* Pas-Gaf Domains : Spectrum of CphA-PG and CphBm-PG expressed in *E. coli* and reconstituted with PCB and BV, respectively.

The crude lysate of B-PG after the reconstitution with BV and irradiation in far red light and red light for 5 minutes showed the Pr - Pfr difference spectra with the broad peak (no distinct photoreversion- Fig. 4.13). Therefore, crude lysate was incubated with BV overnight. After 16 hours of incubation the Pr - Pfr difference spectra obtained was as in figure 4.14. The spectra showed the P_r form blue-shifted to 678 nm and Pfr at 743 nm.

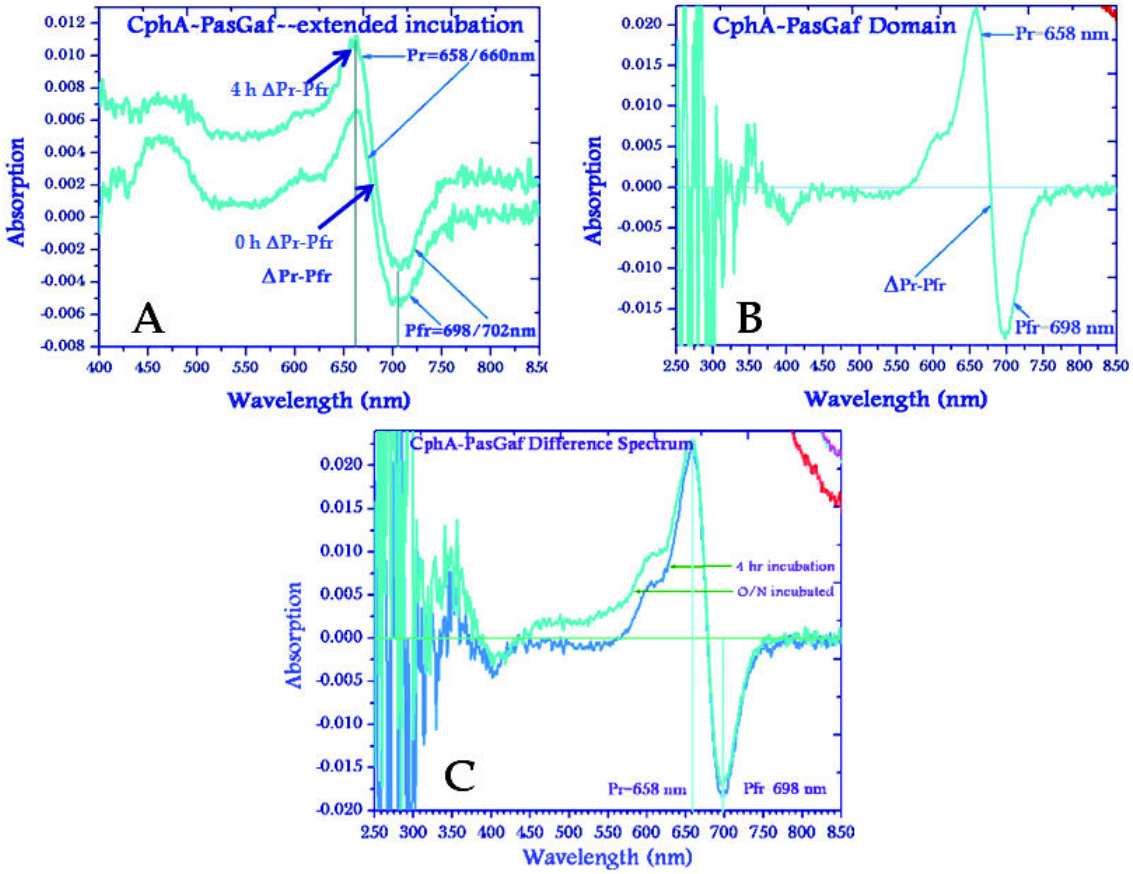

Figure 4.13 Difference Spectrum of CphA-PG at different incubation times : Pr - Pfr difference spectra of *Calothrix* CphA-PG + PCB. (A) Difference spectra of crude protein at 0h and 4h incubation. (B) Difference spectra of CphA-PG after His-tag affinity purification with PCB and (C) Comparative spectra of purified protein at 0 hr (blue spectrum), and after overnight incubation with extra PCB (cyan spectrum).

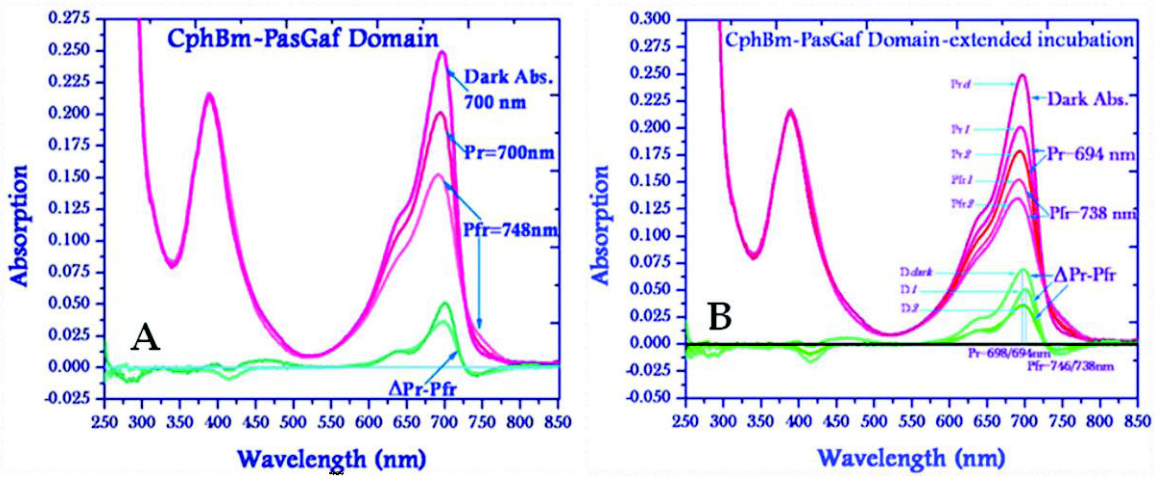

Figure 4.14 Difference Spectrum of CphBm-PG : (A) The graph depicts the Pr and Pfr absorption spectrum alongwith the dark absorption spectra of *Calothrix* CphB-PG expressed in *E. coli* and reconstituted with BV. **(B)** The spectral properties of the protein after extended incubation (overnight with excess BV), obtained after His tag affinity purification and concentration.

After His-tag purification the apoprotein had shown loss of the chromophore due to the probable weak binding, therefore apoprotein was again reconstituted with biliverdin (BV) and incubated overnight. The overnight incubated apoproteins with BV showed the Pr and Pfr absorption spectrum as figure 4.13 and Pr - Pfr (difference) absorption spectrum. The Pr and Pfr absorption spectrum spectrum was obtained as 678 nm and 743 nm.

4.2.3 Histidine Kinase Domains – cloning, expression and purification

Signal transduction in microorganisms and plants is often mediated by His-Asp phosphorelay systems typically involving two centrally conserved families of proteins: histidine protein kinases that binds ATP and, when activated, undergoes autophosphorylation on a specific histidine residues, and phospho-aspartyl response regulators that transfers the phosphoryl group from the phosphohistidine in the kinase to one of its own aspartate residues (Figure 2.7 and 4.4). The kinases generally are assigned with a conserved catalytic core, the activity of which is

regulated by distinct input signals through a wide range of different associated sensory elements differentiating in response to environmental signals. Histidine kinases consequently control the level of phosphorylation of their cognate response regulators, which act in turn to control the activities of associated effector domains, usually DNA-binding proteins that regulate gene expression.

The sensing domains of the histidine protein kinases regulate the rate of autophosphorylation. The phosphorylated kinase in turn interacts with the receiver domain of its cognate response regulator, donating its phosphoryl-group to an invariant aspartate in the receiver domain. A phosphorylation-induced conformational change in the receiver is thought to modify the activities of associated response regulator output domains. Phosphorylation of response regulators with no output domains are thought to cause changes in affinity for target effector proteins.

Phytochromes are photosensory molecules that show significant homology to histidine protein kinases (Schneider-Poetsch *et al*., 1991). The cyanobacterial phytochrome CphA-7601 donates phosphoryl groups to a response regulator, RcpA (Jorrissen *et al*., 2002).

The recent elucidation of the structures of the conserved histidine kinase cores of distinct histidine kinases — *Thermatoga maritima* CheA (Marina et al., 2005) — has added considerably to our understanding of the differences between signal transduction mechanisms in prokaryotes and eukaryotes. The core structure is composed of two domains (Figure 4.16), a dimerization domain with a pair of up-down α-helical segments, and an ATP-binding phosphotransfer domain homologous to the ATPase domains of type II topoisomerases, MutL and the heat-shock protein 90 (Hsp90) class of molecular chaperones.

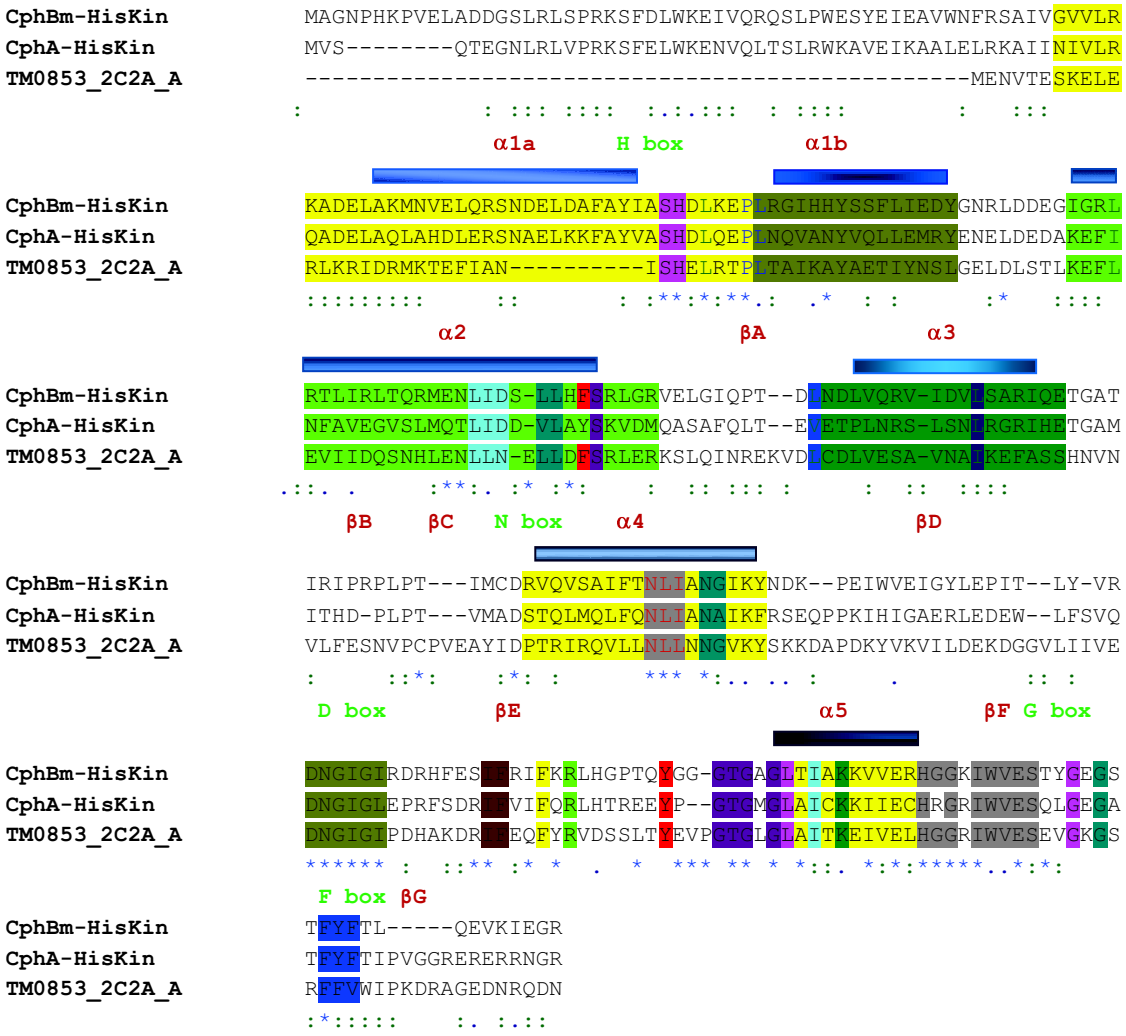

Figure. 4.15. Homologous sequence alignment of Histidine kinase domain with related proteins of known structure (CheA type; TM0853) : Computation was performed by the ClustalW network service of the EMBL-EBI. Alignment of conserved boxes in the phosphoacceptor/dimerization domain (H-box, the site of autophosphorylation in shadowed pink) and in the ATP-binding catalytic domain (N-, D-, F- and G-boxes) of representative His-kinases. Shadowed residues characterize the different boxes. The three amino-acid sequences are aligned based on their protein folds. β-sheets are shown intercepting the yellow and green filled colored boxes (light and dark). Residues identical in all the three sequences are shown in similar color. Highly conserved active site residues are marked with the panels alongwith the different sub domains. CheA histidine kinase has been crystallized successfully where the sub domains resemble the ones from the phytochromes from *Calothrix sp.* (Bilwes et al., 1999; Marina et al., 2005).

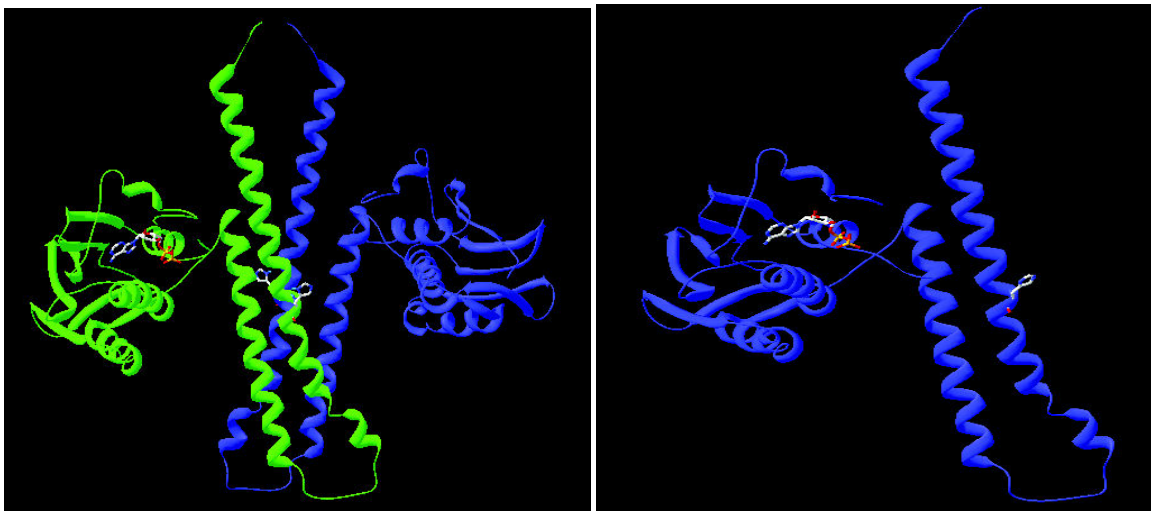

Figure 4.16 : ClusPro docked molecular model : The three dimensional homology modeled structure of histidine kinase from *Thermotoga maritima* (HK-HK853), with the ATPase domains are like butterfly's wings around the Histidine phototransfer domain (HpD): similar leit-motiv motifs but quite different orientations. The right side is the pictorial representation of the modelled CphB histidine kinase (535-753 aa) domain using the ClusPro server.

The histidine kinase domain in both CphA and CphB phytochromes resemble the crystallized domain in the two component system found in *Thermotoga maritima*. Figure 4.15 depicts the homology alignment of the histidine kinase domain between the three proteins. The kinase domains as such were modeled against the backdrop of the available kinase structure, protein data bank identity 2c2a from *Thermotoga*, with nearly 30% identity (Figure 4.16 & 4.17). The systematic design of histidine kinases typically contain two functionally and structurally distinct parts, a variable N-terminal sensor region and a conserved C-terminal kinase core domain that features the phospho-accepting histidine as well as the so called homology boxes. The latter are highly conserved sequence fingerprints that serve to define the family (Stock *et al.* 1988; Parkinson & Kofoid, 1992).

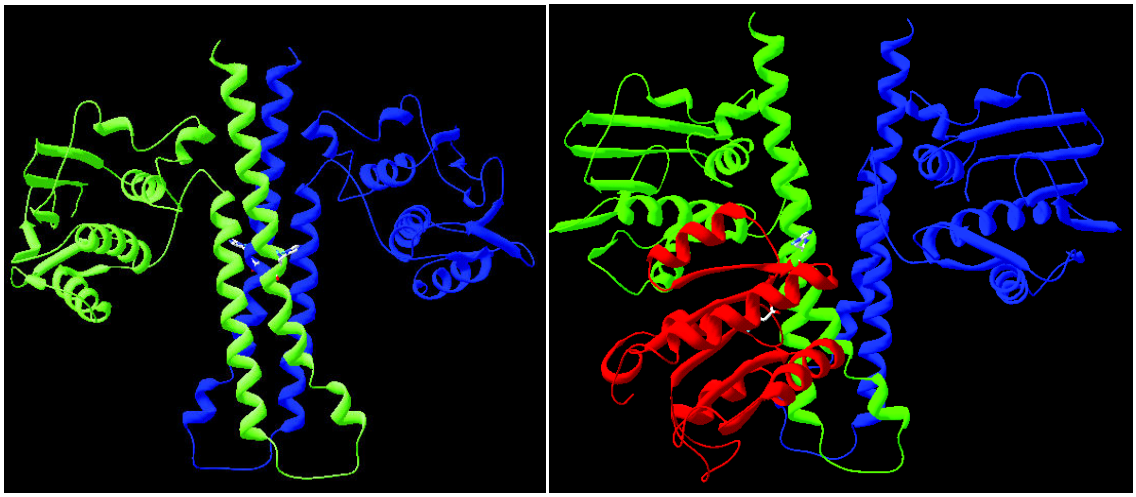

Figure 4.17 : Model of the CphBKinase dimer (DOT software at the ClusPro server): This model includes the His-dimerization and ATPase domains showing similarity in topology between the two inter-protein domains. Two monomers were docked with Cluspro (DOT). In the model cluster 9 is represented in the left panel, while the right picture depicts the Cluster 4 including CphB HisKin dimer+RcpB docked as per the two component signaling system.

Recent structural studies of the histidine protein kinase core have shed considerable light on the function of the other conserved regions (Bilwes *et al.*, 1999). Members of the histidine protein kinase superfamily homologous clusters of highly conserved residues that are presumed to play crucial roles in substrate binding, catalysis, and/or structure. These characteristic sequence fingerprints have been termed homology boxes: the H-, N-, D-, F-, and G-boxes (Stock *et al.*, 1988; Parkinson and Kofoid, 1992; Stock *et al.*, 1995). In phytochromes subfamily of HKs these so called boxes tend to be less conserved, though detailed sequence alignments as done here show a rather conserved similarity (Figure 4.15). The H-box contains the site of histidine phosphorylation. This histidine is generally located at the face of an α-helix within an up-down-updown helix bundle (Zhou *et al.*, 1997). The distribution of charged and hydrophobic residues around the phospho-accepting histidine tends to be different for different subfamilies. In many cases these sequence features can serve as subfamily identifiers. In general, it is the homology boxes that define subfamilies, whereas flanking sequences tend to be are highly variable even within subfamilies.

Cloning

The histidine kinase domains from *Calothrix* were cloned as per the details depicted in Fig. 4.4 and also tabulated in Table 4 (c). The primers were designed so as to get intact secondary structure of the kinase domain. Figure 4.14 shows the graphical depiction of the kinase constructs cloned from the *Calothrix* full length phytochrome genes. The kinase domain poses an interesting domain to be studied in greater details as, after the phytochrome crystal structure, most interesting aspect would be to get information on the two component system under the control of the photo-acceptor. The constructs were carefully chosen to include the conserved secondary structure of the well known histidine kinases, were aimed to study their interaction with the cognate response regulators.

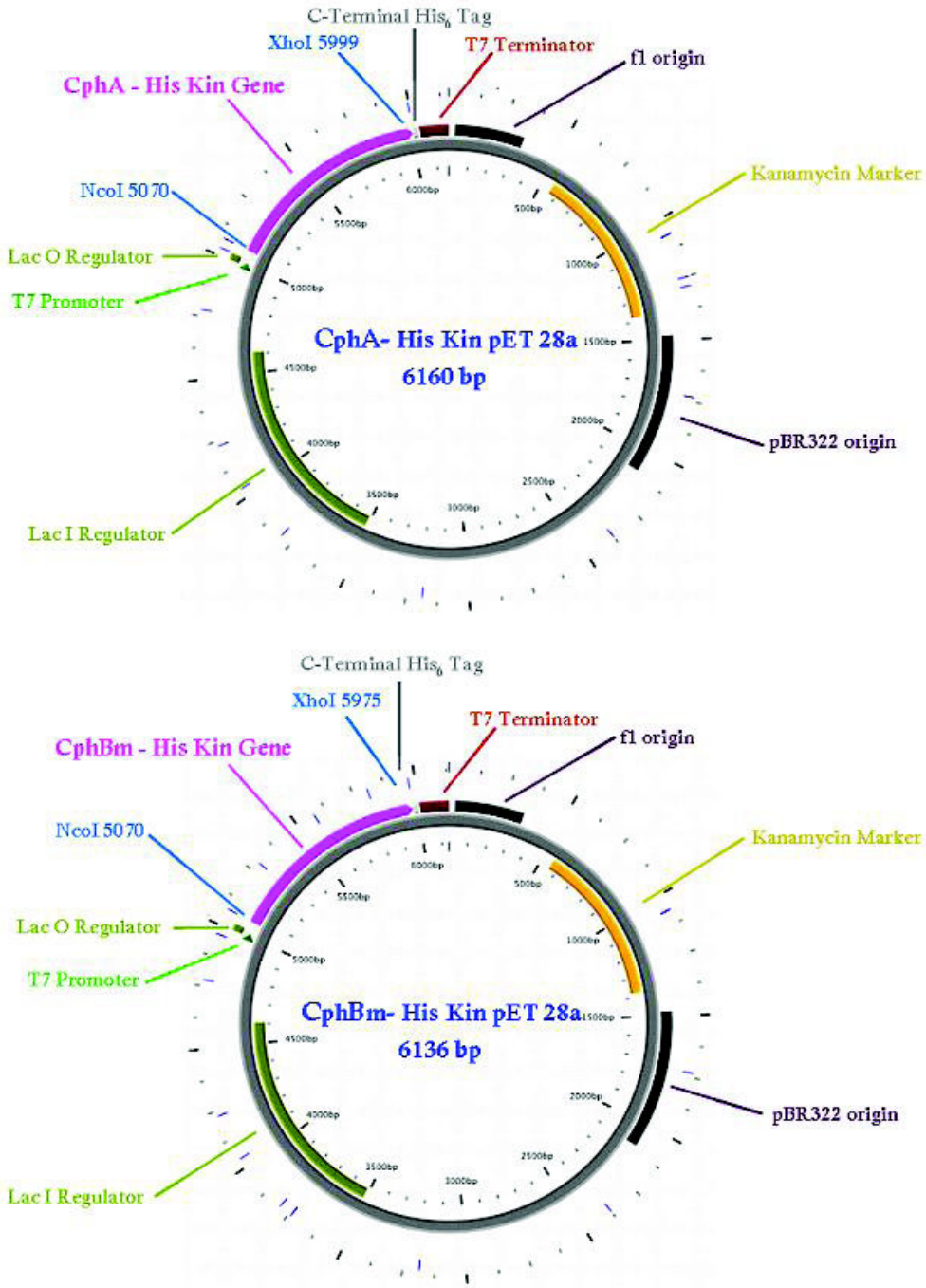

Figure 4.18 Graphical representation of the expression constructs in vector pET28a(+) : CphA-Histidine kinase construct (A-HC) and CphBm-Histidine kinase construct (B-HC) showing detailed vector construction with various components used for directional cloning, selection, expression and purification. E.g. CphA Histidine Kinase ORF with His6 tag, Kan: Kanamycin resistance gene, Ori: origin of replication, T7P: T7 promoter, T7T: T7 terminator.

Expression and Purification

The histidine kinase domain of CphA- HisKA (A-HK) and CphBm-HisKa (B-HK) is the most C-terminal domain of the phytochromes. The ATPase domain is also the part of the gene cloned for expression. The figure below depicts the gel of the purified kinase domains. The CLUSTALW alignment of the histidine kinase domain with various other similar domains across the prokaryotic regime is depicted in Figure 4.15. The domain has been divided into different recognition boxes as elaborated in the figure. The phytochromes have been reported to have a slightly different make-up from the rest of the clan of histidine kinases (Karniol and Vierstra, 2003, 2004).

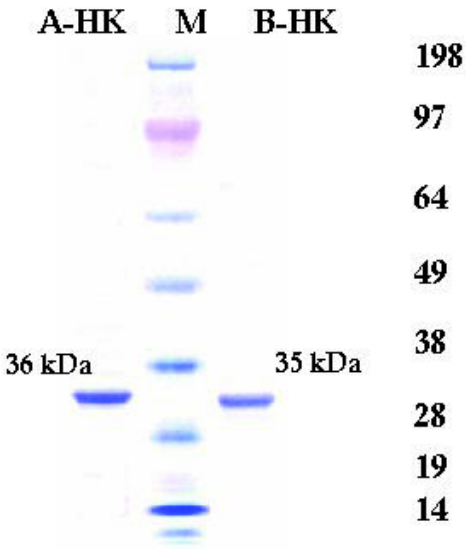

Figure 4.19 Figure showing the coomassie stained SDS-PAGE analysis of the purified fractions of CphA- His Kin and CphBm-His Kin : The denatured protein runs at the expected height near the 36 kD and 28 kD, respectively, for A-HK and B-HK with the marker band (M) in the middle. Protein samples were mixed with an equal volume of sample buffer (3.3.2), heated to 80°C for 5 min and applied to the gel. The gel was run at constant power (180 V) until the lower dye band of the sample buffer reached the lower end of the gel.

The histidine kinase domains form an integral part of the two component signal transduction system of the phytochromes. This domain can be termed as the "operator" for signaling to the cognate response regulator which is the effector

protein while the N-terminus part of the phytochrome is hypothesized to act as a "switch" for the kinase domain. Thus, these kinase domains form an important part for understanding the molecular level of regulation of various physiological functions of the phytochromes.

The two kinase domains from CphA and CphBm i.e. HisKin (A-HK and B-HK) were expressed similarly in *E. coli* BL21 (DE3) RIL+RIPL cells like the other domains of the phytochromes. But recombinant proteins mostly expressed as insoluble inclusion body which was detected through SDS-PAGE. To overcome this problem, the expression induction was reduced to 0.250 mM IPTG. Here, there was sufficient amount of soluble proteins detected by Western blotting give numbers of amounts that were obtained, but B-HK was quite poorly expressed as compared to A-HK. The Western blot analysis shows the expected bands at 36.5 for A-HK while 35.4 for B-HK. The purified truncated domain proteins here served our purpose to understand the kinetic interaction amongst the partners of the two component system as discussed further ahead.

4.3 Micro-Calorimetry Experiments

Isothermal titration calorimetry (ITC)

Isothermal titration calorimetry, also termed as microcalorimetry, is a thermodynamic technique that monitors a chemical reaction initiated by interaction between two reaction partners. Microcalorimetry uses a suite of techniques to directly measure enthalpy and heat capacity changes i.e. heat absorbed or released, arising during chemical reactions / reaction partner interactions. When performed under straight temperature controlled conditions, the measurement of this heat allows accurate determination of binding constants (KB), reaction stoichiometry (n), enthalpy (ΔH) and entropy (ΔS). ITC measures, in aqueous solution, heat flux into or out of the sample i.e. change in heat (enthalpy - kJ/mol) as a result from the interaction of virtually any two molecular species. The characterization of biomolecular interactions, through ITC applies to ligand binding to receptors, changes in the conformation of complex macromolecules (such as proteins or DNA), and in protein-protein or nucleic acids interactions (Ladbury et al., 2004). ITC hence provides a complete thermodynamic profile of molecular interaction in a single experiment.

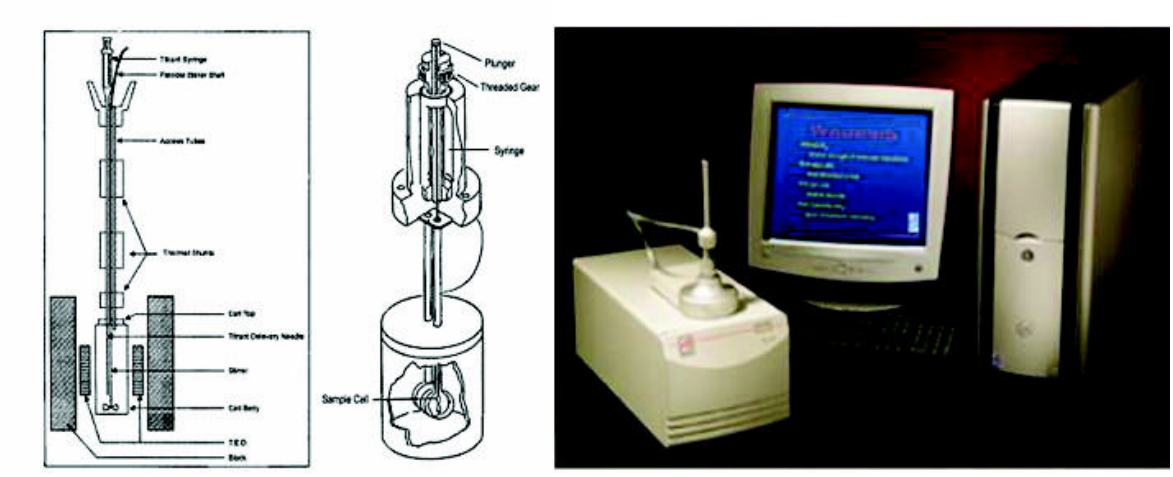

Figure 4.20 Representation of the ITC device : the left panel shows the detailed internal organization of the cell and needle of the calorimeter.

4.3.1 ITC Experiment

The basic set up for the ITC measurements is shown in the figure 4.41. The two basic parts of the instrument – syringe and cell, with the syringe containing the "ligand" solution was titrated into the cell containing the "macromolecule" solution at constant temperature. Here, the full length phytochrome was used in the cell of the micro calorimeter whereas the response regulator proteins was gradually titrated into the cell from a constantly stirring needle, thus there was controlled addition of the amount of the response regulator partner with time, maintaining a constant temperature and other conditions, only increasing the amount of the protein. Heat is released or absorbed in direct proportion to the extent of binding. As the macromolecule becomes saturated with ligand, the heat signal diminishes until only background heat of dilution is observed. The ratio of the proteins used in the cell to needle was initially at 1:10 in micromolar quantities.

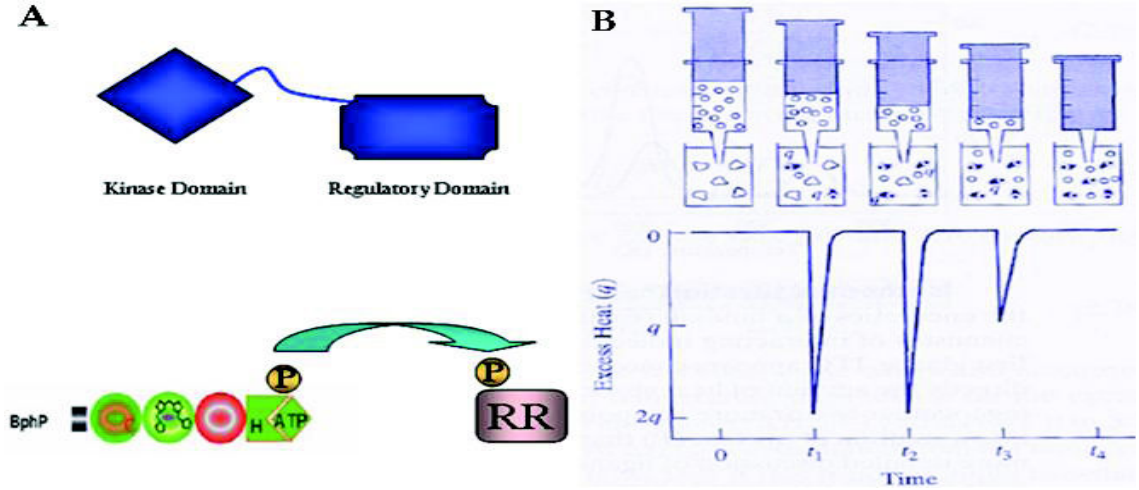

Figure 4.21 Cartoon depicting the reaction mechanism at the molecular level of the ITC measurements : Panel A ; Graphical view of the protein interaction studied during this study using phytochrome two component signaling system ; Panel B : Graphical representation of the reaction mechanism where the upper panel shows the titration of ligand into the cell of calorimeter, while the lower panel shows the measurements of the enthalpy changes.

The data was collected from the continuously reading calorimeter, with 24 consecutive injections of the response regulator solution to the photoreceptor phytochrome protein solution. The area underneath each peak is equal to the heat released for a particular injection. Integrated heat was plotted against the molar ratio of ligand to macromolecule in cell, producing a binding isotherm curve for the interaction. Such data points obtained were fitted based on the (assumed) number of binding sites, in this case one.

4.3.2 Protein –Protein interaction Study

The phytochromes CphA and CphB, alongwith their cognate response regulators (RcpA and RcpB) that are associated in the same operon in the genome, form the light-driven bacterial two component system in the cyanobacterium *Calothrix* PCC7601 (Jorissen et al., 2002). The photoreceptor transmits the signal to a downstream situated response regulator which is implicated in various secondary stage responses or activities. There is phosphorylation of the full length protein as the C-terminal part is a kinase, which is responsible for the transfer of the phosphoryl group to the response regulator. This statement comes from the experimental radioactive transfer of the ^{32}P- phosphate, as previously published (Hübschmann et al., 2002). The two proteins after separate purification steps were analysed for purity through SDS–PAGE, and then used for the above experimentation. We know from radioactive data that these two proteins interact via phosphor-transfer, and here microcalorimetry aims at determining the binding constants of such an interaction.

The protein samples prepared for the experiments were thoroughly degassed prior to each experiment. Initially, blank measurements were performed where the reservoir cell protein, here the photoreceptor as well as the response regulator proteins were titrated against the buffer used for the proteins dissolution, both in the presence of ATP and ATP analogue (non-hydrolyzable ATP), so as to ensure no changes occur with buffer alone (Fig. 4.42). These measurements were

used as control set of experimental data for all the titrations performed with both the proteins.

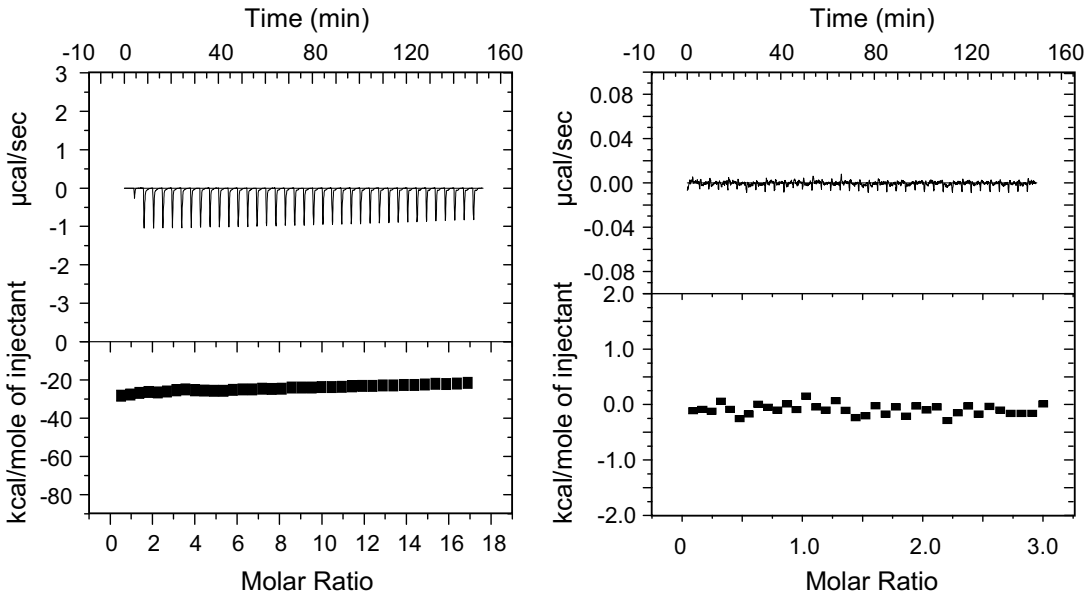

Figure 4.22 : Control experiments of isothermal titration calorimetry measurements: Control experiments of isothermal titration calorimetry measurements. Titration of the buffer into (left) a solution of BV-reconstituted CphBm, and of (right) buffer into a solution of RcpA.

The experimental set-up reaction measured is graphically represented in the Fig. 4.21, where the phosphoacceptor protein, here the full length phytochrome was stepwise titrated against the cognate response regulator in the presence of ATP (1mM). In all experiments, the response regulator (RcpA/B), typically at a concentration of 200 µM, was injected in 15 µM increments into the calorimetry cell, until complete saturation. The calorimetry reservoir cell contained the phytochrome protein (as either the full length CphA/B protein) in 2 ml of buffer at a concentration of 15 µM and ATP at a concentration of 1 mM. The two proteins in the reaction were in the same buffer, and at constant temperature conditions, only varying in the molar ratio between the two partners (Fig. 4.22 – Fig. 4.23).

Although the radioactive data suggests transfer of the phosphoryl group form the phytochrome to the regulator protein when incubated together (Hübschmann et al., 2001, 2002), the titration here did not result in any significant interaction between the two proteins. The experiments showed trivial binding constants between the two proteins even in the presence of ATP, though a titration curve without a clear inflection point could be observed (Fig 4.43 (A & B)).

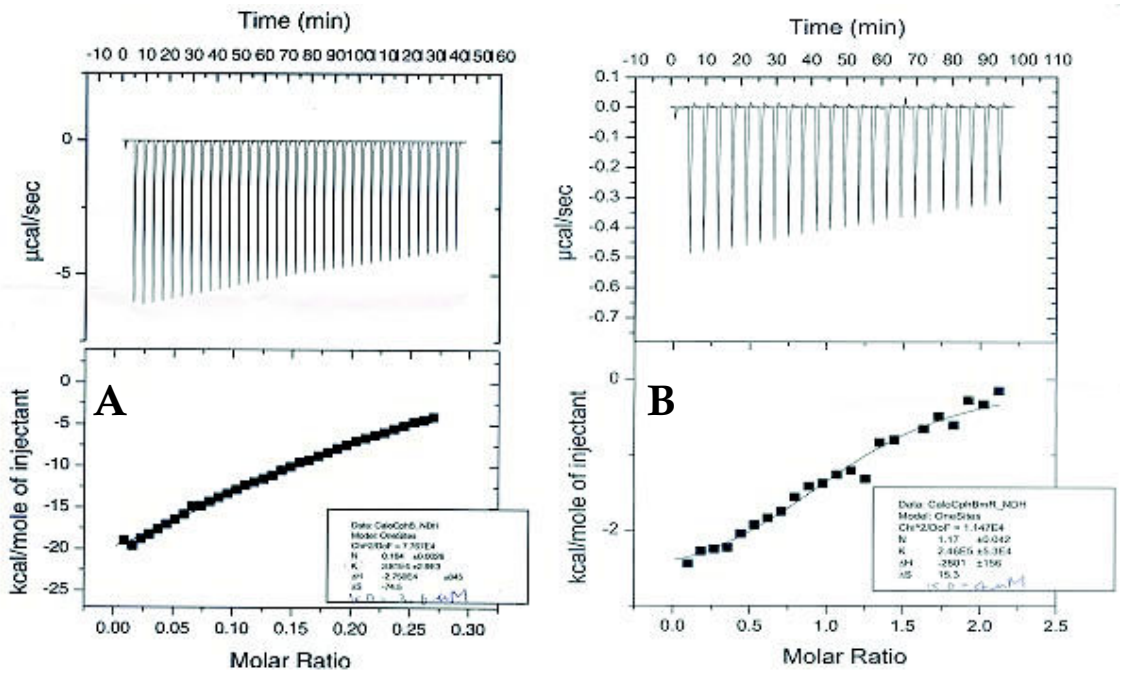

Figure 4.23 Graphical representation of the ITC experiment in presence of ATP: (A) CphBm phytochrome with the buffer-blank reaction, (B) CphBm reaction with RcpB; molar ratio of the protein samples is 1:10 (CphBm : RcpB). Both the experiments were done in the presence of ATP.

The titrations obtained after the above described experimental setup thus pointed towards transient nature binding between the two proteins. The interactive melange of reaction steps (i.e. binding of RcpB to CphB+ATP, hydrolysis of ATP to ADP while phosphorylating RcpB) followed by these two-component binding partners amongst themselves as well as with ATP, during the phosphotransfer mechanism thus form a multifarious approach.

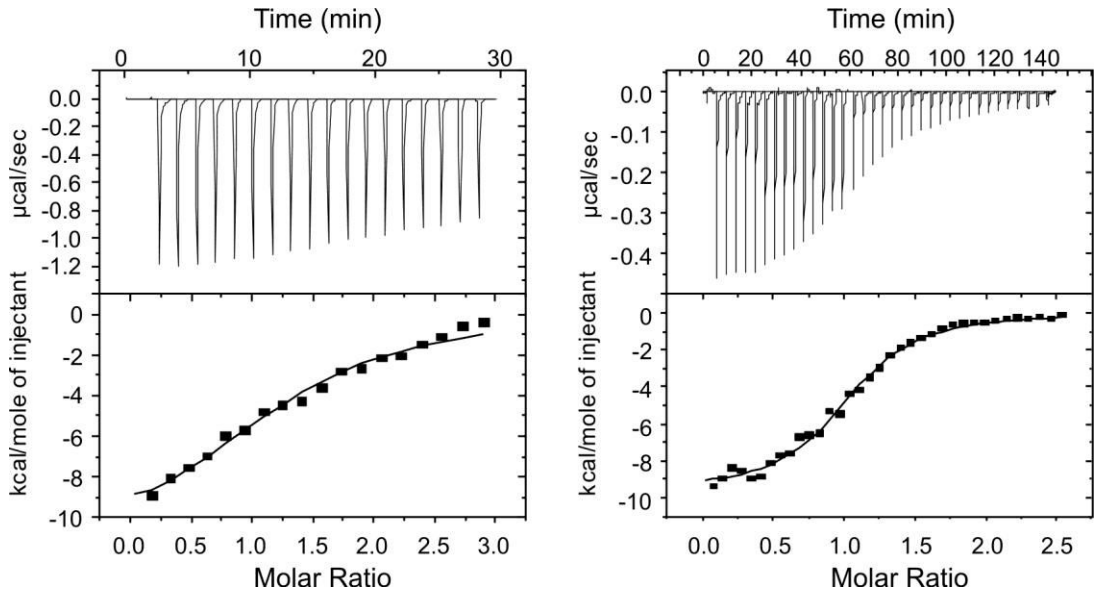

Figure 4.24 Graphical comparison of the ITC experiment in the presence of ATP vs. non-hydrolysable ATP: (A) CphBm reaction with RcpB in the presence of ATP. (B) CphBm titration reaction with RcpB in the presence of non-hydrolysable ATP. Both the experiments were done in the presence of ATP. Molar ratio of the protein samples is 1:5 (CphBm : RcpB).

These results led to a final set of experimentation where a non-hydrolyzable ATP source was provided to look for the binding interaction of the two partners, since in this experiment a kinase with ATP-binding capacity was studied. Thus finally experiments were performed to include the pre-incubation of the photoreceptor protein with non hydrolyzable ATP at a concentration of 1mM for about 10 minutes, after which time the response regulator was titrated into the reaction vessel (Fig. 4.20). A significant binding curve was obtained under such conditions symptomatic of the complex formation between CphB and RcpB.

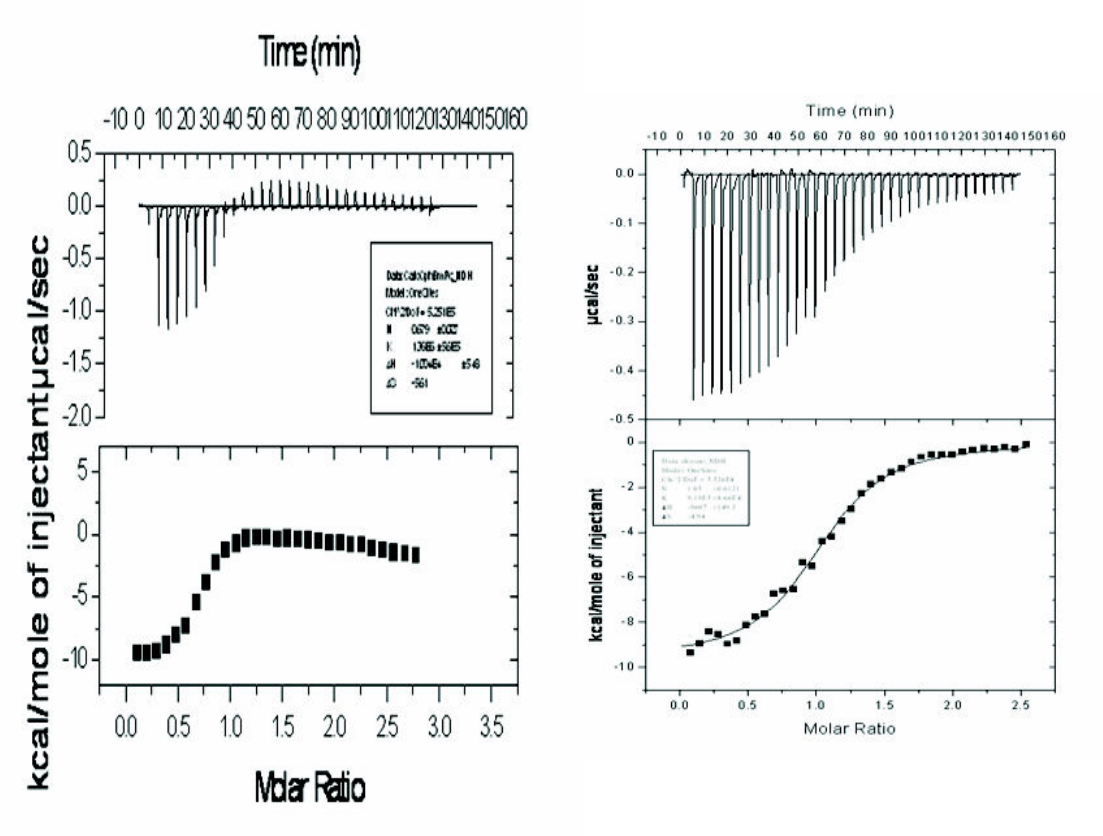

Figure 4.25 Graphical presentation of the ITC experiment : Panel (A) shows the pre-incubated CphBm with non-hydrolysable ATP and RcpB titration into the cell, molar ratio for CphBm : RcpB is 1:10; (B) CphBm with non-hydrolysable ATP and RcpB titration at 1:5 molar ratio for the two proteins respectively. The ratio for the consecutive experiment was done as the 1:10 molar ratio experiment had very fast kinetics.

The results clearly indicate that the interaction in terms of microcalorimetry occurs only when there is a non-hydrolysable binding agent present (here as a non-hydrolyzable ATP-derivative), whereas there is minimal binding of the two proteins without this agent. A binding constant of 1.1 µM for the CphB/RcpB was calculated from the data obtained. The stoichiometry was determined close to 1 (1.5), with CphA/RcpA couple having nearly identical behavior with binding constant calculated to 1.2 µM and stoichiometry of 0.9. These findings evidently advocate the definite role of the non-hydrolyzable ATP in stabilizing the kinetic interaction between the phytochromes and their cognate response regulators to be sufficiently measured by ITC. The phosphorylation condition of the recombinant

proteins obtained from *E. coli* is not ascertained as such here nor is whether there is any effect of irradiation difference in this interaction.

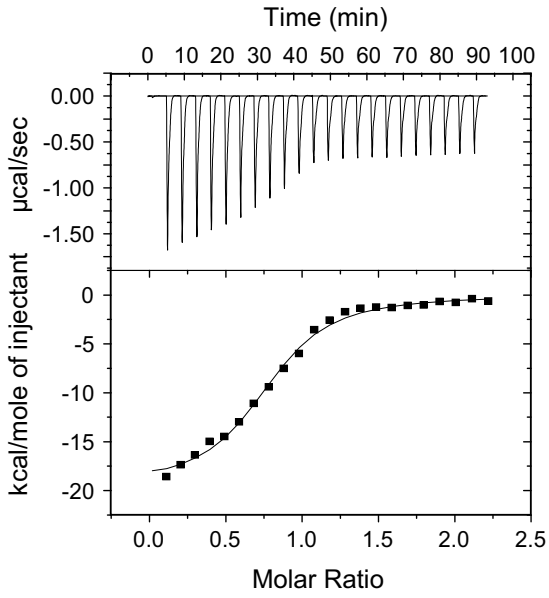

Figure 4.26: Graphical presentation of the titration interaction: The graph epitomizes the interactive thermodynamic sketch for CphA and RcpA proteins, signalling two-component partners, in the presence of non-hydrolyzable ATP derivative.

All the above described reaction set ups were performed with the chromophores assembled phytochrome protein irradiated with far-red light to get the Pr form that was dark incubated and further experimental procedure was carried out under safe green light for the photoreceptor.

The effect of light on the kinetics of this chromophore bound photoreceptor-response regulator interaction transpired as the next logical extension to the above experimental results. The C-terminal histidine kinase part, not involved in light perception by these proteins was a suitable candidate domain to study this interaction in the absence of the photoreceptor core domains. The HK domain was recombinantly expressed and titrated against the response regulator protein under similar conditions as for full length phytochromes. Quite interestingly, the HK

domain alone, either in the presence or absence of non-hydrolyzable ATP did not exhibit any characteristic complex formation with RR, indicative of requirement of the photosensory core for such an interaction. The titration curve obtained pointed towards a completely different interaction between the two proteins here (Fig. 4.27).

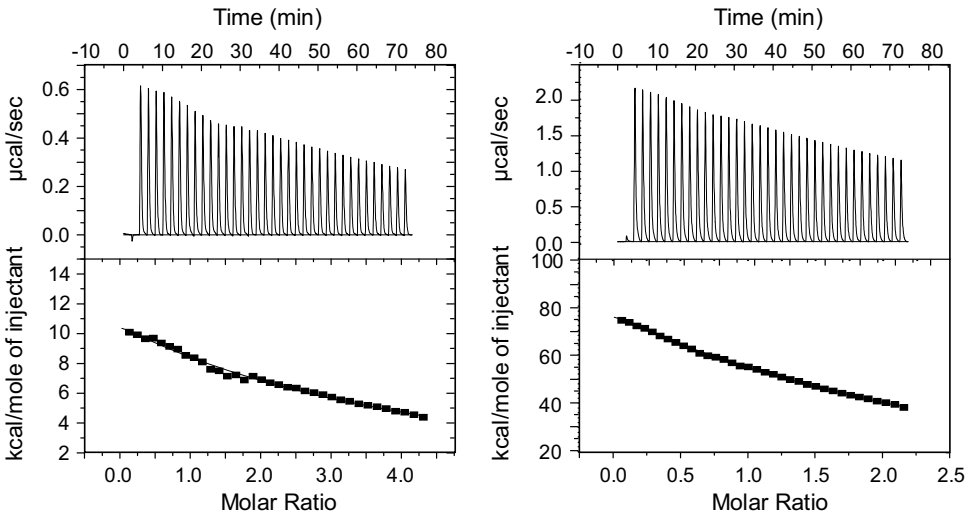

Figure 4.27 : Titration of the heterologously expressed HK domain from CphA and RcpA: Titration of the heterologously expressed HK domain from CphA and RcpA, showing calorimetric interaction in the (left) presence or (absence) absence of non-hydrolyzable ATP derivative. The lower panel shows the binding isotherm of the titration shown in upper panel. The continuous line represents the least-squares fit of the data to a single-site binding model.

The ITC data assaying in totality provide substantial relevance to the radioactive studies on these two proteins (Hübschmann et al., 2001). The two component functionality of auto- and trans-phosphorylation during the transitory complex formed between the phytochrome and its cognate response regulator is established with the molar ratio of the proteins involved as 1:1, though a 2:2 ratio isn't excluded that is herald of the homo-dimerisation adopted by the histidine kinase domains. The Pr endorsed auto-phosphorylation activity, as experimentally seen in the dark assembled or biosynthesized phytochromes (Hübschmann et al.,

2001, 2002) appended us to trail the role of histidine kinase alone in this phosphoryl transfer. The ITC reaction turns on the fact of the inacitivity of the HK domain alone without the regulatory photosensory core of the phytochromes. The tabular representation of the ITC parameters of the experiments performed is depicted below (Table 4(e)).

TABLE 4 (e)

Thermodynamic parameters of CphA-RcpA and CphB-RcpB binding reactions

	$\Delta H°$ (kJ mol^{-1})	K ($M^{-1} \cdot 10^5$)	ΔG (kJ mol^{-1})	$T\Delta S$ (kJ $mol^{-1}K^{-1}$)	K_D (µM)	n
CphB / RcpB(ATP analog)	-9.6	9.19	-8.3	-1.47	1.08	1.05
CphB / RcpB	no binding					
CphA / RcpA (ATP analog)	-19.4	8.05	-8.2	-11.2	1.2	0.9
HK domain / RcpA	no binding					
HK domain/ RcpA (ATP analog)	no binding					

The locked reaction parameters during (CphB/RcpB/ATP) complexing interaction where the non-hydrolyzable ATP (ADPNHP) secede the phosphate transfer from the binding of the two proteins here has allowed the binding parameters using ITC. The transient nature of such binding also illuminate the amplification and transduction aspect of the light signal provided by the phytochromes directed to higher number of regulator protein molecules.

4.4 FTIR - Spectroscopic characterization of recombinant phytochromes

4.4.1 FTIR - Introduction

Fourier Transform Infrared Spectroscopy (FTIR) is a powerful tool for identifying types of chemical bonds (functional groups) in a molecule by producing an infrared absorption spectrum that is like a unique molecular "fingerprint". This technique measures the absorption of various infrared light wavelengths by the material of interest. The wavelength of light absorbed is characteristic of the chemical bond as can be seen in the annotated spectrum.

Thus, infrared absorption bands identify specific molecular components and structures. Absorption bands in the range of 4000 - 1500 wavenumbers are typically due to functional groups (e.g. -OH, C=O, N-H, CH3, etc.). The region between 1500 - 400 wavenumbers is referred to as the fingerprint region. Absorption bands in this region are generally due to intra-molecular phenomena, and are highly specific for each material.

4.4.2 Description of technique - FTIR spectroscopy for proteins

FTIR as a vibrational spectroscopy can yield information on the function and dynamics of a certain system. Vibrational spectra are directly related to structural features of molecules, for example, lengths of bonds, mass of atoms, dipole moments, etc. The frequencies of the bond vibrations here are determined by the electronic nature of the bonds, hence making them sensitive to changes in structure and environment: strength of hydrogen bonds, hydrophobicity, bond angles, etc. The vibrational modes of the peptide amide groups are of prime interest in the study of peptides and proteins, and the amide I band is the most widely used amide mode. The amide I mode principally originates from the carbonyl stretching vibration of the amide group, with some contribution from the C-N stretch, and gives rise to infrared bands between 1600 and 1700 cm^{-1}. These

bands are well established indicators of secondary structure because of their sensitivity to hydrogen bonding, dipole-dipole interactions, and geometry of the peptide backbone.

Qualitative Analysis

The overwhelming intensity of amide-I and -II bands, however, covers any other change, e.g., such of single carboxylic acids de- or reprotonation - which are in the intensity range of 10^{-3} - 10^{-5}. For such reason, FTIR is usually allied as a difference technique where spectra are taken during each change, one before the event and another after the event, and the difference is then considered. Such procedure annihilates the strong amide bands (which are usually not subject of change).

4.4.3 Phytochrome protein FTIR

4.4.3.1 Phytochrome photoreaction

The phytochromes had the intrinsic property of an interconvertible photoreaction between two parent states, *i.e.* the red-absorbing form (Pr) (λmax = 664 nm/ 700 nm) and the physiologically active, far-red–absorbing form (Pfr; λmax = 707 nm/ 750 nm) (Sineshchekov et al., 1995). The photoreactivity is a property by virtue of the linear tetrapyrrole chromophore linked with the apoproteins, which undergoes molecular changes during the photoconversion. These changes have been attributed to a *Z*,*E* isomerization around the C15=C16-methine bridge during the conversion (Rüdiger et al., 1992).

4.4.3.2 FTIR for Phytochromes

The elucidation of phytochrome photoreversibility at the molecular level has been the prime focus of biochemical characterization of the light activated protein systems. Light-induced Fourier-transform infrared (FT-IR) difference spectroscopy has been put to use for the comprehensive biophysical investigations of the biological photoreceptors as the spectra obtained here refer to changes in

both chromophore and protein (Foerstendorf et al., 1996, 2001; Schwinté et al., 2008). In the current work, the photoreactions of CphA and CphBm, i.e. Pr → Pfr and Pfr → Pr, reconstituted with phycocyanobilin and biliverdin respectively, were investigated using optical and FT-IR difference spectroscopy. The assignments of bands in vibrational spectra are done in comparison with the observed spectral homologies to the spectra of *Synechocystis* Cph1 and oat phyA (Foerstendorf et al., 2000; vanThor et al., 2005). The initial aspects of the chromophore-protein interaction changes are studied at low temperature infra red spectra in this work.

We have investigated the low temperature infra-red spectroscopy for the full length phytochromes to gain new insights into the structure and function of the holoproteins bound to their respective ligands; this work was done in collaboration with the research group of F. Siebert, Univ. Freiburg. Samples were prepared as dry films, which then were rehydrated (section 3.13). The degree of rehydration of the protein film was checked using the broad absorption band of water around 3300 cm^{-1}. Sealing the sandwich windows with silicone on the edges prevented dehydration of the film in the cryostat. Since FTIR in that measuring regime is a static method, the sample has to remain in the same state during the whole set of experiments (data acquisition by averaging). This is usually accomplished by low temperatures which freeze the sample in a certain state (intermediate) of the conversion. The samples were irradiated in frozen state at low temperature and then stepwise warmed to slightly higher temperatures, only allowing a conversion to the next following intermediate. The samples were photoconverted within the FTIR spectrometer by irradiation with red and far red light using interference filters of either 660 nm or 710 nm peak transmission. The intermediates were accumulated by irradiation of Pr or Pfr at the temperatures given in the figure captions. In order to ensure that same intermediate states are reached under the given set of conditions, the identical sample subjected to FTIR is in advance controlled by (difference) spectroscopy. Accordingly, first the UV-Vis control experiments are shown, and then followed by the FTIR data under the

same conditions (Fig. 4.28). The final step of the phototransformation, back to the initial state, had to be performed at ambient temperature. For each single-beam spectrum, 512 scans were accumulated with a resolution of 4 cm^{-1}. Photoreversibility of phytochrome in the rehydrated film samples was checked by recording the visible absorption spectra between 500 and 800 nm on a UV/VIS spectrometer.

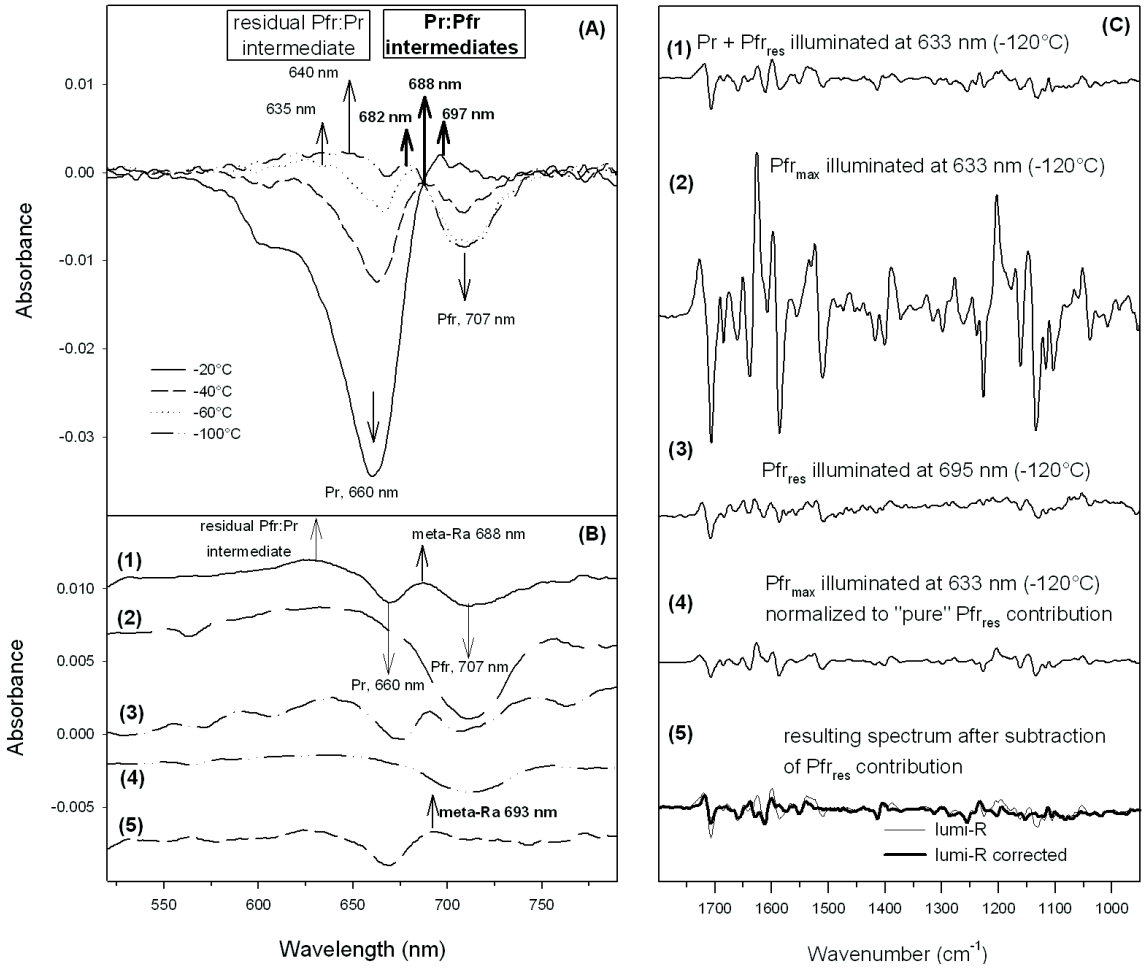

Figure 4.28 : Graphical measurements followed during FTIR spectroscopic analysis. (A) Measured UV-Vis difference spectra of the Pr:Pfr pathway, including a residual backward reaction, upon red illumination (633 nm); (B) Correction procedure applied to the measured UV-Vis spectra of the Pr:Pfr pathway, to subtract the contribution of unwanted backward photoreaction: the example of meta-Ra (-45 °C); steps (1) to (5) are described in section 4.4.3.4; (C) The correction procedure applied to the measured FTIR spectra of the Pr:Pfr pathway in the case of lumi-R (-115 °C).

Since FTIR applied here is a static method, the sample has to remain in the same state during the whole set of experiments (data acquisition by averaging). This is usually accomplished by low temperatures, which freeze the sample in a certain state (intermediate) of conversion. The samples were irradiated in frozen state and then stepwise warmed to slightly higher termperatures, only allowing a conversion to the next following intermediate. In order to ensure that same intermediate states are reached under low temp conditions the identical sample subjected to FTIR is in advance controlled by (difference) spectroscopy. Accordingly, first the UV-Vis control experiments are shown, and then followed by the FTIR data under the same conditions.

4.4.3.3 FTIR measurement facts:

1.) Each FTIR difference spectrum is the average of approximately 10-30 single difference spectra corresponding to several samples and several experiments per sample, each obtained from 5 single-beam spectra recorded before and 3 single-beam spectra recorded after illumination, and taking into account a baseline drift caused by the long measuring time. There is a correction procedure for the solvent heat effect caused due to longer illumination during measurements before we arrive at the final FTIR spectra.

2.) The reading of absorption changes is immediately followed by the actual FTIR measurements, when there is no residual photoreactivity of the sample identified as “light effect”. This reading was substracted from actual FTIR spectra to achieve the final data.

3.) The spectral noise level of the measured spectra was deduced from the baseline above 1750 cm^{-1}, where no bands show up, taking in addition the spectral variation of the IR intensity into account. The band intensities of the spectra can be estimated from the strongest bands which extend from 0.1 milliabsorbance units (mOD) for the early photoproducts (lumi-R, meta-Ra) to 2 mOD for the Pfr-spectrum. Low temperature-caused differences in spectral intensities are due to the

gradual reduction in photoconversion rates. For comparison, the spectra were normalized in the region around 1400 cm^{-1}.

4.) As described above, FTIR measurements were performed alongwith UV-Vis spectroscopy. A residual Pfr form persisted during the forward reaction from Pfr to Pr hence generating corresponding photoproducts. This is due to the overlapping of the absorption spectra of Pr and Pfr. To extract the spectra of "pure" Pr:Pfr intermediates from these mixtures, we applied the procedure described below. This residual Pfr was confirmed by measurements at 0 °C after Pr generation by far-red illumination, showing that in less than 30" a small residual Pfr:Pr-like difference spectrum could be generated by additional far-red illumination (data not shown).

4.4.3.4 Correction procedure for the presence of residual Pfr :

The spectra (UV-Vis as well as FTIR) of "pure" Pr-to-Pfr intermediates from the mixtures containing in addition the photoproducts from Pfr, were deduced from two supplementary illumination experiments. As an example they are described for meta-Ra (res = residual, F-int = intermediate of the Pfr-to-Pr pathway, Pfr,max = maximum amount of Pfr that can be obtained):

(1) $\text{sample} \xrightarrow{695\text{nm},20^{\circ}\text{C}} \text{Pr} + \text{Pfr,res} \xrightarrow{633\text{nm},-45^{\circ}\text{C}} \text{meta - Ra} + \text{F} - \text{int}$

The corresponding difference spectrum is then corrected for the presence of the F-intermediate.

(2) $\text{sample} \xrightarrow{633\text{nm},20^{\circ}\text{C}} \text{Pr} + \text{Pfr,max} \xrightarrow{633\text{nm},-45^{\circ}\text{C}} \text{F} - \text{int} + \text{meta - Ra (small amount)}$

the same illumination procedure as in (1) is used.

(3) $\text{sample} \xrightarrow{695\text{nm},20^{\circ}\text{C}} \text{Pr} + \text{Pfr,res} \xrightarrow{695\text{nm},-45^{\circ}\text{C}} \text{F} - \text{int}$ (pure)

This F-intermediate (pure) spectrum is noisy, since the absorbance changes are small because of the low amount of Pfr, but it contains the same amount of F-

intermediate as in (1). The larger bands, however, can be used for normalization of spectrum 2 on this amount of F-intermediate (Fig. 4.29 (B)). Because of the high amount of F-int, the noise is much less in (2), and therefore, this spectrum is used for correction after normalization.

(4) = (2) normalized on (3)

(1) - (4) = (5) $\mathbf{Pr} \xrightarrow{633nm,-45°C} \mathbf{meta-Ra}$

The small amount of meta-Ra present in (2), and thus also in (4) only reduces the size of the meta-Ra spectrum by a small amount. This correction procedure is presented on Figure 4.28 (A) for UV-Vis spectra and Figure 4.28 (B) for FTIR spectra. The correction seems to be quite small for the intermediates trapped at -25 °C and -45 °C, but it is quite significant at lower temperature such as -120 °C for correction of lumi-R spectra (Figure 4.28 (B). This is due to the fact that the photoproduct yield is reduced for the Pr:Pfr pathway, whereas it is essentially independent of the temperature for the Pfr:Pr pathway.

4.4.4 FTIR for CphA

4.4.4.1 UV-Vis spectroscopy parallel to the FTIR spectroscopy

As mentioned, the samples were subjected to UV-Vis spectroscopy prior to the FTIR measurements. Spectra are depicted in accordance to the conventional way of presenting IR difference spectra, hence the Pr spectrum absorbing at 660 nm is shown negative (parent/ground state) while the Pfr form absorbing at 707 nm is shown positive (Figure 4.29 (A)). The difference spectrum for the two states of CphA was measured at room temperature with the sandwich sample. The spectrum shows the characteristic bands at 660 nm and a shoulder at 605 nm of the Pr form (negative bands) and the band at 707 nm of the Pfr form (positive band).

The photoreactions of both the forward Pr:Pfr pathway and the backward Pfr:Pr pathway were investigated at low temperatures, with temperatures ranging

from -20 °C to -140 °C, at 10 or 20 degrees intervals. The main purpose of these studies is the determination of the temperature for stabilizing intermediates. Because of the shorter measuring time as compared to FTIR spectroscopy, UV–Vis spectroscopy is better suited. By repetitive measurements over 30 min at these temperatures the optimum temperature was selected to obtain a stable photoproduct.

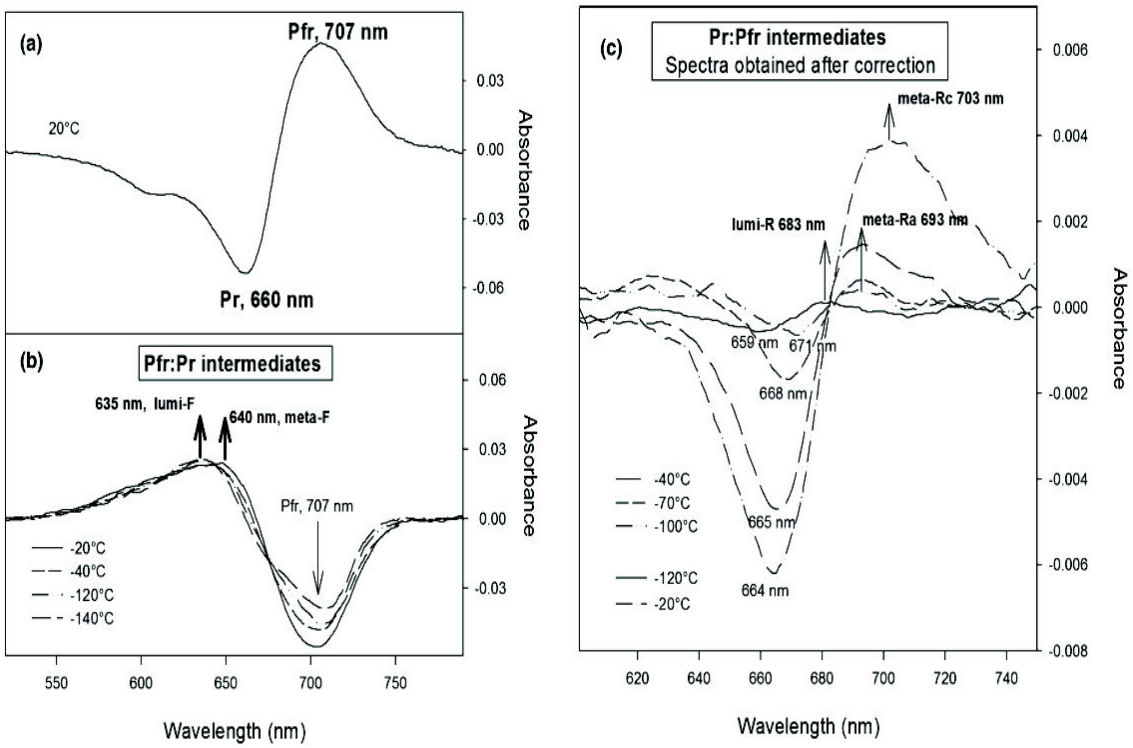

Figure 4.29 : Spectroscopic graphical representation of UV-Vis measurements of CphA phytochrome done in parallel with FTIR spectroscopy: (A) UV-Vis difference spectrum between Pr and Pfr (T=20 °C); (B) Difference spectra of the Pfr:Pr pathway, upon far red illumination (695 nm); (C) Difference spectra of the Pr:Pfr pathway, upon red illumination (633 nm), after correction.

***Pr-to-Pfr pathway* :** Photoreaction yields decreased with lowering temperature affecting the difference band spectrum intensity which went from about 35 mOD at -20 °C to about 5 mOD at -140 °C (Figure 4.28 (A), non-corrected). A striking feature of the spectra for the Pr:Pfr pathway is the simultaneous presence of two

minima below -20 °C. This can be explained such that a residual Pfr state corresponded to the presence of the second minimum, the main minimum at 660 nm corresponding to the disappearance of the Pr state, and the second minimum at 707 nm referring to Pfr. The Pr:Pfr transformation is completed above -10 °C. It can be seen that the relative contribution of residual Pfr to the difference spectra increases at lower temperatures (e.g. temperature less than -20 °C to -100 °C), since the yield of the forward reaction decreases; interestingly, the backward photoreaction does not show such a gradual reduction (see Pfr:Pr pathway). The difference spectra obtained after applying the correction procedure described in Section 4.4.3.4 are shown in Figure 4.29 (C). We now can deduce the absorbance maxima in the difference spectra for the intermediates: meta-Rc (-20 °C to -30 °C) at 703 nm, meta-Ra (-40 °C and -100 °C) at 693 nm. The third intermediate (lumi-R) is only obtained at temperatures lower than -100 °C and the corresponding absorption maxima in the difference spectrum is estimated to 683 nm. As expected, the lower photoproduct yield at lower temperatures is also evident in the corrected spectra.

The data when anticipated after comparison to the corresponding values of Cph1 (Foerstendorf et al., 2000), shows large differences where the values for Pr and Pfr in the Pr:Pfr difference spectrum are 653 and 709 nm, respectively. These values thus essentially represent the actual absorption maxima showing a larger spectral shift in this transition of Cph1. The Cph1 FTIR spectra show that the lumi-R difference spectrum very much resembles that reported here for CphA, i.e. a minimum close to the value of the Pr state and a maximum around 680 nm. The published values for the meta-Ra and meta-Rc difference spectra also resemble those of CphA, i.e. the maxima and minima are rather closely spaced in meta-Ra and exhibit a somewhat larger separation in meta-Rc (Foerstendorf et al., 2000). The different values for the negative bands are caused by varying spectral overlap between the Pr state and the photoproduct states. The different values for the negative bands are caused by varying spectral overlap between the Pr state and the

photoproduct states. Thus, the two cyanobacterial phytochromes behave very similar, although the actual values show small differences. This shows that the chromophore–protein interaction must be very similar, although not identical, in agreement with the homology of the chromophore binding pocket.

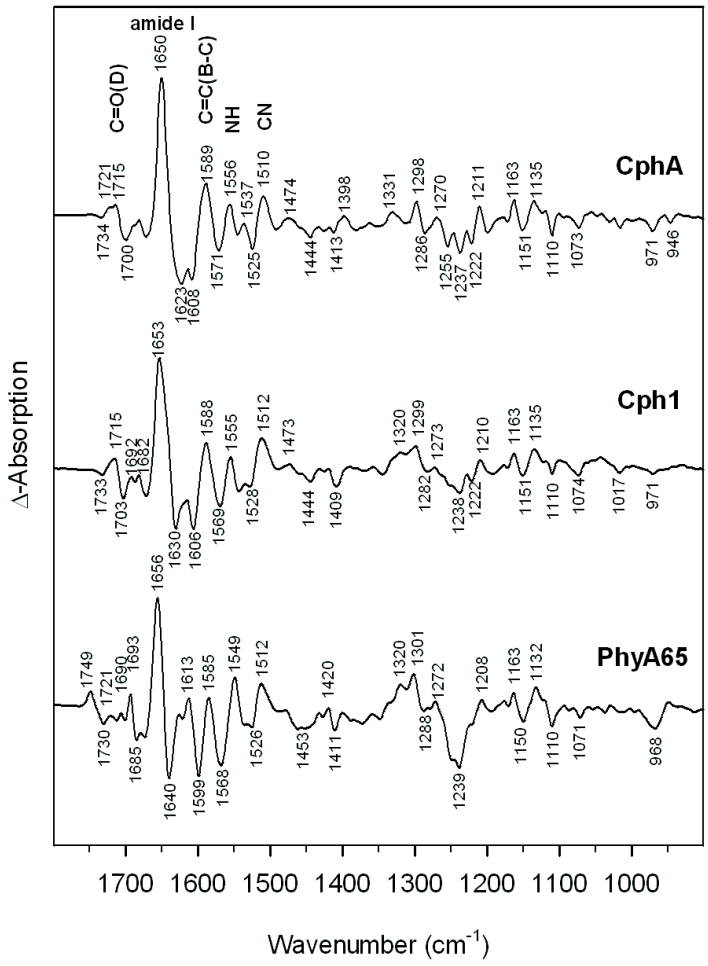

Figure 4.30 : Comparison of the Pr:Pfr FTIR difference spectra (0°C) for various recombinant phytochromes: From top to bottom: CphA from Calothrix (88 kDa), Cph1 from Synechocystis (85 kDa), Cph1D2 (59 kDa) N-terminal fragment (514 residue) and PhyA (65 kDa), all assembled with phycocyanobilin (PCB).

The plant phytochrome, phyA here shows greater deviations, the values are generally red-shifted (Pr absorb at 665 nm and Pfr at 730 nm) since the chromophore phytochromobilin carries an additional double bond (vinyl instead

of ethyl group). The separation between the two values is considerably larger. The principal feature of the lumi-R difference band is similar to those of cyanobacterial phytochrome, taking the general red-shift into account, i.e. a negative band close to absorption maximum of Pr and a positive band around 695 nm. However, for the meta-Ra state, a general reduction of the absorbance has been described with no pronounced shift in the absorption maximum with respect to Pr, whereas in the cyanobacterial phytochromes, a clear difference band is observed with equal size of positive and negative bands (this work and Foerstendorf et al., 2000). On the other side, the meta-Rc difference spectra have similar features. Thus, as expected from the lower homology of the chromophore binding pocket, the deviations from the cyanobacterial phytochromes are larger, although still many spectral features prevail.

Pfr-to-Pr pathway **:** Whereas the intensity of the Pr:Pfr difference spectra strongly depends on the temperature, this is not the case for the intermediate spectra of the backreaction obvious from the relatively constant intensity absorption of 80 mOD in contrast to the forward reaction (Figure 4.29 (B)). In the Pfr:Pr photoreaction, only one minimum at 707 nm, corresponding to the disappearance of the Pfr state, and one maximum, corresponding to the photoproduct, was observed. In the temperature from -20 °C to -100 °C this maximum is located at 640 nm and below -120 °C it is shifted to 635 nm. This observation is similar to that found in Cph1, where the most blue-shifted positive peak is observed in the lumi-F difference spectrum [635 nm for CphA and 640 nm for Cph1], whereas in the meta-F difference spectrum the blueshift of the positive band is reduced by 5 nm (CphA) and 7 nm (Cph1) (Foerstendorf et al., 2000)]. This is in contrast to phyA for which, as compared to the Pr state, a redshifted absorption maximum has been reported (Eilfeld and Rudiger, 1985). The absorption maximum of meta-F is blueshifted as compared to Pr, similarly as that of cyanobacterial meta-F. Again, the varying homologies of the chromophore binding pocket may explain the similar (Cph1 and CphA) and different (phyA) spectral properties.

These low temperature investigations with UV-Vis led to selection of optimal temperature conditions to study these photoproducts by FTIR difference spectroscopy. These selected temperatures are, for the Pr:Pfr pathway, -25 °C for meta-Rc, -45 °C for meta-Ra (smaller correction), and -120 °C for lumi-R, and for the Pfr:Pr pathway, -70 °C for meta-F and -140 °C for lumi-F, respectively.

4.4.4.2 FTIR difference spectroscopy

Pr :Pfr difference spectra : The FTIR difference spectrum for CphA intermediates for the Pr-Pfr pathway are presented in figures 4.31 (H_2O) and 4.32 (D_2O), respectively. The corresponding spectra for the intermediates for the back reaction are shown in Figs. 4.33 and 4.34 for H_2O and D_2O, respectively. In each case, positive bands represent the intermediate state and negative bands represent the parent state. It is beyond the scope of this contribution to discuss all the bands of the intermediates at greater detail. The data presented focus on the comparison of the spectra of CphA with those of published data from Cph1 and from PhyA (Eilfeld and Rudiger, 1985; Foerstendorf et al., 2000). The comparative difference spectra studied were of CphA, Cph1Δ2 (the 59 kDa N-terminal fragment of Cph1 reconstituted with PCB) and of PhyA65 reconstituted with PCB (Fig. 4.30) with details of bands for which in the case of PhyA an unambiguous assignment could be made (Murgida et al., 2007; Schwinté et al., 2008) and to imply the significant differences between the three phytochromes studied.

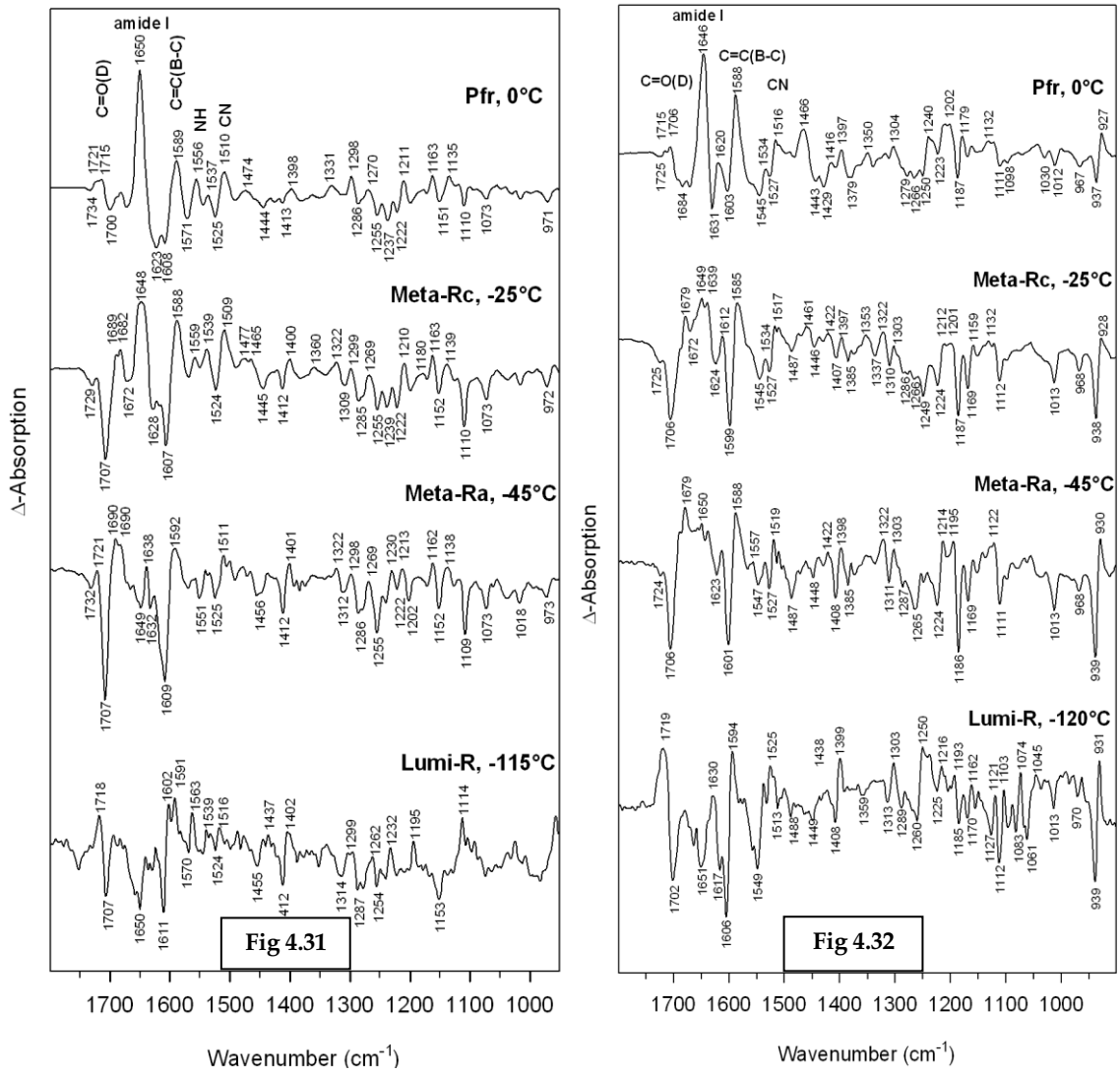

Figure 4.31 & 4.32 : Light-induced FTIR difference spectra of the photoreactions of recombinant bacteriophytochrome CphA recorded in H_2O and in D_2O: Depicted here from top to bottom: Pfr (0 °C), meta-Rc (-25 °C), meta-Ra (- 45 °C), lumi-R (- 70 °C) and lumi-R (-115 °C). Positive bands represent the respective photoproduct, negative bands Pr. (H_2O) measurements represented on the left panel while the D_2O measurements are shown on the right panel.

Pr:Pfr Difference Spectra: In general, the Pfr / Pr difference spectra of the three phytochromes display far-reaching similarities (Fig. 4.34). The band assignments for the proteins are discussed further ahead.

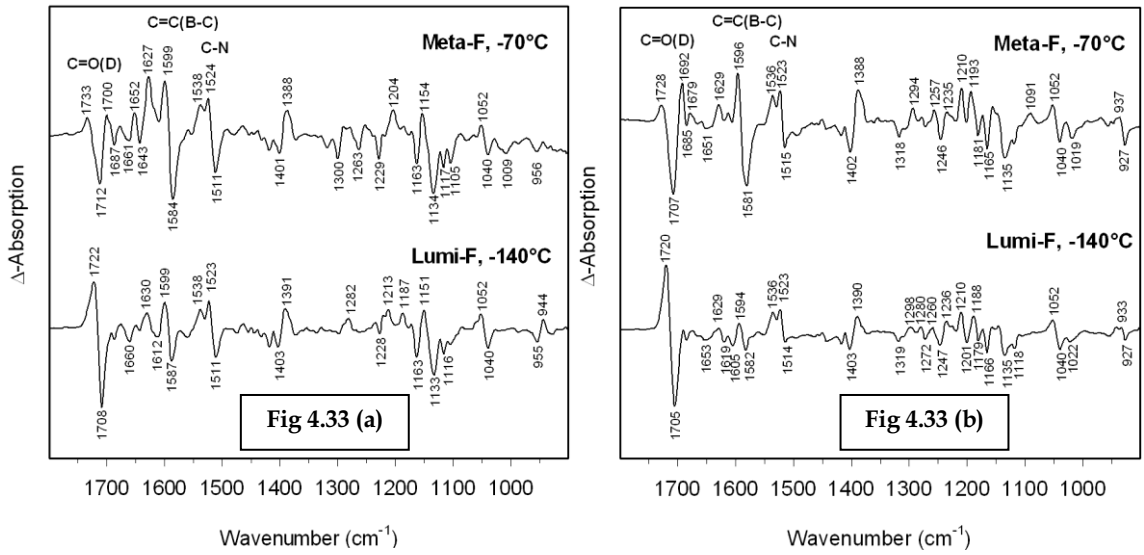

Figure 4.33 (a & b) : Light-induced FTIR difference spectra of the photoreactions of recombinant bacteriophytochrome CphA recorded in H_2O and D_2O: The spectra show intermediates of the Pfr:Pr pathway. Assigned from top to bottom: meta-F (-70 °C) and lumi-F (-140 °C). Positive bands represent the respective photoproduct, negative bands Pfr. Figure 4.33 (a) shows H_2O measurements while Figure 4.33 (b) shows D_2O measurements.

4.4.4.2 (A) FTIR band assignments

Difference band - 1623(-)/1650(+) cm^{-1}: An immense overall similarity was found in the spectra obtained from the above group of proteins studied with the strongest difference band at 1623(-)/1650(+) cm^{-1} in the case of CphA assigned to amide I changes**.** There were only few differences observed in CphA in comparison with Phy A with the band intensities at 1656(-)/1650(+) cm^{-1} for amide I changes as shown previously on the basis of phyA adducts with uniformly ^{13}C labeled PΦB. In this system no shifts of these bands have been induced by the labeling. The 1623 (-)/1650(+) cm^{-1} band showed no significant shift, thereby unanimously corresponding to the protein changes related to the amide I spectral changes in the proteins. This assignment is based on the measurements of PhyA65 reconstituted with uniformly ^{13}C-labeled PCB chromophore (Schwinte et al., 2008). Whereas the positive peaks are at very similar frequencies in all phytochromes, the frequency of the negative peaks shows more significant variations but still remains in the region

characteristic of amide I bands, indicating similar albeit not necessarily identical protein structural changes during the Pr:Pfr transition. Specifically, the band pattern in the amide I band region appears to be more closely related among the cyanobacterial phytochromes. For the comparison, one has to keep in mind that protein moieties of different lengths have been studied.

Bands range 1100- 1300 cm^{-1}: The band width region as observed in CphA between 1100 and 1300 cm^{-1} was assigned to chromophore vibrational modes at the molecular level which evidently occur in the Pr:Pfr transition typically found in Cph1 and PhyA phytochromes. Thus the characteristic Z:E isomerization of the methine bridge double bond between rings C and D of the chromophore (specific band assignments) could be safely projected during the light induced Pr-Pfr transition in cyanobacterial phytochromes. Also here, the congruence is better for the cyanobacterial phytochromes. This indicates that the chromophore structural changes during the Pr:Pfr transition are largely the same for plant and cyanobacterial phytochromes and only minor details may be different for CphA / Cph1 and phyA.

Difference band - 1608 (-)/1589(+) cm^{-1} : The substantial difference band seen at 1608 (-)/1589(+) cm^{-1} in the spectrum of CphA is attributed to the B-C methine bridge stretching mode coupled with the N-H in-plane bending coordinates of the rings B and C of the chromophore. Additional information of the coupling to NH bending modes is gathered by the downshift of this difference band in D_2O to 1603(-)/1588(+) cm^{-1} (Figure 4.33 (b)). The correct position of the positive band is around 1585 (+) cm^{-1}, since it is influenced as a result of the strong negative band at 1571 cm^{-1}. For phyA, it has been linked to special diagnostic value monitoring chromophore-protein interactions.

The downshift of this band in the Pr:Pfr transition cannot solely be attributed to the geometrical changes of the tetrapyrrole with the Z:E isomerization of the C-D bridge (Schwinté et al., 2008). Isotopic labeling of the chromophore in

phyA adducts point towards a similar mode composition in Pr and Pfr. Thus, we propose that a change in chromophore-protein interaction, resulting in the change of π-electronic system and /or in a change of the B-C geometry ((ring B)-C(10)-(ring C)) bond angle or B-C methine dihedral angle may explain this large downshift. Indeed, solid-state ^{15}N NMR studies indicate alterations in the electronic system upon Pr:Pfr conversion (Rohmer et al., 2006). Such changes may be induced by steric and / or electrostatic interactions. Electrostatic effects could be especially important since the protonated chromophore carries a net positive charge on the pyrrole rings B and C. Such alterations in the chromophore–protein interactions may be paralleled by a torsion of the A–B bridge as reflected by the large downshift of the corresponding stretching mode from 1645 to ca. 1620 cm^{-1} observed in the RR spectra (Mgorinski et al., 2004). This scheme of interpretation may be extended to CphA which seems to be justified in view of the similarities in the overall band patterns.

Difference band - 1571(-)/1556(+) cm^{-1} : The 1571(-)/1556(+) cm^{-1} difference band common to all species could be assigned to the protein as has been the case for phyA. Its position and disappearance during D_2O (Figure 4.33) measurements indicate that it must be assigned to amide II changes. They reflect structural changes of the protein backbone similar to the amide I band changes (vide supra). The assignment of amide I / II bands in the Pfr / Pr difference spectra is in agreement with FTIR studies of a Cph1 fragment using isotopic labeling (Murgida et al., 2007).

Difference band - 1525(-)/1510(+) cm^{-1} : The bands in the region between ca. 1600 and 1500 cm^{-1} have been previously assigned for phyA and these assignments hold true also for the cyanobacterial phytochromes due to overlapping spectral agreement in this region (Schwinte et al., 2008). For all three species (Cph1, PhyA and CphA), a difference band (1525(-)/1510(+) cm^{-1} for CphA) is observed that displays a small upshift upon H/D exchange (deuteration) indicating the

involvement of the N-H in- plane bending coordinate (Fig. 4.33). A precise molecular description of this mode will be difficult, since it would require taking the actual interaction of the NH groups with the protein into account (e.g. in case of DrBphP His 260 and Asp 207, and a water molecule (Wagner et al., 2007). Especially, the structural data show that the two NH groups of rings B and C are no longer equivalent. In the case of phyA, this assignment is further supported by the ca. 5 cm^{-1} shift caused by ^{15}N-labeled PCB.

The molecular affect for the observed downshifts of this band and of the band assigned to C_{10} methine stretching mode upon the Pr:Pfr transition needs to be further deciphered. There are two basic molecular changes which have to be considered: changes in the electronic structure similarly as deduced from the published NMR spectra (Rohmer et al., 2006; vanThor et al., 2006) and the geometrical changes of the chromophore. For a clear-cut explanation, extensive calculations would be necessary. However, some insights can be obtained from the spectra of the intermediates.

Negative band - 1734 cm^{-1} : The small negative band around 1734 cm^{-1} for CphA assumingly corresponds to the difference band assigned to the C=O stretch of ring A (Foerstendorf et al., 2001), where this band is upshifted in Pfr state in the spectrum of PhyA. Instead, in the spectra of Cph1 and CphA a downshift probably takes place, rendering the assignment less unequivocal. However, because of the similar positions of the negative bands, we assign also these difference bands to this mode. This is supported by the downshift observed for measurements in D_2O (Figure 4.33). Furthermore, under circumstances not yet completely clarified, also for PhyA a downshift of this band is observed (Schwinté et al., 2008).

4.4.4.2 (B) Intermediate Spectra : Lumi-R, Meta-Ra & Meta-Rc

Lumi-R : For cryogenic trapping of Pr-Pfr photocycle intermediates, the choice of the appropriate temperature was guided by UV–Vis spectroscopy as described

above. Comparing the spectra with those of Cph1 and of phyA published earlier (Foerstendorf et al., 2000, 2001), we note an overall striking similarity, although the absolute positions of bands vary from protein to protein.

The intermediates with their respective temperature points were Lumi-R at -120 ˚C, Meta-Ra at -45 ˚C and Meta-Rc at -25 ˚C. The spectra obtained were generally correlated to those found for Cph1 and PhyA, although the absolute positions of bands varied by a few wave-numbers. A strong negative band observed at 1707 cm^{-1} was the characteristic feature of the spectra of each intermediate during this transition, where there was a decreasing contribution of modes located in the amide I spectral range upon formation of the earlier intermediates. The negative band observed in CphA has been assigned to the C=O stretch of ring D, that is upshifted in lumi-R in case of phyA (Foerstendorf et al., 2001). Thus, it could be safely correlated to the molecular events occurring to form the lumi-R state and the altered chromophore-protein interactions quite similar as found in phyA. As reported previously for Cph1 and here CphA, the high frequency positions of the bands assigned to the C=O stretch of ring D in Pr and Pfr indicate that the chromophore must be protonated in both the states.

The anamoly of assignment of an intermediate with an FTIR spectrum with high similarity to that of lumi-R spectrum measured in this work (Fig. 4.30), to meta-Ra, based on the UV-Vis difference spectrum (Foerstendorf et al., 2000) was corrected for Cph1 as this intermediate can be acquired at a temperature as low as -140 ˚C. Furthermore, the spectrum is very similar to that of CphA. In this context, we like to note that the spectra of lumi-R are associated with more uncertainties than those of the other intermediates. The spectral range above 1750 cm^{-1} shows that the noise is considerably larger than in the other spectra. This is because of the low photoproduct yield. In addition, the contribution of the Pfr photoproduct lumi-F, which is particularly large in this case, decreases the accuracy. Therefore, special care had to be exercised for the interpretation of the spectra. However,

these uncertainties cannot account for the considerable differences compared with the recent picosecond time-resolved IR lumi-R / Pr difference spectrum of the 515 amino acid N-terminal fragment of Cph1. These differences are, for instance, especially evident for the carbonyl bands of ring D (vanThor et al., 2007). It is beyond the scope of this contribution to discuss these differences at greater detail.

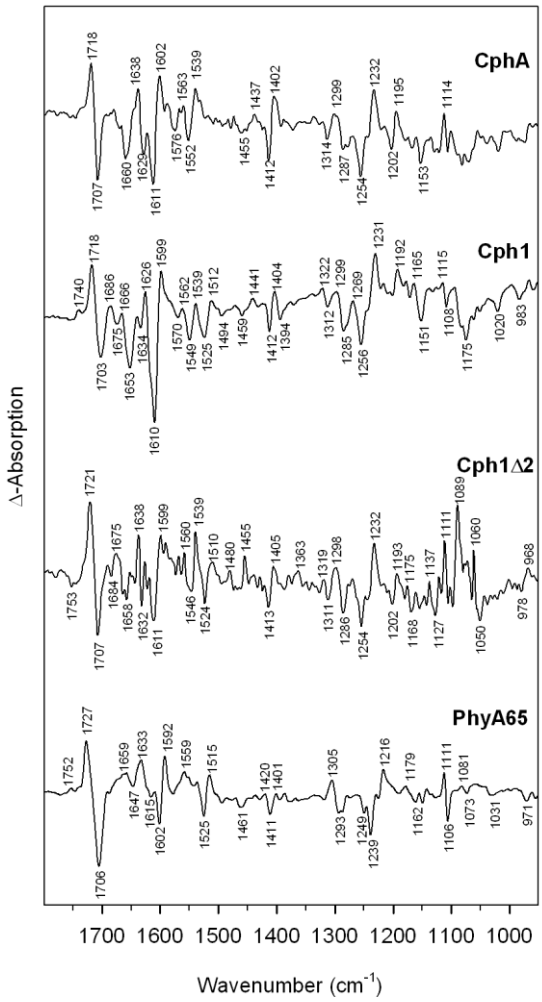

Figure 4.34 : Comparison of the Pr:Lumi-R FTIR difference spectra (- 120 °C to – 140 °C) for various recombinant phytochromes: From top to bottom: CphA from Calothrix (88 kDa), Cph1 from Synechocystis (85 kDa), Cph1D2 (59 kDa) N-terminal fragment (514 residue) and PhyA (65 kDa), all assembled with phycocyanobilin (PCB).

In contrast to the lumi-R spectrum of plant phyA (Schwinté et al., 2008) for which only a small band is observed in the amide I region, for CphA major bands

show up at 1660/1638 cm^{-1} and 1552/1539 cm^{-1}, which are assigned to amide I and amide II modes, respectively. Similar difference signals have been observed in the corresponding spectrum of Cph1 (Foerstendorf et al., 2000), indicating that they represent characteristic feature of cyanobacterial phytochromes. It is reasonable to assume that the underlying protein structural changes are localized in the immediate vicinity of the chromophore (Hauser et al., 2002) since this region will be most strongly affected by its geometrical changes associated with the photoisomerization. The amino acids lining the chromophore are very similar in CphA and Cph1. Therefore, it is not surprising that this amide I signature is similar in the two systems. We admit that in the spectra the size of these bands may be affected by the correction procedure. Artefacts brought about by the ''correction'' procedure may be the origin for the lack of the difference band at ca. 1515 cm^{-1} that is seen in the later intermediates of CphA as well as in lumi-F (Fig. 4.32(a)) but not in lumi-R. In contrast, this difference band is present in the corresponding spectra of Cph1 (Foerstendorf et al., 2000) and phyA.

Meta-Ra & Meta-Rc : The spectra of meta-Ra/Pr and meta-Rc/Pr was documented for only the negative band of the C=O of ring D presenting a identical situation observed for meta-Rc as in Cph1 where it might be that it is downshifted to about 1690 cm^{-1} (Foerstendorf et al., 2000). Measurements done in D_2O support this assignment since they indicate a downshift of this mode. However, an unequivocal assignment using isotopically labeled chromophore has not yet been made.

The spectra show that the position of the B–C methine stretching mode (difference band around 1600 cm^{-1}) shifts to lower frequencies in the later intermediates. The negative Pr-band progressively shifts down from 1611 cm^{-1} (in the lumi-R spectrum), to 1609 cm^{-1} (meta-Ra), and 1607 cm^{-1} (meta-Rc and Pfr spectra). One could assume that the higher position of the Pr band is caused by the overlap between the positive and negative bands, which would be more pronounced in lumi-R and meta-Ra. However, a careful analysis shows that this

overlap has a minor influence on the band positions. In addition, in the case of phyA, where similar increasingly lower frequencies for the bands of the intermediates are observed, the band position of the parent state (Pr) remains unchanged (Foerstendorf et al., 1996; Schwinte et al., 2008). On the other hand, Cph1 displays a similar behavior as CphA (Foerstendorf et al., 2000). Thus, we conclude that the frequency of this band varies with the temperature, i.e. it increases with lowering the temperature. Note that such an effect is not observed for phyA.

This conclusion shows that it is reasonable to discuss the changes of the B–C stretching mode of the intermediates in terms of frequency differences with respect to the respective Pr band at the corresponding temperature. Then, the downshifts observed for the photoproducts are 9, 17, 19 and 19 cm^{-1} for lumi-R, meta-Ra, meta-Rc and Pfr, respectively (Fig. 4.34 - 4.36). In the case of phyA, for which a similar behavior is observed, the maximum downshift (Pfr) is only 14 cm^{-1}, the downshift for lumi-R, however, is the same as for CphA. As mentioned, in our previous study on phyA, we have argued that the Pr structure may be described by a distorted ZZZ_{ssa} geometry, twisted around the A–B methine bridge (Schwinte et al., 2008). Taking into account previous RR results (Murgida et al., 2007), photoisomerization leads to a ZZE_{ssa} configuration in which the distorted syn conformation of the A–B methine bridge is maintained. In Pfr, the torsion of the C–D methine bridge is presumably increased and the conformation of the A–B methine bridge is altered as concluded from the RR spectra (Murgida et al., 2007). The change of the A–B methine bridge could cause the downshift of the C=O stretch of ring A described above. However, as discussed above, these structural changes cannot account for the dramatic downshift of the B–C stretching observed for the Pfr state of phyA, and as possible origins we have suggested changes in the π-electronic system and thus of the force constants and changes of the geometry of the B–C part. The larger downshift of the B–C methine stretching mode as compared to plant phytochrome probably reflects a larger alteration of the this part of the chromophore.

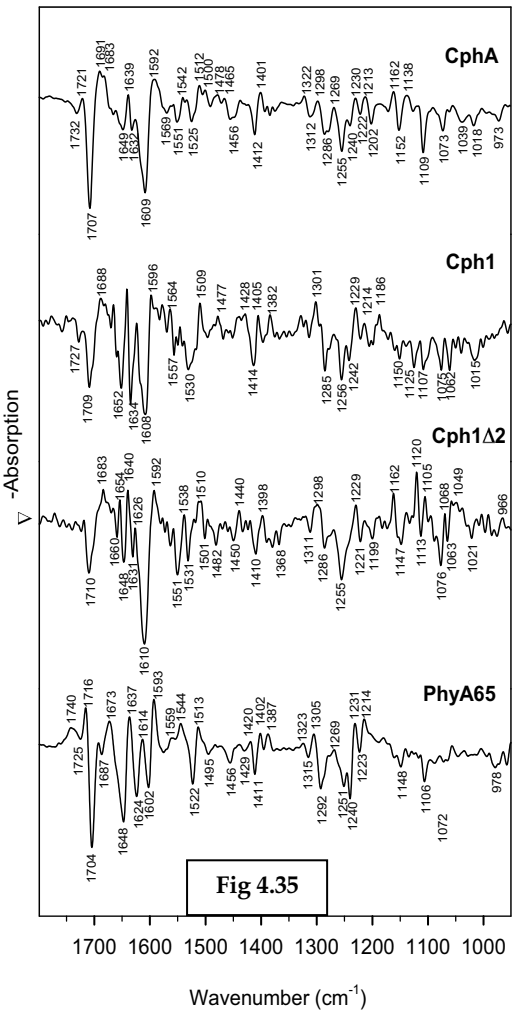

Figure 4.35 : Comparison of the Pr:Meta-Ra FTIR difference spectra (- 45 °C to – 70 °C) for various recombinant phytochromes: From top to bottom: CphA from Calothrix (88 kDa), Cph1 from Synechocystis (85 kDa), Cph1D2 (59 kDa) N-terminal fragment (514 residue) and PhyA (65 kDa), all assembled with phycocyanobilin (PCB).

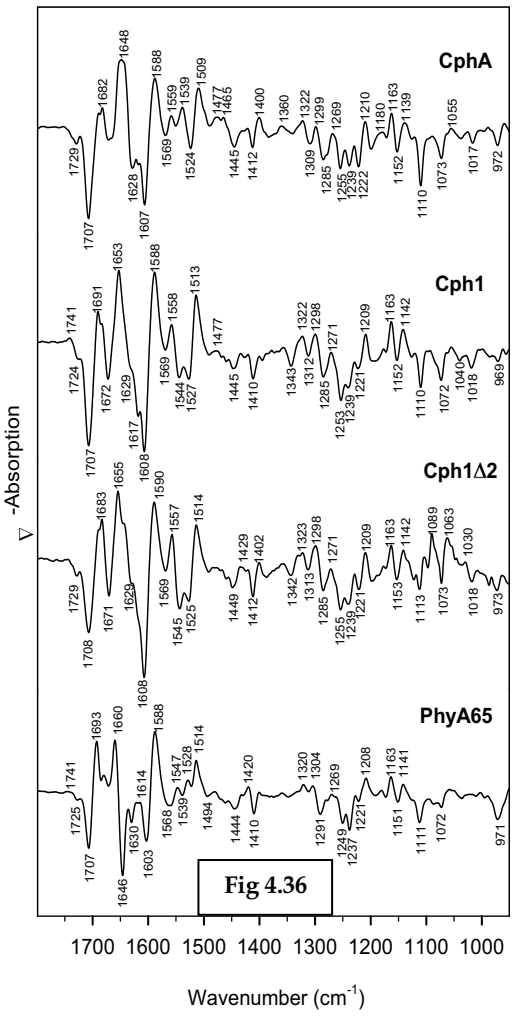

Figure 4.36 : Comparison of the Pr:Meta-Rc FTIR difference spectra (-25°C) for various recombinant phytochromes: From top to bottom: CphA from Calothrix (88 kDa), Cph1 from Synechocystis (85 kDa), Cph1D2 (59 kDa) N-terminal fragment (514 residue) and PhyA (65 kDa), all assembled with phycocyanobilin (PCB).

As visualized in the Pfr / Pr spectrum, also in the meta-Rc / Pr, and meta-Ra / Pr spectra a difference band is present at 1525(-) / 1510(+) cm^{-1}. The Pfr / Pr spectrum measured in D_2O shows that this band undergoes an upshift to 1527(-) / 1516(+) cm^{-1} (Fig. 4.32), indicating that it contains a small contribution of the NH bending coordinate. It is generally accepted that the chromophore is protonated in

Pr, lumi-R and in Pfr. As this mode has the same characteristics in meta-Ra and meta-Rc as in Pr, we conclude that in meta-Ra and, at least in a fraction of the meta-Rc population, the chromophore is also protonated. These findings are consistent with recent RR spectroscopic results on CphA (unpublished) and Cph1 (von Stetten, doctoral thesis 2008) which have revealed a mixture of protonated and deprotonated chromophores in the Meta-Rc states. In this respect, the behavior of CphA (and Cph1) is different compared biliverdin-binding phytochromes for which the Meta-Rc chromophore was found to be largely in the deprotonated state (Borucki et al., 2005; Wagner et al., 2007, 2008).

In the meta-Ra / Pr and meta-Rc / Pr spectra the C=O stretch of ring A in the Pr state is detected at ca. 1730 cm^{-1}, in analogy to the Pfr / Pr spectrum. Since no positive band is seen at higher wavenumbers we conclude that a downshift similar to that of the Pr:Pfr transition also takes place in these intermediates. This downshift cannot be seen because of the strong negative band of the C=O stretch of ring D. Thus, some rearrangements of ring A take place already in meta-Ra.

Phototransformation of Pfr : In the photoreaction of the Pfr:Pr pathway, two intermediates can be identified by IR spectroscopy, i.e. lumi-F and meta-F ((Figs. 4.32 (a & b)), as they were also observed for the other phytochromes (Foerstendorf et al., 1996, 2001). In the lumi-F spectrum, we can identify amide I bands at the same positions as in the lumi-R spectrum (1660 and 1638 cm^{-1}), indicating that the distortions of the chromophore binding pocket are qualitatively similar in the primary photoprocesses of the two parent states. Despite the different chromophore geometries, this could be accomplished by compensating twists around the methine bridges. The B–C methine stretching mode is shifted up in three steps. The apparent position 1599 cm^{-1} is the same in lumi-F and meta-F, however, the amplitude of the difference band is considerably larger in the meta-F / Pfr difference spectrum taking the bands between 1100 and 1200 cm^{-1} as a reference. This finding indicates that in the lumi-F / Pfr spectrum, a considerable overlap between the Pfr and lumi-F bands reduces the amplitude of the difference

band. The significant frequency upshift from 1587 to 1599 cm^{-1} suggests that the bandwidth is correspondingly large in order to account for the amplitude reduction in the difference spectrum. The larger amplitude of the difference band in the meta- F / Pfr spectrum is explained by a larger upshift of the B–C stretching mode as compared with lumi-F. The final upshift occurs with the formation of Pr. The large bandwidths can be explained by a structural heterogeneity of the chromophore. A heterogeneity has been identified before by thermochromism studies (Schmidt et al., 1996). The behavior of the B–C methine stretching mode is different from that in the Pr:Pfr pathway. Here, the size of the difference band remains the same, indicating smaller bandwidths, and thus, better defined protein states.

The two intermediates exhibit a characteristic band at 1538 cm^{-1}, similar to that observed for phyA (Schwinté et al., 2008) for which it could be assigned to the chromophore. However, a clear description in terms of normal modes was not yet possible. It might reflect a special distortion of the chromophore and / or a special interaction with the protein being relaxed with the formation of Pr, since the band disappears in the last step of the backreaction.

In meta-F a small positive band is noted at 1733 cm-1, which can be assigned to the C=O stretch of ring A. This assignment is supported by the 5-cm^{-1} downshift induced by H/D exchange (Fig. 4.32 (b)). The position of this band is similar to that of Pr. In the lumi-F / Pfr spectrum, the strong band of the C=O stretch of ring D partially obscures the corresponding region. However, this band is broader and of lower amplitude in lumi-F than in Pfr. Thus, it could be that even in lumi-F the C=O stretch of ring A has already the frequency of the Pr state. It is interesting to note that Fig. 4.28 shows that the UV–Vis spectra of the intermediates have already pronounced similarities to the spectrum of Pr, i.e. some properties of the Pr state are already anticipated in the intermediates. This is clearly different from the Pr:Pfr pathway.

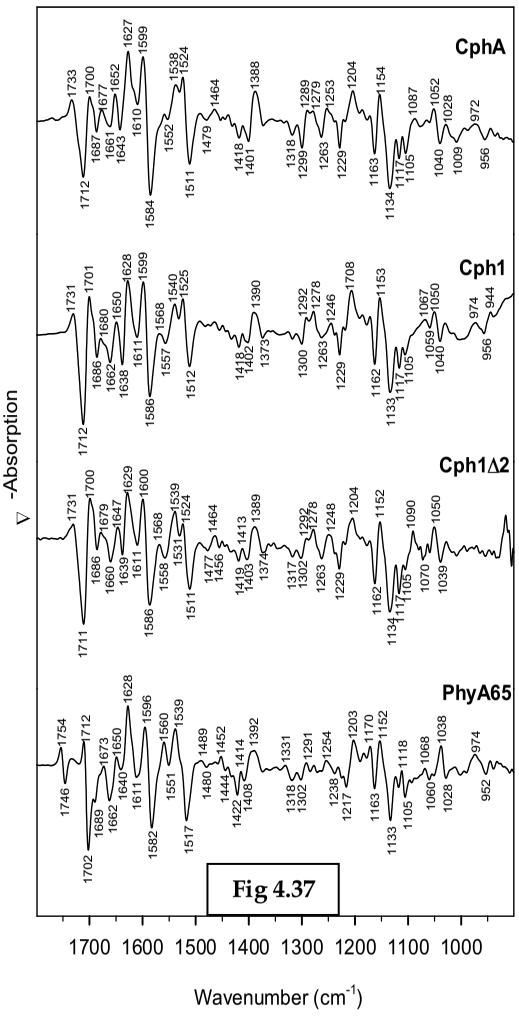

Figure 4.37 : Comparison of the Pfr:Meta-F FTIR difference spectra (- 80 °C) for various recombinant phytochromes: From top to bottom: CphA from Calothrix (88 kDa), Cph1 from Synechocystis (85 kDa), Cph1D2 (59 kDa) N-terminal fragment (514 residue) and PhyA (65 kDa), all assembled with phycocyanobilin (PCB).

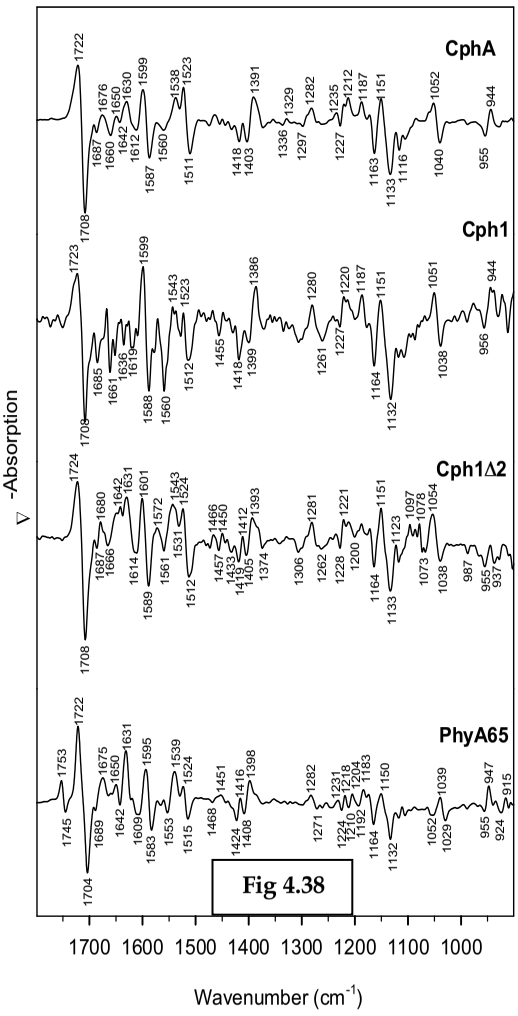

Figure 4.38 : Comparison of the Pfr:Lumi-F FTIR difference spectra (- 140 °C) for various recombinant phytochromes: From top to bottom: CphA from Calothrix (88 kDa), Cph1 from Synechocystis (85 kDa), Cph1D2 (59 kDa) N-terminal fragment (514 residue) and PhyA (65 kDa), all assembled with phycocyanobilin (PCB).

Difference band - 1608 cm^{-1}: The next band mentioned in the discussion of the Pr:Pfr difference spectrum is the difference band around 1608 cm^{-1}. In all the intermediates it undergoes a downshift as in Pfr. In the case of PhyA we could show by $^{13}C_{10}$ isotope labeling and by measurements in D_2O that this downshifted

band has the same character, i.e. being composed mainly from the stretching vibration of the C10 methine bridge coupled to neighboring NH bending modes. Similarly, a difference band around 1520 cm^{-1} is seen in all spectra, and again for PhyA the same assignment could be made for the photoproduct bands as for the negative band described above.

The spectra of the intermediates show that the downshift of the C10 methine mode becomes larger for the later intermediates. What molecular changes could cause a shift of a mode located primarily in the middle of the chromophore? From the structure of the chromophore being composed of the four pyrrole rings connected by the three methine bridges it appears unlikely that the Z:E isomerization of the CD methine bond directly affects the BC methine stretching vibration. It appears more likely that by this geometrical change the interaction of ring D with the environment, especially the NH group, is altered, resulting in a change of the conjugated system, which then alters the force constants especially of the methine bridges. The downshift observed in lumi-R could be caused by the new interaction of the NH group of rind D with the protein after chromophore isomerization. This region appears to be special since it is also able to stabilize the positive charge of the chromophore. The additional shift occurring for the later intermediates may be caused by further relaxation of ring D, as evidenced by the change in the C=O mode but also by additional geometrical changes of the chromophore as suggested recently (Lamparter et al., 2001). These further changes could again influence the conjugated system.

The NH mode described above only shows up in the Pr:Pfr spectrum with large amplitude. Since there is no negative band of comparable size in the meta-Rc spectrum, a deprotonation of the chromophore in this state must be excluded. In the earlier intermediates a small difference band shows up in this region which also disappears upon H/D exchange. Therefore, it probably represents the same

mode. The small size indicates that the two NH groups of rings B and C undergo only minor changes in the interaction with the protein.

Difference band - 1515 cm^{-1} : The last band discussed above is the difference band around 1515 cm^{-1}. The band is very small in lumi-R, at noise level. It becomes somewhat larger in meta-Ra, but reaches the final size and the largest downshift in meta-Rc and Pfr. Again, in the case of PhyA the same shifts caused by isotopic labeling are observed as described above for the parent state (to be published). Due to its C-N, NH, and C5-methine character (derived from DFT calculations), this band will be influenced by the electronic structure of the conjugated system, but also directly by the interaction of the NH group of ring B. Therefore, it is more difficult to interpret the downshift in molecular terms, since probably both factors contribute. However, since this mode is the same in meta-Rc and in Pfr it appears that in CphA no further rearrangements of ring A takes place. This is further supported by the presence of a negative band in the spectra of meta-Ra (1732 cm^{-1}), meta-Rc (1729 cm^{-1}) and Pfr (1734 cm^{-1}), which is downshifted in Pfr, and as explained above, is assigned to C=O stretch of ring A. The downshift cannot be seen in meta-Ra and meta-Rc, since the corresponding positive band overlaps with the strong negative band due to C=O stretch of ring D. In PhyA the situation may be different. We have previously published that only in the transition to Pfr an upshift of this band takes place, clearly demonstrating that here an additional relaxation of ring A takes place.

4.4.4.2 (C) Conclusion

The overall band pattern of the FTIR difference spectra of phyA and the cyanobacterial phytochromes is strikingly similar, although greater similarities exist between the cyanobacterial systems CphA and Cph1. All phytochromes discussed here show the temperature-dependent yield of the forward photoreaction (Foerstendorf et al., 2000, 2001; Schwinte et al., 2008), which can probably be explained by a barrier in the electronic excited state as suggested for

phyA on the basis of ultrafast UV–Vis spectroscopy (Bischoff et al., 2001). Further, in all systems discussed here, the yield of the backreaction is temperature-independent, indicating a barrier-free reaction path. Since little is known about the excited state properties of bilin chromophores, we cannot decide whether this behavior of the excited states is an intrinsic property of the chromophores or caused by special chromophore– protein interactions. Besides these overall similarities, notable differences refer to the positions of amide I bands in the Pfr / Pr spectra, and the band positions of the B–C methane stretching mode which indicate different structural changes of the protein and protein–chromophore interactions during the phototransformation in the cyanobacterial phytochromes. An unexpected observation for CphA is the fast thermal reaction from Pr to Pfr within 30 s which is not observed in Cph1. Despite the considerable homology in the amino acid composition between Cph1 and CphA, especially in the chromophore binding pocket, there must be specific chromophore–protein interactions in CphA which facilitate this reaction. It is hoped that the molecular structures of the systems will help to explain the somewhat deviating properties.

4.4.5 FTIR - CphBm

4.4.5.1 UV-Vis spectroscopy

The UV-Vis difference spectrum was recorded between the Pr and Pfr states of CphB at room temperature, with the same protein liquid film (sandwich sample) prepared for FTIR (Fig.4.39 (A)). The typical bands in the red-far red region were observed respectively at 701 nm for the Pr form (negative band) and at 753 nm for the Pfr form (positive band). CphB has a distinction of having biliverdin as its natural chromophore (Quest et al., 2004) when compared with CphA from *Calothrix*, *Synechocystis* Cph1 or PhyA, which assemble PCB or PΦB chromophores covalently. The Pr and Pfr bands were significantly red-shifted compared to bacteriophytochrome CphA (660, 707 nm), Cph1 (653, 709 nm) or PhyA65 (663, 730 nm). The red-shift observed on the Pr maximum was respectively 41, 48 and 38 nm compared to CphA, Cph1, PhyA while that for Pfr, the observed red-shift was 46, 44 and 23 nm, as the B type phytochromes have a longer conjuganted system.

The two absorption maxima of the biliverdin chromophore in CphB, at about 400 and 700 nm are reminiscent of the biliverdin spectrum obtained in polar organic solvents such as methanol or DMSO (McDonagh, 1980; Scheer, 1976) which would mimic the hydrophobic protein pocket. The positions and relative intensity of the two bands are even closer to what is obtained in the acidified medium, for example 5% HCl in MeOH , with a red shift as well as a markedly increased absorption coefficient of the long wavelength band (increase about twice in intensity), relative to the non-acidified medium, as determined by McDonagh : in MeOH the bands are at λ_{max} 376 nm (ε=50800 $M^{-1}.cm^{-1}$) and λ_{max} 666 nm (ε =14400 $M^{-1}.cm^{-1}$), in 5% HCl-MeOH they are shifted to λ_{max} 377 nm (ε =66200 $M^{-1}.cm^{-1}$) and λmax 696 nm (ε =30800 $M^{-1}.cm^{-1}$) (McDonagh 1980). This change on the long wavelength band is attributed to the formation of the cationic form of biliverdin (Scheer 1976). On the other hand, the overall red shift observed from the PCB or

PΦB chromophore to biliverdin is ascribed to the increased conjugation in the latter: the position of the red band has been correlated empirically with the size of the conjugated system.

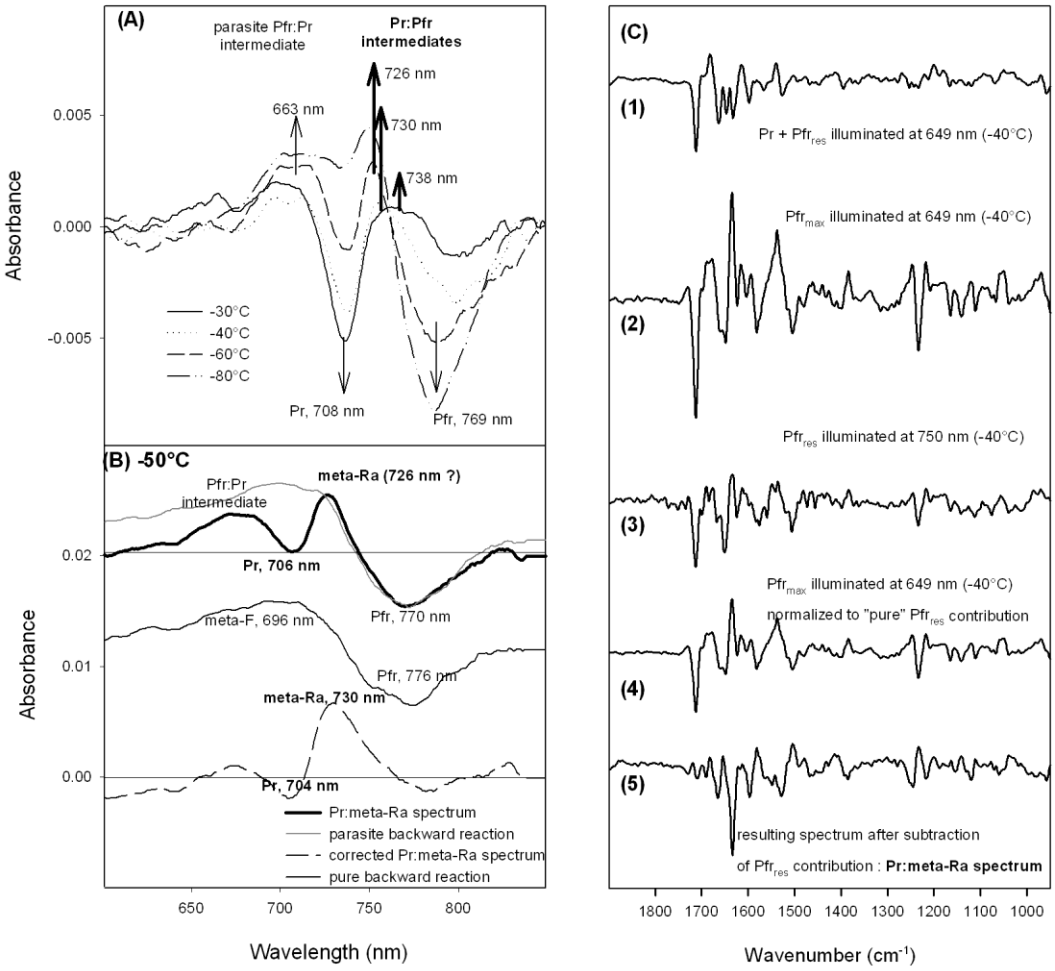

Figure 4.39 : Spectroscopic graphical representation of UV-Vis measurements CphB phytochrome done in parallel with FTIR spectroscopy: (A) Measured UV-vis difference spectra of the Pr:Pfr pathway, with residual backward reaction, upon red illumination (649 nm); (B) Correction procedure applied to the measured UV-vis spectra of the Pr:Pfr pathway, to subtract the contribution of unwanted backward photoreaction: the example of meta-Ra (-50°C); (C) Correction procedure applied to the measured FTIR spectra of the Pr:Pfr pathway in the case of meta-Ra (-40°C). The spectra depicted in the figures are that of CphBm.

The photoreactions of both the forward Pr:Pfr pathway and the backward Pfr:Pr pathway were investigated at low temperatures, ranging from -20°C to

-140°C, at 10 or 20 degrees intervals. The difference spectra after correction are presented on Fig. 4.40 (C) for the forward reaction and Fig. 4.40 (B) for the backward reaction. The negative band represents the initial state and the positive band some photoproduct. Again, as outlined for the CphA case, a correction procedure had to be applied in order to account for a photochemical contribution of a small amount of the Pfr form.

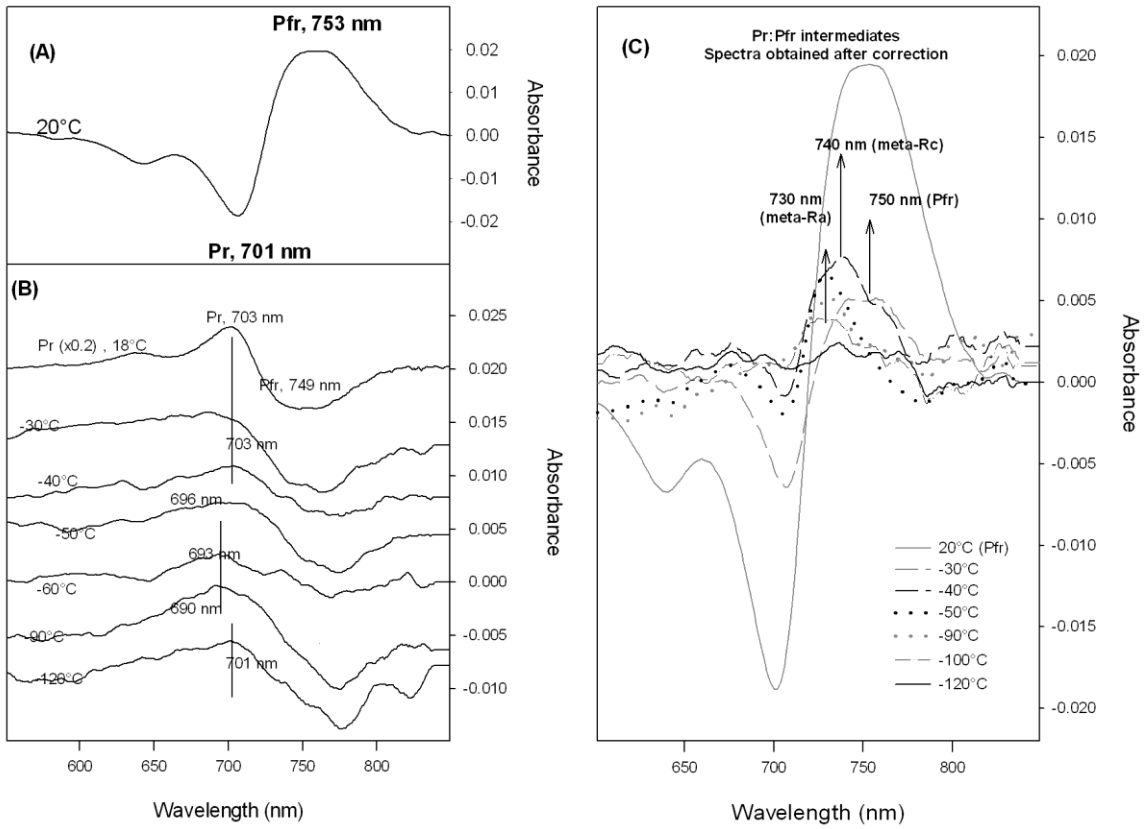

Figure 4.40 : Graphical measurements followed during FTIR spectroscopic analysis. (A) UV-vis difference spectrum between Pr and Pfr (T=20°C); (B) Difference spectra of the Pfr:Pr pathway, upon far red illumination (750 nm); (C) Difference spectra of the Pr:Pfr pathway, upon red illumination (649 nm), after correction.

Pr:Pfr pathway. The amplitude of the difference bands observed ranges from 5 mOD at -30°C to about 2 mOD at -140°C. Above -30°C the Pr:Pfr transformation is realized (λ_{max} at 750 nm). At -40°C the maximum of the Pr:Pfr pathway intermediate is located at 740 nm. At -50°C this maximum is shifted to 730 nm,

where it stays up to -100°C and below -100°C the signal is at noise level: one cannot detect any third intermediate (lumi-R). These intermediates correspond respectively to "Meta-Rc", "Meta-Ra", to keep the denomination of plant phytochrome intermediates, but their absorption values are significantly red-shifted (as is Pr and Pfr) compared to those found for the intermediates of other corresponding phytochromes. Although CphB, as CphA, differs from Cph1 and PhyA on the existence of a residual backward photoreaction, all proteins show a similarity in red shifts observed between the successive intermediates, meta-Ra to meta-Rc to Pfr (CphB: successively from Pr to Pfr: 701, 730(Δ=29), 740(Δ=10), 753(Δ=13); CphA: 660, 683(Δ=23), 693(Δ=10), 703 (Δ=10), 707(Δ=4); Cph1: 653, 689 (Δ=), 698 (Δ=11)). This could indicate that a similar path is followed by CphB, CphA and Cph1 in the course of the photoreaction from Pr to Pfr, and this path might be different from the one in PhyA, at least in the early step of the photoreaction, as evidenced by the curious blue shift encountered in PhyA from Lumi-R to Meta-Ra (PhyA-Pr 663 nm; PhyA-Lumi-R 695 nm; PhyA-Meta-Ra 691 nm; PhyA-Meta-Rc 718 nm). Unfortunately we cannot tell precisely the wavelength for lumi-R in CphB because the signal is on the noise level (see figure 4.41).

Pfr:Pr pathway. The amplitude of the Pfr:Pr photoreaction difference spectra also ranges between 5 and 2 mOD. One main minimum is observed at about 770 nm, corresponding to the disappearance of the Pfr state. Above –40°C we still get Pr. From -50°C to -90°C the maximum is located at about 693 nm. Below -90°C it seems to be back to 701 nm. For this, refer please to figures (Fig 4.40 (A) and (B)). These two photoproducts might correspond respectively to Meta-F and Lumi-F following the plant phytochrome denomination, and are also significantly red-shifted compared to the CphA corresponding intermediates which can be trapped at -70°C and -140°C with absorption maxima at 640 nm and 635 nm. The intermediates of the reverse photoreaction could be trapped in all phytochromes at the same temperatures (-140°C for Lumi-F and -70°C for Meta-F), but here the extent and direction of the shifts encountered from Pfr to Lumi-F, Meta-F and then

Pr, suggests a similarity in the Pfr:Pr reaction pathway for CphA and Cph1 (CphA: 707, 635(Δ=–72), 640(Δ=5), 660(Δ=20); Cph1: 709, 640(Δ=-69), 647(Δ=7), 653(Δ=6)), which is different in PhyA as well as in CphB in the early steps of the photoreaction with a blue shift from Lumi-F to Meta-F (PhyA-Lumi-F 670 nm, PhyA-Meta-F 663 nm (Δ=-7); CphB-Lumi-F 701 nm, CphB-Meta-F 693 nm (Δ=-8)).

4.4.5.2 FTIR difference spectroscopy

Pr:Pfr pathway : Figure 4.33 shows the FTIR difference spectra of CphB intermediates for the Pr:Pfr pathway in water and in D_2O, respectively. As before, positive bands represent the intermediate state and negative bands the parent state. Comparisons of all intermediate spectra with corresponding species for PhyA65-PCB, *Synechocystis* Cph1 and Cph1Δ2, and *Calothrix* CphA phytochromes are displayed as separate figures in the **Supporting Information.**

4.3.5.2 (A) FTIR Band Assignments :

On the contrary to CphA which was found to display a behavior very similar to plant phytochrome or better bacterial phytochrome Cph1, the spectra for the intermediates of the forward reaction for CphB show noticeable changes, however some general features are retained.

It is obvious that the Pfr spectrum for CphB shows some similarities with the other phytochromes in the chromophore bands (discussed in CphA) but it is quite different in the amide I region:

- The negative band at around 1620 cm^{-1} (amide I spectral changes in the proteins) is here positive in CphB, in contrary to other phytochromes;
- The changes in protein band structure are more numerous, but not as intense as in other phytochromes.

The **chromophore bands** appear quite similar as in CphA, but slightly shifted in wave-numbers.

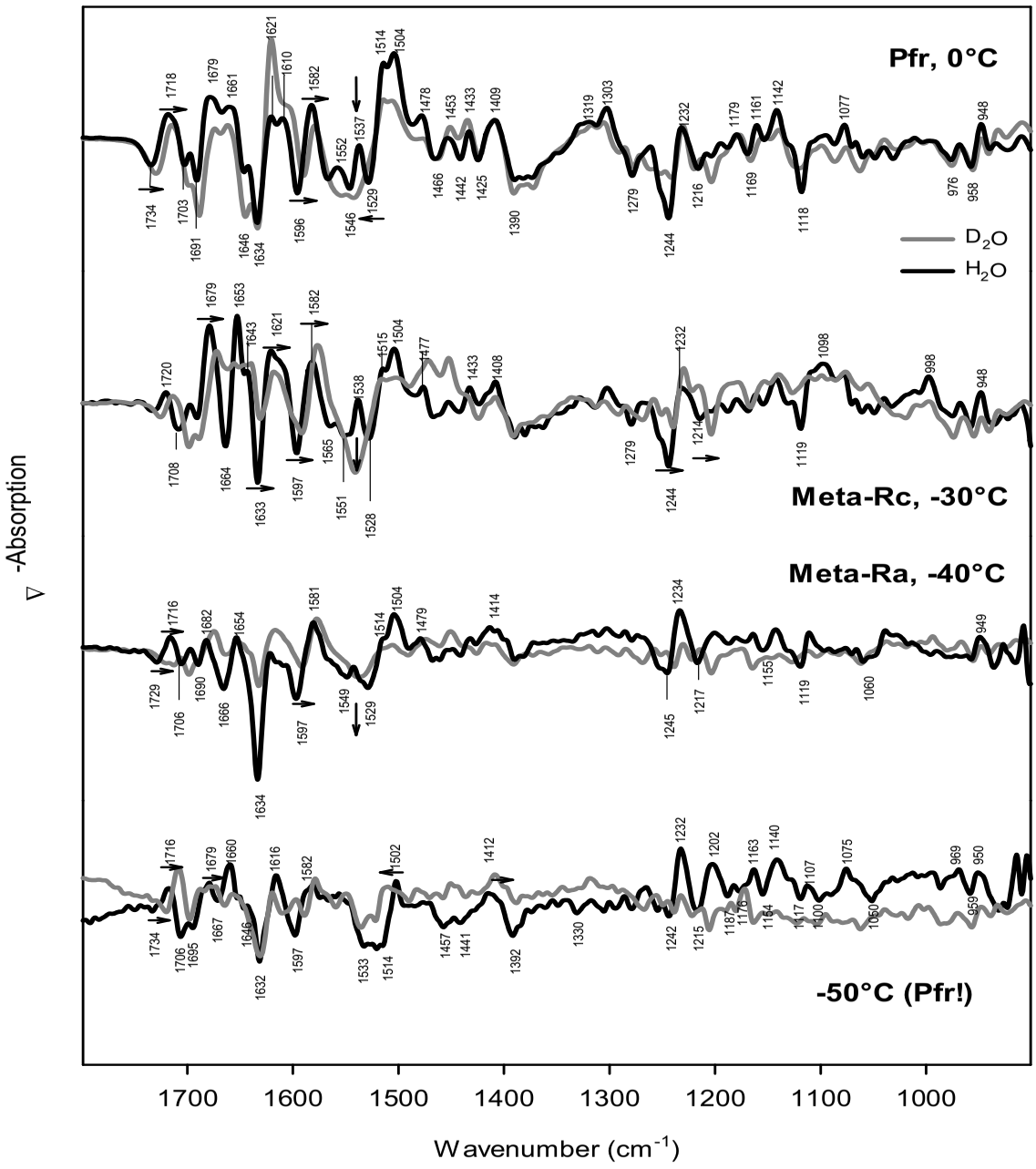

Figure 4.41 : Light-induced FTIR difference spectra of the photoreactions of recombinant bacteriophytochrome CphB recorded in H_2O (black) and D_2O (grey): From top to bottom: Pfr (0°C), meta-Rc (-30°C), meta-Ra (-40°C); lumi-R could not be obtained. Positive bands represent the respective photoproduct, negative bands Pr.

From the assignment in CphA, we can deduce :

- The difference band at 1596(-)/1582(+) cm^{-1} corresponds to the 1608/1589 cm^{-1} band in CphA, which was assigned to a combination of $C=C_{10}$ stretching modes coupled to neighboring NH. This coupling is here also supported by the downshift in D_2O.
- The difference bands at 1565(-)/1552(+) cm^{-1} and 1546(-)/1537(+) cm^{-1}, which disappear in D_2O, correspond to the 1571/1556 cm^{-1} band in CphA, and were assigned to NH(B,C) modes. Present as positive and negative band, it confirms that the chromophore is protonated both in the Pr and in the Pfr state. As in CphA, here in CphB there is a downshift of these NH vibrations when going from Pr into Pfr, suggesting also a weakening of the H-bond array around these NH vibrations in Pfr; this was explained for CphA by the increased delocalization of the positive charge in Pfr (Schwinté et al., 2008).
- The band at 1529(-)/1514(+) cm^{-1} corresponds to the 1525/1510 cm^{-1} band in CphA. It is here in CphB much more intense: some comparisons in CphA (D_2O, the chromophore labeled all ^{13}C) have suggested that this band is a mixture of CN chromophore modes and some protein modes; it is probably this latter component which is here so intense. The CN component presence is also confirmed in CphB by the upshift in D_2O. As in CphA, this band is here also downshifted upon Pfr formation.
- The band at 1703(-)/1715(+) cm^{-1} should correspond to C=O(D), from CphA assignments; as in CphA, the band is upshifted upon Pfr formation.
- The band at 1734(-)/1718(+) cm^{-1} corresponds to the band at 1734/1721 cm^{-1} in CphA, which was assigned to C=O (A), and it is here again downshifted upon Pfr formation.

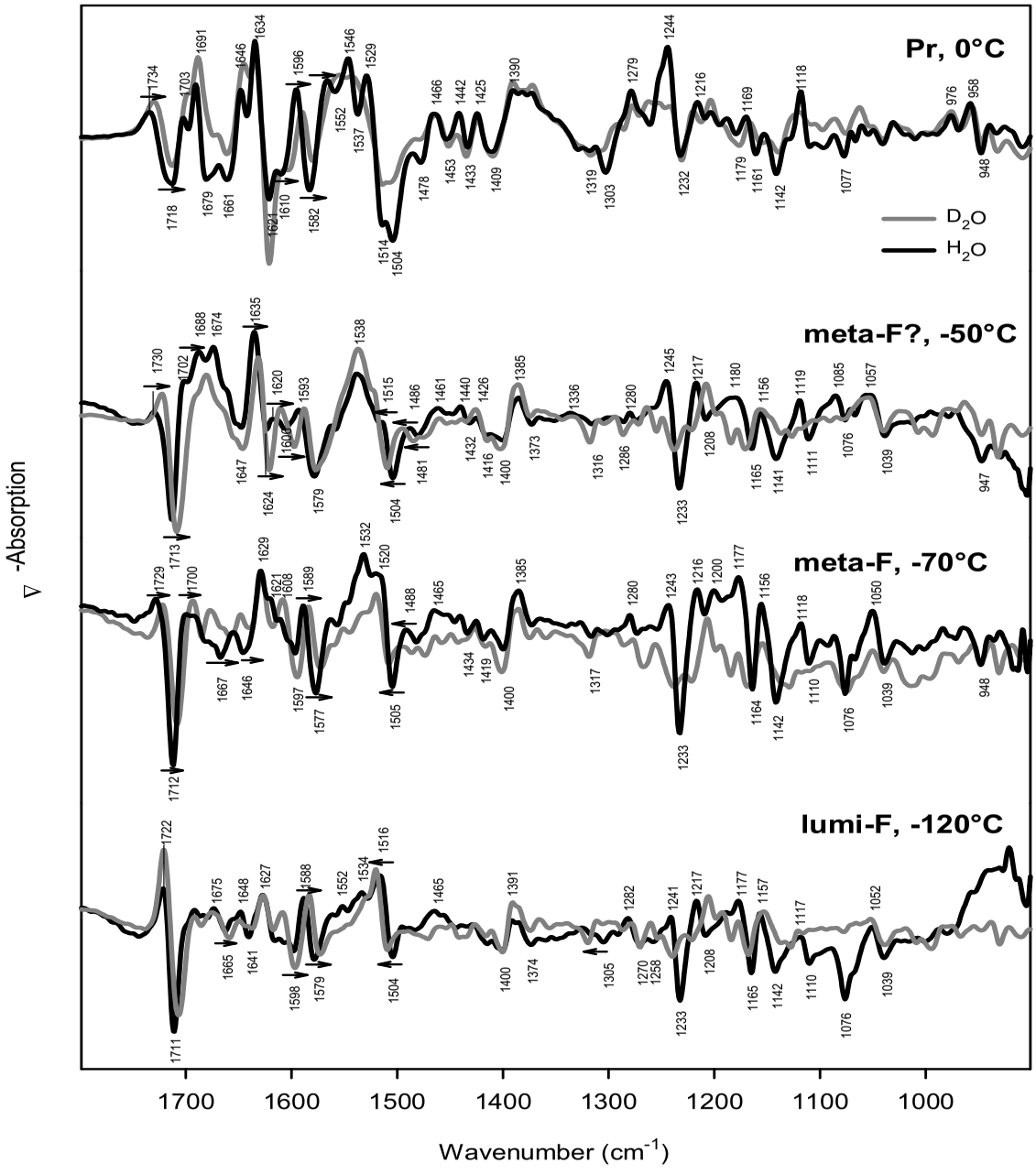

Figure 4.42 : Light-induced FTIR difference spectra of the photoreactions of recombinant bacteriophytochrome CphB recorded in H_2O (black) and D_2O (grey): From top to bottom: Pr (0°C), meta-F (-70°C) and lumi-F (-120°C). Positive bands represent the respective photoproduct, negative bands Pfr.

4.4.5.2 (B) FTIR intermediates Spectra:

The spectra of the Pr:Pfr intermediates meta-Ra and meta-Rc are quite different from those in other phytochromes, specially in the amide I region.

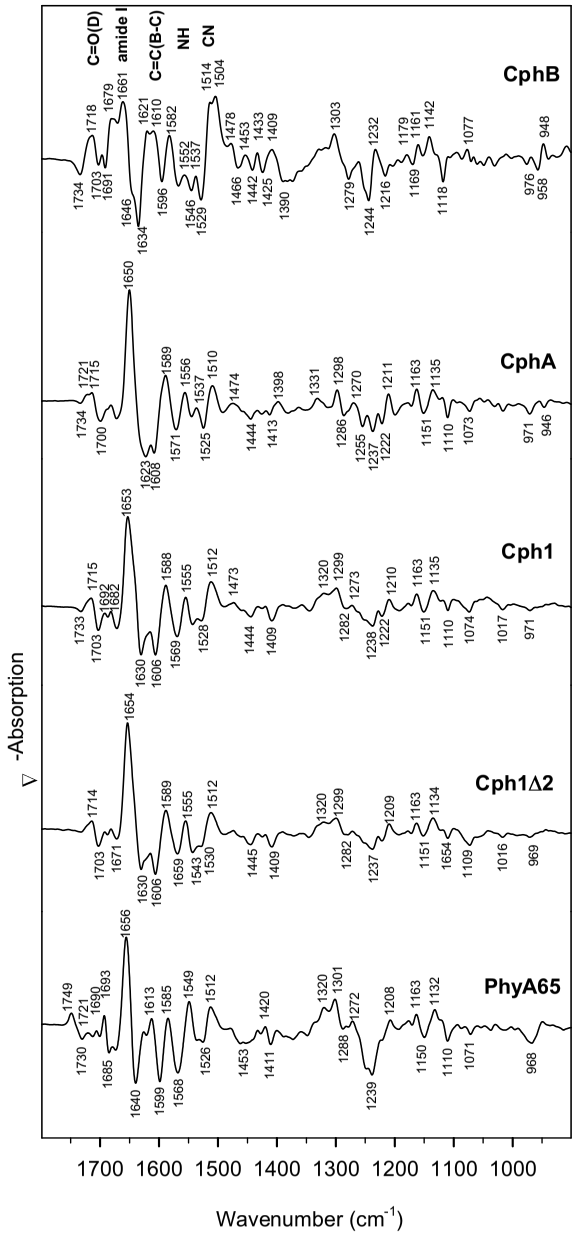

Figure 4.43 : Comparison of the Pr:Pfr FTIR difference spectra for various recombinant phytochromes: From top to bottom: CphB from *Calothrix* (84 kDa), CphA from *Calothrix* (88 kDa), Cph1 from *Synechocystis* (85 kDa), PhyA assembled with PCB (65 kDa).

- A strong band at 1633(-) cm^{-1} is seen on the CphB meta-Ra spectrum, which is new. On the other hand, the C=O(D) band, which is very intense in other phytochromes' (Cph1 or PhyA), meta-Ra and meta-Rc spectra is here surprisingly very weak on both, which means it is only little affected in the Pr:Pfr transformation.
- The $C=C_{10}$ band is downshifted in all intermediates as it is in CphA (same explanation: new initial interaction between middle of the chromophore and NH(D) after isomerization) but in the other phytochromes the downshift is worth 10 cm^{-1}, whereas here it is 20 cm^{-1}. This could be due to a bigger delocalization inducing a bigger electronic effect.
- The NH modes in Pfr appear also in the late meta-Rc spectrum, at 1538(+) cm^{-1}, and the signal is stronger. On the other hand, in meta-Ra not much happens on the NH.
- The "CN" band clearly has a NH contribution because it is reduced in D_2O, in all intermediates. The intensity of the band increases when going from meta-Ra to meta-Rc and Pfr, indicating an increasing effect of this interaction.

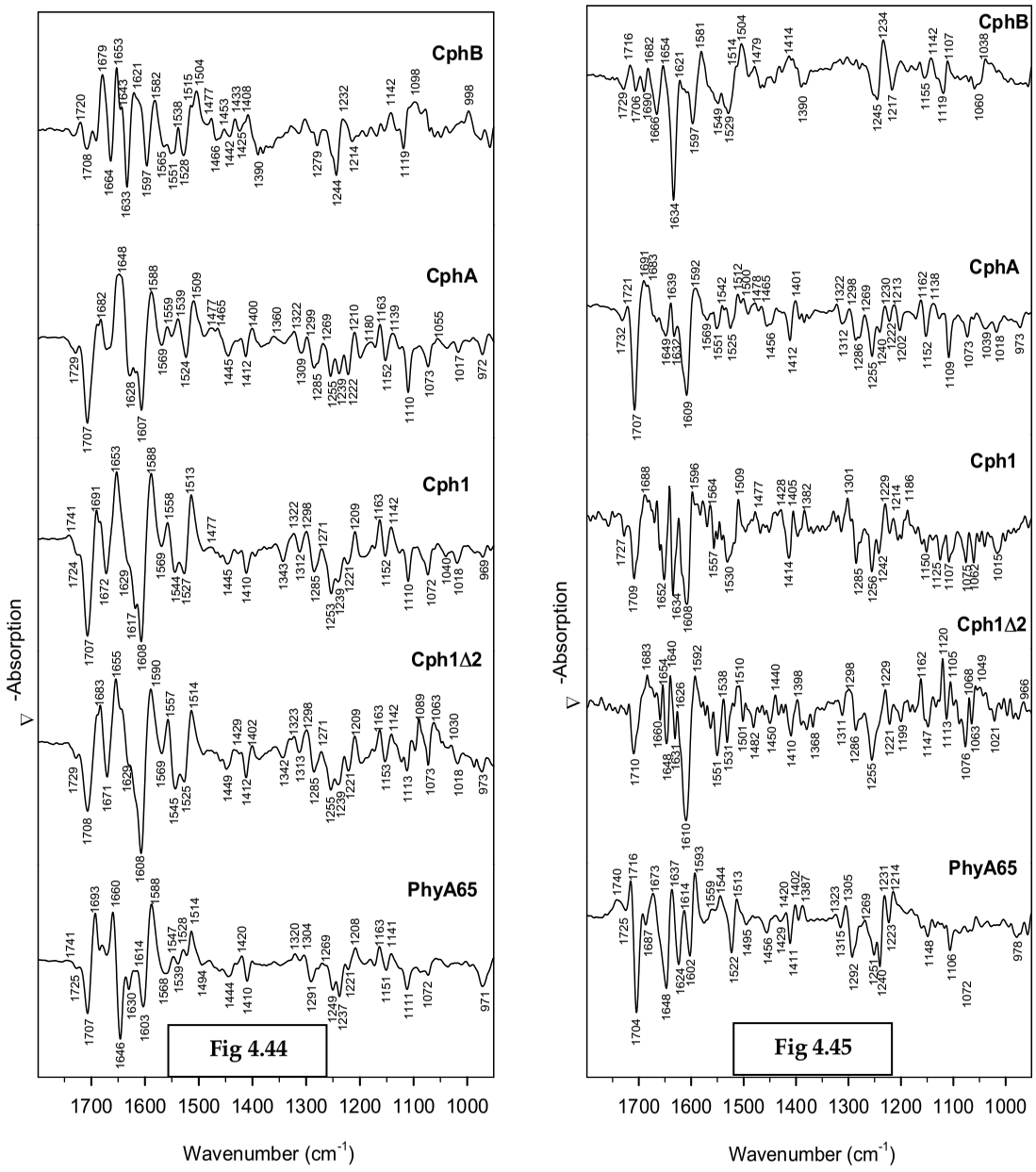

Figure 4.44 & Figure 4.45 : Comparison of the meta-Rc and meta-Ra spectra, respectively for various recombinant phytochromes: From top to bottom: CphB from *Calothrix* (84 kDa), CphA from *Calothrix* (88 kDa), Cph1 from *Synechocystis* (85 kDa), PhyA assembled with PCB (65 kDa).

Pfr:Pr pathway : Figure 4.41 shows the FTIR difference spectra of CphB intermediates for the Pfr:Pr pathway in water, and in D_2O. As before, positive bands represent the intermediate state and negative bands the parent state. The most striking observation is that , unlike the Pr:Pfr pathway, the intermediates in the back reaction display spectra quite similar to "normal" meta-F and lumi-F species, mostly characterized by a prominent change in C=O(D).

- The early intermediate Pfr:lumi-F difference spectrum presents the same characteristics as other phytochrome lumi-F intermediates, except for bigger signals in chromophore bands below 1300 cm^{-1}.
- The meta-F intermediate shows smaller protein changes than in CphA or other phytochromes, so most of these protein changes actually take place in the meta-F: Pr transformation. The C=O(D) band is finer, suggesting that some other minor C=O contribution arising there normally is absent.

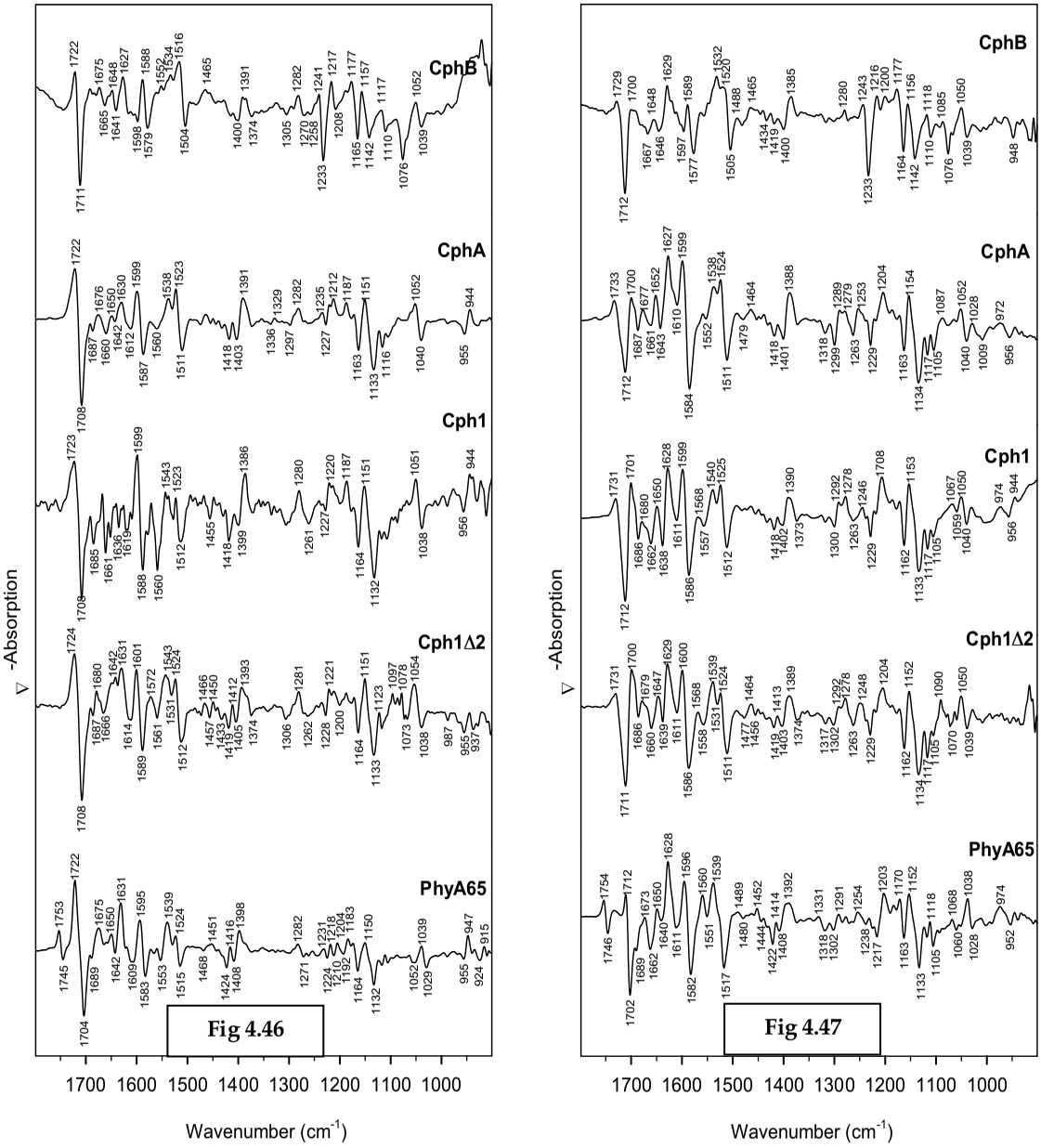

Figure 4.46 & Figure 4.47 : Comparison of the lumi-F and meta-F spectra, respectively, for various recombinant phytochromes: From top to bottom: CphB from *Calothrix* (84 kDa), CphA from *Calothrix* (88 kDa), Cph1 from *Synechocystis* (85 kDa), PhyA assembled with PCB (65 kDa).

Chapter 5

Discussion

DISCUSSION

5.1 Chromophore – phytochrome interactions

The red / far –red light absorbing photoreceptors in *Calothrix* sp. PCC 7601 i.e. CphA and CphB, are the most abundant phytochrome types now found in various genera. This cyanobacterium embraces two types of phytochromes, the Cphs (CphA) and the Bphs (CphB) that differ in the bound chromophore. While CphA attaches PCB to the GAF domain cysteine, CphB tethers the evolutionarily more ancient BV to the cysteine in the N-terminal PAS domain. Though the position of the cysteine residue differs, the crystal structures now available for allied proteins clearly portray that the chromophore lies in a cleft buried in the protein folds formed by both types, thus coming to fall into a relatively similar structural spatial zone.

5.2 Sub-domain phytochrome structural analysis

The present study on the two phytochromes has put some more light on the biochemical aspects of these bili-proteins, and maximal purity of the full length phytochromes at high concentrations was achieved. The crystallography trials on the full length proteins were hampered by the fact that in most screens the protein precipitated immediately after plating them with varied solvents. The full length proteins were then truncated at specified positions to obtain the bi-domain (PAS-GAF), tri-domain (PAS-GAF-PHY) and C-terminal (HK) modules of the phytochromes. The biochemical and spectroscopical assignments for these truncated proteins yielded valuable data on the stability of phytochromes and photoreversibility as related to the different domains.

5.3 Molecular level phytochrome transformations

The FTIR spectroscopy gave the bio-physical assessment of the photoreversible mechanism in the full length phytochromes in accordance with

that observed for homologous proteins in plants as well as in other cyanobacteria. The data from such studies can be interpreted along with the crystal structure data for reaching the physiological functioning of such protein systems.

5.4 Thermodynamic interactions of phytochrome – signaling proteins

The kinetic analysis of the phytochromes using the isothermal titration calorimetry provides the thermodynamic parameters for the protein - protein and intra – domain function in the phytochrome two–component system alongwith its cognate response regulator protein. These interaction studies form the basis to make way for the downstream signaling pathway study that would give the ultimate goal for the protein study as related to its function in the cell at the molecular level. This study comprehensively formed the elementary description into the biochemical and thermodynamic profiling of the phytochromes' proteins crucial to the further dissection of the functional machinery of the light activated two-component protein signals.

Chapter 6

Bibliography

LITERATURE CITED

[1] (1994) *Photomorphogenesis in plants*, 2nd edn. Kluwer Academic Publishers, Dordrecht, The Netherlands.

[2] Ababou,A. & Ladbury,J.E. (2007) Survey of the year 2005: literature on applications of isothermal titration calorimetry. *J. Mol. Recognit.* **20,** 4-14.

[3] Ahmad,M. (1999) Seeing the world in red and blue: insight into plant vision and photoreceptors. *Curr. Op. Plant. Biol.* **2,** 230-235.

[4] Al-Sady,B., Ni,W.M., Kircher,S., Schäfer,E., & Quail,P.H. (2006) Photoactivated phytochrome induces rapid PIF3 phosphorylation prior to proteasorne-mediated degradation. *Molecular Cell* **23,** 439-446.

[5] Andel,F., III, Lagarias,D.M., & Mathies,R.A. (1996) Resonance Raman analysis of chromophore structure in the Lumi-R photoproduct of phytochrome. *Biochemistry* **35,** 15997-16008.

[6] Andel,F., III, Murphy,J.T., Haas,J.A., McDowell,M.T., van,d.H., I, Lugtenburg,J., Lagarias,J.C., & Mathies,R.A. (2000) Probing the photoreaction mechanism of phytochrome through analysis of resonance Raman vibrational spectra of recombinant analogues. *Biochemistry* **39,** 2667-2676.

[7] Anderson,S., Dragnea,V., Masuda,S., Ybe,J., Moffat,K., & Bauer,C. (2005) Structure of a novel photoreceptor, the BLUF domain of AppA from Rhodobacter sphaeroides. *Biochemistry* **44,** 7998-8005.

[8] Aravind,L. & Ponting,C.P. (1997) The GAF domain: an evolutionary link between diverse phototransducing proteins. *Trends Biochem. Sci.* **22,** 458-459.

[9] Arciero,D.M., Bryant,D.A., & Glazer,A.N. (1988) In vitro attachment of bilins to apophycocyanin. I. Specific covalent adduct formation at cysteinyl residues involved in phycocyanobilin binding in C-phycocyanin. *J. Biol. Chem.* **263,** 18343-18349.

[10] Ashby,M.K. & Houmard,J. (2006) Cyanobacterial two-component proteins: Structure, diversity, distribution, and evolution [Review]. *Microbiology & Molecular Biology Reviews* **70,** 472-509.

[11] Azuma,N., Kanamaru,K., Matsushika,A., Yamashino,T., Mizuno,T., Kato,M., & Kobayashi,T. (2007) In vitro analysis of His-Asp phosphorelays in Aspergillus nidulans: The first direct biochemical evidence for the existence of His-Asp phosphotransfer systems in filamentous fungi. *Bioscience, Biotechnology & Biochemistry* **71,** 2493-2502.

[12] Baker,B.M. & Murphy,K.P. (1996) Evaluation of linked protonation effects in protein binding reactions using isothermal titration calorimetry. *Biophys. J.* **71,** 2049-2055.

[13] Batschauer,A. (1999) Light perception in higher plants. *Cell. Mol. Life Sci.* **55,** 153-165.

[14] Beale,S.I. & Cornejo,J. (1983) Biosynthesis of phycocyanobilin from exogenous labeled biliverdin in Cyanidium caldarium. *Arch. Biochem. Biophys.* **227,** 279-286.

[15] Beale,S.I. & Cornejo,J. (1984) Enzymic Transformation of Biliverdin to Phycocyanobilin by Extracts of the Unicellular Red Alga Cyanidium caldarium. *Plant Physiol* **76,** 7-15.

[16] Beale,S.I. & Cornejo,J. (1991) Biosynthesis of phycobilins. 3(Z)-phycoerythrobilin and 3(Z)-phycocyanobilin are intermediates in the formation of 3(E)-phycocyanobilin from biliverdin IX alpha. *J. Biol. Chem.* **266,** 22333-22340.

[17] Beale,S.I. & Cornejo,J. (1991) Biosynthesis of phycobilins. Ferredoxin-mediated reduction of biliverdin catalyzed by extracts of Cyanidium caldarium. *J. Biol. Chem.* **266,** 22328-22332.

[18] Benda,C. & Gärtner,W. (2002) Conformational changes of the N-terminal part of phytochromes during the light-induced Pr-to-Pfr transformation. *Photochem. Photobiol.* (unpublished).

[19] Benda,C., Scheufler,C., Tandeau de,M.N., & Gärtner,W. (2004) Crystal structures of two cyanobacterial response regulators in apo- and phosphorylated form reveal a novel dimerization motif of phytochrome-associated response regulators. *Biophys. J.* **87,** 476-487.

[20] Benda,C., Scheufler,C., Tandeau de Marsac,N., & Gärtner,W. (2004) A new dimerization motif in the structures of two light-inducible response regulators from the cyanobacterium Calothrix PCC7601. *Biophys. J.*

[21] Bhoo,S.H., Hirano,T., Jeong,H.Y., Lee,J.G., Furuya,M., & Song,P.S. (1997) Phytochrome photochromism probed by site-directed mutations and chromophore esterfication. *J. Am. Chem. Soc.* **119,** 11717-11718.

[22] Bhoo,S.H., Davis,S.J., Walker,J.M., Karniol,B., & Vierstra,R.D. (2001) Bacteriophytochromes are photochromic histidine kinases using a biliverdin chromophore. *Nature* **414,** 776-779.

[23] Bilwes,A.M., Alex,L.A., Crane,B.R., & Simon,M.I. (1999) Structure of CheA, a signal-transducing histidine kinase. *Cell* **96,** 131-141.

[24] Birnboim,H.C. & Doly,J. (1979) A rapid alkaline extraction procedure for screening recombinant plasmid DNA. *Nucleic Acids Res.* **7,** 1513-1523.

[25] Bischoff,M., Hermann,G., Rentsch,M., & Strehlow,D. (2001) First steps in the phytochrome phototransformation: A comparative femtosecond study on the forward (Pr -> Pfr) and the back reaction (Pfr->Pr). *Biochemistry* **40,** 181-186.

[26] Blumenstein,A., Vienken,K., Tasler,R., Purschwitz,J., Veith,D., Frankenberg-Dinkel,N., & Fischer,R. (2005) The Aspergillus nidulans phytochrome FphA represses sexual development in red light. *Curr. Biol.* **15,** 1833-1838.

[27] Borucki,B., Otto,H., Rottwinkel,G., Hughes,J., Heyn,M.P., & Lamparter,T. (2003) Mechanism of Cph1 phytochrome assembly from stopped-flow kinetics and circular dichroism. *Biochemistry* **42,** 13684-13697.

[28] Borucki,B., von,S.D., Seibeck,S., Lamparter,T., Michael,N., Mroginski,M.A., Otto,H., Murgida,D.H., Heyn,M.P., & Hildebrandt,P. (2005) Light-induced proton release of

phytochrome is coupled to the transient deprotonation of the tetrapyrrole chromophore. *J. Biol. Chem.* **280,** 34358-34364.

[29] Bowler,C., Neuhaus,G., Yamagata,H., & Chua,N.-H. (1994) Cyclic GMP and calcium mediate phytochrome phototransduction. *Cell* **77,** 73-81.

[30] Bradford,M. (1976) A rapid and sensitive method for the quantitation of microgram quantities of protein utilizing the principle of protein-dye binding. *Anal. Biochem.* **72,** 248-254.

[31] Brandt,S., von,S.D., Gunther,M., Hildebrandt,P., & Frankenberg-Dinkel,N. (2008) The fungal phytochrome FphA from Aspergillus nidulans. *J. Biol. Chem.* **283,** 34605-34614.

[32] Braslavsky,S.E., Gärtner,W., & Schaffner,K. (1997) Phytochrome photoconversion. *Plant Cell Env.* **20,** 700-706.

[33] Briggs,W.R. & Olney,M.A. (2001) Photoreceptors in plant photomorphogenesis to date. five phytochromes, two cryptochromes, one phototropin, and one superchrome. *Plant Physiol.* **125,** 85-88.

[34] Brown,S.B., Houghton,J.D., & Vernon,D.I. (1990) Biosynthesis of phycobilins. Formation of the chromophore of phytochrome, phycocyanin and phycoerythrin. *J. Photochem. Photobiol. B* **5,** 3-23.

[35] Brudler,R., Rammelsberg,R., Woo,T.T., Getzoff,E.D., & Gerwert,K. (2001) Structure of the I1 early intermediate of photoactive yellow protein by FTIR spectroscopy. *Nat. Struct. Biol.* **8,** 265-270.

[36] Butler,W.L., Norris,K.H., Siegelman,H.W., & Hendricks,S.B. (1959) Detection, assay and preliminary purification of the pigment controlling photoresponsive development of plants. *Proc. Natl. Acad. Sci. USA* **45,** 1703-1708.

[37] Butler,W.L., Siegelman,H.W., & Miller,C.O. (1964) Denaturation of phytochrome. *Biochemistry* **3,** 851-857.

[38] Butler,W.L., Hendricks,S.B., & Siegelman,H.W. (1964) Action spectra of phytochrome *in vitro*. *Photochem. Photobiol.* **3,** 521-528.

[39] Casal,J.J., Sanchez,R.A., & Botto,J.F. (1998) Modes of action of phytochromes. *J. exp. botany* **49,** 127-138.

[40] Casal,J.J. (2000) Phytochromes, cryptochromes, phototropin: Photoreceptor interactions in plants. *Photochem. Photobiol.* **71,** 1-11.

[41] Cashmore,A.R. (1998) Higher-plant phytochrome: "I used to date histidine, but now I prefer serine". *Proc. Natl. Acad. Sci. USA* **95,** 13358-13360.

[42] Cashmore,A.R. (2003) Cryptochromes: enabling plants and animals to determine circadian time. *Cell* **114,** 537-543.

[43] Catlett,N.L., Yoder,O.C., & Turgeon,B.G. (2003) Whole-genome analysis of two-component signal transduction genes in fungal pathogens. *Eukaryot. Cell* **2,** 1151-1161.

[44] Chapman,D.J., Cole,W.J., & Siegelman,H.W. (1967) Chromophores of allophycocyanin and R-phycocyanin. *Biochem. J.* **105,** 903-905.

[45] Chen,M., Chory,J., & Fankhauser,C. (2004) Light signal transduction in higher plants. *Annu. Rev. Genet.* **38,** 87-117.

[46] Chen,M., Tao,Y., Lim,J., Shaw,A., & Chory,J. (2005) Regulation of phytochrome B nuclear localization through light-dependent unmasking of nuclear-localization signals. *Curr. Biol.* **15,** 637-642.

[47] Choi,G., Yi,H., Kwon,Y.K., Soh,M.S., Shin,B.C., Luka,Z.A., Hahn,T.-R., & Song,P.-S. (1999) Phytochrome signalling is mediated through nucleoside diphosphate kinase 2. *Nature* **401,** 610-613.

[48] Chory,J. & Wu,D. (2001) Weaving the complex web of signal transduction. *Plant Physiol* **125,** 77-80.

[49] Christie,J.M. (2007) Phototropin blue-light receptors. *Annu. Rev. Plant Biol.* **58,** 21-45.

[50] Clack,T., Mathews,S., & Sharrock,R.A. (1994) The phytochrome apoprotein family in Arabidopsis is encoded by five genes: the sequences and expression of PHYD and PHYE. *Plant Mol. Biol.* **25,** 413-427.

[51] Cliff,M.J. & Ladbury,J.E. (2003) A survey of the year 2002 literature on applications of isothermal titration calorimetry. *J. Mol. Recognit.* **16,** 383-391.

[52] Cliff,M.J., Gutierrez,A., & Ladbury,J.E. (2004) A survey of the year 2003 literature on applications of isothermal titration calorimetry. *J. Mol. Recognit.* **17,** 513-523.

[53] Cole,W.J., hEocha,O., Moscowitz,A., & Krueger,W.R. (1967) The optical activity of urobilins derived from phycoerythrobiln. *Eur. J. Biochem.* **3,** 202-207.

[54] Connelly,P.R., Varadarajan,R., Sturtevant,J.M., & Richards,F.M. (1990) Thermodynamics of protein-peptide interactions in the ribonuclease S system studied by titration calorimetry. *Biochemistry* **29,** 6108-6114.

[55] Cornilescu,G., Ulijasz,A.T., Cornilescu,C.C., Markley,J.L., & Vierstra,R.D. (2008) Solution structure of a cyanobacterial phytochrome GAF domain in the red-light-absorbing ground state. *J. Mol. Biol.* **383,** 403-413.

[56] Crosson,S., Rajagopal,S., & Moffat,K. (2003) The LOV domain family: photoresponsive signaling modules coupled to diverse output domains. *Biochemistry* **42,** 2-10.

[57] Davies,D.R., Sarma,R., Labaw,L.W., Silverton,E., Segal,D., & Terry,W.D. (1971) X-ray diffraction and electron microscope studies on a crystalline human immunoglobulin. *Ann. N. Y. Acad. Sci.* **190,** 122-129.

[58] Davis,S.J., Vener,A.V., & Vierstra,R.D. (1999) Bacteriophytochromes: Phytochrome-like photoreceptors from nonphotosynthetic eubacteria. *Science* **286,** 2517-2520.

[59] Davis,S.J., Bhoo,S.H., Durski,A.M., Walker,J.M., & Vierstra,R.D. (2001) The heme-oxygenase family required for phytochrome chromophore biosynthesis is necessary for proper photomorphogenesis in higher plants. *Plant Physiology* **126,** 656-669.

[60] Devlin,P.F. & Kay,S.A. (2000) Cryptochromes are required for phytochrome signaling to the circadian clock but not for rhythmicity. *Plant Cell* **12,** 2499-2510.

[61] Dutta,R., Qin,L., & Inouye,M. (1999) Histidine kinases: diversity of domain organization. *Mol. Microbiol.* **34,** 633-640.

[62] Edgerton,M.D. & Jones,A.M. (1994) Subunit interactions in the carboxy-terminal domain of phytochrome. *Biochemistry* **32,** 8239-8245.

[63] Edgerton,M.D., Santos,M.O., & Jones,A.M. (1994) In vivo suppression of phytochrome aggregation by the GroE chaperonins in *Escherichia coli*. *Plant Mol. Biol.* **21,** 1191-1194.

[64] Eilfeld,P.A. & Eilfeld,P.G. (1988) Circular dichroism of phytochrome intermediates. *Physiol. Plant.* **74,** 169-175.

[65] Essen,L.O., Mailliet,J., & Hughes,J. (2008) The structure of a complete phytochrome sensory module in the Pr ground state. *Proc. Natl. Acad. Sci. U. S. A* **105,** 14709-14714.

[66] Esteban,B., Carrascal,M., Abian,J., & Lamparter,T. (2005) Light-induced changes of cyanobacterial phytochrome Cph1 probed by limited proteolysis and autophosphorylation. *Biochemistry* **44,** 450-461.

[67] Evans,K., Grossmann,J.G., Fordham-Skelton,A.P., & Papiz,M.Z. (2006) Small-angle X-ray scattering reveals the solution structure of a bacteriophytochrome in the catalytically active Pr state. *J. Mol. Biol.* **364,** 655-666.

[68] Fairchild,C.D. & Glazer,A.N. (1994) Oligomeric structure, enzyme kinetics, and substrate specificity of the phycocyanin alpha subunit phycocyanobilin lyase. *J. Biol. Chem.* **269,** 8686-8694.

[69] Fairchild,C.D. & Glazer,A.N. (1994) Nonenzymatic bilin addition to the alpha subunit of an apophycoerythrin. *J. Biol. Chem.* **269,** 28988-28996.

[70] Falk,H. (1989) *The Chemistry of Linear Oligopyrroles and Bile Pigments* .

[71] Fankhauser,C. (2000) Phytochromes as light-modulated protein kinases. *Seminars in Cell & Developmental Biology* **11,** 467-473.

[72] Fankhauser,C. (2001) The phytochromes, a family of red/far-red absorbing photoreceptors. *J. Biol. Chem.* **276,** 11453-11456.

[73] Fiedler,B., Broc,D., Schubert,H., Rediger,A., Borner,T., & Wilde,A. (2004) Involvement of cyanobacterial phytochromes in growth under different light qualities and quantities. *Photochem. Photobiol.* **79,** 551-555.

[74] Fischer,A.J. & Lagarias,J.C. (2004) Harnessing phytochrome's glowing potential. *Proc. Natl. Acad. Sci. U. S. A* **101,** 17334-17339.

[75] Fischer,A.J., Rockwell,N.C., Jang,A.Y., Ernst,L.A., Waggoner,A.S., Duan,Y., Lei,H., & Lagarias,J.C. (2005) Multiple roles of a conserved GAF domain tyrosine residue in cyanobacterial and plant phytochromes. *Biochemistry* **44,** 15203-15215.

[76] Foerstendorf,H., Mummert,E., Schäfer,E., Scheer,H., & Siebert,F. (1996) Fourier-transform infrared spectroscopy of phytochrome: Difference spectra of the intermediates of the photoreactions. *Biochemistry* **35,** 10793-10799.

[77] Foerstendorf,H., Parbel,A., Scheer,H., & Siebert,F. (1997) Z,E isomerization of the alpha-84 phycoviolobilin chromophore of phycoerythrocyanin from Mastigocladus laminosus investigated by Fourier-transform infrared difference spectroscopy. *FEBS Lett.* **402,** 173-176.

[78] Foerstendorf,H., Lamparter,T., Hughes,J., Gärtner,W., & Siebert,F. (2000) The photoreactions of recombinant phytochrome from the cyanobacterium Synechocystis: a low-temperature UV-Vis and FT-IR spectroscopic study. *Photochem. Photobiol.* **71,** 655-661.

[79] Foerstendorf,H., Benda,C., Gärtner,W., Storf,M., Scheer,H., & Siebert,F. (2001) FTIR studies of phytochrome photoreactions reveal the C=O bands of the chromophore: consequences for its protonation states, conformation, and protein interaction. *Biochemistry* **40,** 14952-14959.

[80] Frankenberg-Dinkel,N. (2004) Bacterial heme oxygenases. *Antioxid. Redox. Signal.* **6,** 825-834.

[81] Frankenberg,N., Mukougawa,K., Kohchi,T., & Lagarias,J.C. (2001) Functional genomic analysis of the HY2 family of ferredoxin-dependent bilin reductases from oxygenic photosynthetic organisms. *Plant Cell* **13,** 965-978.

[82] Frankenberg,N. & Lagarias,J.C. (2003) Phycocyanobilin:ferredoxin oxidoreductase of Anabaena sp. PCC 7120. Biochemical and spectroscopic. *J. Biol. Chem.* **278,** 9219-9226.

[83] Franklin,K.A., Larner,V.S., & Whitelam,G.C. (2005) The signal transducing photoreceptors of plants. *Int. J. Dev. Biol.* **49,** 653-664.

[84] Freire,E., Schon,A., & Velazquez-Campoy,A. (2009) Isothermal titration calorimetry: general formalism using binding polynomials. *Methods Enzymol.* **455,** 127-155.

[85] Froehlich,A.C., Liu,Y., Loros,J.J., & Dunlap,J.C. (2002) White Collar-1, a circadian blue light photoreceptor, binding to the *frequency* promoter. *Science* **297,** 815-819.

[86] Froehlich,A.C., Noh,B., Vierstra,R.D., Loros,J., & Dunlap,J.C. (2005) Genetic and molecular analysis of phytochromes from the filamentous fungus Neurospora crassa. *Eukaryot. Cell* **4,** 2140-2152.

[87] Fu,E., Friedman,L., & Siegelman,H.W. (1979) Mass-spectral identification and purification of phycoerythrobilin and phycocyanobilin. *Biochem. J.* **179,** 1-6.

[88] Galperin,M.Y., Nikolskaya,A.N., & Koonin,E.V. (2001) Novel domains of the prokaryotic two-component signal transduction systems. *FEMS Microbiology Letters* **203,** 11-21.

[89] Gambetta,G.A. & Lagarias,J.C. (2001) Genetic engineering of phytochrome biosynthesis in bacteria. *Proc. Natl. Acad. Sci. U. S. A* **98,** 10566-10571.

[90] Gärtner,W., Hill,C., Worm,K., Braslavsky,S.E., & Schaffner,K. (1996) Influence of expression system on chromophore binding and preservation of spectral properties in recombinant phytochrome. *Eur. J. Biochem.* **236,** 978-983.

[91] Gärtner,W. & Braslavsky,S.E. (2003) The Phytochromes: Spectroscopy and Function. In Photoreceptors and Light Signaling (Batschauer,A., ed), pp. 137-180. Royal Society of Chemistry, Cambrige, UK.

[92] Giraud,E., Fardoux,L., Fourrier,N., Hannibal,L., Genty,B., Bouyer,P., Dreyfus,B., & Vermeglio,A. (2002) Bacteriophytochrome controls photosystem synthesis in anoxygenic bacteria. *Nature* **417,** 202-205.

[93] Giraud,E., Zappa,S., Vuillet,L., Adriano,J.M., Hannibal,L., Fardoux,J., Berthomieu,C., Bouyer,P., Pignol,D., & Vermeglio,A. (2005) A new type of bacteriophytochrome acts in tandem with a classical bacteriophytochrome to control the antennae synthesis in Rhodopseudomonas palustris. *J. Biol. Chem.* **280,** 32389-32397.

[94] Giraud,E. & Vermeglio,A. (2008) Bacteriophytochromes in anoxygenic photosynthetic bacteria. *Photosynth. Res.* **97,** 141-153.

[95] Grimm,R., Donaldson,G.K., van,d., V, Schafer,E., & Gatenby,A.A. (1993) Chaperonin-mediated reconstitution of the phytochrome photoreceptor. *J. Biol. Chem.* **268,** 5220-5226.

[96] Grossman,A.R., Bhaya,D., & He,Q. (2001) Tracking the light environment by cyanobacteria and the dynamic nature of light harvesting. *J. Biol. Chem.* **276,** 11449-11452.

[97] Hagiwara,Y., Sugishima,M., Takahashi,Y., & Fukuyama,K. (2006) Crystal structure of phycocyanobilin:ferredoxin oxidoreductase in complex with biliverdin IXalpha, a key enzyme in the biosynthesis of phycocyanobilin. *Proc. Natl. Acad. Sci. U. S. A* **103,** 27-32.

[98] Hahn,J., Strauss,H.M., Landgraf,F.T., Gimenez,H.F., Lochnit,G., Schmieder,P., & Hughes,J. (2006) Probing protein-chromophore interactions in Cph1 phytochrome by mutagenesis. *The FEBS Journal* **273,** 1415-1429.

[99] Hahn,J., Kuhne,R., & Schmieder,P. (2007) Solution-state (15)N NMR spectroscopic study of alpha-C-phycocyanin: implications for the structure of the chromophore-binding pocket of the cyanobacterial phytochrome Cph1. *Chembiochem.* **8,** 2249-2255.

[100] Han,Y.J., Song,P.S., & Kim,J.I. (2007) Phytochrome-mediated photomorphogenesis in plants [Review]. *Journal of Plant Biology* **50,** 230-240.

[101] Heyne,K., Herbst,J., Stehlik,D., Esteban,B., Lamparter,T., Hughes,J., & Diller,R. (2002) Ultrafast dynamics of phytochrome from the cyanobacterium *Synechocystis,* reconstituted with phycocyanobilin and phycoerythrobilin. *Biophys. J.* **82,** 1004-1016.

[102] Hildebrandt,P., Hoffmann,A., Lindemann,P., Heibel,G., Braslavsky,S.E., Schaffner,K., & Schrader,B. (1992) Fourier transform resonance Raman spectroscopy of phytochrome. *Biochemistry* **31,** 7957-7962.

[103] Ho,J.Y.S., Burden,M., & Hurley,J.H. (2000) Structure of the GAF domain, a ubiquitous signaling motif and a new class of cyclic GMP receptor. *The EMBO Journal* **19,** 5288-5299.

[104] Hughes,J., Mittmann,F., Wilde,A., Gärtner,W., Börner,T., Hartmann,E., & Lamparter,T. (1997) A prokaryotic phytochrome. *Nature* **386,** 663.

[105] Hughes,J. & Lamparter,T. (1999) Prokaryotes and Phytochrome. The Connection to Chromophores and Signaling. *Plant Physiol.* **121,** 1059-1068.

[106] Huq,E., Al-Sady,B., & Quail,P.H. (2003) Nuclear translocation of the photoreceptor phytochrome B is necessary for its biological function in seedling photomorphogenesis. *Plant J.* **35,** 660-664.

[107] Hübschmann,T., Yamamoto,H., Gieler,T., Murata,N., & Borner,T. (2005) Red and far-red light alter the transcript profile in the cyanobacterium Synechocystis sp. PCC 6803: impact of cyanobacterial phytochromes. *FEBS Lett.* **579,** 1613-1618.

[108] Hübschmann,T., Jorissen,H.J.M.M., Börner,T., Gärtner,W., & Tandeau de Marsac, N. (2001) Phosphorylation of proteins in the light-dependent signalling pathway of a filamentous cyanobacterium. *European Journal of Biochemistry* **268,** 3383-3389.

[109] Hübschmann,T., Börner,T., Hartmann,E., & Lamparter,T. (2001) Characterization of the Cph1 holo-phytochrome from Synechocystis sp PCC 6803. *European Journal of Biochemistry* **268,** 2055-2063.

[110] Inomata,K., Noack,S., Hammam,M.A.S., Khawn,H., Kinoshita,H., MURATA,Y., Michael,N., Scheerer,P., Krauss,N., & Lamparter,T. (2006) Assembly of synthetic locked chromophores with Agrobacterium phytochromes AGP1 and AGP2. *J. Biol. Chem.* **281,** 28162-28173.

[111] Jancarik,J., Scott,W.G., Milligan,D.L., Koshland,D.E., Jr., & Kim,S.H. (1991) Crystallization and preliminary X-ray diffraction study of the ligand-binding domain of the bacterial chemotaxis-mediating aspartate receptor of Salmonella typhimurium. *J. Mol. Biol.* **221,** 31-34.

[112] Jelesarov,I. & Bosshard,H.R. (1999) Isothermal titration calorimetry and differential scanning calorimetry as complementary tools to investigate the energetics of biomolecular recognition. *J. Mol. Recognit.* **12,** 3-18.

[113] Jiang,Z., Swem,L.R., Rushing,B.G., Devanathan,S., Tollin,G., & Bauer,C.E. (1999) Bacterial photoreceptor with similarity to photoactive yellow protein and plant phytochromes. *Science* **285,** 406-409.

[114] Jiao,Y.L., Lau,O.S., & Deng,X.W. (2007) Light-regulated transcriptional networks in higher plants [Review]. *Nature Reviews Genetics* **8,** 217-230.

[115] Jones,A.M. & Quail,P.H. (1989) Phytochrome structure: peptide fragments from the amino-terminal domain involved in protein-chromophore interactions. *Planta* **178,** 147-156.

[116] Jones,A.M. & Edgerton,M.D. (1994) The anatomy of phytochrome, a unique photoreceptor in plants. *Semin. Cell Biol.* **5,** 295-302.

[117] Jones,A.M., Ecker,J.R., & Chen,J.G. (2003) A re-evaluation of the role of the heterotrimeric G-protein in coupling light responses in Arabidopsis. *Plant Physiol.* **131,** 1623-1627.

[118] Jones,D.T. (1999) Protein secondary structure prediction based on position-specific scoring matrices. *J. Mol. Biol.* **292,** 195-202.

[119] Jorissen,H.J.M.M., Quest,B., Lindner,I., Tandeau de Marsac, N., & Gärtner,W. (2002) Phytochromes with Noncovalently Bound Chromophores: The Ability of Apophytochromes to Direct Tetrapyrrole Photoisomerization. *Photochem. Photobiol.* **75,** 554-559.

[120] Jorissen,H.J.M.M., Quest,B., Remberg,A., Coursin,T., Braslavsky,S.E., Schaffner,K., Tandeau de Marsac, N., & Gärtner,W. (2002) Two independent, light-sensing two-component systems in a filamentous cyanobacterium. *Eur. J. Biochem.* **269,** 2662-2671.

[121] Jung,C. (2000) Insight into protein structure and protein-ligand recognition by Fourier transform infrared spectroscopy. *J. Mol. Recognit.* **13,** 325-351.

[122] Karlin-Neumann,G.A., Brusslan,J.A., & Tobin,E.M. (1991) Phytochrome control of the tms2 gene in transgenic Arabidopsis: a strategy for selecting mutants in the signal transduction pathway. *Plant Cell* **3,** 573-582.

[123] Karniol,B. & Vierstra,R.D. (2003) The pair of bacteriophytochromes from Agrobacterium tumefaciens are histidine kinases with opposing photobiological properties. *Proc. Natl. Acad. Sci. U. S. A* **100,** 2807-2812.

[124] Karniol,B. & Vierstra,R.D. (2004) The HWE histidine kinases, a new family of bacterial two-component sensor kinases with potentially diverse roles in environmental signaling. *J. Bacteriol.* **186,** 445-453.

[125] Karniol,B., Wagner,J.R., Walker,J.M., & Vierstra,R.D. (2005) Phylogenetic analysis of the phytochrome superfamily reveals distinct microbial subfamilies of photoreceptors. *Biochem. J.* **392,** 103-116.

[126] Kehoe,D.M. & Grossman,A.R. (1996) Similarity of a chromatic adaptation sensor to phytochrome and ethylene receptors. *Science* **273,** 1409-1412.

[127] Kevei,E. & Nagy,F. (2003) Phytochrome controlled signalling cascades in higher plants. *Physiologia Plantarum* **117,** 305-313.

[128] Kim,D.H., Kang,J.G., Yang,S.S., Chung,K.S., Song,P.S., & Park,C.M. (2002) A phytochrome-associated protein phosphatase 2A modulates light signals in flowering time control in Arabidopsis. *Plant Cell* **14,** 3043-3056.

[129] Kim,J., Yi,H., Choi,G., Shin,B., Song,P.S., & Choi,G. (2003) Functional characterization of phytochrome interacting factor 3 in phytochrome-mediated light signal transduction. *Plant Cell* **15,** 2399-2407.

[130] Kim,J.I., Kozhukh,G.V., & Song,P.S. (2002) Phytochrome-mediated signal transduction pathways in plants. *Biochem. Biophys. Res. Commun.* **298,** 457-463.

[131] Kim,J.I., Shen,Y., Han,Y.J., Park,J.E., Kirchenbauer,D., Soh,M.S., Nagy,F., Schafer,E., & Song,P.S. (2004) Phytochrome phosphorylation modulates light signaling by influencing the protein-protein interaction. *Plant Cell* **16,** 2629-2640.

[132] Kim,J.I., Park,J.E., Zarate,X., & Song,P.S. (2005) Phytochrome phosphorylation in plant light signaling. *Photochem. Photobiol. Sci.* **4,** 681-687.

[133] Kneip,C., Parbel,A., Foerstendorf,H., Scheer,H., Siebert,F., & Hildebrandt,P. (1998) Fourier transform near-infrared resonance Raman spectroscopic study of the alpha-subunit of phycoerythrocyanin and phycocyanin from the cyanobacterium Mastigocladus laminosus. *J. Raman Spectr.* **29,** 939-944.

[134] Kneip,C., Hildebrandt,P., Schlamann,W., Braslavsky,S.E., Mark,F., & Schaffner,K. (1999) Protonation state and structural changes of the tetrapyrrole chromophore during the Pr to Pfr phototransformation: A Resonance Raman Spectroscopic Study. *Biochemistry* **38,** 15185-15192.

[135] Krall,L. & Reed,J.W. (2000) The histidine kinase-related domain participates in phytochrome B function but is dispensable. *Proc. Natl. Acad. Sci. U. S. A* **97,** 8169-8174.

[136] Kufer,W. & Scheer,H. (1979) Chemical modification of biliprotein chromophores. *Z. Naturforsch. C.* **34,** 776-781.

[137] Kunkel,T., Tomizawa,K.-I., Kern,R., Furuya,M., Chua,N.-H., & Schäfer,E. (1993) *In vitro* formation of a photoreversible adduct of phycocyanobilin and tobacco apophytochrome B. *Eur. J. Biochem.* **215,** 587-594.

[138] Kurokawa,H., Lee,D.S., Watanabe,M., Sagami,I., Mikami,B., Raman,C.S., & Shimizu,T. (2004) A redox-controlled molecular switch revealed by the crystal structure of a bacterial heme PAS sensor. *J. Biol. Chem.* **279,** 20186-20193.

[139] Laan,W., Gauden,M., Yeremenko,S., van,G.R., Kennis,J.T., & Hellingwerf,K.J. (2006) On the mechanism of activation of the BLUF domain of AppA. *Biochemistry* **45,** 51-60.

[140] Ladbury,J.E. & Chowdhry,B.Z. (1996) Sensing the heat: the application of isothermal titration calorimetry to thermodynamic studies of biomolecular interactions. *Chem. Biol.* **3,** 791-801.

[141] Lagarias,J.C. & Rapoport,H. (1980) Chromopeptides from phytochrome. The structure and linkage of the P_r form of the phytochrome chromophore. *J. Am. Chem. Soc.* **102,** 4821-4828.

[142] Lagarias,J.C., Klotz,A.V., Dallas,J.L., Glazer,A.N., Bishop,J.E., O'Connell,J.F., & Rapoport,H. (1988) Exclusive A-ring linkage for singly attached phycocyanobilins and phycoerythrobilins in phycobiliproteins. Absence of singly D-ring-linked bilins. *J. Biol. Chem.* **263,** 12977-12985.

[143] Lagarias,J.C. & Lagarias,D.M. (1989) Self-assembly of synthetic phytochrome holoprotein *in vitro*. *Proc. Natl. Acad. Sci. USA* **86,** 5778-5780.

[144] Lamparter,T., Mittmann,F., Gärtner,W., Börner,T., Hartmann,E., & Hughes,J. (1997) Characterization of recombinant phytochrome from the cyanobacterium *Synechocystis*. *Proc. Natl. Acad. Sci. USA* **94,** 11792-11797.

[145] Lamparter,T., Esteban,B., & Hughes,J. (2001) Phytochrome Cph1 from the cyanobacterium Synechocystis PCC6803 - Purification, assembly, and quaternary structure. *Eur. J. Biochem.* **268,** 4720-4730.

[146] Lamparter,T., Michael,N., Mittmann,F., & Esteban,B. (2002) Phytochrome from *Agrobacterium tumefaciens* has unusual spectral properties and reveals an N-terminal chromophore attachment site. *Proc. Natl. Acad. Sci. USA* **99,** 11628-11633.

[147] Lamparter,T., Michael,N., Caspani,O., Miyata,T., Shirai,K., & Inomata,K. (2003) Biliverdin binds covalently to Agrobacterium phytochrome Agp1 via its ring a vinyl side chain. *J. Biol. Chem.* **278,** 33786-33792.

[148] Lamparter,T. (2004) Evolution of cyanobacterial and plant phytochromes. *FEBS Lett.* **573,** 1-5.

[149] Lamparter,T., Carrascal,M., Michael,N., Martinez,E., Rottwinkel,G., & Abian,J. (2004) The biliverdin chromophore binds covalently to a conserved cysteine residue in the N-terminus of Agrobacterium phytochrome Agp1. *Biochemistry* **43,** 3659-3669.

[150] Lamparter,T. & Michael,N. (2005) Agrobacterium phytochrome as an enzyme for the production of ZZE bilins. *Biochemistry* **44,** 8461-8469.

[151] Li,L. & Lagarias,J.C. (1992) Phytochrome assembly. Defining chromophore structural requirements for covalent attachment and photoreversibility. *J. Biol. Chem.* **267,** 19204-19210.

[152] Li,L., Murphy,J.T., & Lagarias,J.C. (1995) Continuous fluorescence assay of phytochrome assembly in vitro. *Biochemistry* **34,** 7923-7930.

[153] Lin,C. (2002) Blue light receptors and signal transduction. *Plant Cell* **14 Suppl,** S207-S225.

[154] Lin,C. & Shalitin,D. (2003) Cryptochrome structure and signal transduction. *Annu. Rev. Plant Biol.* **54,** 469-496.

[155] Liscum,E., Hodgson,D.W., & Campbell,T.J. (2003) Blue light signaling through the cryptochromes and phototropins. So that's what the blues is all about. *Plant Physiol* **133,** 1429-1436.

[156] Losi,A. & Gärtner,W. (2008) Bacterial bilin- and flavin-binding photoreceptors. *Photochem. Photobiol. Sci.* **7,** 1168-1178.

[157] Losi,A. & Gärtner,W. (2008) Shedding (blue) light on algal gene expression. *Proc. Natl. Acad. Sci. U. S. A* **105,** 7-8.

[158] Marina,A., Waldburger,C.D., & Hendrickson,W.A. (2005) Structure of the entire cytoplasmic portion of a sensor histidine-kinase protein. *EMBO J.* **24,** 4247-4259.

[159] Masuda,S. & Bauer,C.E. (2002) AppA is a blue light photoreceptor that antirepresses photosynthesis gene expression in Rhodobacter sphaeroides. *Cell* **110,** 613-623.

[160] Mathews,S. (2006) Seeing the light. *Nat. Genet.* **38,** 606-608.

[161] Matsushita,T. (2006) Photoreponses and functions of different domains in phytochrome molecule. *Plant & Cell Physiology* **47,** S8.

[162] Matute,R.A., Contreras,R., Perez-Hernandez,G., & Gonzalez,L. (2008) The Chromophore Structure of the Cyanobacterial Phytochrome Cph1 As Predicted by Time-Dependent Density Functional Theory. *J. Phys. Chem. B*. **112 (51),** 16253-16256.

[163] Matysik,J., Hildebrandt,P., Schlamann,W., Braslavsky,S.E., & Schaffner,K. (1995) Fourier-transform resonance Raman spectroscopy of intermediates of the phytochrome photocycle. *Biochemistry* **34,** 10497-10507.

[164] McDonagh,A.F., Palma,L.A., & Lightner,D.A. (1980) Blue light and bilirubin excretion. *Science* **208,** 145-151.

[165] McDonagh,A.F. & Palma,L.A. (1980) Preparation and properties of crystalline biliverdin IX alpha. Simple methods for preparing isomerically homogeneous biliverdin and [14C[biliverdin by using 2,3-dichloro-5,6-dicyanobenzoquinone. *Biochem. J.* **189,** 193-208.

[166] McDonell,M.W., Simon,M.N., & Studier,F.W. (1977) Analysis of restriction fragments of T7 DNA and determination of molecular weights by electrophoresis in neutral and alkaline gels. *J. Mol. Biol.* **110,** 119-146.

[167] Montgomery,B.L. (2007) Sensing the light: photoreceptive systems and signal transduction in cyanobacteria [Review]. *Molecular Microbiology* **64,** 16-27.

[168] Mozley,D., Remberg,A., & Gärtner,W. (1997) Large-scale generation of affinity-purified recombinant phytochrome chromopeptide. *Photochem. Photobiol.* **66,** 710-715.

[169] Mroginski,M.A., Murgida,D.H., & Hildebrandt,P. (2007) The chromophore structural changes during the photocycle of phytochrome: A combined resonance raman and quantum chemical approach. *Accounts of Chemical Research* **40,** 258-266.

[170] Murgida,D.H., von,S.D., Hildebrandt,P., Schwinte,P., Siebert,F., Sharda,S., Gärtner,W., & Mroginski,M.A. (2007) The chromophore structures of the Pr States in plant and bacterial phytochromes. *Biophys. J.* **93,** 2410-2417.

[171] Murphy,K.P., Freire,E., & Paterson,Y. (1995) Configurational effects in antibody-antigen interactions studied by microcalorimetry. *Proteins* **21,** 83-90.

[172] Mutsuda,M., Michel,K.P., Zhang,X., Montgomery,B.L., & Golden,S.S. (2003) Biochemical properties of CikA, an unusual phytochrome-like histidine protein kinase that resets the circadian clock in Synechococcus elongatus PCC 7942. *J. Biol. Chem.* **278,** 19102-19110.

[173] Nagy,F. & Schäfer,E. (2000) Nuclear and cytosolic events of light-induced, phytochrome-regulated signalling in higher plants. *EMBO J.* **19,** 157-163.

[174] Nagy,F. & Schafer,E. (2002) Phytochromes control photomorphogenesis by differentially regulated, interacting signaling pathways in higher plants. *Annu. Rev. Plant Biol.* **53,** 329-355.

[175] Neff,M.M., Fankhauser,C., & Chory,J. (2000) Light: an indicator of time and place. *Genes Dev.* **14,** 257-271.

[176] Neuhaus,G., Bowler,C., Kern,R., & Chua,N.-H. (1993) Calcium/calmodulin dependent and -independent phytochrome signal transduction pathways. *Cell* **73,** 937-952.

[177] Newton,C.R., Holland,D., Heptinstall,L.E., Hodgson,I., Edge,M.D., Markham,A.F., & McLean,M.J. (1993) The production of PCR products with 5' single-stranded tails using primers that incorporate novel phosphoramidite intermediates. *Nucleic Acids Res.* **21,** 1155-1162.

[178] Ni,M., Tepperman,J.M., & Quail,P.H. (1999) Binding of phytochrome B to its nuclear signalling partner PIF3 is reversibly induced by light. *Nature* **400,** 781-784.

[179] Ni,M. (2005) Integration of light signaling with photoperiodic flowering and circadian rhythm. *Cell Res.* **15,** 559-566.

[180] Noack,S. & Lamparter,T. (2007) Light modulation of histidine-kinase activity in bacterial phytochromes monitored by size exclusion chromatography, crosslinking, and limited proteolysis. *Methods Enzymol.* **423,** 203-221.

[181] Noack,S., Michael,N., Rosen,R., & Lamparter,T. (2007) Protein conformational changes of Agrobacterium phytochrome Agp1 during chromophore assembly and photoconversion. *Biochemistry* **46,** 4164-4176.

[182] Ohmori,M., Terauchi,K., Okamoto,S., & Watanabe,M. (2002) Regulation of cAMP-mediated photosignaling by a phytochrome in the cyanobacterium *Anabaena cylindrica*. *Photochem. Photobiol.* **75,** 675-679.

[183] Oka,Y., Matsushita,T., Mochizuki,N., Suzuki,T., Tokutomi,S., & Nagatani,A. (2004) Functional Analysis of a 450–Amino Acid N-Terminal Fragment of Phytochrome B in Arabidopsis. *Plant Cell* **16(8):** 2104-2116.

[184] Okamota,H., Matsui,M., & Deng,X.W. (2001) Overexpression of the heterotrimeric G-protein alpha subunit enhances phytochrome-mediated inhibition of hypocotyl elongation. *Plant Cell* **13,** 1639-1652.

[185] Okhrimenko,O. & Jelesarov,I. (2008) A survey of the year 2006 literature on applications of isothermal titration calorimetry. *J. Mol. Recognit.* **21,** 1-19.

[186] Park,C.M., Bhoo,S.H., & Song,P.S. (2000) Inter-domain crosstalk in the phytochrome molecules. *Seminars in Cell & Developmental Biology* **11,** 449-456.

[187] Park,C.M., Shim,J.-Y., Yang,S.-S., Kang,J.-G., Kim,J.-I., Luka,Z.A., & Song,P.-S. (2000) Chromophore-apoprotein interactions in Synechocystis sp PCC6803 phytochrome Cph1. *Biochemistry* **39,** 1409-1412.

[188] Pratt,L.H. (1995) Phytochromes:differential properties, expression patterns and molecular evolution. *Photochem. Photobiol.* **61,** 10-21.

[189] Quail,P.H., Boylan,M.T., Parks,B.M., Short,T.W., Xu,Y., & Wagner,D. (1995) Phytochromes: Photosensory perception and signal transduction. *Science* **268,** 675-680.

[190] Quail,P.H. (1997) The phytochromes: a biochemical mechanism of signaling in sight? *BioEssays* **19,** 571-579.

[191] Quail,P.H. (2000) Phytochrome-interacting factors. *Semin. Cell Dev. Biol.* **11,** 457-466.

[192] Quail,P.H. (2002) Photosensory perception and signalling in plant cells: new paradigms? *Curr. Opin. Cell Biol.* **14,** 180-188.

[193] Quail,P.H. (2002) Phytochrome photosensory signalling networks. *Nature Reviews Molecular Cell Biology* **3,** 85-93.

[194] Quest,B. & Gärtner,W. (2004) Chromophore selectivity in bacterial phytochromes: dissecting the process of chromophore attachment. *Eur. J. Biochem.* **271,** 1117-1126.

[195] Quest,B., Hübschmann,T., Sharda,S., Tandeau de Marsac, N., & Gärtner,W. (2007) Homologous expression of a bacterial phytochrome - The cyanobacterium Fremyella

diplosiphon incorporates biliverdin as a genuine, functional chromophore. *FEBS Journal* **274,** 2088-2098.

[196] Remberg,A., Lindner,I., Lamparter,T., Hughes,J., Kneip,C., Hildebrandt,P., Braslavsky,S.E., Gärtner,W., & Schaffner,K. (1997) Raman spectroscopic and light-induced kinetic characterization of a recombinant phytochrome of the cyanobacterium Synechocystis. *Biochemistry* **36,** 13389-13395.

[197] Remberg,A., Ruddat,A., Braslavsky,S.E., Gärtner,W., & Schaffner,K. (1998) Chromophore incorporation, P_r to Pfr kinetics and Pfr thermal reversion of recombinant N-terminal fragments of phyA and phyB phytochrome chromoproteins. *Biochemistry* **37,** 9983-9990.

[198] Remberg,A., Schmidt,P., Braslavsky,S.E., Gärtner,W., & Schaffner,K. (1999) Differential effects of mutations in the chromophore pocket of recombinant phytochrome on chromoprotein assembly and P_r-to-P_{fr} photoconversion. *Eur. J. Biochem.* **266,** 201-208.

[199] Rockwell,N.C. & Lagarias,J.C. (2006) The structure of phytochrome: a picture is worth a thousand spectra. *Plant Cell* **18,** 4-14.

[200] Rockwell,N.C., Su,Y.S., & Lagarias,J.C. (2006) Phytochrome structure and signaling mechanisms. *Annu. Rev. Plant Biol.* **57,** 837-858.

[201] Rohmer,T., Strauss,H., Hughes,J., de,G.H., Gärtner,W., Schmieder,P., & Matysik,J. (2006) N-15 MAS NMR studies of Cph1 phytochrome: Chromophore dynamics and intramolecular signal transduction. *Journal of Physical Chemistry B* **110,** 20580-20585.

[202] Rohmer,T., Lang,C., Hughes,J., Essen,L.O., Gärtner,W., & Matysik,J. (2008) Light-induced chromophore activity and signal transduction in phytochromes observed by 13C and 15N magic-angle spinning NMR. *Proc. Natl. Acad. Sci. U. S. A* **105,** 15229-15234.

[203] Rüdiger,W. (1987) Phytochrome: the chromophore and photoconversion. *Photobiochem. Photobiophys. ,Suppl.* 217-227.

[204] Rüdiger,W. (1992) Events in the phytochrome molecule after irradiation. *Photochem. Photobiol.* **56,** 803-809.

[205] Saiki,R.K., Gelfand,D.H., Stoffel,S., Scharf,S.J., Higuchi,R., Horn,G.T., Mullis,K.B., & Erlich,H.A. (1988) Primer-directed enzymatic amplification of DNA with a thermostable DNA polymerase. *Science* **239,** 487-491.

[206] Sambrook,J., Fritsch,E.F., & Maniatis,T. (1989) *Molecular Cloning*, 2nd edn. Cold Spring Harbor Laboratory Press, New York.

[207] Sancar,A. (2003) Structure and function of DNA photolyase and cryptochrome blue-light photoreceptors. *Chem. Rev.* **103,** 2203-2237.

[208] Sancar,A. (2004) Photolyase and cryptochrome blue-light photoreceptors. *Adv. Protein Chem.* **69,** 73-100.

[209] Sanger,F., Nicklen,S., & Coulson,A.R. (1977) DNA sequencing with chain-terminating inhibitors. *Proc. Natl. Acad. Sci. U. S. A* **74,** 5463-5467.

[210] Sanger,F., Coulson,A.R., Barrell,B.G., Smith,A.J., & Roe,B.A. (1980) Cloning in single-stranded bacteriophage as an aid to rapid DNA sequencing. *J. Mol. Biol.* **143,** 161-178.

[211] Schafer,E. & Bowler,C. (2002) Phytochrome-mediated photoperception and signal transduction in higher plants. *EMBO Reports* **3,** 1042-1048.

[212] Schäfer,E. & Nagy,F. (2006) *Photomorphogenesis in plants and bacteria*, 3 edn. Springer, Dordrecht, The Netherlands.

[213] Schägger,H. & von Jagow,G. (1987) Tricine-sodium dodecyl sulfate-polyacrylamide gel electrophoresis for the separation of proteins in the range from 1 to 100 kDa. *Anal. Biochem.* **166,** 368-379.

[214] Scheerer,P., Michael,N., Park,J.H., Noack,S., Forster,C., Hammam,M.A., Inomata,K., Choe,H.W., Lamparter,T., & Krauss,N. (2006) Crystallization and preliminary X-ray crystallographic analysis of the N-terminal photosensory module of phytochrome Agp1, a biliverdin-binding photoreceptor from Agrobacterium tumefaciens. *J. Struct. Biol.* **153,** 97-102.

[215] Schmidt,P., Westphal,U.H., Worm,K., Braslavsky,S.E., Gärtner,W., & Schaffner,K. (1996) Chromophore-protein interaction controls the complexity of the phytochrome photocycle. *J. Photochem. Photobiol. B* **34,** 73-77.

[216] Schmitz,O., Katayama,M., Williams,S.B., Kondo,T., & Golden,S.S. (2000) CikA, a bacteriophytochrome that resets the cyanobacterial clock. *Science* **289,** 765-768.

[217] Schneider-Poetsch,H.A.W., Braun,B., Marx,S., & Schaumberg,A. (1991) Phytochromes and bacterial sensor proteins are related by structural and functional homologies. Hypothesis on phytochrome-mediated signal-transduction. *FEBS Lett.* **281,** 245-249.

[218] Schneider-Poetsch,H.A.W. (1992) Signal transduction by phytochrome: phytochromes have a module related to the transmitter modules of bacterial sensor proteins. *Photochem. Photobiol.* **56,** 839-846.

[219] Schumann,C., Gross,R., Wolf,M.M., Diller,R., Michael,N., & Lamparter,T. (2008) Subpicosecond midinfrared spectroscopy of the Pfr reaction of phytochrome Agp1 from Agrobacterium tumefaciens. *Biophys. J.* **94,** 3189-3197.

[220] Schwinte,P., Foerstendorf,H., Hussain,Z., Gärtner,W., Mroginski,M.A., Hildebrandt,P., & Siebert,F. (2008) FTIR study of the photoinduced processes of plant phytochrome phyA using isotope-labeled bilins and density functional theory calculations. *Biophys. J.* **95,** 1256-1267.

[221] Schwinte,P., Gärtner,W., Sharda,S., Mroginski,M.A., Hildebrandt,P., & Siebert,F. (2009) The photoreactions of recombinant phytochrome CphA from the cyanobacterium Calothrix PCC7601: a low-temperature UV-Vis and FTIR study. *Photochem. Photobiol.* **85,** 239-249.

[222] Segal,D.M., Powers,J.C., Cohen,G.H., Davies,D.R., & Wilcox,P.E. (1971) Substrate binding site in bovine chymotrypsin A-gamma. A crystallographic study using peptide chloromethyl ketones as site-specific inhibitors. *Biochemistry* **10,** 3728-3738.

[223] Sharda,S., Shah,R., & Gärtner,W. (2007) Domain interaction in cyanobacterial phytochromes as a prerequisite for spectral integrity. *European Biophysics Journal* **36,** 815-821.

[224] Sharda,S., Koay,M.S., Kim,Y.J., Engelhard,M., & Gärtner,W. (2009) A non-hydrolyzable ATP derivative generates a stable complex in a light-inducible two-component system. *J. Biol. Chem.* **284,** 33999-34004.

[225] Sharrock,R.A. & Clack,T. (2002) Patterns of expression and normalized levels of the five Arabidopsis phytochromes. *Plant Physiol* **130,** 442-456.

[226] Sharrock,R.A. (2008) The phytochrome red/far-red photoreceptor superfamily. *Genome Biol.* **9,** 230.

[227] Siebert,F., Mäntele,W., & Gerwert,K. (1983) Fourier-transform infrared spectroscopy applied to rhodopsin. The problem of the protonation state of the retinylidene Schiff base re-investigated. *Eur. J. Biochem.* **136,** 119-127.

[228] Siebert,F., Grimm,R., Rudiger,W., Schmidt,G., & Scheer,H. (1990) Infrared spectroscopy of phytochrome and model pigments. *Eur. J. Biochem.* **194,** 921-928.

[229] Siebert,F. (1997) Monitoring the mechanism of biological reactions by infrared spectroscopy. *Mikrochim Acta* **14,** 43-50.

[230] Sineshchekov,V., Koppel',L., Esteban,B., Hughes,J., & Lamparter,T. (2002) Fluorescence investigation of the recombinant cyanobacterial phytochrome (Cph1) and its C-terminally truncated monomeric species (Cph1Delta2): implication for holoprotein assembly, chromophore-apoprotein interaction and photochemistry. *J. Photochem. Photobiol. B* **67,** 39-50.

[231] Sineshchekov,V.A., Hughes,J., Hartmann,E., & Lamparter,T. (1998) Fluorescence and photochemistry of recombinant phytochrome from the cyanobacterium Synechocystis. *Photochem. Photobiol.* **67,** 263-267.

[232] Smith,H. (2000) Phytochromes and light signal perception plants- an emerging synthesis. *Nature* **407,** 585-591.

[233] Song,P.-S. (1999) Inter-Domain Signal Transmission within the Phytochromes. *J. Biochemistry and Molec. Biol.* **32,** 215-225.

[234] Southern,E.M. (1979) Measurement of DNA length by gel electrophoresis. *Anal. Biochem.* **100,** 319-323.

[235] Stock,A.M., Robinson,V.L., & Goudreau,P.N. (2000) Two-component signal transduction. *Annu. Rev. Biochem.* **69,** 183-215.

[236] Stock,A.M. & West,A.H. (2003) Response regulator proteins and their interactions with histidine protein kinases. In: Histidine Kinases in Signal Transduction, (Inoyue,M. & Dutta,R., eds), pp. 237-271. San Diego, CA: Academic Press, New York.

[237] Stowe-Evans,E.L. & Kehoe,D.M. (2004) Signal transduction during light-quality acclimation in cyanobacteria: a model system for understanding phytochrome-response pathways in prokaryotes. *Photochem. Photobiol. Sci.* **3,** 495-502.

[238] Strauss,H.M., Schmieder,P., & Hughes,J. (2005) Light-dependent dimerisation in the N-terminal sensory module of cyanobacterial phytochrome 1. *FEBS Lett.* **579,** 3970-3974.

[239] Suetsugu,N. & Wada,M. (2003) Cryptogam blue-light photoreceptors. *Curr. Opin. Plant Biol.* **6,** 91-96.

[240] Suetsugu,N. & Wada,M. (2007) Phytochrome-dependent photomovement responses mediated by phototropin family proteins in cryptogam plants [Review]. *Photochemistry & Photobiology* **83,** 87-93.

[241] Tandeau de Marsac,N., Mazel,D., Damerval,T., Guglielmi,G., Capuano,V., & Houmard,J. (1988) Photoregulation of gene expression in the filamentous cyanobacterium *Calothrix* sp. PCC 7601: light-harvesting complex and cell differentiation. *Photosynthesis Research* **18,** 132-133.

[242] Tarutina,M., Ryjenkov,D.A., & Gomelsky,M. (2006) An unorthodox bacteriophytochrome from Rhodobacter sphaeroides involved in turnover of the second messenger c-di-GMP. *J. Biol. Chem.* **281,** 34751-34758.

[243] Tasler,R., Moises,T., & Frankenberg-Dinkel,N. (2005) Biochemical and spectroscopic characterization of the bacterial phytochrome of Pseudomonas aeruginosa. *FEBS J.* **272,** 1927-1936.

[244] Terauchi,K., Montgomery,B.L., Grossman,A.R., Lagarias,J.C., & Kehoe,D.M. (2004) RcaE is a complementary chromatic adaptation photoreceptor required for green and red light responsiveness. *Mol. Microbiol.* **51,** 567-577.

[245] Terry,M.J., Maines,M.D., & Lagarias,J.C. (1993) Inactivation of phytochrome- and phycobiliprotein-chromophore precursors by rat liver biliverdin reductase. *J. Biol. Chem.* **268,** 26099-26106.

[246] Terry,M.J., Wahleithner,J.A., & Lagarias,J.C. (1993) Biosynthesis of the plant photoreceptor phytochrome. *Arch. Biochem. Biophys.* **306,** 1-15.

[247] Thümmler,F. & Rüdiger,W. (1983) Models for the photoreversibility of phytochrome. Z,E-isomerization of chromopeptides from phycocyanin and phytochrome. *Tetrahedron* **39,** 1943-1951.

[248] Thümmler,F., Algarra,P., & Fobo,G.M. (1995) Sequence similarities of phytochrome to protein kinases: implication for the structure, function and evolution of the phytochrome gene family. *FEBS Lett.* **357,** 149-155.

[249] Tobin,E.M. & Kehoe,D.M. (1994) Phytochrome regulated gene expression. *Semin. Cell Biol.* **5,** 335-346.

[250] Towbin,H., Staehelin,T., & Gordon,J. (1979) Electrophoretic transfer of proteins from polyacrylamide gels to nitrocellulose sheets: Procedure and some applications. *Proc. Natl. Acad. Sci. USA* **76,** 4350-4354.

[251] van der Horst,M.A. & Hellingwerf,K.J. (2004) Photoreceptor proteins, "star actors of modern times": a review of the functional dynamics in the structure of representative members of six different photoreceptor families. *Acc. Chem. Res.* **37,** 13-20.

[252] van Thor,J.J., Borucki,B., Crieelard,W., Otto,H., Lamparter,T., Hughes,J., Hellingwerf,K.J., & Heyn,M.P. (2001) Light-induced proton release and proton uptake reactions in the cyanobacterial phytochrome Cph1. *Biochemistry* **40,** 11460-11471.

[253] van Thor,J.J., Fisher,N., & Rich,P.R. (2005) Assignments of the Pfr-Pr FTIR difference spectrum of cyanobacterial phytochrome Cph1 using 15N and 13C isotopically labeled phycocyanobilin chromophore. *J. Phys. Chem. B* **109,** 20597-20604.

[254] van Thor,J.J., Mackeen,M., Kuprov,I., Dwek,R.A., & Wormald,M.R. (2006) Chromophore structure in the photocycle of the cyanobacterial phytochrome Cph1. *Biophys. J.* **91,** 1811-1822.

[255] van Thor,J.J., Ronayne,K.L., & Towrie,M. (2007) Formation of the early photoproduct Lumi-R of cyanobacterial phytochrome Cph1 observed by ultrafast mid-infrared spectroscopy. *Journal of the American Chemical Society* **129,** 126-132.

[256] Velazquez-Campoy,A., Leavitt,S.A., & Freire,E. (2004) Characterization of protein-protein interactions by isothermal titration calorimetry. *Methods Mol. Biol.* **261,** 35-54.

[257] Velazquez-Campoy,A., Ohtaka,H., Nezami,A., Muzammil,S., & Freire,E. (2004) Isothermal titration calorimetry. *Curr. Protoc. Cell Biol.* **17,** Unit.

[258] Velazquez-Campoy,A. & Freire,E. (2006) Isothermal titration calorimetry to determine association constants for high-affinity ligands. *Nat. Protoc.* **1,** 186-191.

[259] Velazquez,C.A. & Freire,E. (2005) ITC in the post-genomic era...? Priceless. *Biophys. Chem.* **115,** 115-124.

[260] Vierstra,R.D. (1993) Illuminating phytochrome functions. *Plant Physiol.* **103,** 679-684.

[261] Vierstra,R.D. (1994) Phytochrome degradation. In Photomorphogenesis in plants - 2nd Edition (Kendrick,R.E. & Kronenberg,G.H.M., eds), pp. 141-160. Kluwer Academic Publishers, Netherland.

[262] Vierstra,R.D. & Davis,S.J. (2000) Bacteriophytochromes: new tools for understanding phytochrome signal transduction. *Seminars in Cell & Developmental Biology* **11,** 511-521.

[263] Vogel,R. & Siebert,F. (2003) Fourier transform IR spectroscopy study for new insights into molecular properties and activation mechanisms of visual pigment rhodopsin. *Biopolymers* **72,** 133-148.

[264] Vogelstein,B. & Gillespie,D. (1979) Preparative and analytical purification of DNA from agarose. *Proc. Natl. Acad. Sci. USA* **76,** 615-619.

[265] von,S.D., Seibeck,S., Michael,N., Scheerer,P., Mroginski,M.A., Murgida,D.H., Krauss,N., Heyn,M.P., Hildebrandt,P., Borucki,B., & Lamparter,T. (2007) Highly conserved residues Asp-197 and His-250 in Agp1 phytochrome control the proton affinity of the chromophore and Pfr formation. *J. Biol. Chem.* **282,** 2116-2123.

[266] von,S.D., Gunther,M., Scheerer,P., Murgida,D.H., Mroginski,M.A., Krauss,N., Lamparter,T., Zhang,J., Anstrom,D.M., Vierstra,R.D., Forest,K.T., & Hildebrandt,P. (2008) Chromophore heterogeneity and photoconversion in phytochrome crystals and solution studied by resonance Raman spectroscopy. *Angew. Chem. Int. Ed Engl.* **47,** 4753-4755.

[267] Vuillet,L., Kojadinovic,M., Zappa,S., Jaubert,M., Adriano,J.M., Fardoux,J., Hannibal,L., Pignol,D., Vermeglio,A., & Giraud,E. (2007) Evolution of a bacteriophytochrome from light to redox sensor. *EMBO J.* **26,** 3322-3331.

[268] Wagner,J.R., Brunzelle,J.S., Forest,K.T., & Vierstra,R.D. (2005) A light-sensing knot revealed by the structure of the chromophore-binding domain of phytochrome. *Nature* **438,** 325-331.

[269] Wagner,J.R., Zhang,J., Brunzelle,J.S., Vierstra,R.D., & Forest,K.T. (2007) High resolution structure of Deinococcus bacteriophytochrome yields new insights into phytochrome architecture and evolution. *J. Biol. Chem.* **282,** 12298-12309.

[270] Wagner,J.R., Zhang,J., von,S.D., Gunther,M., Murgida,D.H., Mroginski,M.A., Walker,J.M., Forest,K.T., Hildebrandt,P., & Vierstra,R.D. (2008) Mutational analysis of Deinococcus radiodurans bacteriophytochrome reveals key amino acids necessary for the photochromicity and proton exchange cycle of phytochromes. *J. Biol. Chem.* **283,** 12212-12226.

[271] West,A.H. & Stock,A.M. (2001) Histidine kinases and response regulator proteins in two-component signaling systems. *Trends Biochem. Sci.* **26,** 368-376.

[272] Wilde,A., Churin,Y., Schubert,H., & Borner,T. (1997) Disruption of a Synechocystis sp. PCC 6803 gene with partial similarity to phytochrome genes alters growth under changing light qualities. *FEBS Lett.* **406,** 89-92.

[273] Wilde,A., Fiedler,B., & Borner,T. (2002) The cyanobacterial phytochrome Cph2 inhibits phototaxis towards blue light. *Mol. Microbiol.* **44,** 981-988.

[274] Wu,S.H. & Lagarias,J.C. (2000) Defining the bilin lyase domain: lessons from the extended phytochrome superfamily. *Biochemistry* **39,** 13487-13495.

[275] Yang,X., Stojkovic,E.A., Kuk,J., & Moffatt,K. (2007) Crystal structure of the chromophore binding domain of an unusual bacteriophytochrome, RpBphP3, reveals residues that modulate photoconversion. *Proc. Natl. Acad. Sci.* **104,** 12571-12576.

[276] Yang,X., Kuk,J., & Moffat,K. (2008) Crystal structure of Pseudomonas aeruginosa bacteriophytochrome: photoconversion and signal transduction. *Proc. Natl. Acad. Sci. U. S. A* **105,** 14715-14720.

[277] Yeh,K.-C., Wu,S.-H., Murphy,J.T., & Lagarias,J.C. (1997) A cyanobacterial phytochrome two-component light sensory system. *Science* **277,** 1505-1508.

[278] Yeh,K.C. & Lagarias,J.C. (1998) Eukaryotic phytochromes: light-regulated serine/threonine protein kinases with histidine kinase ancestry. *Proc. Natl. Acad. Sci. U. S. A* **95,** 13976-13981.

[279] Yoon,J.M., Hahn,T.R., Cho,M.H., Jeon,J.S., Bhoo,S.H., & Kwon,Y.K. (2008) The PHY domain is required for conformational stability and spectral integrity of the bacteriophytochrome from Deinococcus radiodurans. *Biochem. Biophys. Res. Commun.* **369,** 1120-1124.

[280] Zhao,K.H., Ran,Y., Li,M., Sun,Y.N., Zhou,M., Storf,M., Kupka,M., Bohm,S., Bubenzer,C., & Scheer,H. (2004) Photochromic biliproteins from the cyanobacterium Anabaena sp. PCC 7120: lyase activities, chromophore exchange, and photochromism in phytochrome AphA. *Biochemistry* **43,** 11576-11588.

Chapter 7

Appendix

Abbreviations

aa	Amino acid(s)
Abs	Absorption
Amp	Ampicillin
AP	Alkaline phosphatase
APS	ammonium peroxodisulfate
ATP	Adenosine 5 ‘-triphosphate
BBP	Bilin binding pocket
bp	Base pairs
BCIP	5-bromo-4-chloro-3-indolyl phosphate
BLD	Bilin lyase domain
Bph	Bacteriophytochrome
BSA	Bovine serum albumin
BV	Biliverdin IXα
°C	Degree Celsius
Cm	Chloramphenicol
CBD	Chromophore binding domain
CCA	Complementary chromatic adaptation
cDNA	Complementary DNA
cGMP	Cyclic guanosine monophosphate
CIP	Calf intestinal phosphatase
Cph	Cyanobacterial phytochrome
Cry	Cryptochrome
Cys	Cysteine

ADDENDUM

DMSO	Dimethyl sulfoxide
DNA	Deoxyribonucleic acid
dNTP	Deoxyribonucleoside triphosphate
DrBphP	Deinococcus radiodurans bacteriophytochrome
DrCBD	Chromophore binding domain of DrBphP
DTT	Dithiothreitol
EDTA	Ethylene diamine tetra-acetic acid
EtOH	Ethanol
FhLA	Bacterial formiethyl hydrogen lyase transcriptor activatorA
Fph	Fungal phytochrome
Fig.	Figure
FR	Far-red light
g	Grams or gravity (context sensitive)
GAF	Vertebrate cGMP specific phosphodiesterase- cyanobacterial Adenyl cyclase- bacterial Formiethyl hydrogen lyase transcriptor activator A
h	Hour
His_6 tag	6 - Histidine residues identification tag
HK/HKD	Histidine kinase domain
HKRD	Histidine kinase related domain
HO	Heme oxygenase
Hpt	Histidine phosphotransferase
HPLC	High performance liquid chromatography
IDA	Imino diacetic acid
IMAC	Immobilized metal affinity chromatography
IPTG	Isopropyl-β-D-thiogalactopyranoside

ADDENDUM

Kan	Kanamycin
kb	Kilobase
kDa	Kilo dalton
l	Litre
LB	Luria Bertani broth
M	Molar (mol/l)
MCS	Multiple cloning site
mg	Milligram
min	Minute
ms	Millisecond
MW	Molecular weight
NBT	Nitro blue tetrazolium
ng	Nanogram
nm	Nanometer
ns	Nanosecond
NMR	Nuclear magnetic resonance
OD	Optical density
ORF	Open reading frame
PAC	PAS associated /C-terminal PAS domain
PAS	Per-Arnt-Sim domain
PaBphP	Pseudomonas aeruginosa bacteriophytochrome
PAGE	Polyacrylamide gel electrophoresis
PBS	Phosphate buffered saline
PCB	Phycocyanobilin
PCC	Pasteur Culture Collection

PCR	Polymerase chain reaction
Pefabloc	4-(2-aminoethyl)-benzene-sulfonylfluoride hydrochloride
PEG	Polyethylene glycol
Pfr	Phytochrome, far-red light absorbing form
Phot	Phototropin
Phy	Phytochrome
PHY	Phytochrome specific GAF related domain
Pr	Phytochrome, red light absorbing form
PVDF	Polyvinylidene difluoride
PΦB	Phytochromobilin
PYP	Photoactive yellow protein
R	Red light
RBS	Ribosome binding site
RcP(s)	Response regulator of cyanobacterial phytochrome (plural)
Ref	Reference
rpm	Rotations per minute
RR(s)	Response regulator(s)
RT	Room temperature
s	Seconds
SAP	Shrimp alkaline phosphatase
SAR	Specific absorption ratio (ratio of Pr absorption maxima and absorbance at 280 nm
SDM	Site directed mutagenesis
SDS	Sodium dodecyl sulfate
SDS-PAGE	Sodium dodecyl sulfate-polyacrylamide gel electrophoresis

Tab.	Table
TAE	Tris- acetate /EDTA
TB	Terrific broth
TBY	Terrific broth/ yeast extract excess
TCEP	Tris(2-carboxyethyl)phosphine HCl
TE	Tris /EDTA
TEMED	N,N,N`,N`-Tetramethyl ethylene diamine
Tris	2-amino-2-(hydroxymethyl)-1,3-propanediol
Triton X-100	t-octylphenoxypolyethoxyethanol
TWEEN	Poly-oxyethylene-sorbitan
UV-Vis	Ultra-violet visible spectrum / spectroscopy
V	Volt
Vol	Volume
v/v	Volume per volume
WT	Wild type
w/v	Weight per volume
X-Gal	5-Brom-3-Chlor-3-Inoyl-β-D-galactopyranoside
β-ME	Beta-mercaptoethanol
λ	Wavelength
λ_{max}	Wavelength of the absorption maximum
μM	Micromolar
μS	Microseconds
ΔA	Absorbance difference
ε	Extinction coefficient (in M^{-1} cm^{-1})

Appendix II

Cryo I sparse matrix crystallization screen – Hampton Research

	Crystallant Buffer	Additive(s)
1.	40% (v/v) 2-methyl-2,4-pentanediol phosphate-citrate pH 4.2	none
2.	40% (v/v) ethylene glycol acetate pH 4.5	none
3.	50% (v/v) PEG-200 citrate pH 5.5	none
4.	40% (v/v) PEG-300 HEPES pH 7.5	0.2 M NaCl
5.	40% (v/v) PEG-400 citrate pH 5.5	0.2 M $MgCl_2$
6.	40% (v/v) PEG-600 cacodylate pH 6.5	0.2 M $Ca(OAc)_2$
7.	40% (v/v) ethanol Tris pH 8.5	0.05 M $MgCl_2$
8.	35% (v/v) 2-ethoxyethanol cacodylate pH 6.5	none
9.	35% (v/v) 2-propanol phosphate-citrate pH 4.2	none
10.	45% (v/v) glycerol imidazole pH 8.0	none
11.	35% (v/v) 2-methyl-2,4-pentanediol Tris pH 8.5	0.2 M $(NH4)_2SO_4$
12.	50% (v/v) ethylene glycol acetate pH 4.5	5% (w/v) PEG-1000
13.	30% (v/v) PEG-200 MES pH 6.0	5% (w/v) PEG-3000
14.	20% (v/v) PEG-300 phosphate-citrate pH 4.2	0.2 M $(NH4)2SO_4$, 10% glycerol
15.	50% (v/v) PEG-400 CHES pH 9.5	0.2 M NaCl
16.	30% (v/v) PEG-600 MES pH 6.0	5% PEG-1000, 10% glycerol
17.	40% (v/v) 1, 2-propanediol HEPES pH 7.5	none
18.	35% (v/v) 2-ethoxyethanol imidazole pH 8.0	0.05 M $Ca(OAc)_2$
19.	35% (v/v) 2-propanol Tris pH 8.5	none
20.	30% (v/v) 1,2-propanediol citrate pH 5.5	20% 2-methyl-2,4-pentanediol
21.	40% (v/v) 1,2-propanediol acetate pH 4.5	0.05 M $Ca(OAc)_2$
22.	40% (v/v) ethylene glycol Na/K phosphate pH 6.2	none
23.	40% (v/v) 2-methyl-2,4-pentanediol Tris pH 7.0	0.2 M $(NH4)_2SO_4$
24.	40% (v/v) PEG-400 Na/K phosphate pH 6.2	0.2 M NaCl
25.	30% (v/v) PEG-200 Tris pH 8.5	0.2 M $(NH4)_2HPO_4$
26.	40% (v/v) PEG-300 CHES pH 9.5	0.2 M NaCl
27.	30% (v/v) PEG-400 CAPS pH 10.5	0.5 M $(NH4)_2SO_4$, 10% glycerol
28.	30% (v/v) PEG-600 HEPES pH 7.5	0.05 M Li2SO4, 10% glycerol
29.	40% (v/v) PEG-300 CHES pH 9.5	0.2 M sodium citrate
30.	35% (v/v) 2-ethoxyethanol citrate pH 5.5	none
31.	35% (v/v) 2-propanol citrate pH 5.5	5% (w/v) PEG-1000
32.	40% (v/v) 1,2-propanediol CHES pH 9.5	0.2 M sodium citrate
33.	25% (v/v) 1, 2-propanediol imidazole pH 8.0	0.2 M $Zn(OAc)_2$, 10% glycerol
34.	40% (v/v) 2-methyl-2,4-pentanediol imidazole pH 8.0	0.2 M MgCl2
35.	40% (v/v) ethylene glycol HEPES pH 7.5	5% (w/v) PEG-3000
36.	50% (v/v) PEG-200 Tris pH 7.0	0.05 M $Li2SO_4$
37.	40% (v/v) PEG-300 cacodylate pH 6.5	0.2 M $Ca(OAc)_2$
38.	40% (v/v) PEG-400 Tris pH 8.5	0.2 M $Li2SO_4$
39.	40% (v/v) PEG-600 phosphate-citrate pH 4.2	none
40.	40% (v/v) ethanol phosphate-citrate pH 4.2	5% (w/v) PEG-1000
41.	25% (v/v) 1, 2-propanediol phosphate-citrate pH 4.2	5% PEG-3000, 10% glycerol
42.	40% (v/v) ethylene glycol Tris pH 7.0	none
43.	50% (v/v) ethylene glycol Tris pH 8.5	0.2 M $MgCl_2$
44.	50% (v/v) PEG-200 cacodylate pH 6.5	0.2 M $Zn(OAc)_2$
45.	20% (v/v) PEG-300 Tris pH 8.5	5% PEG-8000, 10% glycerol
46.	40% (v/v) PEG-400 MES pH 6.0	5% (w/v) PEG-3000
47.	50% (v/v) PEG-400 acetate pH 4.5	0.2 M $Li2SO_4$
48.	40% (v/v) PEG-600 imidazole pH 8.0	0.2 M $Zn(OAc)_2$

Cryo II sparse matrix crystallization screen – Hampton Research

	Crystallant Buffer	Additive(s)
1.	40% (v/v) 2-methyl-2,4-pentanediol cacodylate pH 6.5	5% (w/v) PEG-8000
2.	50% (v/v) PEG-200 CHES pH 9.5	none
3.	40% (v/v) ethylene glycol phosphate-citrate pH 4.2	0.2 M $(NH4)_2SO_4$
4.	40% (v/v) PEG-400 HEPES pH 7.5	0.2 M $Ca(OAc)_2$
5.	40% (v/v) PEG-300 Tris pH 7.0	5% (w/v) PEG-1000
6.	30% (v/v) PEG-600 cacodylate pH 6.5	1 M NaCl, 10% (v/v) glycerol
7.	40% (v/v) ethanol Tris pH 7.0	none
8.	35% (v/v) 2-ethoxyethanol Na/K phosphate pH 6.2	0.2 M NaCl
9.	35% (v/v) 2-propanol imidazole pH 8.0	0.05 M $Zn(OAc)_2$
10.	40% (v/v) 1,2-propanediol acetate pH 4.5	none
11.	25% (v/v) 1, 2-propanediol Na/K phosphate pH 6.2	10% (v/v) glycerol
12.	40% (v/v) 1,2-propanediol citrate pH 5.5	0.2 M NaCl
13.	35% (v/v) 2-methyl-2,4-pentanediol cacodylate pH 6.5	0.05 M $Zn(OAc)_2$
14.	40% (v/v) ethylene glycol imidazole pH 8.0	0.2 M $Ca(OAc)_2$
15.	50% (v/v) PEG-200 Na/K phosphate pH 6.2	0.2 M NaCl
16.	20% (v/v) PEG-300 imidazole pH 8.0	1 M $(NH4)_2SO4$, 10% glycerol
17.	50% (v/v) PEG-400 MES pH 6.0	none
18.	40% (v/v) PEG-300 phosphate-citrate pH 4.2	none
19.	40% (v/v) PEG-600 acetate pH 4.5	0.2 M $MgCl_2$
20.	50% (v/v) ethylene glycol CHES pH 9.5	0.5 M K/Na tartrate
21.	35% (v/v) 2-ethoxyethanol Tris pH 8.5	0.2 M $Li2SO_4$
22.	35% (v/v) 2-propanol cacodylate pH 6.5	0.2 M $MgCl_2$
23.	30% (v/v) 1,2-propanediol HEPES pH 7.5	20% (v/v) PEG-400
24.	25% (v/v) 1, 2-propanediol Tris pH 8.5	0.2 M MgCl2, 10% glycerol
25.	40% (v/v) 2-methyl-2,4-pentanediol CAPS pH 10.5	none
26.	40% (v/v) ethylene glycol MES pH 6.0	0.2 M $Zn(OAc)_2$
27.	50% (v/v) PEG-200 Tris pH 7.0	none
28.	40% (v/v) PEG-300 imidazole pH 8.0	0.2 M $Zn(OAc)_2$
29.	30% (v/v) PEG-400 HEPES pH 7.5	5% PEG-3000, 10% glycerol
30.	40% (v/v) PEG-600 citrate pH 5.5	none
31.	40% (v/v) PEG-600 CHES pH 9.5	none
32.	35% (v/v) 2-propanol acetate pH 4.5	none
33.	45% (v/v) glycerol cacodylate pH 6.5	0.2 M $Ca(OAc)_2$
34.	25% (v/v) 1, 2-propanediol Tris pH 7.0	0.2 M $(NH4)_2SO4$, 10% glycerol
35.	40% (v/v) 2-methyl-2,4-pentanediol citrate pH 5.5	none
36.	50% (v/v) PEG-200 cacodylate pH 6.5	0.2 M $MgCl_2$
37.	50% (v/v) ethylene glycol imidazole pH 8.0	none
38.	40% (v/v) PEG-400 acetate pH 4.5	none
39.	30% (v/v) PEG-600 Tris pH 7.0	0.5 M $(NH4)_2SO_4$, 10% glycerol
40.	40% (v/v) 2-methyl-2,4-pentanediol CHES pH 9.5	none
41.	50% (v/v) ethylene glycol HEPES pH 7.5	0.2 M $Li2SO_4$
42.	30% (v/v) PEG-200 acetate pH 4.5	0.1 M NaCl
43.	40% (v/v) PEG-400 imidazole pH 8.0	none
44.	35% (v/v) 2-methyl-2,4-pentanediol acetate pH 4.5	10% (v/v) glycerol
45.	40% (v/v) PEG-300 acetate pH 4.5	0.2 M NaCl
46.	30% (v/v) PEG-200 CAPS pH 10.5	0.2 M $(NH4)_2SO_4$
47.	50% (v/v) PEG-200 HEPES pH 7.5	none
48.	50% (v/v) PEG-200 phosphate-citrate pH 4.2	0.2 M NaCl

Crystal Screen 1- Hampton Research

	Crystallant Buffer	Additive(s)
1.	30% MPD, 0.1 M Na Acetate pH 4.6	0.02 M $CaCl_2$
2.	0.4 M K, Na Tartrate	none
3.	0.4 M Ammonium Phosphate	none
4.	2.0 M Ammonium Sulfate	0.1 M Tris HCl pH 8.5
5.	30% MPD, 0.1 M Na Hepes pH 7.5	0.2 M Sodium Citrate
6.	30% PEG 4000, 0.1 M Tris HCl pH 8.5	0.2 M $MgCl_2$
7.	1.4 M Sodium Acetate	0.1 M Na Cacodylate pH 6.5
8.	30% iso-Propanol, 0.1 M Na Cacodylate pH 6.5	0.2 M Sodium Citrate
9.	30% PEG 4000, 0.1 M Na Citrate pH 5.6	0.2 M Ammonium Acetate
10.	30% PEG 4000, 0.1 M Na Acetate pH 4.6	0.2 M Ammonium Acetate
11.	1.0 M Ammonium Phosphate	0.1 M Na Citrate pH 5.6
12.	30% iso-Propanol, 0.1 M Na Hepes pH 7.5	0.2 M $MgCl_2$
13.	30% PEG 400, 0.1 M Tris HCl pH 8.5	0.2 M Sodium Citrate
14.	28% PEG 400, 0.1 M Na Hepes pH 7.5	0.2 M $CaCl_2$
15.	30% PEG 8000, 0.1 M Na Cacodylate pH 6.5	0.2 M $(NH4)2SO_4$
16.	1.5 M Lithium Sulfate	0.1 M Na Hepes pH 7.5
17.	30% PEG 4000, 0.1 M Tris HCl pH 8.5	0.2 M $Li2SO_4$
18.	20% PEG 8000, 0.1 M Na Cacodylate pH 6.5	0.2 M Magnesium Acetate
19.	30% iso-Propanol, 0.1 M Tris HCl pH 8.5	0.2 M Ammonium Acetate
20.	25% PEG 4000, 0.1 M Na Acetate pH 4.6	0.2 M Ammonium Sulfate
21.	30% MPD, 0.1 M Na Cacodylate pH 6.5	0.2 M Magnesium Acetate
22.	30% PEG 4000, 0.1 M Tris HCl pH 8.5	0.2 M Sodium Acetate
23.	30% PEG 400, 0.1 M Na Hepes pH 7.5	0.2 M $MgCl_2$
24.	20% iso-Propanol, 0.1 M Na Acetate pH 4.6	0.2 M $CaCl_2$
25.	1.0 M Sodium Acetate	0.1 M Imidazole pH 6.5
26.	30% MPD, 0.1 M Na Citrate pH 5.6	0.2 M Ammonium Acetate
27.	20% iso-Propanol, 0.1 M Na Hepes pH 7.5	0.2 M Sodium Citrate
28.	30% PEG 8000, 0.1 M Na Cacodylate pH 6.5	0.2 M Sodium Acetate
29.	0.8 M K, Na Tartrate	0.1 M Na Hepes pH 7.5
30.	30% PEG 8000	0.2 M Ammonium Sulfate
31.	30% PEG 4000	0.2 M Ammonium Sulfate
32.	2.0 M Ammonium Sulfate	none
33.	4.0 M Sodium Formate	none
34.	2.0 M Sodium Formate	0.1 M Na Acetate pH 4.6
35.	1.6 M Na, K Phosphate	0.1 M Na Hepes pH 7.5
36.	8% PEG 8000	0.1 M Tris HCl pH 8.5
37.	8% PEG 4000	0.1 M Na Acetate pH 4.6
38.	1.4 M Sodium Citrate	0.1 M Na Hepes pH 7.5
39.	2% PEG 400, 0.1 M Na Hepes pH 7.5	2 M $(NH4)_2SO_4$
40.	20% iso-Propanol, 0.1 M Na Citrate pH 5.6	20% PEG 4000
41.	10% iso-Propanol, 0.1 M Na Hepes pH 7.5	20% PEG 4000
42.	20% PEG 8000, 0.05 M Potassium Phosphate	30% PEG 1500
43.	0.2 M Magnesium Formate	none
44.	18% PEG 8000, 0.1 M Na Cacodylate pH 6.5	0.2 M Zinc Acetate
45.	18% PEG 8000, 0.1 M Na Cacodylate pH 6.5	0.2 M Calcium Acetate
46.	2.0 M Ammonium Sulfate	0.1 M Sodium Acetate pH 4.6
47.	2.0 M Ammonium Phosphate	0.1 M Tris HCl pH 8.5
48.	20% PEG 8000	1.0 M Lithium Sulfate

Crystal Screen 2 – Hampton Research

	Crystallant Buffer	Additive(s)
1.	10% PEG 6000	2.0 M Sodium Chloride
2.	0.5 M Sodium Chloride, 0.01 M CTAB	0.01 M Magnesium Chloride
3.	25% Ethylene Glycol	none
4.	35% Dioxane	none
5.	5% iso-Propanol	2.0 M Ammonium Sulfate
6.	1.0 M Imidazole pH 7.0	none
7.	10% PEG 1000, 10% PEG 8000	none
8.	10% Ethanol	1.5 M Sodium Chloride
9.	2.0 M Sodium Chloride	0.1 M Na Acetate pH 4.6
10.	30% MPD, 0.1 M Na Acetate pH 4.6	0.2 M Sodium Chloride
11.	1.0 M 1,6 Hexanediol, 0.1 M Na Acetate pH 4.6	0.01 M Cobalt Chloride
12.	30% PEG 400, 0.1 M Na Acetate pH 4.6	0.1 M Cadmium Chloride
13.	30% PEG MME 2000, 0.1 M Na Acetate pH 4.6	0.2 M Ammonium Sulfate
14.	2.0 M Ammonium Sulfate, 0.1 M Na Citrate pH 5.6	0.2 M K/Na Tartrate
15.	1.0 M Lithium Sulfate, 0.1 M Na Citrate pH 5.6	0.5 M Ammonium Sulfate
16.	2% Polyethyleneimine, 0.1 M Na Citrate pH 5.6	0.5 M Sodium Chloride
17.	35% tert-Butanol, 0.1 M Na Citrate pH 5.6	none
18.	10% Jeffamine M-600, 0.1 M Na Citrate pH 5.6	0.01 M Ferric Chloride
19.	2.5 M 1,6 Hexanediol, 0.1 M Na Citrate pH 5.6	none
20.	1.6 M Magnesium Sulfate, 0.1 M MES pH 6.5	none
21.	2.0 M Sodium Chloride, 0.1 M MES pH 6.5	0.2 M Na/K Phosphate
22.	12% PEG 20,000, 0.1 M MES pH 6.5	none
23.	10% Dioxane, 0.1 M MES pH 6.5	1.6 M Ammonium Sulfate
24.	30% Jeffamine M-600, 0.1 M MES pH 6.5	0.05 M Cesium Chloride
25.	1.8 M Ammonium Sulfate, 0.1 M MES pH 6.5	0.01 M Cobalt Chloride
26.	30% PEG MME 5000, 0.1 M MES pH 6.5	0.2 M Ammonium Sulfate
27.	25% PEG MME 550, 0.1 M MES pH 6.5	0.01 M Zinc Sulfate
28.	1.6 M Sodium Citrate pH 6.5	none
29.	30% MPD, 0.1 M Hepes pH 7.5	0.5 M Ammonium Sulfate
30.	10% PEG 6000, 0.1 M Hepes pH 7.5	5% MPD
31.	20% Jeffamine M-600, 0.1 M Hepes pH 7.5	none
32.	1.6 M Ammonium Sulfate, 0.1 M Hepes pH 7.5	0.1 M Sodium Chloride
33.	2.0 M Ammonium Formate, 0.1 M Hepes pH 7.5	none
34.	1.0 M Sodium Acetate, 0.1 M Hepes pH 7.5	0.05 M Cadmium Sulfate
35.	70% MPD, 0.1 M Hepes pH 7.5	none
36.	4.3 M Sodium Chloride, 0.1 M Hepes pH 7.5	none
37.	10% PEG 8000, 0.1 M Hepes pH 7.5	8% Ethylene Glycol
38.	20% PEG 10,000, 0.1 M Hepes pH 7.5	none
39.	3.4 M 1,6 Hexanediol, 0.1 M Tris pH 8.5	0.2 M Magnesium Chloride
40.	25% tert-Butanol, 0.1 M Tris pH 8.5	none
41.	1.0 M Lithium Sulfate, 0.1 M Tris pH 8.5	0.01 M Nickel (II) Chloride
42.	12% Glycerol, 0.1 M Tris pH 8.5	1.5 M Ammonium Sulfate
43.	50% MPD, 0.1 M Tris pH 8.5	0.2 M Ammonium Phosphate
44.	20% Ethanol, 0.1 M Tris pH 8.5	none
45.	20% PEG MME 2000, 0.1 M Tris pH 8.5	0.01 M Nickel (II) Chloride
46.	20% PEG MME 550, 0.1 M Bicine pH 9.0	0.1 M Sodium Chloride
47.	2.0 M Magnesium Chloride, 0.1 M Bicine pH 9.0	none
48.	10% PEG 20,000, 0.1 M Bicine pH 9.0	2% Dioxane

Appendix III

Figure 2.1 : Diagrammatic display of the electromagnetic light spectrum with identified photoreceptor groups active under the respective light wavelengths.

Figure 2.2 : Depiction of the three types of photoreceptors comprehensible for the plants with the assigned functions of each photoreceptor as described by various studies.

Figure 2.3 : Diversity of bilin chromophores utilized by the phytochrome systems found in proteobacteria, plants and cyanobacteria.

Figure 2.4 : Spectral properties of typical cyanobacterial phytochrome.

Figure 2.5 : Structural modulation of the phytochrome chromophore.

Figure 2.6 : Schematic domain architecture of phytochromes and phytochrome like proteins.

Figure 2.7 : Schematic organization of the phytochrome structural domains.

Figure 2.8 : Three dimensional phytochrome bi-domain structure of the N-terminus PAS-GAF of *Deinococcus radiodurans.*

Figure 2.9 : Crsytal structure of the PAS-GAF-PHY tri-domain of the *Synechocystis* PCC 6803 phytochrome, Cph1□ 2, in the Pr state.

Figure 2.10 : Chromophore bound to the protein in the biling binding pocket formed in the crystal structure of Cph1.

Figure 2.11 : The chromophore tethered to the cysteine residue in the PLD domain of bacteriophytochromes as seen through the crystal structure lens.

Figure 2.12 : Schematic representations of isothermal titration calorimetry (ITC) instruments.

Table 3.1 : Bacterial strains used with detailed genotypes.

Table 3.2 : Extinction coefficient (ε) of Bilins PCB (Cole et al., 1967), and BV (McDonagh, 1979).

Table 4 (a) : Detailed depiction of the heterologously expressed phytochromes

Figure 4.1 : UV/VIS Absorption spectra of CphA and CphBm.

Figure 4.2 : Spectrum of CphBm expressed in different competent cells.

ADDENDUM

ADDENDUM

Figure 4.20 : Representation of the ITC device.

Figure 4.21 : Cartoon depicting the reaction mechanism at the molecular level of the ITC measurements.

Figure 4.22 : Control experiments of isothermal titration calorimetry measurements.

Figure 4.23 : Graphical representation of the ITC experiment in presence of ATP.

Figure 4.24 : Graphical comparison of the ITC experiment in the presence of ATP vs. non-hydrolysable ATP.

Figure 4.25 : Graphical presentation of the ITC experiment.

Figure 4.26 : Graphical presentation of the titration interaction.

Figure 4.27 : Titration of the heterologously expressed HK domain from CphA and RcpA.

TABLE 4 (e) : Thermodynamic parameters of CphA-RcpA and CphB-RcpB binding reactions.

Figure 4.28 : Graphical measurements followed during FTIR spectroscopic analysis.

Figure 4.29 : Spectroscopic graphical representation of UV-Vis measurements of CphA phytochrome done in parallel with FTIR spectroscopy.

Figure 4.30 : Comparison of the Pr:Pfr FTIR difference spectra (0°C) for various recombinant phytochromes.

Figure 4.31 & 4.32 : Light-induced FTIR difference spectra of the photoreactions of recombinant bacteriophytochrome CphA recorded in H_2O and in D_2O.

Figure 4.33 (a & b) : Light-induced FTIR difference spectra of the photoreactions of recombinant bacteriophytochrome CphA recorded in H_2O and D_2O.

Figure 4.34 : Comparison of the Pr:Lumi-R FTIR difference spectra (- 120 °C to – 140 °C) for various recombinant phytochromes.

Figure 4.35 : Comparison of the Pr:Meta-Ra FTIR difference spectra (- 45 °C to – 70 °C) for various recombinant phytochromes.

Figure 4.36 : Comparison of the Pr:Meta-Rc FTIR difference spectra (-25°C) for various recombinant phytochromes.

Figure 4.37 : Comparison of the Pfr:Meta-F FTIR difference spectra (- 80 °C) for various recombinant phytochromes.

Figure 4.38 : **Comparison of the Pfr:Lumi-F FTIR difference spectra (- 140 °C) for various recombinant phytochromes.**

Figure 4.39 : **Spectroscopic graphical representation of UV-Vis measurements of CphB phytochrome done in parallel with FTIR spectroscopy.**

Figure 4.40 : **Graphical measurements followed during FTIR spectroscopic analysis.**

Figure 4.41 : **Light-induced FTIR difference spectra of the photoreactions of recombinant bacteriophytochrome CphB recorded in H_2O (black) and D_2O (grey).**

Figure 4.42 : **Light-induced FTIR difference spectra of the photoreactions of recombinant bacteriophytochrome CphB recorded in H_2O (black) and D_2O (grey).**

Figure 4.43 : **Comparison of the Pr:Pfr FTIR difference spectra for various recombinant phytochromes.**

Figure 4.44 : **Comparison of the meta-Rc spectra for various recombinant phytochromes.**

Figure 4.45 : **Comparison of the meta-Ra spectra for various recombinant phytochromes.**

Figure 4.46 : **Comparison of the lumi-F spectra for various recombinant phytochromes.**

Figure 4.47 : **Comparison of the meta-F spectra for various recombinant phytochromes.**

Die hier vorgelegte Dissertation habe ich eigenständig und ohne unerlaubte Hilfe
angefertigt. Die Dissertation wurde in der vorgelegten oder in ähnlicher Form noch
bei keiner anderen Institution eingereicht. Ich habe bisher keine erfolglosen Promotionsversuche unternommen.

Unterschrift Düsseldorf, den
...../...../2010

Aus dem Max-Planck Institut für
Bioanorganische Chemie in Mülheim an der Ruhr

Gedruckt mit der Genehmigung der
Mathematisch-Naturwissenschaftlichen Fakultät der
Heinrich-Heine-Universität Düsseldorf

Referent: Prof. Dr. Wolfgang Gärtner

Koreferent: Prof. Dr. Georg Groth

Tag der mündlichen Prüfung:
(-----28-----/---10-------/ 2010)